Rip Currents in Lake Michigan and in Lake Superior

By
Yuli Liu

A dissertation submitted in partial fulfillment of
the requirements for the degree of

Doctor of Philosophy
(Civil and Environmental Engineering)

at the
UNIVERSITY OF WISCONSIN-MADISON
2020

Date of final oral examination: 08/10/2020

The dissertation is approved by the following members of the Final Oral Committee:

Chin H. Wu, Professor, Civil and Environmental Engineering
Paul J. Block, Associate Professor, Civil and Environmental Engineering
Daniel B. Wright, Assistant Professor, Civil and Environmental Engineering
James P. Hurley, Professor, Civil and Environmental Engineering
Fengyan Shi, Associate Professor, Civil and Environmental Engineering, University of Delaware

Abstract

Rip currents are narrow, fast-moving offshore-directed flows that can sweep swimmers out from surf zone into deeper water. Hundreds of fatalities and incidents reported on the Great Lakes coasts are caused by rip currents, which impose severe hazards to the Great Lakes beach users. The objective of this dissertation is to characterize rip currents in Lake Michigan and in Lake Superior, and to develop assessment tools for effective warning of the rip current hazards to coastal communities.

Flash rips are transient and intermittent rip currents. To provide real-time flash rip warnings to beach users, a Lifeguarding Operational Camera Kiosk System (LOCKS) is developed and implemented at the North Beach of Port Washington, WI. LOCKS has three components. First, a real-time environmental observation system acquires timely beach view images and local environmental condition data. Second, an integrated nowcast forecast operational system, high performance and distributed computing infrastructure, digitally detects and assesses flash rip hazards in high, moderate, or low risks. Third, an automated kiosk dynamically issues real-time on-site warnings by a three-color dynamic light and a digital display monitor. Results show that LOCKS can detect flash rips in both sunny and cloudy days with an overall accuracy of 83%. Characteristics of flash rips are observed to have nonstationary locations and intermittent occurrences. The developed flash rip occurrence checklist is demonstrated to reliably assess the likelihood of hazardous flash rips by using two new proxies of visual images and convective storms. The observed co-occurrence of convective storms and flash rips suggests future studies on investigating the meteorologically induced water level oscillations in generating flash rips.

Flash rips generated by meteorologically induced water level oscillations (MIWLOs) are revealed to pose unrecognized hazards to the unawareness of beach users. Occurrences and

causative processes of generating flash rips are investigated in Lake Michigan at the North Beach of Port Washington, by compiling images, hydrodynamic and atmospheric observations with reconstructed velocity fields from integrated atmospheric-hydrodynamic modeling. Results show that meteotsunamis, seiches, wind waves, and combined effects are all pathways to generate flash rips. Temporal transiency, intermittency, and spatial ubiquity and unpredictability are characteristics of flash rips induced by MIWLOs and elevated the hidden danger to beach swimmers. Rip currents generated by MIWLOs are found to be associated with 70% of current related incidents on the Great Lakes coasts. Statistics evidence also suggests that causes of many incidents on United States ocean coasts can be related to the unrecognized flash rip hazards.

Hidden flash rips can be wide-spread hazards, as several drowning incidents occurred across Lake Michigan during a series of convective storms. Features of storm disturbances and hydrodynamic forcing are characterized to depict possible causes of the drowning incidents. Nearshore processes generating unexpected flash rips through storm-induced energetic wind waves, meteotsunami-induced longshore currents, water level drawdowns, and seiches are revealed. Hidden flash rip hazards are frequent under both low meteorologically induced water level oscillations and low wind waves, a condition has not been recognized before. The time delay in flash rip occurrences relative to convective storms further elevates the risk of the hidden danger to the unaware beach swimmers.

Rip currents near coastal structures are one cause for drownings in the Great Lakes. A Structure Rip Checklist and Assessment Matrix (SRiCAM) is developed by characterizing rip currents near breakwaters and aims to provide timely warnings to beach users. Rip currents occurrences near the north breakwater of Port Washington, are associated with environmental proxies. Results show that rip currents can occur when the water appears seemingly calm near the

structure, thus imposing hidden dangers to unalerted beach users. The performance of the SRiCAM shows consistency and inclusiveness by using the four-level tier assessment. Furthermore, the SRiCAM is integrated into a cyberinfrastructure with a data contingency plan to provide real-time warnings to the public. The applicability of the SRiCAM is also demonstrated by applying to thirty-eight other locations and shows great potential to be widely extended to wider regions of the Great Lakes to foster the resilience of recreational water users to the rip current hazards.

Lastly, rip currents are characterized on the western shore of Lake Superior. Remote-sensing data including aerial imagery, coastal LiDAR elevations, and nearshore webcam images are analyzed to detect bathymetry features like nearshore bars where rip currents are prone to occur at two beaches, the 12th St Beach and the 22nd St Beach in Duluth, MN. Results show that double crescent bar systems, experiencing dynamic evolution on the time scale from years to hours, are dominant along the western shore of Lake Superior. The documented bathymetric characteristics provide information about hotspots and can be used to facilitate the future studies of rip currents on the western shore of Lake Superior for the resilience to rip current hazards for the Great Lakes coastal communities.

Acknowledgments

I would like to thank many people who have supported me throughout my graduate studies at the University of Wisconsin-Madison. First of all, I must thank my advisor Dr. Chin Wu. He has inspired me and led me to research, which opened a world I would not consider before. I appreciate the opportunities he has provided for me all the way along to do all kinds of interesting works. His continuous mentoring in both technical and non-technical aspects are essential to me as a researcher and as a person in society. I also would like to thank my committee members Dr. Paul J. Block and Dr. Daniel B. Wright, Dr. James P. Hurley, and Dr. Fengyan Shi. Thanks to Dr. Block and Dr. Wright for their insightful comments and research suggestions. Thanks to Dr. Hurley for his perspectives and providing opportunities for me to work on projects to help people. Thanks to Dr. Shi for his guidance on numerical modeling and his encouragement. Also, I would like to thank Dr. Adam Bechle and Alex Campbell for their mentoring about camera techniques and help in my early days of research, Dr. Josh Anderson for his guidance and assistance in instrumentation, computing, and field works, and Dr. Alvaro Linares for his advice in meteotsunamis and rip current studies and supports.

Organizations and project partners for their gracious support and assistance must be acknowledged. Funding sources for this work include the University of Wisconsin Sea Grant Institute, Wisconsin Coastal Management Program, the National Oceanic and Atmospheric Administration Coastal Storms Program, and the Becker Travel Grant. I would like to thank many people and staff from the City of Port Washington, City of Ashland, Minnesota Sea Grant, University of Minnesota Duluth Natural Resources Research Institute, Great Lakes Environmental Research Laboratory, and many others. Particularly I would like to thank Mr. Dennis Cherny, Mr. Dan Buehler, and Mr. Jerry Henneck for assistance in fieldwork over the past six years. An especial

thank is to Mr. Todd Breiby, thank you for your coordination in the projects and always being supportive and believing in the work I do and I am thankful for all the things I learned from you.

The support and help I received from peers and professors of the Water Resources Engineering group and Coastal Sustainability & Environmental Fluid Mechanics Lab are important to me from the past to the present. People I have worked together with in all kinds of fieldwork are too numerous to name, but their help and assistance and deeply appreciated. I'd like to thank my TA peers during the 8-semester of time in "re-learning" Fluid Mechanisms. I have learned a lot from them in different ways of teaching. Also, thanks to professors Dr. Ken Potter, Dr. Steve Loheide, and Dr. Nimish Pujara, and everyone else in the WRE for continuing to improve our program and creating a supportive environment. I am honored and proud to be part of the WRE.

Lastly, I want to thank my friends and family for their support and encouragement throughout my journey of graduate studies. There are so many friendships and supports I have earned over the years in Madison. I am grateful for all their help, support, and fun time I experienced. Especially I would like to thank my friends Biyun and Weijuan for willing to listening to me and cheering me up. Last but definitely not least, I want to thank my parents for everything they gave me. Their advice and perspectives are valuable in every stage of my life. Their unconditional love and supports are the momentum for me to become a better person. I feel lucky and grateful to be in such a family.

Table of contents

List of Tables

List of Figures

1. Introduction

1.1 Background

Rip currents are narrow, rapid seaward water jets that can sweep swimmers out from the surf zone to into deeper water (Dalrymple et al., 2011; MacMahan et al., 2006), where exhaustion and panic often result in drowning (Castelle et al., 2016). Hundreds of incidents due to rip currents have been reported over the world (Arozarena et al., 2015; Brighton et al., 2013; Gensini and Ashley, 2010; Short and Hogan, 1994). In the United States, an annual average of 57 fatalities was estimated based on incident statistics of 2008 – 2017 (*Summary of Natural Hazard Statistics for 2018 in the United States*, 2018), including both ocean coasts and the Great Lakes (Linares et al., 2019; Meadows et al., 2011). According to the Great Lakes Current Incident Database (GLCID, 2019), a total of 624 incidents including 195 fatalities had occurred during 2002 – 2019. In Lake Michigan, at a hotspot like the Holland State Park, Michigan, a total of 28 incidents occurred on a single day of August 3, 2011 (GLCID, 2019). On the western shore, unexpected incidents including 8 drownings and more than 10 rescues were reported near the harbor of Port Washington, Wisconsin (GLCID, 2019; *Great Lakes Surf Rescue Project Statistics*, 2019). While Lake Michigan has the predominant number of incidents that contribute to 72% of all incidents across the Great Lakes, Lake Superior, though perceived "less swimmable" due to low water temperature, also has had more than 49 incidents including 17 fatalities (GLCID, 2019). A vivid example was on August 17, 2003, near Park Point Beach in Duluth, Minnesota, when rip currents caused the drowning of a 21-year old young man, and 7 others were rescued (Schomberg, 2009). Overall, rip currents impose a deadly and prevalent threat to water users. In view of these consequences, effective warnings based on systematic characterizations of rip currents are critical to foster the resilience of coastal communities to the hazards the Great Lakes.

Three types of rip currents are examined in this dissertation. The first type is *hydrodynamically-controlled rip currents*, known as *flash rips* (Castelle et al., 2016). Mostly occurring in featureless or alongshore-uniform beaches, flash rips are generated by mechanisms including (1) shear instability of strong longshore currents (Özkan-Haller and Kirby, 1999), (2) breaking vorticities of single short-crested waves (Feddersen, 2014; Kirby and Derakhti, 2019), (3) interactions of incident waves with infra-gravity waves (Dalrymple, 1975; Johnson and Pattiaratchi, 2006) or edge waves (Sasaki and Horikawa, 1978; Symonds and Ranasinghe, 2001), as well as (4) meteorologically induced water level oscillations, such as the meteotsunamis (Linares et al., 2019) that have been recently revealed as a new mechanism of flash rips in the Great Lakes. The second type is *boundary-controlled rip currents*, which occur near natural headlands or anthropogenic structures such as breakwaters, groyns, and piers (Dalrymple et al., 2011). The boundary-controlled rips usually develop in two forms. One is *deflection rips* generated on the wave-side of the boundary due to longshore currents being physically deflected when encountering rigid structures (Castelle and Coco, 2013; Scott et al., 2016). The other form is *shadow rips* on the leeside as recirculation eddies generated by wave set-up differences due to shadowing effect (Gourlay, 1974; Pattiaratchi et al., 2009; Shi et al., 2003; Wind and Vreugdenhil, 1986). The third type is *bathymetry-controlled rip currents*, that usually occur in two kinds of bathymetry features. One kind is the *channel rips* in the deep region (rip channels) between nearshore sand bars (Castelle et al., 2016), where alongshore gradients of radiation stress due to non-uniform breaking drive the narrow jet of offshore-directed rip currents (Dalrymple et al., 2011; MacMahan et al., 2006). The second kind is the *focused rips*, generated from wave refraction due to offshore bathymetric anomalies, such as transverse ridges (Houser et al., 2011), sorted bedforms (Coco et al., 2007), submarine canyon outside of surf zones (Long and Özkan-Haller, 2005), and

multiple-barred beaches (Castelle et al., 2007). Three types of rip currents all can impose critical beach hazards, yet currently limited characterization for rip currents in the Great Lakes have been documented.

Warning of rip currents is essential to providing beach users the timely information of dangerous water conditions and can influence people's decisions of entering the water (Matthews et al., 2014; White and Hyde, 2010). Three approaches of rip current warnings are commonly used. First, static signage has been widely promoted at beaches since the NOAA "Break the Grip of the Rip!" campaign (Houser et al., 2017). The signage approach has been proven valuable in educating people the strategies to escape from rip currents (Brannstrom et al., 2015), while sometimes people may not be fully aware of the hazard (Houser et al., 2017). One possible reason is that the static signage is less eye-catching. Another possible cause is that users may not able to correctly recognize hazardous conditions based upon schematic illustrations on the signage (Brannstrom et al., 2015). Second, dynamic flags are thereby used by beach patrols, lifeguards, and local law enforcement officials (Brander et al., 2011; Sherker et al., 2010). The flag system is found effective (Brannstrom et al., 2015) while placing flags at unpatrolled beaches during rapid moving storm conditions remains challenging (Houser et al., 2017). Third, cyberinfrastructure has also recently become a popular way to provide real-time rip current warnings (Alvarez-Ellacuria et al., 2009; Arun Kumar and Prasad, 2014; Austin et al., 2012; Voulgaris et al., 2011). In the United States, the NOAA National Weather Service (NWS) developed rip current outlook webpage on oceanic and Great Lakes coasts (https://www.weather.gov/safety/ripcurrent-forecasts). The outlook provides advisory for rip current hazard in tiers (high-medium-low), which are assessed using empirical relations of environmental proxies (Lushine, 1991) or statistical model to predict rip current likelihoods (Dusek and Seim, 2013). The continuous advancements in developing rip

current risk assessment and cyberinfrastructures have served as valuable tools for rip current warnings. Nevertheless, effective real-time warnings at local beaches remain sporadic and overall underserved for the Great Lakes coastal communities.

Knowledge gaps and warning needs of rip currents in the Great Lakes lead to questions:

i. First, *what are the characteristics of flash rips in the Great Lakes?* Due to the nature of unpredictability and transiency (Castelle et al., 2016), flash rips are difficult to capture but can impose high risks as unexpected and hidden hazards to beach swimmers (Linares et al., 2019). Occurrences of flash rips in the Great Lakes have not yet been observed. Furthermore, the recent study (Linares et al., 2019) revealing that flash rips can be generated by meteotsunamis also leads to an additional question, *what are the roles of meteorologically induced water level oscillations and associated processes in generating flash rips?*

ii. Second, *what are the environmental conditions/proxies of boundary-controlled rips occurring near breakwater structures in the Great Lakes*? Characterization for boundary-controlled rips near groyn fields (Pattiaratchi et al., 2009; Scott et al., 2016) and headlands (Castelle and Coco, 2013) have been well documented, but limited information about rips occurring near breakwater structures are found in the literature (Liu and Mei, 1976). In the Great Lakes, breakwaters are common coastal structures and can have lengths on the order of several hundred meters in comparison to those of groyns and headlands. Studies have shown that rip occurrences depend on both hydrodynamic conditions and boundary lengths (Castelle and Coco, 2013; Scott et al.,

2016), but it is yet unclear if the breakwater geometry affects the rip current characteristics and the conditions of occurrences.

iii. Third, *what are typical patterns of bathymetry features that induce bathymetry-controlled rips in the Great Lakes*? Bathymetry-controlled rips are persistent and spatially fixed (Castelle et al., 2016; Moulton et al., 2017), thus bathymetric features like rip channels or crescent bars can be used as indicators of hotspots of rip currents. Though bathymetry-controlled rips that occurring on sandy barred beaches have been widely reported as likely causes for many drownings in the Great Lakes (GLCID, 2019), yet there is no detailed characterization on the bathymetry features of rip currents.

iv. Lastly, *how to assess rip current hazards to provide effective warnings to the Great Lakes communities*? Existing assessments are mostly developed based on characteristics of bathymetry-controlled rips (Lushine, 1991; Meadows et al., 2011), including the Great Lakes Rip Current Checklist (GLRCC). The GLRCC employs factors like wave height, wave period, wind speed, wind direction, and water level (Meadows et al., 2011). Recently, new factors like storm disturbances (Anderson and Wu, 2018), image visual evidence (Murray et al., 2013), high-frequency water level oscillations such as meteotsunamis (Linares et al., 2019) also found to be possible proxies for flash rips and boundary-controlled rips near coastal structures, but no corresponding assessment tools are yet available.

1.2 Research objectives

The aim of this dissertation is to characterize the three types of rip currents in Lake Michigan and in Lake Superior for providing warnings of rip current hazards to coastal communities. Guided by the key knowledge gaps in the characterization of rip currents and the need for effective rip current warnings in the Great Lakes, four overarching objectives of this dissertation are as follows:

1) Reveal occurrences, characteristics and causative processes of *flash rips* associated with meteorologically induced water level oscillations in Lake Michigan
2) Characterize environmental proxies for *boundary-controlled rips* occurring near breakwater structures in Lake Michigan
3) Examine bathymetric features of *bathymetry-controlled rips* in Lake Superior.
4) Develop assessment tools for effective and timely *warnings* of rip current hazards to the Great Lakes coastal communities.

1.3 Outline of the dissertation

Chapter 2 aims to characterize flash rips and provide timely warnings in Lake Michigan. A Lifeguarding Operational Camera Kiosk System (LOCKS) is developed to capture, compute, and communicate flash rip occurrences for real-time warnings to beach users. The LOCKS incorporates real-time environmental observation systems, high-performance computing infrastructures, and an automated kiosk with warnings signal lights. The system was implemented and has been in operation at the North Beach of Port Washington, WI since 2019. The key contributions of this chapter include two folds: first, flash rip occurrences were first time observed and characterized in the Great Lakes; second, the LOCKs provides real-time flash rip warnings to beach users for the first time. Chapter 2 was published in *Coastal Engineering 152* (2019).

In Chapter 3, the objective is to elucidate temporal and spatial characteristics of flash rips induced by meteorologically induced water level oscillations for revealing unrecognized beach hazards for beachgoers. Observation data including camera images, surface winds, atmospheric pressures, nearshore waves, water level fluctuation, and state-of-the-art integrated atmospheric-hydrodynamic modeling are employed to characterize flash rips. The key contribution of this chapter is revealing the unrecognized dangers in flash rips related to meteorologically induced water level oscillations. Chapter 3 is in preparation to be submitted to *Scientific Reports*.

In Chapter 4, the objective is to depict the causes of several drowning incidents in Lake Michigan and reveal nearshore processes that generate flash rips. Observations are used to characterize features of atmospheric storm disturbances and hydrodynamic forcings that lead to the possible occurrences of flash rips across Lake Michigan. The integrated atmospheric-hydrodynamic modeling is employed to uncover processes of generating hidden flash rips at reported incidents. In this chapter, the key contribution is uncovering the hidden dangers of flash

rips related to convective storms, a critical message to be delivered to the Great Lakes coastal communities. Chapter 4 has been submitted to *Nature Communications.*

Chapter 5 aims to characterize boundary-controlled rip currents and develop assessment tools for rip currents near breakwater structures for providing timely warnings to beach users in Lake Michigan. Field measurements of current velocities and nearshore environmental conditions were collected near the North Breakwater at Port Washington and are analyzed to characterize rip flow patterns and environmental proxies associated with the occurrences. A Structure Rip Checklist and Assessment Matrix (SRiCAM) is developed to assess potential occurrences using real-time data. The key contribution of this chapter is the development of SRiCAM that particularly addresses rip currents occurring near coastal structures and shows great potential for wider applications to many other places on the Great Lakes. Chapter 5 is in preparation to be submitted to *Journal of Great Lakes Research.*

Chapter 6 aims to characterize bathymetry features like nearshore bars that may lead to rip currents at the 12th St. Beach and the 22nd St. Beach in Duluth, MN of Lake Superior. Remote sensing data include aerial imagery, LiDAR elevations, and nearshore camera images that are processed to extracting the temporal and spatial changes of bathymetric features. The key contribution of this chapter is to examine bathymetric characteristics at rip hotspots to provide information for revealing rip currents in Lake Superior. Chapter 6 is in preparation to be submitted to *Natural Hazards.*

Lastly, in Chapter 7, summary, conclusions, and recommendations for future work are presented.

1.4 References

Alvarez-Ellacuria, A., Orfila, A., Olabarrieta, M., Gómez-pujol, L., Medina, R., Tintoré, J., 2009. An Alert System for Beach Hazard Management in the Balearic Islands. Coast. Manag. 37, 569–584. https://doi.org/10.1080/08920750903150662

Anderson, J.D., Wu, C.H., 2018. Development and application of a real-time water environment cyberinfrastructure for kayaker safety in the Apostle Islands, Lake Superior. J. Great Lakes Res. 44, 990–1001. https://doi.org/10.1016/J.JGLR.2018.07.006

Arozarena, I., Houser, C., Echeverria, A.G., Brannstrom, C., 2015. The rip current hazard in Costa Rica. Nat. Hazards 77, 753–768. https://doi.org/10.1007/s11069-015-1626-9

Arun Kumar, S.V. V., Prasad, K.V.S.R., 2014. Rip current-related fatalities in India: a new predictive risk scale for forecasting rip currents. Nat. Hazards 70, 313–335. https://doi.org/10.1007/s11069-013-0812-x

Austin, M.J., Scott, T.M., Russell, P.E., Masselink, G., 2012. Rip Current Prediction: Development, Validation, and Evaluation of an Operational Tool. J. Coast. Res. 29, 283. https://doi.org/10.2112/JCOASTRES-D-12-00093.1

Brander, R.W., Bradstreet, A., Sherker, S., MacMahan, J., 2011. Responses of Swimmers Caught in Rip Currents: Perspectives on Mitigating the Global Rip Current Hazard. Int. J. Aquat. Res. Educ. 5. https://doi.org/10.25035/ijare.05.04.11

Brannstrom, C., Lee Brown, H., Houser, C., Trimble, S., Santos, A., 2015. "You can't see them from sitting here": Evaluating beach user understanding of a rip current warning sign. Appl. Geogr. 56, 61–70. https://doi.org/10.1016/J.APGEOG.2014.10.011

Brighton, B., Sherker, S., Brander, R., Thompson, M., Bradstreet, A., 2013. Rip current related drowning deaths and rescues in Australia 2004–2011. Nat. Hazards Earth Syst. Sci. 13, 1069–

1075. https://doi.org/10.5194/nhess-13-1069-2013

Castelle, B., Bonneton, P., Dupuis, H., Sénéchal, N., 2007. Double bar beach dynamics on the high-energy meso-macrotidal French Aquitanian Coast: A review. https://doi.org/10.1016/j.margeo.2007.06.001

Castelle, B., Coco, G., 2013. Surf zone flushing on embayed beaches. Geophys. Res. Lett. 40, 2206–2210. https://doi.org/10.1002/grl.50485

Castelle, B., Scott, T., Brander, R.W.W., McCarroll, R.J.J., 2016. Rip current types, circulation and hazard, Earth-Science Reviews. Elsevier. https://doi.org/10.1016/j.earscirev.2016.09.008

Coco, G., Murray, A.B., Green, M.O., Thieler, E.R., Hume, T.M., 2007. Sorted bed forms as self-organized patterns: 2. Complex forcing scenarios. J. Geophys. Res. 112, F03016. https://doi.org/10.1029/2006JF000666

Dalrymple, R.A., 1975. A mechanism for rip current generation on an open coast. J. Geophys. Res. 80, 3485–3487. https://doi.org/10.1029/JC080i024p03485

Dalrymple, R.A., MacMahan, J.H., Reniers, A.J.H.M., Nelko, V., 2011. Rip Currents. Annu. Rev. Fluid Mech. 43, 551–581. https://doi.org/10.1146/annurev-fluid-122109-160733

Dusek, G., Seim, H., 2013. A Probabilistic Rip Current Forecast Model. J. Coast. Res. 289, 909–925.

Feddersen, F., 2014. The Generation of Surfzone Eddies in a Strong Alongshore Current. J. Phys. Oceanogr. 44, 600–617. https://doi.org/10.1175/JPO-D-13-051.1

Gensini, V.A., Ashley, W.S., 2010. An examination of rip current fatalities in the United States. Nat. Hazards 54, 159–175. https://doi.org/10.1007/s11069-009-9458-0

Gourlay, M.R., 1974. Wave Set-Up and Wave Generated Currents in the Lee of a Breakwater or Headland. American Society of Civil Engineers, New York, NY.

https://doi.org/10.1061/9780872621138.118

Great Lakes Current Incident Database [WWW Document], 2019. URL https://www.michiganseagrant.org/dcd/dcdsearch.php (accessed 12.9.19).

Great Lakes Surf Rescue Project Statistics [WWW Document], 2019. URL http://www.glsrp.org/statistics/ (accessed 12.9.19).

Houser, C., Barrett, G., Labude, D., 2011. Alongshore variation in the rip current hazard at Pensacola Beach, Florida. Nat. Hazards 57, 501–523. https://doi.org/10.1007/s11069-010-9636-0

Houser, C., Trimble, S., Brander, R., Chris Brewster, B., Dusek, G., Jones, D., Kuhn, J., 2017. Public perceptions of a rip current hazard education program: "Break the Grip of the Rip!" Nat. Hazards Earth Syst. Sci. 17, 1003–1024. https://doi.org/10.5194/nhess-17-1003-2017

Johnson, D., Pattiaratchi, C., 2006. Boussinesq modelling of transient rip currents. Coast. Eng. 53, 419–439. https://doi.org/10.1016/J.COASTALENG.2005.11.005

Kirby, J.T., Derakhti, M., 2019. Short-crested wave breaking. Eur. J. Mech. - B/Fluids 73, 100–111. https://doi.org/10.1016/J.EUROMECHFLU.2017.11.001

Linares, Á., Wu, C.H., Bechle, A.J., Anderson, E.J., Kristovich, D.A.R., 2019. Unexpected rip currents induced by a meteotsunami. Sci. Rep. 9, 2105. https://doi.org/10.1038/s41598-019-38716-2

Liu, P.L.-F., Mei, C.C., 1976. Water motion on a beach in the presence of a breakwater: 2. Mean currents. J. Geophys. Res. 81, 3085–3094. https://doi.org/10.1029/jc081i018p03085

Long, J.W., Özkan-Haller, H.T., 2005. Offshore controls on nearshore rip currents 110. https://doi.org/10.1029/2005JC003018

Lushine, J.B., 1991. A Study of Rip Current Drownings and Related Weather Factors. NATL.

WEA. DIG 13--19.

MacMahan, J.H., Thornton, E.B., Reniers, A.J.H.M., 2006. Rip current review. Coast. Eng. 53, 191–208.

Matthews, B., Andronaco, R., Adams, A., 2014. Warning signs at beaches: Do they work? Saf. Sci. 62, 312–318. https://doi.org/10.1016/J.SSCI.2013.09.003

Meadows, G., Purcell, H., Guenther, D., Meadows, L., Kinnunen, R.E., Clark, G., 2011. Rip Currents in the Great Lakes: An Unfortunate Truth, in: Leatherman, S., Fletemeyer, J. (Eds.), Rip Currents: Beach Safety, Physical Oceanography, and Wave Modeling. CRC Press, pp. 199–214.

Moulton, M., Elgar, S., Raubenheimer, B., Warner, J.C., Kumar, N., 2017. Rip currents and alongshore flows in single channels dredged in the surf zone. J. Geophys. Res. Ocean. 122, 3799–3816. https://doi.org/10.1002/2016JC012222

Murray, T., Cartwright, N., Tomlinson, R., 2013. Video-imaging of transient rip currents on the Gold Coast open beaches. J. Coast. Res. 165, 1809–1814. https://doi.org/10.2112/SI65-306.1

Özkan-Haller, H.T., Kirby, J.T., 1999. Nonlinear evolution of shear instabilities of the longshore current: A comparison of observations and computations. J. Geophys. Res. Ocean. 104, 25953–25984. https://doi.org/10.1029/1999JC900104

Pattiaratchi, C., Olsson, D., Hetzel, Y., Lowe, R., 2009. Wave-driven circulation patterns in the lee of groynes. Cont. Shelf Res. 29, 1961–1974. https://doi.org/10.1016/j.csr.2009.04.011

Sasaki, T.O., Horikawa, K., 1978. Observation of Nearshore Current and Edge Waves, in: Coastal Engineering 1978. American Society of Civil Engineers, New York, NY, pp. 791–809. https://doi.org/10.1061/9780872621909.047

Schomberg, J., 2009. Rip Currents: A Survey of Beach Users.

Scott, T., Austin, M., Masselink, G., Russell, P., 2016. Dynamics of rip currents associated with groynes — field measurements, modelling and implications for beach safety. Coast. Eng. 107, 53–69. https://doi.org/10.1016/J.COASTALENG.2015.09.013

Sherker, S., Williamson, A., Hatfield, J., Brander, R., Hayen, A., 2010. Beachgoers' beliefs and behaviours in relation to beach flags and rip currents. Accid. Anal. Prev. 42, 1785–1804. https://doi.org/10.1016/J.AAP.2010.04.020

Shi, F., Svendsen, I.A., Kirby, J.T., Smith, J.M.K., McKee Smith, J., 2003. A curvilinear version of a quasi-3D nearshore circulation model. Coast. Eng. 49, 99–124. https://doi.org/10.1016/S0378-3839(03)00049-8

Short, A.D., Hogan, C.L., 1994. Rip Currents and Beach Hazards: Their Impact on Public Safety and Implications for Coastal Management. J. Coast. Res. 197–209.

Summary of Natural Hazard Statistics for 2018 in the United States, 2018.

Symonds, G., Ranasinghe, R., 2001. On the Formation of Rip Currents on a Plane Beach, in: Coastal Engineering 2000. American Society of Civil Engineers, Reston, VA, pp. 468–481. https://doi.org/10.1061/40549(276)37

Voulgaris, G., Kumar, N., Warner, J.C., 2011. Methodology for prediction of rip currents using a three-dimensional numerical, coupled, wave current model, in: Leatherman, S., Fletemeyer, J. (Eds.), Rip Currents: Beach Safety, Physical Oceanography, and Wave Modeling. CRC Press, pp. 107–124.

White, K.M., Hyde, M.K., 2010. Swimming between the flags: A preliminary exploration of the influences on Australians' intentions to swim between the flags at patrolled beaches. Accid. Anal. Prev. 42, 1831–1838. https://doi.org/10.1016/J.AAP.2010.05.004

Wind, H.G., Vreugdenhil, C.B., 1986. Rip-current generation near structures. J. Fluid Mech. 171,

459. https://doi.org/10.1017/S0022112086001520

2. Lifeguarding Operational Camera Kiosk System (LOCKS) for Flash Rip Warning: Development and Application

The following has been published at *Coastal Engineering*

Liu, Y., Wu, C.H., 2019. Lifeguarding Operational Camera Kiosk System (LOCKS) for flash rip warning: Development and application. Coast. Eng. 152, 103537. https://doi.org/10.1016/j.coastaleng.2019.103537

2.1 Introduction

Flash rips, or known as transient rips, are rip currents that appear at featureless beaches (Castelle et al., 2016). Bathymetrically-controlled rip currents (Dalrymple et al., 2011), in contrast, are usually associated with morphological features including deeper channels between submerged sandbars (Reniers et al., 2006; Winter et al., 2014), offshore transverse ridges (Houser et al., 2011), sorted bedforms (Coco et al., 2007), and submarine canyon outside of surf zones (Long and Özkan-Haller, 2005). Different from stationary boundary-controlled rip currents at locations near natural headlands and anthropogenic structures (Castelle and Coco, 2013; Scott et al., 2016; Silva et al., 2010), flash rips, induced by shear instability of longshore currents (Özkan-Haller and Kirby, 1999) or migrating surfzone eddies (Feddersen, 2014), intermittently appear at nonstationary locations (Dalrymple et al., 2011). Intermittency in flash rips can be also caused by meteorologically-induced water level oscillations (MIWLO) in the Great Lakes (Linares et al., 2019; Meadows et al., 2011). Due to the nature of unpredictability, flash rips are hazardous to swimmers by unexpectedly sweeping people away from the surf zone to deeper water to cause drowning (Castelle et al., 2016; Dalrymple et al., 2011; MacMahan et al., 2006). Fatalities due to rip currents were reported globally (Gensini and Ashley, 2010). In the United States, an annual average was 58 fatalities based on incident statistics of 2008 – 2018 (National Weather Service,

2018). In the Great Lakes, a total of 185 fatalities and 591 incidents during 2002 – 2018 were recorded (Great Lake Current Incident Database, 2018). Overall, flash rips are intermittency and nonstationary at featureless beaches, imposing hidden hazards and high risks to beach users.

Warnings for rip currents to notify beach users about dangerous water conditions (Matthews et al., 2014) can influence people's decisions of entering water (White and Hyde, 2010). For example, warning signage for rip currents as part of the "Break the Grip of the Rip!" campaign has been widely used at beaches (Brannstrom et al., 2015). Static signage for rip current warning is proven valuable for escape strategy education. Studies find that sometimes people may not be fully aware of the hazards and disasters (Houser et al., 2017). One possible reason is that the static signage is less eye-catching. Another possible cause is that users may not able to correctly recognize the actual hazardous conditions based upon schematic illustrations on the signage (Brannstrom et al., 2015). Dynamic flags for rip current warning are thereby used by beach patrols, lifeguards, and local law enforcement officials (Brander and MacMahan, 2011; Sherker et al., 2010; White and Hyde, 2010). While the flag system has been found effective (Brannstrom et al., 2015), timely placing flags at unpatrolled beaches during rapid moving storm conditions can be challenging (Houser et al., 2017). Continuous efforts have been called for effectively issuing rip current warning, which requires reliably assessing occurrences of intermittent and nonstationary flash rips.

In the past, assessing flash rip occurrences have been conducted in several ways. First, proxies or environmental factors including wave climates, wind conditions, tidal elevations, or morphological status have been statistically correlated with or empirically related to rip current occurrences. For example, there are several rip current assessing tools like the Lushine Rip Currents scale (LURCS, Lushine, 1991), the East-Central Florida beaches scale (e.g. ECFL

LURCS, Engle, 2003; Lascody, 1998; Schrader, 2004), and the Great Lakes Rip Current Checklist (GLRCC, Meadows et al., 2011). This type of assessing tools is efficient but requires site specific data and uncertainty evaluation. Second, in-situ sensors such as acoustic Doppler velocimeters or current profilers at fixed locations (Clark et al., 2010; Johnson and Pattiaratchi, 2004) can measure offshore-directed rip currents. Dense arrays of sensors at fixed locations would be required due to non-stationarity nature of flash rips (Haus, 2011). Lagrangian drifters have been employed for tracking flash rips in the surf zone (Castelle et al., 2014; Johnson and Pattiaratchi, 2004; Scott et al., 2018). Nevertheless, use of in-situ sensors to reveal flash rips can be expensive and not practical. Third, trained lifeguards often identify presences of flash rips as sediment- or bubble-laden water jets based on visual clues of water color differences and patterns of wave breaking in surf zone (Dalrymple et al., 2011; Floćh et al., 2018; Leatherman and Leatherman, 2017). Observations by trained lifeguards are limited to patrolled beaches, which are infeasible to achieve in all beaches. Last but not least, remote sensors like optical cameras can provide long-term observations with large field of view and required spatial-temporal resolutions (Holman et al., 2006). For example, the well-known ARGUS (Holman and Stanley, 2007), the SIRENA (Nieto et al., 2010), and COSMOS (Taborda and Silva, 2012) have been used in monitoring rip currents (Orzech et al., 2011; Radermacher et al., 2018). Studies by Murray et al. (2013) and Floćh et al. (2018) showed that flash rips can be potentially detected based on color thresholds for rip-induced sediment plumes. To date, reliably and practically assessing the likelihood of hazardous flash rips remains a challenging research topic.

In recent years, cyberinfrastructure technology has greatly advanced to serve as an automated tool for rip current information (Alvarez-Ellacuria et al., 2009; Arun Kumar and Prasad, 2014; Voulgaris et al., 2011). For example, a Rip Risk Prediction Tool has been used to provide

the hazard level of bathymetry-controlled rip currents based on forecasted flow speeds and patterns through a coupled wave and circulation model (Austin et al., 2012). Based upon the wave forecast models with the spatial resolutions >2 km on the Great Lakes (Alves et al., 2014), outlooks with three tiers of high, moderate, and low risks have been used to issue daily rip current warnings on the regional scale (https://www.weather.gov/safety/ripcurrent-forecasts) by the National Weather Service (NWS). Recently, a statistical model of rip current likelihood maps (Dusek and Seim, 2013), based on forecasts outputs of the higher resolution (~500 m) Nearshore Wave Prediction System (NWPS, van der Westhuysen, 2013) have been developed and validated on the U.S ocean coasts, but not yet for the Great Lakes (Churma and Churma, 2017; Moulton et al., 2017). While continuous advancements of rip current cyberinfrastructures have been made, no system with the capability of assessing the likelihood of hazardous flash rips and providing timely warnings of intermittent and nonstationary flash rips have been developed and implemented, as far as the authors are aware.

The objective of this paper is to develop and implement a Lifeguarding Operational Camera Kiosk System (LOCKS) to characterize flash rips and provide timely warnings in Lake Michigan. The LOCKS has three components. First, a Real Time Environmental Observation System is designed and deployed to capture whole beach views and measure nearshore waves and local wind conditions. Second, an Integrated Nowcast Forecast Operational System, a high performance and distributed computing platform, is used to process acquired data and assess likelihood of flash rip occurrences. Lastly, a Beach Lights and Notifying Kiosk is designed and built at the study site to deliver real-time warnings to beach users. The paper is structured as follows. The study site is described in Section 2. Section 3 details the methods including the hardware and software of the real time observation system, the computing infrastructure and data processing algorithms, and the

development and implementation of the kiosk and dynamic beach lights. Section 4 shows results of flash rip characteristics obtained by the LOCKS at the study site. In Section 5, possible mechanisms of flash rips, applications of the LOCKS for different types of rip currents, and public communications are discussed. Finally, summary and conclusions are given in Section 6.

2.2 Site Description

The study site is the North Beach at the City of Port Washington, Wisconsin, located on the western shore of Lake Michigan (see Fig. 2-1). The beach shoreline forms a 30-degree angle clockwise from the North. The surf zone is approximated 60 m wide away from the shoreline with a mean bottom slope of 0.04. The beach is exposed to northeast and southwest dominated winds with a mean significant wave height of 0.61 m and a mean peak wave period of 4.0 sec (WIS-USACE, 1979 – 2014). Each year the beach opens from 6 AM to 10 PM daily. Visitors and recreational water users enter the beach from two routes, as shown in the yellow dotted lines in Fig. 2-1. One route, denoted as R1, is the lakeshore path starting from the south end of the Waste Water Treatment Plant (WWTP). The other route, denoted as R2, is the staircase path that links to the Upper Lake Park. Like many beaches in the Great Lakes, there are no lifeguards at the North Beach. Over the last several years, eight drownings and more than ten rescue incidents have been reported (GLCID, 2018; Great Lakes Surf Rescue Project, 2018). Specifically, unexpected fatalities occurred on September 2, 2012, March 16, 2016 and August 29, 2018, respectively.

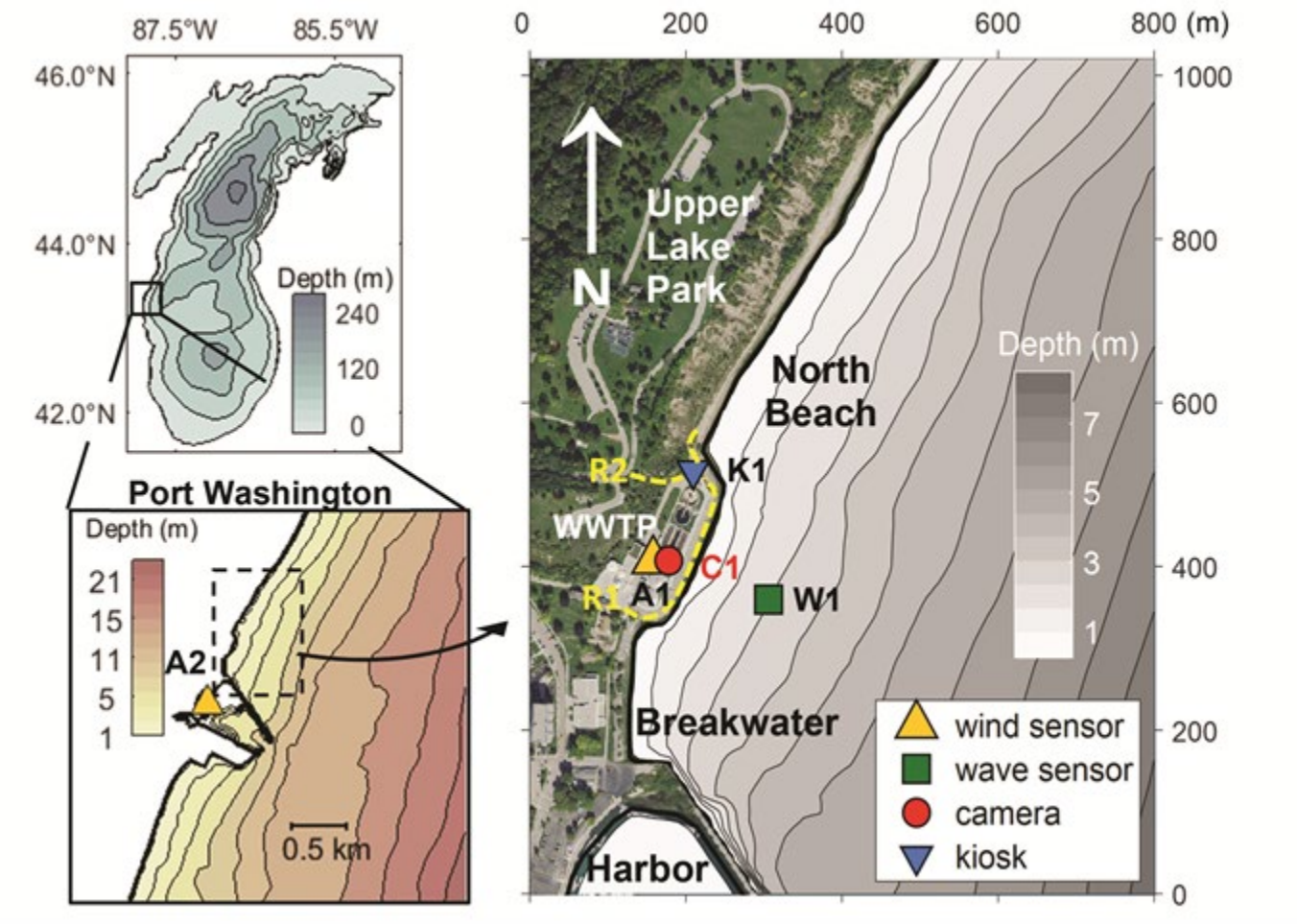

Fig. 2-1. The North Beach in Lake Michigan at Port Washington, WI. The two zoom-in map view show locations of two wind sensors A1 and A2 (orange triangle), a wave sensor W1 (green square), an Ethernet camera C1 (red dot), and a kiosk K1 (blue flipped triangle). Two routes to access the North Beach are shown in yellow dotted lines. Bathymetry are represented by the depth contours and color bars.

2.3 Methods

2.3.1. Real Time Environmental Observation System (RTEOS)

Data acquisition including nearshore water surface images, wind conditions, and wave climates are achieved by the RTEOS with an Ethernet camera, a wind sentry, and a wave sensor, respectively. Fig. 2-2 shows the RTEOS components. For acquiring images, a MOBOTIX S15

Ethernet camera (see C1 in Fig. 2-1) is mounted on a 2-meter galvanized steel pole at a building rooftop, at approximately 30 meters above the ground and 120 meters from the North Beach entrance. A 7.9 mm focal lens with a 45° x 34° field of view with a CMOS sensor captures the whole view of the North Beach from an oblique view. Live streaming of nearshore water is provided in continuous 1 MP videos at 2 HZ. High-resolution 6 MP images are sampled every 5 seconds. Fig. 2-2 shows a sample image, in which a region of interest (ROI) bounded by white solid lines. Uninterrupted power and continuous Internet are provided through a Power-Over-Ethernet (POE) switch in the WWTP building. For acquiring wind conditions, the wind sentry (see A1 in Fig. 2-1), a RM Young model (#03001) with a three-cup anemometer and a wind vane, is mounted on the same pole (see Fig. 2-2). Wind speeds and directions are sampled at 2 HZ with a 1-min average through a Campbell Scientific CR800 data logger. For acquiring wave climates, an Echologger ECT400 hydro-acoustic sounder (see W1 in Fig. 2-1) on an aluminum tripod frame, deployed at a water depth of approximately 3.1 meters and at 70 meters from the shore, is connected by a RS485-based protocol cable to the data logger. Wave displacements were sampled at 5 HZ and water temperatures were sampled on a 1-minute interval. The ECT400 sensor, different from the permanently installed IP camera and wind sentry, is deployed and retrieved between early June and late August for the swimming season. In addition to environmental data acquired by the RTEOS, wind data on a 10-min interval are available through a NOAA meteorological station PWAW3 inside the Port Washington Harbor (see A2 in Fig. 2-1).

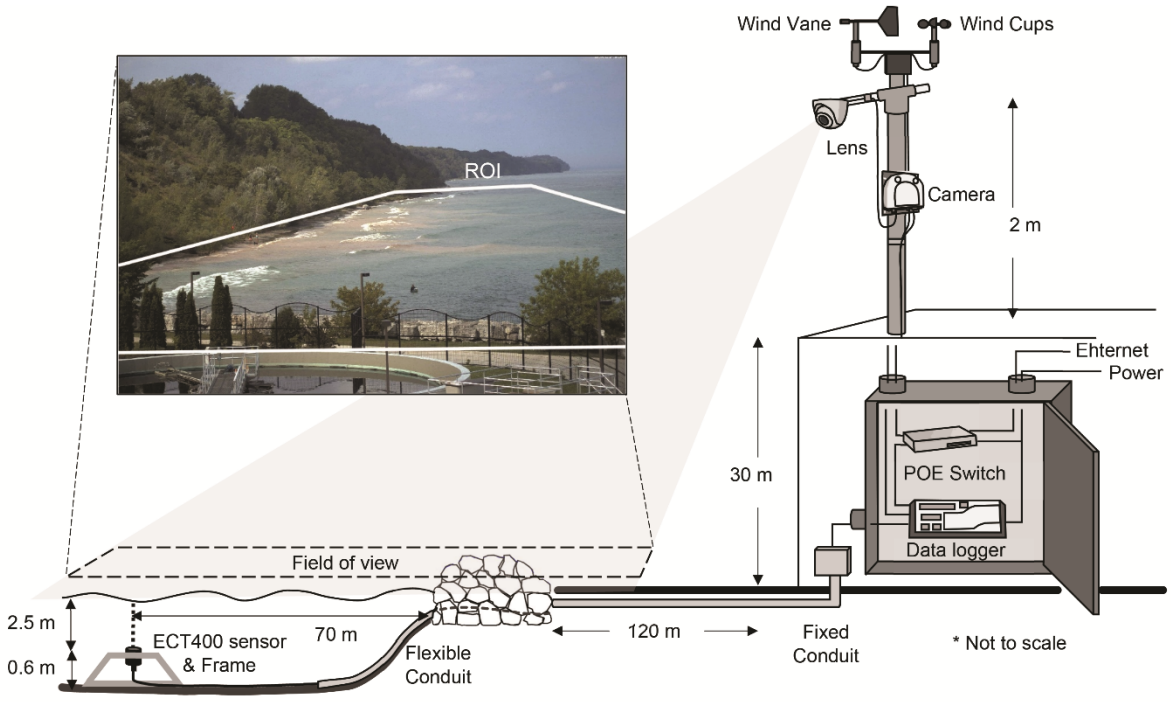

Fig. 2-2. The Real Time Environmental Observation System (RTEOS) consists of an Ethernet camera, a wind sentry on the rooftop, and an ECT 400 wave sensor deployed underwater connected to a data logger and a PoE switch for power and data transfer. The embedded image, a snapshot acquired at 2017/07/12 16:24 PM, shows flash rip-induced sediment plumes within a region of interest (ROI) defined by white solid lines.

2.3.2. Integrated Nowcast Forecast Operational System (INFOS)

2.3.2.1. Computing infrastructure

General description of the INFOS is described here while the details of INFOS cyberinfrastructure can refer to Reimer and Wu (2016) and Anderson and Wu (2018). Fig. 2-3a shows the three components of computing infrastructure of INFOS: a locally-based High-Performance Computing (HPC) cluster, a cloud-based distributed HPC grid, and a secure web server. The local HPC cluster, situated in the Coastal Sustainability and Environment Fluid Mechanics Lab at the University of Wisconsin – Madison, contains a master node and 128 computing nodes from eight AMD Phenom hex-core processors, a Gigabit Ethernet switch that

connects to the high-speed Internet provided by the UW College of Engineering Computer-Aided Engineering (CAE) network, and an Uninterrupted Power Supply (UPS) device for power backups. The distributed HPC has a submitting server at the Center for High Throughput Computing in UW-Madison and utilizes computing nodes on the Open Science Grid (OSG). The secure web server is hosted by the CAE stack system. To schedule automated processing, MATLAB scripts are written in the master node. Recorded image snapshots and other environmental data are distributed to the local HPC computing nodes for immediate processing while the 10-min video images are submitted to the distributed HPC grids on the waiting queue to available free nodes. After computations are completed, processed data is compiled in the master node and then uploaded onto the INFOS web server. Image processing and flash rip hazard likelihood assessment are described in the following two sub-sections.

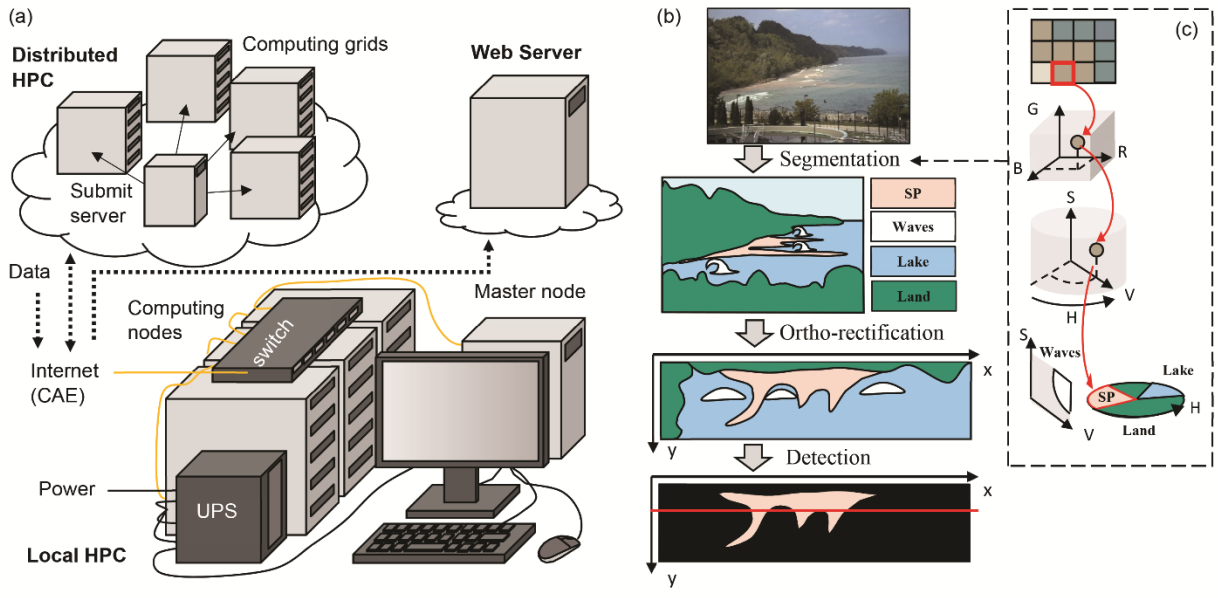

Fig. 2-3. (a) Computing infrastructure of the Integrated Nowcast Forecast Operation System (INFOS) consists of a local HPC, a distributed HPC, and a web server. (b) Three-step image processing of INFOS are segmentation, ortho-rectification, and flash rip detection. (c) In segmentation step, each pixel is transformed from RGB values to HSV values.

2.3.2.2. Image processing

Fig. 2-3b depicts the three-step image processing. In the first step, an image is segmented into regions of different morphological features - sediment plumes (SP), white-capping waves, the lake, and the land which includes trees, bluffs and other man-made structures. Note that pixels of same morphological features tend to have similar values in the Hue-Saturation-Value (*HSV*) space, which resembles closely human perceived colors. For instances, sediment plumes have hues generally less than 1/6 and values greater than 0.5 while white-capped breaking waves have high Saturations and Values $\sqrt{S^2 + V^2} > 0.8$ (Floćh et al., 2018). Therefore, we transform images of the Red-Green-Blue (*RGB*) color space (a Cartesian coordinate system) into those of the HSV space (a cylindrical coordinate system), as shown in Fig. 2-3c. A k-means clustering method is then applied so pixels are partitioned into k segments. Afterwards, segments are identified as sediment plumes based on the HSV values of the segment centroids. At last, morphological operations by removing connected regions and small scatter pixels are performed so that flash rip features are represented.

In the second step, ortho-rectification, which transforms original oblique images into orthophotos with geo-referenced coordinates, is executed. A pin-hole camera model is assumed to describes the 2D image coordinates (x, y) in relation to 3D world coordinates (X, Y, Z) using the Direct Linear Transform (DLT) equations (Holland et al., 1997)

$$x - x_o = -f\left[\frac{m_{11}(X-X_c)+m_{11}(Y-Y_c)+m_{13}(Z-Z_c)}{m_{31}(X-X_c)+m_{31}(Y-Y_c)+m_{33}(Z-Z_c)}\right] \quad (1a)$$

$$y - y_o = -f\left[\frac{m_{21}(X-X_c)+m_{21}(Y-Y_c)+m_{23}(Z-Z_c)}{m_{31}(X-X_c)+m_{31}(Y-Y_c)+m_{33}(Z-Z_c)}\right] \quad (1b)$$

where (x_o, y_o) is the image center, (X_c, Y_c, Z_c) is the camera center, m_{ij} represents a 3 by 3 rotation matrix for the lens orientation angles, α (azimuth), τ (tilt), θ (swing), and f is the focal lens. The

interior parameters (x_o, y_o) and f were calibrated using a checkerboard before the camera was installed at the study site. The exterior parameters (X_c, Y_c, Z_c) and (α, τ, θ) were calibrated (Wanek and Wu, 2006) by using 42 ground control points (GCP) surveyed with a Nikon Nivo C Series Reflector-less Total Station. Based on the DLT equations, the georeferenced (X, Y) coordinates corresponding to the image pixels (x,y) are solved by approximating a mean lake level elevation Z (Bechle et al., 2012). The orthophoto is then obtained by interpolating pixel colors for a 2D grid in world coordinates (Bechle and Wu, 2011). Fig. 2-3b shows that orthophotos contain geometric dimensions of segmented SPs, thus providing additional information to identify flash rips.

In the third step, detection of flash rips is achieved by meeting the two criteria: (i) a segment is identified as sediment plumes (see the pink region in Fig. 2-3b) and (ii) the offshore length of the sediment plume segment is greater than a threshold (see the red line in Fig. 2-3b). The threshold is determined by minimizing the number of discrepancies by comparing with the occurrence of flash rips perceived by human eye visualizations.

2.3.2.3. Flash rip hazard likelihood assessment

In this study, we assess possible occurrences of flash rips using both site-specific environmental data and image detection. Table 2-1 shows the Flash Rip Occurrence Checklist (FROC), adapted from the Great Lakes Rip Current Checklist (GLRCC) previously used by the NOAA NWS Great Lakes offices (Meadows et al., 2011). There are seven factors in the FROC. Four environmental factors, wind speed (U_w) in m/s, wind direction (Dir_w) in degrees (zero degree means that wind comes from the true North), nearshore significant wave height (H_s) in meter, and peak wave period (T_p) in sec, are based on local and nearshore observations, different from those based upon offshore forecasts in the GLRCC. Specific criteria of the four factors in the FROC are

wind speed U_w > 4.5 m/s (equivalent to 10 mph), southwestern wind direction ($|Dir_w - 225| < 45°$) or significant direction shift ($\Delta Dir_w > 15°$ within 10 minutes), and nearshore wave condition (H_s > 0.46 m (equivalent to 1.5 ft) and T_p > 3 sec). In addition, the fifth environmental factor is the lake level change (ΔLL) referenced to the lake-wide monthly average water level of the 1985 International Great Lakes Datum (IGLD) reported in the Great Lakes Dashboard Project (Smith et al., 2016), which accounts for the effect of oscillating water levels on rip current occurrences in the closed-basin environment of the Great Lakes (Meadows et al., 2011), with the criteria LL < -0.15 m (equivalent to -6 in), which is modified from those used in the GLRCC. To specifically account for the occurrence of flash rips, two new factors are added in the FROC. A storm factor considers the effects of moving storm that has crossed the Lake Michigan up to 12 hours ahead. A visual observation factor accounts for detected flash rips based on sediment plumes described in previous section. To assess the possible occurrences of hazardous flash rips, each factor is assigned with a pre-calibrated likelihood contribution in percentages, as shown in Table 2-1. The total likelihood (TL) of hazardous flash rips is assessed in three tiers of risk: low (L) for TL < 40%, moderate (M) for 40% ≤ TL < 70%, and high (H) for TL ≥70%. At the L risk level, flash rips are unlikely to occur and people are safe to enter the water. At the M risk level, life-threatening flash rips are possible to occur and people are not encouraged to enter the water. At the H risk level, devastating flash rips are likely to be present and people should not enter the water.

Table 2-1. Flash Rip Occurrence Checklist (FROC)

Factors	Criteria	Likelihood
U_w	$U_w > 4.5$ m/s (10 mph)	15 %
Dir_w	$\|Dir_w - 225\| < 45°$ or $\Delta Dir_w > 15°$	15 %
H_s	$H_s > 0.46$ m (1.5 ft)	15 %
T_p	$T_p > 3$ sec	5 %
Lake level change	> -0.15 m (6 in)	5 %
Storm	Occurred in past 12 hours	15 %
Visual	Flash rips identified	30 %

Likelihood	< 40 %	40 – 70 %	> 70 %
Tier	Low	Moderate	High

2.3.3. Beach Lights and Notifying Kiosk (BLINK)

To timely issue warnings to beach users, we design and implement a Beach Lights and Notifying Kiosk (BLINK) as shown in Fig. 2-4. The BLINK design is highlighted in three components. First, the communication unit is an Ubiquiti's NanoBrigde RF wireless disk bridge, installed on an aluminum pole to receive wireless signals boosted from nearby buildings. Second, the control unit, connected through a POE switch to the wireless bridge, is a Raspberry Pi 3B model housed in a 50 cm by 48 cm watertight enclosure with an anti-glare screen and cooling fans. We program in Python language to recursively execute the Raspbian shell CRON task scheduler and fetch the latest flash rip information from the INFOS web server. Third, the alerting unit consists of a sun-bright 19'' LCD monitor and three-color LED beacon lights. As shown in the specially designed "Rip Currents Safety Advisory" signage in Fig. 2-4, the LED light exhibits to the corresponding color of red, yellow or green, based on three tiers of likelihood for flash rip in high, moderate or low occurrence, respectively. The automatic selection is achieved by a circuit that wires MOSFETs (Metal-Oxide Semiconductor Field-Effect Transistors) to the General-Purpose Input Output (GPIO) utility pins of the Raspberry Pi to control the on-and-off of each LED beacon light. Simultaneously, the monitor displays an INFOS webpage for real-time flash rip information.

Fig. 2-4 shows that the BLINK is constructed at the entrance to the North Beach in City of Port Washington (see K1 in Fig. 2-1). The BLINK are placed to the location most visible to people from the both two routes. The LED beacon lights are mounted on at a height of approximately 7.6 meter above the ground to alert visitors before entering the beach. To ensure the information displayed on the monitor readable to both adults and children users, the enclosure is installed to a height of about 1.5 m above the ground. Reliable power is provided though the nearby street light

pole that connects to the City's street power system. With the established internet connectivity to the City's networks, the implementation can allow sustainable operations of the BLINK.

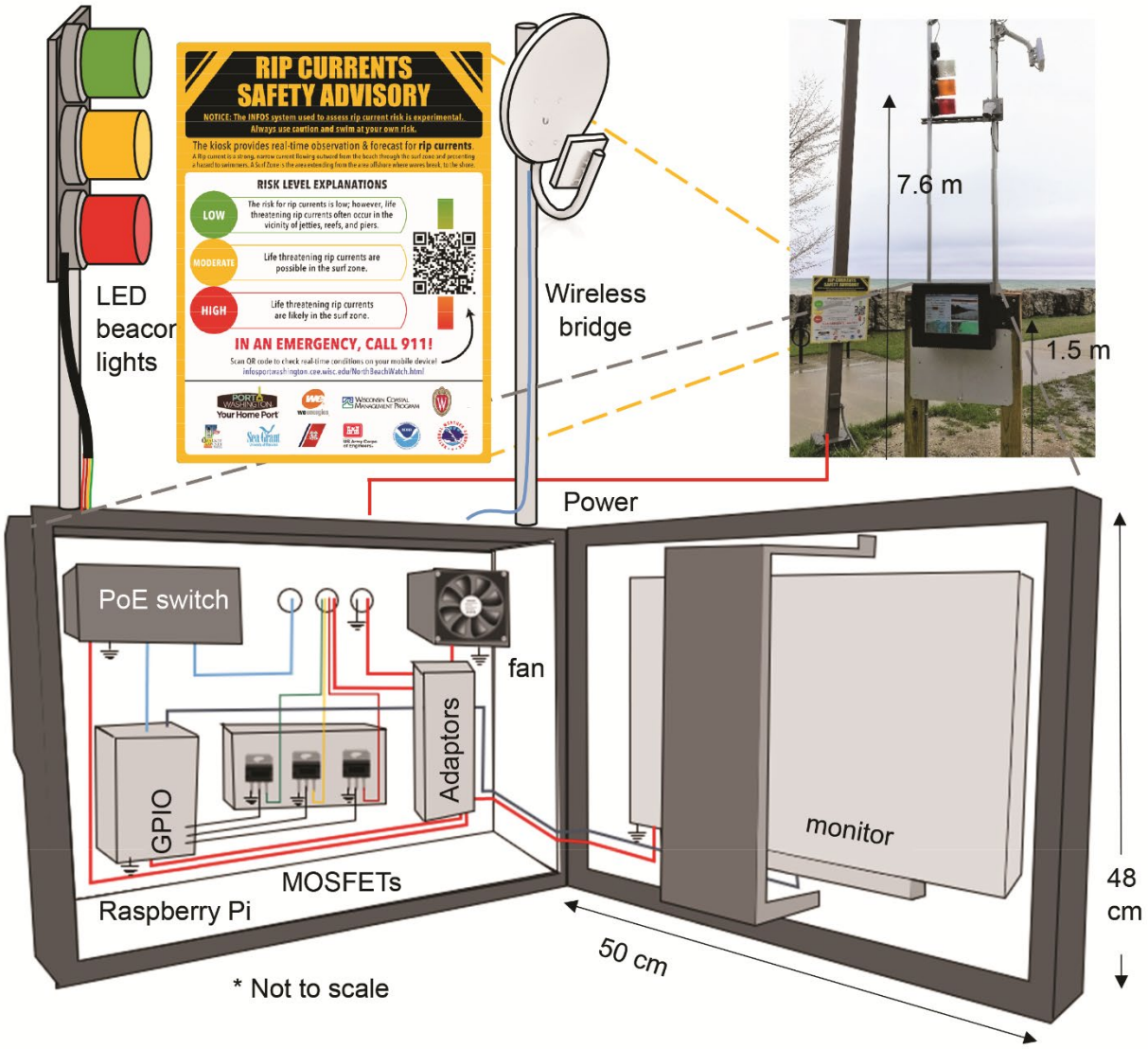

Fig. 2-4. Beach lights and Notifying Kiosk (BLINK) with three components: a communication unit consists of a wireless bridge; a control unit consists of a Raspberry Pi connected through a PoE to the wireless bridge, housed in the enclosure; and an alerting unit consists of a digital LCD monitor in the enclosure and a three-color LED beacon lights. A "Rip Current Safety Advisory" signage is attached to a light pole by the BLINK.

2.4 Results

2.4.1. Detection of Flash Rips

Detection of flash rips using different image processing methods are illustrated in three representative conditions: flash rip occurrences in a sunny day, those in a cloudy day, and no occurrence in a sunny day corresponding to the three images of 2017/07/12 16:24 PM, 2017/10/15 11:09 AM, and 2017/07/12 11:24 AM in Fig. 2-5 a1, a2, and a3, respectively. Results of flash rip detection by applying segmentation in the RGB color space (see Fig. 2-5b), segmentation in the HSV color space (see Fig. 2-5c), and an offshore length threshold of 15-m (represented as red solid lines) in addition to the HSV segmentation (see Fig. 2-5d), are compared. Note that the 15-m length threshold is equivalent to the wavelength of nearshore waves with period of 4 seconds at a water depth of 2 meters in the surf zone at the study site, thus wave-induced sediments can be distinguished from being detected as flash rips. For flash rips in the sunny day (see the first column of Fig. 2-5), all three methods successfully detect flash rip-induced sediment plumes (Fig. 2-5b1, 2-5c1, and 2-5d1). Nevertheless, for flash rips in the cloudy day (see the second column of Fig. 2-5), the RGB-based segmentation fails in detecting flash rips (Fig. 2-5b2) since the colors of the sediment plume region appear similar to those of the lake water under low ambient lights. The HSV-based segmentation only (Fig. 2-5c2) and the combined length threshold and HSV segmentation (Fig. 2-5d2) both effectively detect flash rip-induced sediment plumes, demonstrating the advantage of using HSV colors under the low-light cloudy condition. For no flash rips in the sunny day (see the third column in Fig. 2-5), both the RGB-based (Fig. 2-5b3) and the HSV-based segmentation (Fig. 2-5c3) detect breaking-induced detached sediments which have similar color characteristics as those of flash-rip induced sediment plumes. The combined length threshold and HSV-based segmentation (Fig. 2-5c3) can check if the sediment plumes have an

elongated shape caused by flash rips, yielding no false detection. In short, the RGB-based segmentation is capable of detecting flash rip in sunny days. The HSV-based segmentation can be used to detect flash rips in both sunny and cloudy days with low ambient lighting. By adding the length threshold, the false alarms of flash rips in sunny days can be avoided.

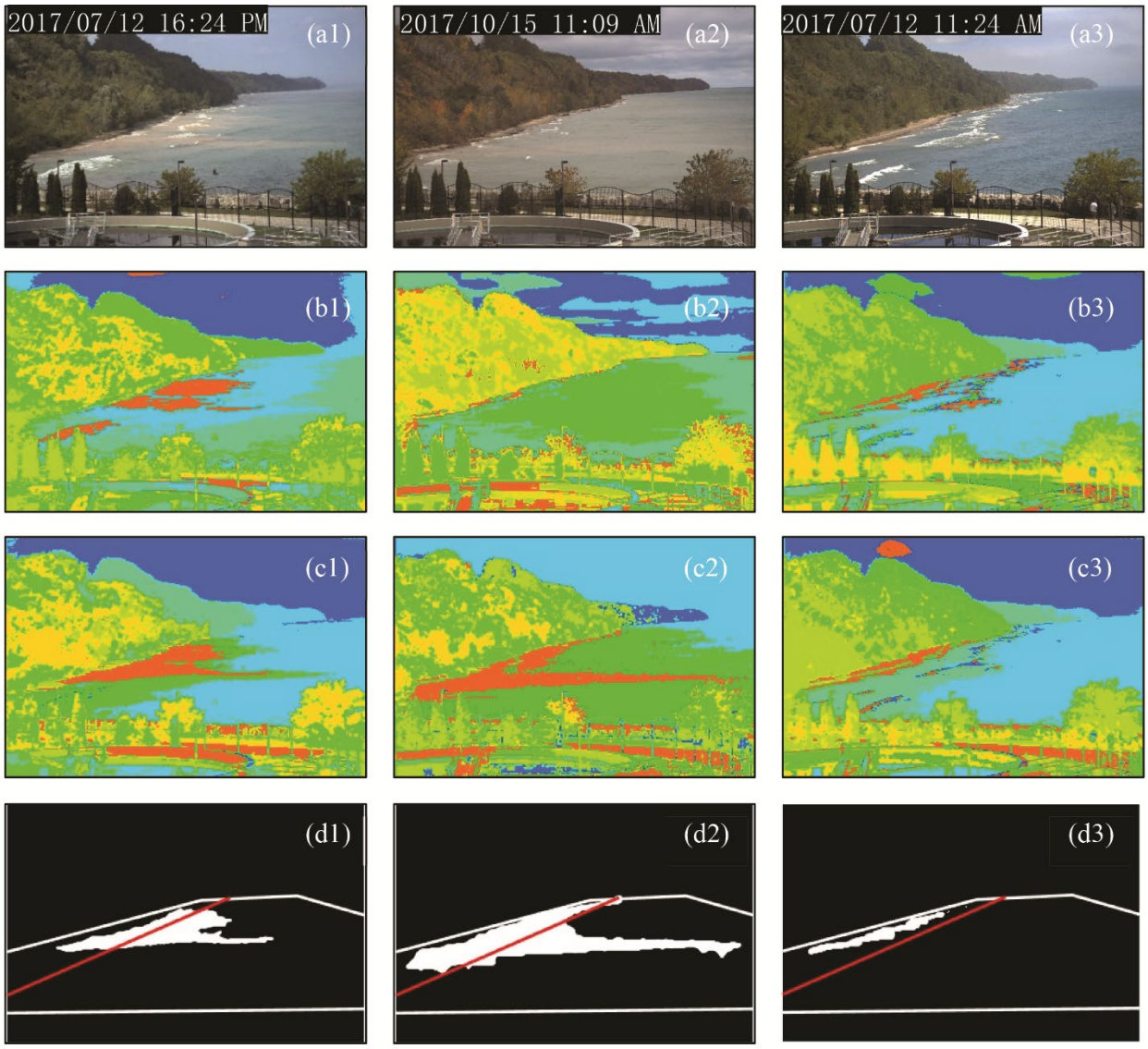

Fig. 2-5. Detection of flash rips under three representative conditions: (a1) flash rips in a sunny day at 16:24 PM, 2017/07/12; (a2) flash rips in a cloudy day at 11:09 AM, 2017/10/15; (a3) no flash rip in a sunny day at 11:24 AM, 2017/07/12 by using (b) RGB color space segmentation, (c) HSV color space segmentation, and (d) HSV color space segmentation and the length threshold (red solid lines) in ROI (white solid lines).

Statistics of flash rip detection using the three image processing methods are calculated and compared here. Table 2-2 shows the percentages of three outcomes: correct detection, false alarm, and miss. Correct detection is counted when the flash rip detection is in consistent with that viewed by human visual observation. False alarm is counted when flash rip is falsely identified in the image but not perceived by human eyes (e.g. Fig. 2-5b3 or 2-5c3). Miss is counted when flash rip is not detected in the image but are perceived by human eyes (e.g. Fig. 2-5b2). In the column of the correct detection, the RGB segmentation has a 55% accuracy compared to the greatly improved 75 % accuracy of the HSV segmentation. Adding the length threshold further improves the accuracy to 83%. In the column of false alarm, errors of the three methods show a similar trend. Particularly, adding the length threshold effectively reduces false alarm with the lowest percentage of 8%. In the column of miss, percentage errors for the three methods indicate the advantage of the HSV-based segmentation and the combined method to reliably detect flash rip under sunny and cloudy conditions. Overall, the statistics for flash rip detection using the RGB-based and the HSV-based segmentation methods in this study supports the previous results that flash rips can be detected based on color thresholds for rip-induced sediment plumes (Murray et al., 2013, Floćh et al., 2018). The combined length threshold and HSV segmentation method further improves flash rip detection, consistent to human eye observations. For general applications of the image-based method to other beaches, we suggest adjusting the length threshold based on local nearshore conditions including wave climates, beach slope and surf zone depth, and adjusting the number of clustering in the HSV-based segmentation by examining captured images for complexity of color features, average color tones of sediment plumes in water, and potential view obstructions from land or human structures.

Table 2-2. Statistics of flash rip detection

Outcome / Method	Correct detection	False alarm	Miss
RGB segmentation	55 %	32 %	13 %
HSV segmentation	75 %	16 %	9 %
Length threshold & HSV segmentation	83 %	8 %	9 %

2.4.2. Location of Flash Rips

Spatial occurrences of flash rips are nonstationary, as shown on the orthophotos in Fig. 2-6. Flash rip-induced sediment plumes occurred at various locations in the Region Of Interest (ROI) that spans 500 m in the longshore x direction and 50 m in the cross-shore y direction y (see Fig. 2-2). For instances, two flash rips (red arrows in Fig. 2-6a) occurred at x = 150 m and x = 200 m at 14:34 PM on July 12, 2017; three (see Fig. 2-6b) occurred at x = 125 m, x = 190 m and x = 250 m at 16:24 PM on the same day; and eight (see Fig 2-6c) occurred at multiple locations from x = 25 m to x = 400 m at 11:49 AM on August 3, 2017, indicating that the occurrence of flash rips were not fixed. For a total of 152 images with flash rip detected, the calculated occurrence frequency of flash rips with 5m x 5m spatial grid resolution over the ROI is shown in Fig. 2-6 (d). The frequency of occurrences in all cells within y < 25 m are larger than zero, indicating that flash rips occurred everywhere. Overall, several notes are drawn here. First, images recorded from the Ethernet camera can be effectively rectified through the INFOS image processing to reveal the locations of flash rip-induced sediment plumes. Second, occurrences of flash rips are ubiquitous but hotspots

of flash rips at the study site have been identified, at locations x = 120 m to x = 150 m and y = 20 m based on the highest probability of 48%. Third, the spacing between flash rips can range from 20 m to 60 m. Last but not least, flash rip-induced sediment plumes identified within the ROI can range from 10 m beyond the surf zone to a distance greater than 50m (equivalent to a length of a standard long course swimming pool) in Lake Michigan, comparable to 50 ~ 100 m reported in oceanic coastal areas (Floćh et al., 2018).

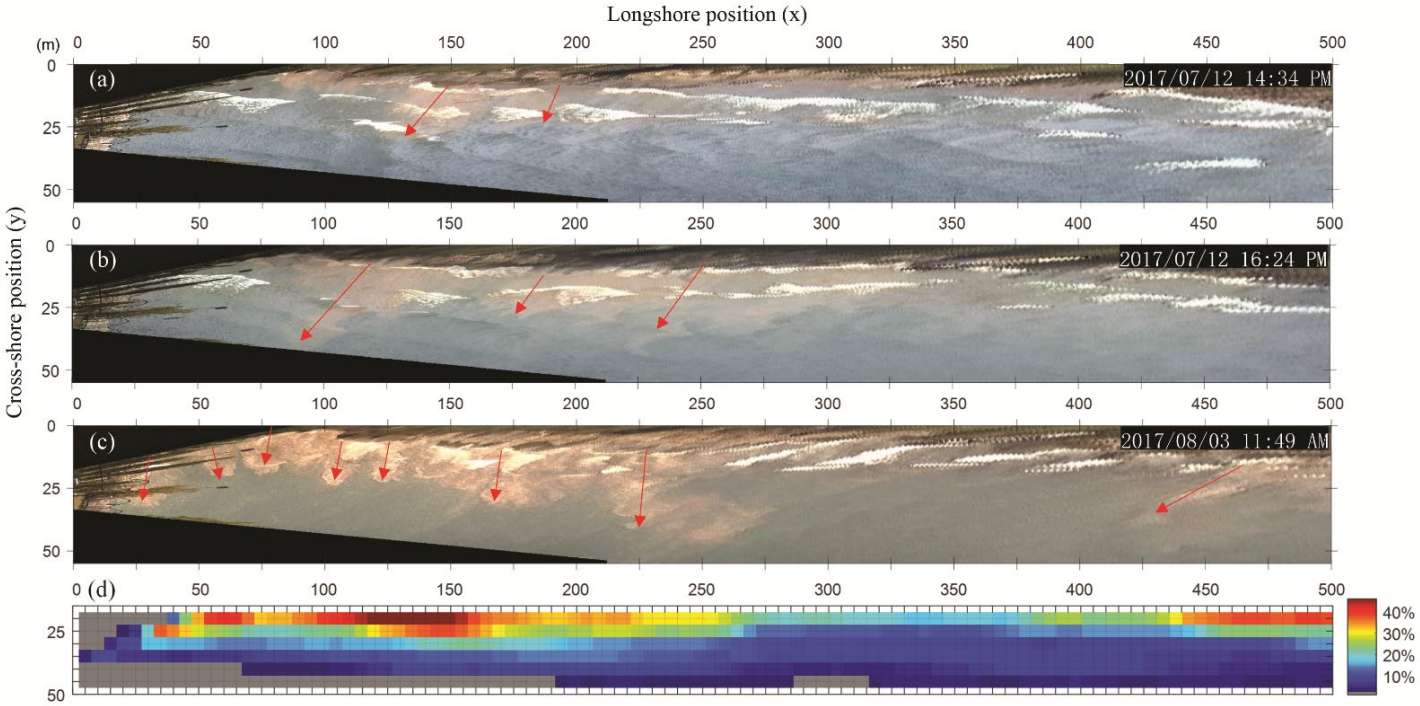

Fig. 2-6. Orthophotos for the ROI of images at (a) 14:34 PM on July 12, 2017, (b) 16:24 PM on July 12, 2017, and (c) 11:49 AM on August 3, 2017 with red arrows representing locations of flash rip-induced sediment plumes. (d) Frequency occurrence of flash rips at 5m by 5m spatial grid resolution spanning over the ROI.

2.4.3. Duration of Flash Rips

Intermittency of occurred flash rips are examined here. We calculate the durations (T) from the images acquired by the RTEOS. For example, flash rip-induced sediment plumes occurred at 14:17:04 PM on July 12, 2017 (Fig. 2-7a1) and were gone at 14:18:14 PM for a duration of 70-sec (Fig. 2-7a2). Another example shows that flash rips started at 16:44:04 PM (Fig. 7b1) and were no longer visible at 16:49:09 PM (see Fig. 2-7b2), yielding a duration of T = 305 seconds. Statistics of flash rip durations in Fig. 2-7c. Overall, several findings are noticed. First, the image acquisition protocol of the Ethernet camera shows the capability to capture the intermittent occurrences of flash rips. The durations of each flash rip can thereby be reliably obtained. Second, 65% of flash rips had the duration less than 2 minutes, comparable to the 60% oceanic flash rips reported by Floćh et al. (2018). Third, approximately 5 % of flash rips had the duration longer than 5 minutes. Fourth, the maximum, average, and minimum durations are found to be 345 seconds, 115 seconds, and 30 seconds, respectively, indicating that flash rips have a short-lifespan and decay after a few minutes. The statistics are consistent to those by Slattery (2010) and Murray et al. (2013). Last but not least, flash rips tend to occur on and off many times throughout the same day, suggesting that water users in Lake Michigan should be cautious about not only intermittency but also recurrence of flash rips.

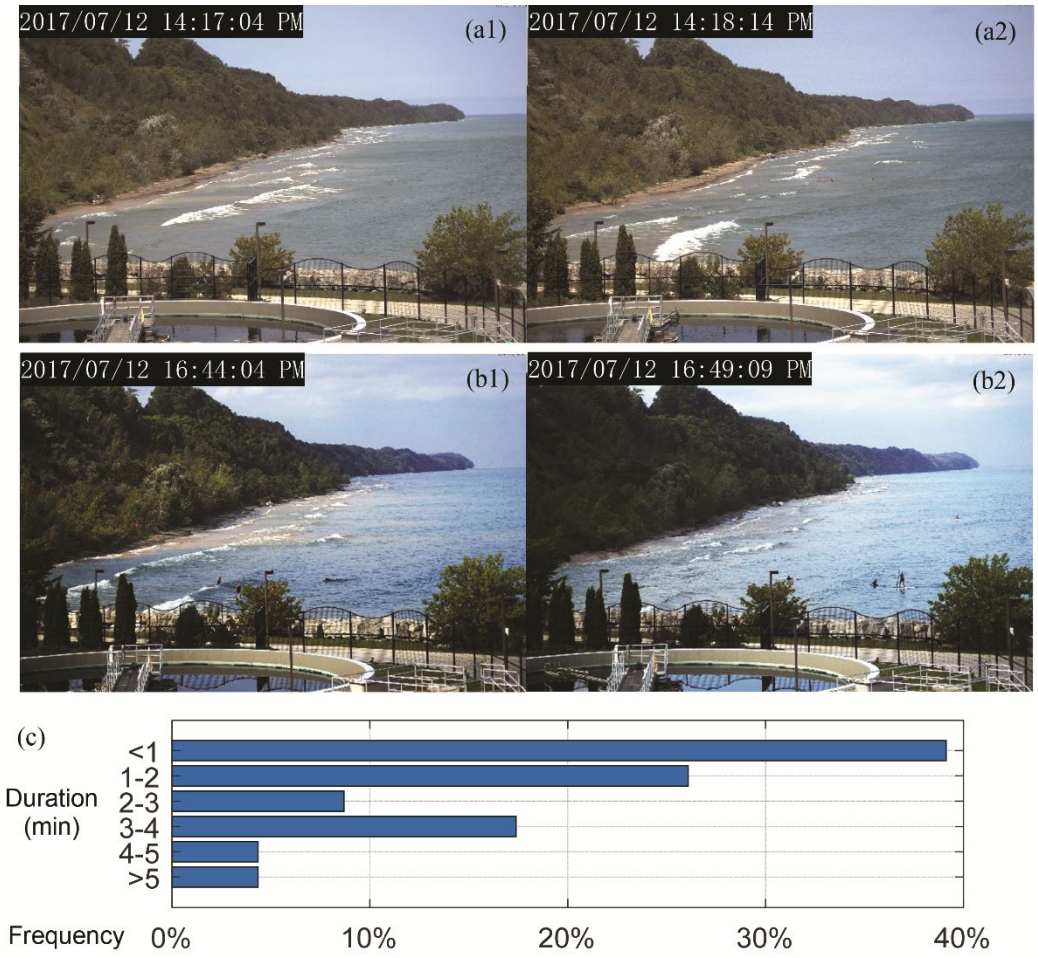

Fig. 2-7. Two examples of flash rips with (a) a short duration of $T = 70$ sec and (b) a long duration of $T = 305$ sec. (c) the frequency histogram of flash rip durations at a 1-minute bin interval.

2.4.4. Likelihood of Flash Rip Hazards

The likelihood of flash rip hazards is assessed based upon the FROC. For example, the time series of the total likelihood (*TL*) and the seven factors in the assessment matrix for July 12, 2017 event are plotted in Fig. 2-8. At 14:17 PM, a *H* risk tier of flash rip is assessed at 95 % total likelihood (*TL*) with 30 % contributed from the visual observation factor of flash rips identified in the image (Fig. 2-8b), 15 % from the storm factor (Fig. 2-8c), and 50 % from the four local environmental factors - wind speed U_w = 5.2 m/s (Fig. 2-8d) and direction from SW of $\mathrm{Dir_w}$ = 221° (Fig. 2-8c), significant wave height H_s = 0.61 m (Fig. 2-8e), wave period T_p = 5.0 sec (Fig. 2-8g), but no contribution from lake level change of < 0.15 m (Fig. 2-8h). At 16:44 PM, a *M* risk tier is assessed at 65 % *TL* with 30 % from the visual observation factor, 15 % from the storm factor, and 20 % from the wave factor (H_s = 0.64 m and T_p = 5.1 sec). Shortly after, at 16:49 PM, an *L* risk tier is assessed at 35% with 15 % from the storm factor and the 20 % from the wave factors (H_s = 0.55 m and T_p = 4.7 sec). The results of likelihood flash rip hazards (Fig. 2-8) assessed by the FROC are consistent to the human-eye observed occurrence from the events on July 12, 2017 (Fig. 2-7a1 and 7b1) and other days (not shown here for brevity) including at 11:09 AM on Oct 15, 2017 (Fig. 2-5a2) and at 11:40 AM on Aug 3, 2017 (Fig. 2-6c). Note that sediment plumes are used as visual observation factor for this study site, while applying this method to other beaches where sediment plumes may not be available, we suggest using other indicative visual signatures such as water foams and bubbles (Leatherman and Leatherman, 2017) and calibrating the checklist by adjusting the relative contribution percentage. Overall, the Flash Rip Occurrence Checklist provides a tool for reliably and practically assessing the likelihood of hazardous flash rips in Lake Michigan for the first time, as far as the authors are aware.

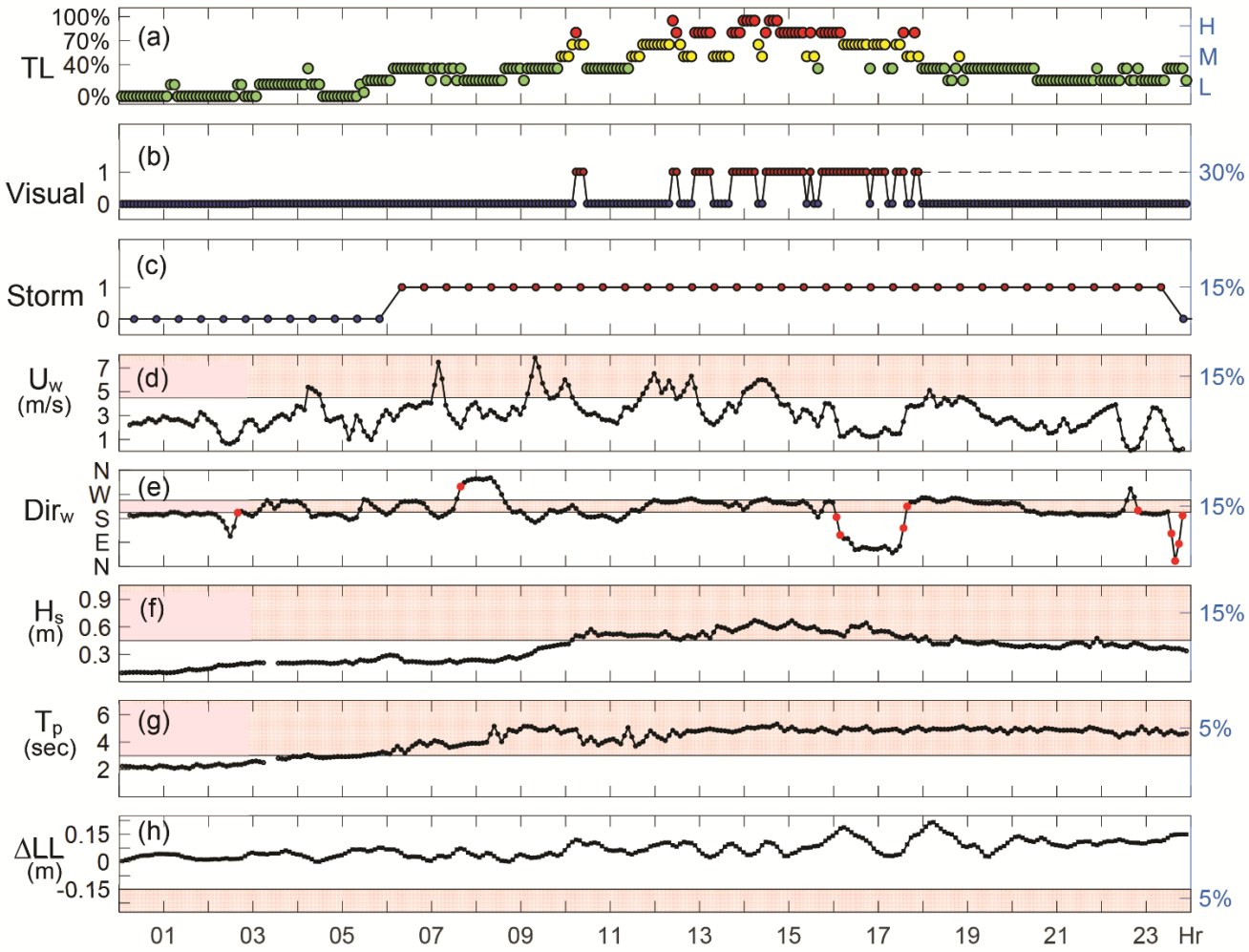

Fig. 2- 8. Likelihood of flash rip hazards on July 12, 2017: (a) total likelihood (TL) ranging from 0 to 100%, and the three tiers of risk in high (red), moderate (yellow), and low (green); (b) image observation factor, with 1 (red) for flash rips detected in the image and 0 (blue) otherwise; (c) storm factor, with 1 (red) for storm occurred in the past 12 hours and 0 (blue) otherwise; (d-h) five environmental factors: wind speed U_w, wind direction Dir_w, wave height H_s, wave period T_p, and lake level change ΔLL. Red shading represents criteria met and the red dots in (e) represent shifting wind criterion met. Percentage contributions of each factor are labeled on right side of axis.

2.4.5. Real-time Warning of Flash Rips

In this study, timely warnings of intermittent and nonstationary flash rips have been developed and implemented as the Beach Lights and Notifying Kiosk (BLINK). Specifically, at the entrance to the North Beach in City of Port Washington, the BLINK provides the real-time flash rip warning on the webpage (http://infosportwashington.cee.wisc.edu/Northbeachwatch1.html). Fig. 2-9 shows an example of flash rips at 14:29 PM on July 12, 2017. At the top of the page, the assessed flash rip risk is "HIGH" in bolded texts with the text color in red. If assessed risk is moderate or low level, bolded texts would accordingly be changed to yellow or green, respectively. Underneath, a table with detailed explanations about three tiers of risk of flash rips is provided. Wordings in the table are adapted from those used in rip current forecasts by the NOAA National Weather Service (https://www.weather.gov/safety/ripcurrent-forecasts). On the left is the real-time view of the North Beach from the RTEOS camera. A message that alerts users of watching out for sediment plumes is overlaid at the bottom of on the image. The text background and the image border are shown in red, yellow or green accordingly. At the page bottom left, a table summarizes the latest environmental conditions including wave height, period, wind speed and direction, and air temperature. At the bottom right, safety recommendations and the "flip, float and follow" escape strategy (Great Lakes Surf Rescue Project, 2018) in graphics are displayed. Overall, the BLINK provides a real-time flash rip warning with color that is consistent to that used in the dynamic flag system. In addition, text explanation, visual and environmental conditions, and safety recommendation allow beach users to learn about flash rip hazards and escape strategy. The real-time BLINK, based on outcomes of the reliable assessments of flash rip likelihood, provides a new approach for the first time to issue flash rip warnings to beach users effectively.

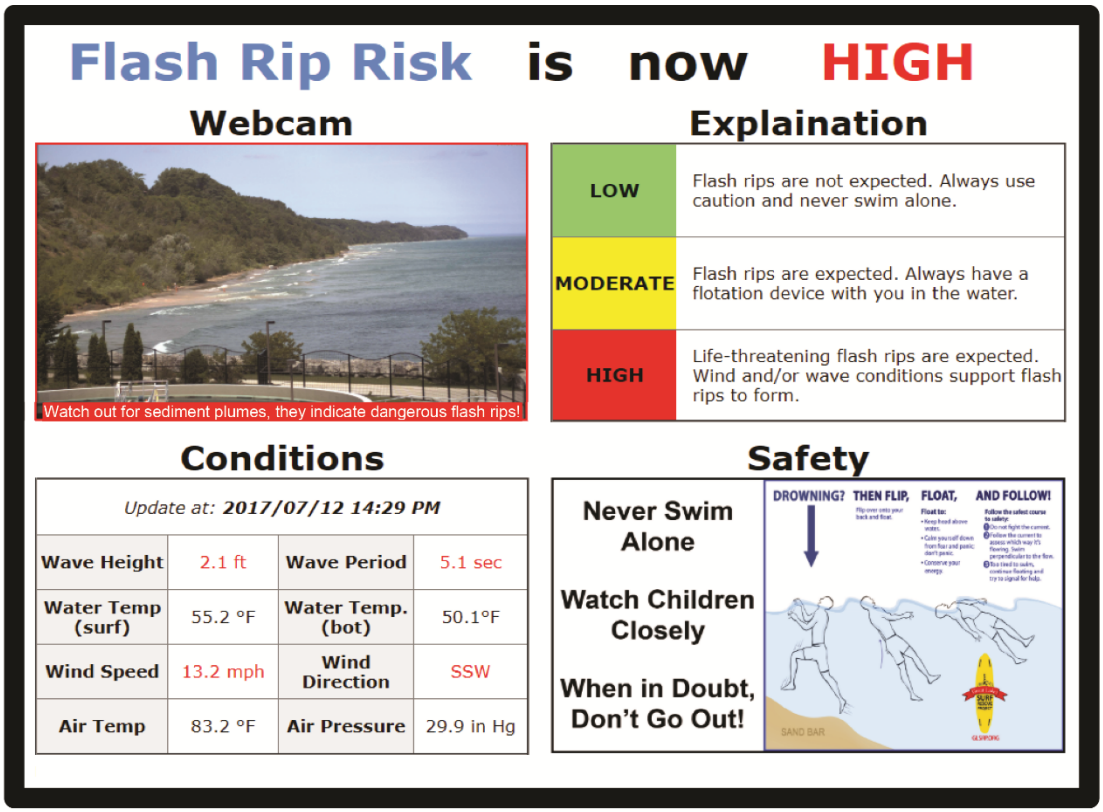

Fig. 2-9. Real-time display of the BLINK shows a high risk of flash rips at 14:29 PM on July 12, 2017. The display consists of a webcam view, a table for risk level explanation, a table for real-time environmental conditions, and safety advisory.

2.5 Discussion

2.5.1. Mechanisms for Flash Rips

Two mechanisms for generating flash rips have been reported in literature. First, shear instabilities of longshore currents (Castelle et al., 2016; Özkan-Haller and Kirby, 1999) under obliquely incident waves can generate unsteady vortices, resulting in locally strong and narrow offshore-directed out-bursting flows as transient and nonstationary rips (Castelle et al., 2014; Feddersen, 2014). Flash rips observed on Aug 3, 2017 (Fig. 2-10a) could possibly be caused by this mechanism as observed waves approached to shore at wave height of 0.67 m, wave period of 6.3 sec, and wave angle at approximately 20° (Fig. 2-10b). Second, alongshore variation of

vorticity caused by the passage of breaking and nonbreaking regions of short-crest waves under normal incident angle (Clark et al., 2012; Peregrine, 1998) can cascade into large-scale surf zone eddies (Feddersen, 2014; Spydell et al., 2009), leading to episodic and unpredictable bursts of water jetting offshore (Castelle et al., 2016; Johnson and Pattiaratchi, 2006). Flash rips observed on March 30, 2017 (Fig. 2-10c) could likely be related to this mechanism as the detected sediment plume (red arrow in Fig. 2-10d) is located right in the gap between of two wave crests, with a near-normal incidence and approximated wave height of 1.8 m and wave period of 7.1 sec.

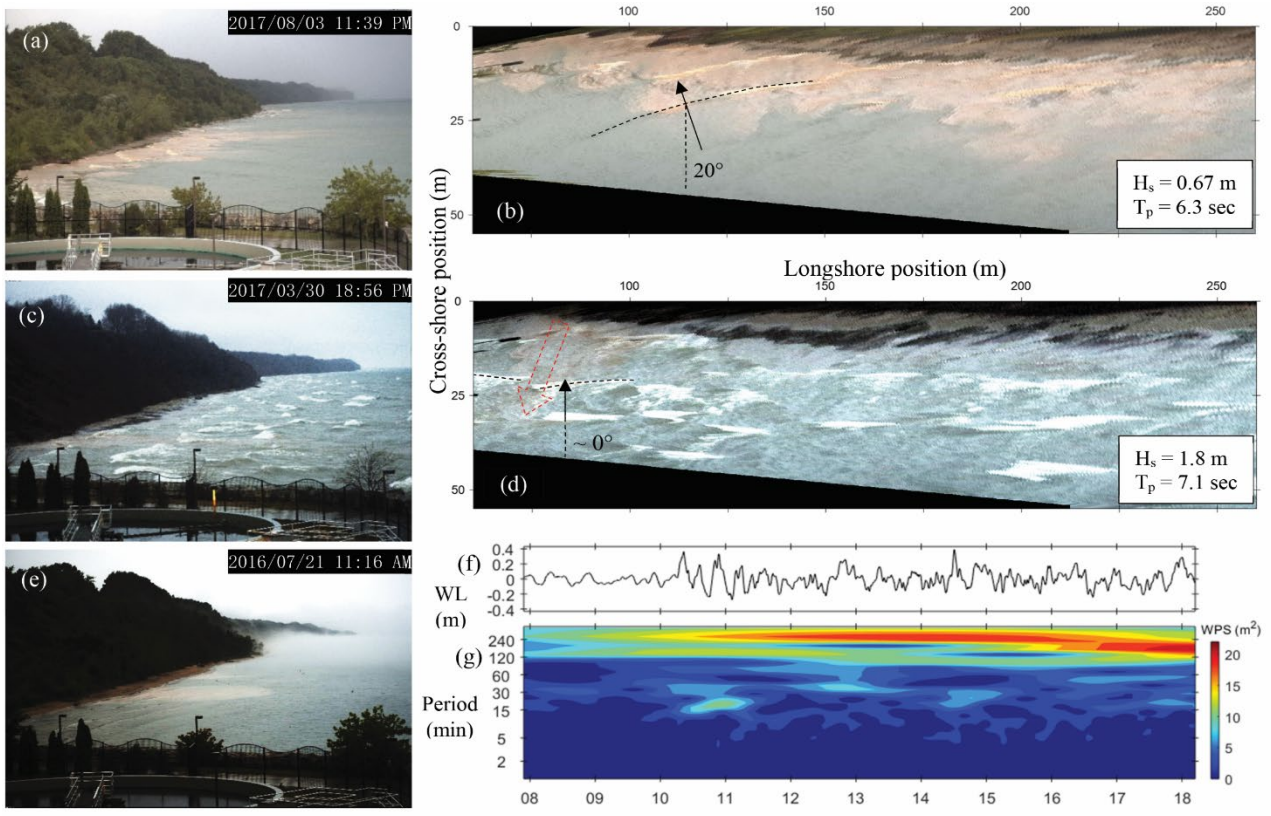

Fig. 2-10 (a) An oblique image shows shear instability induced flash rips at 11:39 PM on Aug 3, 2017 and (b) the corresponding orthophoto shows the incident wave angle of 20°. (c) An oblique image shows vorticity of breaking short-crest waves induced flash rips at 18:56 PM on Mar 3, 2017 and (d) the corresponding orthophoto shows sediment plumes between crests of shore-normal incidence waves. (e) An oblique image shows MIWLO-induced flash rips at 11:16 AM on Jul 21, 2017. (f) The time series of water level displacements on Jul 21, 2017 and (g) the corresponding wavelet power spectrum shows a meteotsunami event at 10:30 AM with maximum height of 0.57 m and periods of 15 min.

A new mechanism to generate flash rips associated with meteorological-induced water level oscillations (MIWLO) in the Lake Michigan has been recently reported by Linares et al. (2019). Specifically, meteotsunamis, one type of MIWLO with periods ranging from a few minutes to 2 hours, are propagating waves generated by fast moving atmospheric disturbances in barometric pressure or wind (Bechle et al., 2016; Monserrat et al., 2006). Bechle and Wu (2014) investigated the large MIWLO of 1954 meteotusnami event that caused seven people drownings. Anderson et al. (2015) reported that the large nearshore currents of meteotsunamis generated by two convective storms swept three swimmers about 0.5 miles offshore in Lake Erie. Linares et al. (2019) revealed that unexpected rip currents can be caused by rapidly receding water levels and generated vorticities in strong longshore currents. In this study, we summarize flash rip currents dates and images, wave characteristics (Hs and Tp), wind speed (Uw) and direction (Dirw), and radar reflectivity images obtained from NOAA National Climatic Data Center in Table 2-3. It is of interest that eight out of the nine flash rip days are associated with moving atmospheric storm disturbances. For example, Fig. 2-10e shows an image of flash rip-induced sediment plumes on July 21, 2017. The maximum height of water level oscillations was 0.57 m around 10:20 AM, as shown in Fig. 2-10f. Using the wavelet power spectrums (Linares et al., 2016), the period of the water level oscillation at the time was 15 minutes, as shown in Fig. 2-10g. Based upon storm type classification described in (Bechle et al., 2015), a bow type storm had crossed the Lake Michigan and reached Port Washington around the same time. All these characteristics meet the criteria (Bechle et al., 2015; Linares et al., 2016) to be a meteotsunami-induced water level fluctuation event. The co-occurrence of the meteotsunami events and flash rips suggest that the mechanism described by Linares et al. (2019) could possibly be the cause for observed flash rips. Future study should investigate the roles of MIWLO and associated processes in generating flash rips.

Table 2-3. Summary for dates and conditions of flash rip occurrences and corresponding radar reflectivity images

Dates	Image	H_s (m)	T_p (sec)	U_w (m/s)	Dir_w	Reflectivity image
2016-06-26		0.49	4.0	6.7	SW	
2016-07-21		0.46	3.3	8.0	SW	
2016-08-24		0.91	3.3	5.8	SW	
2016-09-21		0.49*	4.1*	4.0	S	
2017-03-30		1.8*	7.1*	12	NE	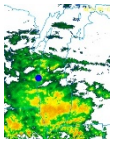
2017-07-12		0.67	4.1	6.7	SW	
2017-08-03		0.91	6.5	8.5	SW	
2017-10-03		0.76*	4.7*	5.8	SW	
2017-10-15		1.6*	6.7*	8.0	SW	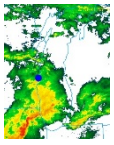

* indicates nearshore wave characteristics estimated from the NOAA National Data Buoy 45007 in Lake Michigan.

2.5.2. Other Types of Rip Currents

Two other types of rip currents at the study site are observed. First, potential locations of bathymetry-controlled rips are obtained by processing recorded RTEOS images. Specifically, we employ the time-averaged (or timex) imaging technique (Holman et al., 2006; Holman and Stanley, 2007) to identify rip channels as the darker region located in between brighter regions that represent sandbars due to depth-limited wave breaking. Fig. 2-11a shows a daily timex orthophoto on Aug 11, 2016. Two oblique rip channels (at x =~ 145 m and at x = ~185 m) in the gaps between three curved sandbars at 10-20 m offshore are clearly observed. The daily timex orthophoto on Sep 14, 2016 (Fig. 2-11b) shows that the rip channels had entirely disappeared and were replaced by a long and straight bar at about 20 m offshore. At later time, the daily timex orthophoto on Oct 11, 2016 (Fig. 2-11c) shows that a new rip channel formed (at x = ~170 m) in the gap of a single bar and doubled bars. The dynamic evolution of sandbars suggests the possible occurrence of bathymetry-controlled rip currents at the study site. Second, boundary-controlled rip currents are observed using another camera with field of view towards the breakwater of the Port Washington Harbor on Jun 5, 2017, as shown in Fig. 2-11d. Rip-induced sediment plumes were along the coastal breakwater (red solid arrow) and near the shore towards the breakwater (red dashed arrow). The incident waves were propagating in a highly oblique angle, as shown in black arrow in Fig. 2-11e. The observed rips were likely caused by wave-generated longshore currents (Longuet-Higgins, 1970) being deflected when encountering the rigid breakwater structure, resulting in the offshore-directed currents (Dalrymple et al., 2011; Wind and Vreugdenhil, 1986). Overall, observations using the camera in the RTEOS reveal several types of rip current occurrences, which may explain eight drownings and more than ten rescue incidents at Port Washington, WI during the last several years.

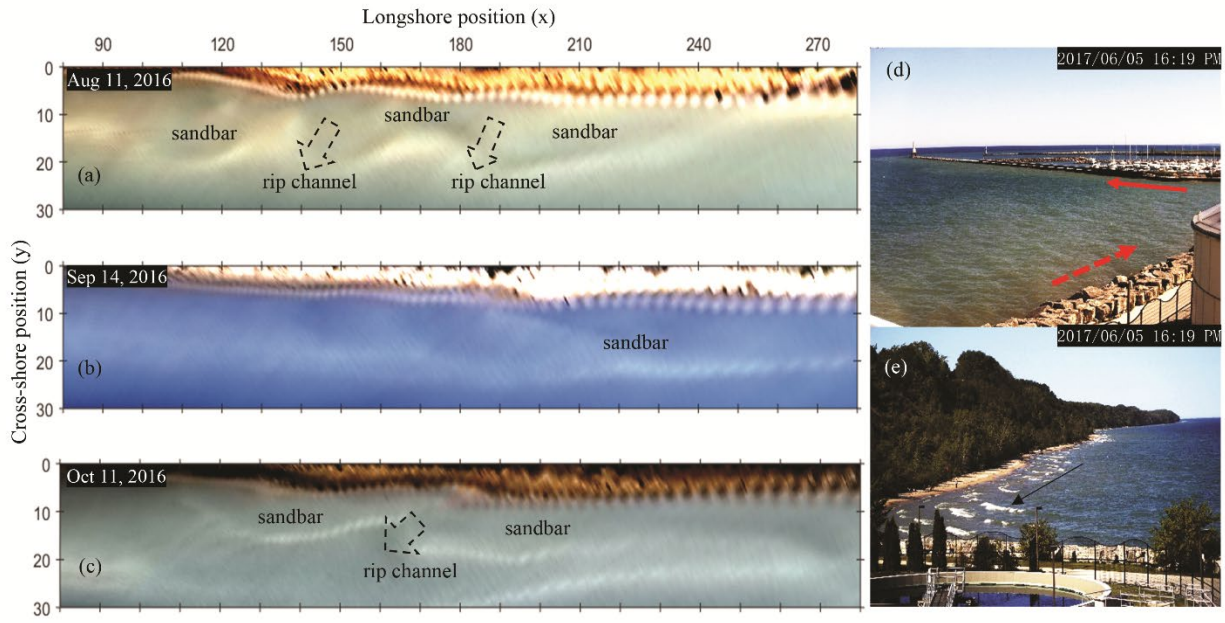

Fig. 2-11 Daily timex orthorectified images show three time stamps: (a) two rip channels (black dotted arrows) on Aug 11, 2016 as potential locations for bathymetry-controlled rip currents, (b) the channels disappeared on Sep 14, and (c) a new formed rip channel on Oct 11, 2016. (d) An oblique image acquired by the RTEOS camera with a field of view towards the Breakwater shows sediment plumes induced by boundary-controlled rip currents (red solid arrow) on Jun 5, 2017, likely due to deflection of longshore currents (red dashed arrow) at the breakwater. (e) An oblique image of the North Beach shows wave propagating in highly oblique incidence (black arrow).

2.5.3. Public Communications

Media mentions and news releases on local (City of Port Washington, Ozaukee Press, Milwaukee Journal Sentinel) and regional (UW Sea Grant, Phy.org) channels have greatly promoted the usages of LOCKS by residents and visitors. Outcomes of public communications are summarized here based upon usage statistics in three perspectives. First, page views of the INFOS website (*http://infosportwashington.cee.wisc.edu/*), tracked by Google Analytics, show a monthly average of 9,650 page views since the website was online in September 2015. A maximum 34,200 page views was reached in August 2016 shortly after several media mentions and news releases. In 2017 and 2018, monthly page views in beach season months maintained at 16,500 and at 19,000

respectively, indicating continuous public uses and interests in rip current safety information. Second, user behaviors are inferred based upon usage logs on when and how the INFOS webpages were accessed. In terms of time, heavy loads of views were usually in early mornings starting at 6 AM on Fridays, Saturdays and Sundays. It is conjectured that people likely checked the water information before they made the decision to go to the beach. In terms of devices, 61 % views were made from desktops and tablets versus 39% from mobile devices, supporting the previous conjecture that people were likely at home when they accessed the information. As we see that large amounts of INFOS usages were made beforehand, which could be up to hours ahead of when people were actually at the beach, BLINK as the in-situ device can be of great help to provide the most updated information about the dangerous rip current conditions. Last but not least, BLINK usages, tracked by a nearby security camera, show that the daily maximum of 55 visits and the average of 20 visits were achieved in May 2019. In each visit, the number of people ranged from 1 person to up to 5 people. Approximately 30% of total tracked visits were families with young children. 75% of people passing by had stopped to check the monitor, showing that BLINK can attract people to notice any potential dangerous rip current and water conditions. With these user statistics, the LOCKS has not only shown the continuous public interests and needs for timely water condition, but also demonstrated that BLINK can be an effective approach to issue rip current warnings.

2.6 Summary and Conclusion

The Lifeguarding Operational Camera Kiosk System (LOCKS) is developed and implemented at the North Beach on Lake Michigan in City of Port Washington, WI. The three components of the LOCKS are the Real Time Environmental Observation System for data

acquisition, the Integrated Nowcast Forecast Operational System for image and data processing, and the Beach Lights and Notifying Kiosk for timely and dynamic warnings of flash rips. Results of flash rip detection show that the combined length threshold and HSV-based segmentation method can be used in both sunny and cloudy days with an overall accuracy of 83%, better than the RGB-based or HSV-based segmentation methods. Nonstationary locations and intermittent occurrences of flash rips in Lake Michigan are observed and characterized for the first time. Flash rip-induced sediment plumes can range from 10 m beyond the surf zone to a distance greater than 50 m. The spacing between flash rips can range from 20 m to 60 m. Flash rips tend to occur on and off many times throughout the same day. The duration of flash rips varies from 1 to 5 minutes with 65% of flash rips less than 2 minutes, indicating that flash rips have a short-lifespan and decay after a few minutes. Consistent to human-eye observed occurrences, the Flash Rip Occurrence Checklist including both environmental factors and two new (storm and visual observation) factors reliably assesses the likelihood of hazardous flash rips. General applications of this method can be achieved in other beaches by adjusting thresholds and the visual observation factor based site-specific wave and water conditions. The design of the Beach Lights and Notifying Kiosk system employs automated three-color LED beacon lights that mimics the dynamic flag system used by beach patrols. The kiosk and dynamic lights, implemented at the entrance to the North Beach most visible to beach users, can provide real-time water conditions and issue warnings of potential dangerous flash rips. Public communication through media mentions, news releases, and website usages show the strong interest and support of the LOCKS as a new approach to effectively issue flash rip warnings to beach users for the first time. The LOCKS can be further used to issue warnings of other types of dangerous currents including bathymetry-controlled and boundary-controlled rips, which were also observed in this study. Future study is suggested to reveal the co-

occurrence of meteotsunamis and flash rips and investigate the roles of meteorologically induced water level oscillations and associated processes in generating flash rips.

2.7 **Acknowledgement**

This study and the LOCKS were supported by the National Oceanic and Atmospheric Administration (NOAA) Coastal Storms Program, Wisconsin Coastal Management Program (WCMP), University of Wisconsin Sea Grant Institute (UW-Sea Grant), and gift funds from WE Energies and local friends of Port Washington group. The authors specially thank Mr. Tom Malda, former Mayor of City of Port Washington, for his vision to develop the cyberinfrastructure to ensure rip current warning for beach safety. We would like to thank Mr. Todd Breiby, Mr. Michael Friis, and Ms. Angel Kathleen from WCMP for funding the beach lights and kiosk system and their support in coordination, education, and outreach for rip current safety. We also thank Mr. Gene Clark, a coastal specialist from UW Sea Grant, for providing valuable knowledge related to nearshore processes near coastal structures. In addition, Ms. Moira Harrington and Ms. Marie Zhuikov at UW-Sea Grant for their dedication to communicating rip current hazards to the Great Lakes community are acknowledged. Outreach activities related to the NOAA rip current rip current outlook by Mr. Marc Kavinsky, Lead Forecaster of Marine Program Leader at NOAA-National Weather Service – Milwaukee/Sullivan, are noted and acknowledged. Last but not least, the authors acknowledge Mr. Marty Becker, Ms. Kiley Schulte, Mr. Dennis Cherny, Mr. Dan Buehler, Mr. Charlie Imig, Ms. Lisa Rathke, Mr. Randy Tetzlaff, and many staff at the City of Port Washington, WI for the assistances in deployment and operation of the LOCKS.

2.8 References

Alvarez-Ellacuria, A., Orfila, A., Olabarrieta, M., Gómez-pujol, L., Medina, R., Tintoré, J., 2009. An Alert System for Beach Hazard Management in the Balearic Islands. Coast. Manag. 37, 569–584. https://doi.org/10.1080/08920750903150662

Alves, J.-H.G.M., Chawla, A., Tolman, H.L., Schwab, D., Lang, G., Mann, G., Alves, J.-H.G.M., Chawla, A., Tolman, H.L., Schwab, D., Lang, G., Mann, G., 2014. The Operational Implementation of a Great Lakes Wave Forecasting System at NOAA/NCEP*. Weather Forecast. 29, 1473–1497. https://doi.org/10.1175/WAF-D-12-00049.1

Anderson, E.J., Bechle, A.J., Wu, C.H., Schwab, D.J., Mann, G.E., Lombardy, K.A., 2015. Reconstruction of a meteotsunami in Lake Erie on 27 May 2012: Roles of atmospheric conditions on hydrodynamic response in enclosed basins. J. Geophys. Res. Ocean. 120, 8020–8038. https://doi.org/10.1002/2015JC010883

Anderson, J.D., Wu, C.H., 2018. Development and application of a real-time water environment cyberinfrastructure for kayaker safety in the Apostle Islands, Lake Superior. J. Great Lakes Res. 44, 990–1001. https://doi.org/10.1016/J.JGLR.2018.07.006

Arun Kumar, S.V. V., Prasad, K.V.S.R., 2014. Rip current-related fatalities in India: a new predictive risk scale for forecasting rip currents. Nat. Hazards 70, 313–335. https://doi.org/10.1007/s11069-013-0812-x

Austin, M.J., Scott, T.M., Russell, P.E., Masselink, G., 2012. Rip Current Prediction: Development, Validation, and Evaluation of an Operational Tool. J. Coast. Res. 29, 283. https://doi.org/10.2112/JCOASTRES-D-12-00093.1

Bechle, A.J., Wu, C.H., 2014. The Lake Michigan meteotsunamis of 1954 revisited. Nautral Hazards. 74(1), 155–177. https://doi.org/10.1007/s11069-014-1193-5

Bechle, A.J., Kristovich, D.A.R., Wu, C.H., 2015. Meteotsunami occurrences and causes in Lake Michigan. J. Geophys. Res. Ocean. 120, 8422–8438. https://doi.org/10.1002/2015JC011317

Bechle, A.J., Wu, C.H., 2011. Virtual wave gauges based upon stereo imaging for measuring surface wave characteristics. Coast. Eng. 58, 305–316. https://doi.org/10.1016/J.COASTALENG.2010.11.003

Bechle, A.J., Wu, C.H., Kristovich, D.A.R., Anderson, E.J., Schwab, D.J., Rabinovich, A.B., 2016. Meteotsunamis in the Laurentian Great Lakes. Sci. Rep. 6, 37832. https://doi.org/10.1038/srep37832

Bechle, A.J., Wu, C.H., Liu, W.-C., Kimura, N., 2012. Development and Application of an Automated River-Estuary Discharge Imaging System. J. Hydraul. Eng. 138, 327–339. https://doi.org/10.1061/(ASCE)HY.1943-7900.0000521

Brander, R.W., MacMahan, J.H., 2011. Future Challenges for Rip Current Research and Outreach, in: Leatherman, S., Fletemeyer, J. (Eds.), Rip Currents: Beach Safety, Physical Oceanography, and Wave Modeling. CRC Press, pp. 1–29.

Brannstrom, C., Lee Brown, H., Houser, C., Trimble, S., Santos, A., 2015. "You can't see them from sitting here": Evaluating beach user understanding of a rip current warning sign. Appl. Geogr. 56, 61–70. https://doi.org/10.1016/J.APGEOG.2014.10.011

Castelle, B., Almar, R., Dorel, M., Lefebvre, J.-P., Senechal, N., Anthony, E.J., Laibi, R., Chuchla, R., Penhoat, Y. du, 2014. Rip currents and circulation on a high-energy low-tide-terraced beach (Grand Popo, Benin, West Africa). J. Coast. Res. 70, 633–638. https://doi.org/10.2112/SI70-107.1

Castelle, B., Coco, G., 2013. Surf zone flushing on embayed beaches. Geophys. Res. Lett. 40,

2206–2210. https://doi.org/10.1002/grl.50485

Castelle, B., Scott, T., Brander, R.W., McCarroll, R.J., 2016. Rip current types, circulation and hazard. Earth-Science Rev. 163, 1–21. https://doi.org/10.1016/J.EARSCIREV.2016.09.008

Churma, M.E., Churma, M.E., 2017. Observation Methodologies for NOAA Operational Rip Current Forecast Models.

Clark, D.B., Elgar, S., Raubenheimer, B., 2012. Vorticity generation by short-crested wave breaking. Geophys. Res. Lett. 39, 2012GL054034. https://doi.org/10.1029/2012GL054034

Clark, D.B., Feddersen, F., Guza, R.T., 2010. Cross-shore surfzone tracer dispersion in an alongshore current. J. Geophys. Res. 115, C10035. https://doi.org/10.1029/2009JC005683

Coco, G., Murray, A.B., Green, M.O., Thieler, E.R., Hume, T.M., 2007. Sorted bed forms as self-organized patterns: 2. Complex forcing scenarios. J. Geophys. Res. 112, F03016. https://doi.org/10.1029/2006JF000666

Dalrymple, R.A., MacMahan, J.H., Reniers, A.J.H.M., Nelko, V., 2011. Rip Currents. Annu. Rev. Fluid Mech. 43, 551–581. https://doi.org/10.1146/annurev-fluid-122109-160733

Dusek, G., Seim, H., 2013. A Probabilistic Rip Current Forecast Model. J. Coast. Res. 289, 909–925. https://doi.org/10.2112/JCOASTRES-D-12-00118.1

Engle, J., 2003. Formulation of a rip current forecasting technique through statistical analysis of rip current-related rescues. Univ. Florida.

Feddersen, F., 2014. The Generation of Surfzone Eddies in a Strong Alongshore Current. J. Phys. Oceanogr. 44, 600–617. https://doi.org/10.1175/JPO-D-13-051.1

Floćh, F., Mabiala, G.R., Almar, R., Castelle, B., Hall, N., Du Penhoat, Y., Scott, T., Delacourt, C., 2018. Flash Rip Statistics from Video Images. J. Coast. Res. 81, 100–106.

https://doi.org/10.2112/SI81-013.1

Gensini, V.A., Ashley, W.S., 2010. An examination of rip current fatalities in the United States. Nat. Hazards 54, 159–175. https://doi.org/10.1007/s11069-009-9458-0

Great Lake Current Incident Database, 2018 Swim Season: Rip Current and Channel Current Incident Summary. http://www.crh.noaa.gov/mqt/?n=glcidyearlystats, 2018 (accessed 27 May 2019).

Great Lakes Surf Rescue Project, Great Lakes Drownings. http://www.glsrp.org/statistics/, 2018 (accessed 27 May 2019).

Haus, B.K., 2011. Remote sensing applied to rip current forecasts and identification, in: Leatherman, S., Fletemeyer, J. (Eds.), Rip Currents: Beach Safety, Physical Oceanography, and Wave Modeling. CRC Press, pp. 133–146.

Holland, K.T., Holman, R.A., Lippmann, T.C., Stanley, J., Plant, N., 1997. Practical use of video imagery in nearshore oceanographic field studies. IEEE J. Ocean. Eng. 22, 81–92. https://doi.org/10.1109/48.557542

Holman, R.A., Stanley, J., 2007. The history and technical capabilities of Argus. Coast. Eng. 54, 477–491. https://doi.org/10.1016/J.COASTALENG.2007.01.003

Holman, R.A., Symonds, G., Thornton, E.B., Ranasinghe, R., 2006. Rip spacing and persistence on an embayed beach. J. Geophys. Res. 111, C01006. https://doi.org/10.1029/2005JC002965

Houser, C., Barrett, G., Labude, D., 2011. Alongshore variation in the rip current hazard at Pensacola Beach, Florida. Nat. Hazards 57, 501–523. https://doi.org/10.1007/s11069-010-9636-0

Houser, C., Trimble, S., Brander, R., Brewster, B.C., Dusek, G., Jones, D., Kuhn, J., 2017. Public

perceptions of a rip current hazard education program: “Break the Grip of the Rip!” Nat. Hazards Earth Syst. Sci. 17, 1003–1024. https://doi.org/10.5194/nhess-17-1003-2017

Johnson, D., Pattiaratchi, C., 2006. Boussinesq modelling of transient rip currents. Coast. Eng. 53, 419–439. https://doi.org/10.1016/J.COASTALENG.2005.11.005

Johnson, D., Pattiaratchi, C., 2004. Transient rip currents and nearshore circulation on a swell-dominated beach. J. Geophys. Res. 109, C02026. https://doi.org/10.1029/2003JC001798

Lascody, R.L., 1998. EAST CENTRAL FLORIDA RIP CURRENT PROGRAM, National Weather Digest.

Leatherman, S.P., Leatherman, S.B., 2017. Techniques for Detecting and Measuring Rip Currents. Int. J. Earth Sci. Geophys. Cit. Leatherman SB 2017, 14.

Linares, Á., Bechle, A.J., Wu, C.H., 2016. Characterization and assessment of the meteotsunami hazard in northern Lake Michigan. J. Geophys. Res. Ocean. 121, 7141–7158. https://doi.org/10.1002/2016JC011979

Linares, Á., Wu, C.H., Bechle, A.J., Anderson, E.J., Kristovich, D.A.R., 2019. Unexpected rip currents induced by a meteotsunami. Sci. Rep. 9, 2105. https://doi.org/10.1038/s41598-019-38716-2

Long, J.W., Özkan-Haller, H.T., 2005. Offshore controls on nearshore rip currents. J. Geophys. Res. 110, C12007. https://doi.org/10.1029/2005JC003018

Longuet-Higgins, M.S., 1970. Longshore currents generated by obliquely incident sea waves: 1. J. Geophys. Res. 75, 6778–6789. https://doi.org/10.1029/JC075i033p06778

Lushine, J.B., 1991. A Study of Rip Current Drownings and Related Weather Factors. NATL. WEA. DIG 13--19.

MacMahan, J.H., Thornton, E.B., Reniers, A.J.H.M., 2006. Rip current review. Coast. Eng. 53,

191–208. https://doi.org/10.1016/J.COASTALENG.2005.10.009

Matthews, B., Andronaco, R., Adams, A., 2014. Warning signs at beaches: Do they work? Saf. Sci. 62, 312–318. https://doi.org/10.1016/J.SSCI.2013.09.003

Meadows, G., Purcell, H., Guenther, D., Meadows, L., Kinnunen, R.E., Clark, G., 2011. Rip Currents in the Great Lakes: An Unfortunate Truth, in: Leatherman, S., Fletemeyer, J. (Eds.), Rip Currents: Beach Safety, Physical Oceanography, and Wave Modeling. CRC Press, pp. 199–214.

Monserrat, S., Vilibić, I., Rabinovich, A.B., 2006. Meteotsunamis: atmospherically induced destructive ocean waves in the tsunami frequency band. Nat. Hazards Earth Syst. Sci. 6, 1035–1051. https://doi.org/10.5194/nhess-6-1035-2006

Moulton, M., Dusek, G., Elgar, S., Raubenheimer, B., Moulton, M., Dusek, G., Elgar, S., Raubenheimer, B., 2017. Comparison of Rip Current Hazard Likelihood Forecasts with Observed Rip Current Speeds. Weather Forecast. 32, 1659–1666. https://doi.org/10.1175/WAF-D-17-0076.1

Murray, T., Cartwright, N., Tomlinson, R., 2013. Video-imaging of transient rip currents on the Gold Coast open beaches. J. Coast. Res. 165, 1809–1814. https://doi.org/10.2112/SI65-306.1

National Weather Service. Natural Hazard Statistics – Weather Fatalities 2018. https://www.nws.noaa.gov/om/hazstats.shtml, 2018 (accessed 27 May 2019).

Nieto, M.A., Garau, B., Balle, S., Simarro, G., Zarruk, G.A., Ortiz, A., Tintoré, J., Álvarez-Ellacuría, A., Gómez-Pujol, L., Orfila, A., 2010. An open source, low cost video-based coastal monitoring system. Earth Surf. Process. Landforms 35, 1712–1719. https://doi.org/10.1002/esp.2025

Orzech, M.D., Reniers, A.J.H.M., Thornton, E.B., MacMahan, J.H., 2011. Megacusps on rip channel bathymetry: Observations and modeling. Coast. Eng. 58, 890–907. https://doi.org/10.1016/J.COASTALENG.2011.05.001

Özkan-Haller, H.T., Kirby, J.T., 1999. Nonlinear evolution of shear instabilities of the longshore current: A comparison of observations and computations. J. Geophys. Res. Ocean. 104, 25953–25984. https://doi.org/10.1029/1999JC900104

Peregrine, D.H., 1998. Surf Zone Currents. Theor. Comput. Fluid Dyn. 10, 295–309. https://doi.org/10.1007/s001620050065

Radermacher, M., de Schipper, M.A., Reniers, A.J.H.M., 2018. Sensitivity of rip current forecasts to errors in remotely-sensed bathymetry. Coast. Eng. 135, 66–76. https://doi.org/10.1016/J.COASTALENG.2018.01.007

Reimer, J.R., Wu, C.H., 2016. Development and Application of a Nowcast and Forecast System Tool for Planning and Managing a River Chain of Lakes. Water Resour. Manag. 30, 1375–1393. https://doi.org/10.1007/s11269-016-1228-7

Reniers, A.J.H.M., MacMahan, J.H., Thornton, E.B., Stanton, T.P., 2006. Modelling infragravity motions on a rip-channel beach. Coast. Eng. 53, 209–222. https://doi.org/10.1016/J.COASTALENG.2005.10.010

Schrader, M., 2004. EVALUATION OF THE MODIFIED ECFL LURCS RIP CURRENT FORECASTING SCALE AND CONDITIONS OF SELECTED RIP CURRENT EVENTS IN FLORIDA.

Scott, T., Austin, M., Masselink, G., Russell, P., 2016. Dynamics of rip currents associated with groynes — field measurements, modelling and implications for beach safety. Coast. Eng. 107, 53–69. https://doi.org/10.1016/J.COASTALENG.2015.09.013

Scott, T., Castelle, B., Almar, R., Senechal, N., Floćh, F., Detandt, G., 2018. Controls on Flash Rip Current Hazard on Low-Tide Terraced Tropical Beaches in West Africa. J. Coast. Res. 81, 92. https://doi.org/10.2112/SI81-012.1

Sherker, S., Williamson, A., Hatfield, J., Brander, R., Hayen, A., 2010. Beachgoers' beliefs and behaviours in relation to beach flags and rip currents. Accid. Anal. Prev. 42, 1785–1804. https://doi.org/10.1016/J.AAP.2010.04.020

Silva, R., Baquerizo, A., Losada, M.Á., Mendoza, E., 2010. Hydrodynamics of a headland-bay beach—Nearshore current circulation. Coast. Eng. 57, 160–175. https://doi.org/10.1016/J.COASTALENG.2009.10.003

Slattery, M.P., 2010. Assessing the nature of rip currents along the south shore of Long Island, NY: Dominant rip type and insights into possible forcing mechanisms. The Graduate School, Stony Brook University: Stony Brook, NY.

Smith, J.P., Hunter, T.S., Clites, A.H., Stow, C.A., Slawecki, T., Muhr, G.C., Gronewold, A.D., 2016. An expandable web-based platform for visually analyzing basin-scale hydro-climate time series data. Environ. Model. Softw. 78, 97–105. https://doi.org/10.1016/J.ENVSOFT.2015.12.005

Spydell, M.S., Feddersen, F., Guza, R.T., 2009. Observations of drifter dispersion in the surfzone: The effect of sheared alongshore currents. J. Geophys. Res. 114, C07028. https://doi.org/10.1029/2009JC005328

Taborda, R., Silva, A., 2012. COSMOS: A lightweight coastal video monitoring system. Comput. Geosci. 49, 248–255. https://doi.org/10.1016/J.CAGEO.2012.07.013

van der Westhuysen, A.J., 2013. Development and validation of the Nearshore Wave Prediction System.

Voulgaris, G., Kumar, N., Warner, J.C., 2011. Methodology for prediction of rip currents using a three-dimensional numerical, coupled, wave current model, in: Leatherman, S., Fletemeyer, J. (Eds.), Rip Currents: Beach Safety, Physical Oceanography, and Wave Modeling. CRC Press, pp. 107–124.

Wave Information Studies – United States Army Corps of Engineers. Lake Michigan (1979-2014). http://wis.usace.army.mil/hindcasts.html (accessed 27 May 2019)

Wanek, J.M., Wu, C.H., 2006. Automated trinocular stereo imaging system for three-dimensional surface wave measurements. Ocean Eng. 33, 723–747. https://doi.org/10.1016/J.OCEANENG.2005.05.006

White, K.M., Hyde, M.K., 2010. Swimming between the flags: A preliminary exploration of the influences on Australians' intentions to swim between the flags at patrolled beaches. Accid. Anal. Prev. 42, 1831–1838. https://doi.org/10.1016/J.AAP.2010.05.004

Wind, H.G., Vreugdenhil, C.B., 1986. Rip-current generation near structures. J. Fluid Mech. 171, 459. https://doi.org/10.1017/S0022112086001520

Winter, G., van Dongeren, A.R., de Schipper, M.A., van Thiel de Vries, J.S.M., 2014. Rip currents under obliquely incident wind waves and tidal longshore currents. Coast. Eng. 89, 106–119. https://doi.org/10.1016/J.COASTALENG.2014.04.001

3. Flash rips induced by meteorologically induced water level oscillations

The following is in preparation to be submitted to *Scientific Reports*.

3.1 Introduction

Flash rips impose an unexpected and hidden hazard to communities on oceanic and the Great Lakes coasts[1,2]. Flash rips, also known as the transient rip currents, are strong and narrow seaward flows in featureless or alongshore-uniform beaches[3]. Non-fixed, unpredictable occurrences of flash rips are different from other types of rip currents generated near morphological features, such as rip channels between sandbars[4,5], near natural headlands[6], and anthropogenic coastal structures[7,8]. Spatially, flash rips tend to migrate alongshore[9,10] and can extend beyond surf zone widths of up to 50-100 meters offshore[11,12]. Temporally, flash rips have transient lifespans of seconds to several minutes and tend to pulse in intervals from minutes to hours[10,12]. The occurrences of flash rips are documented to happen under breaking waves[1], but until recently studies have found that unexpected flash rips[13] also occur under low to moderate waves. The unexpected flash rips are associated with the processes of meteorologically induced high-frequency water level oscillations (MIWLOs), such as meteotsunamis in the Great Lakes[14]. Evidence of drowning incidents and image-based observations has shown that flash rips due to MIWLOs can occur more frequently than expected but were rarely recognized by coastal communities[13]. In consequence, flash rips can sweep unaware water users into deeper water where panic and exhaustion often lead to drowning[1]. In view of the hundreds to thousands of drowning incidents reported globally due to rip currents[1,2], flash rips, with the nature of transiency, unpredictability in locations, and unexpected occurrences associated with MIWLOs, are likely one of the most risky and hidden hazards.

Mechanisms to generate flash rips can be classified into two categories, based upon causes of meteorologically induced water level oscillations (MIWLOs) or wind waves (see Fig 3-1). Meteotsunamis[14], one kind of MIWLOs, are induced by fast-moving atmospheric disturbances of pressures and winds[15–19] due to Proudman resonance[21] or Greenspan resonance[22,23]. Meteotsunamis can propagate as non-trapped long waves or trapped edge waves[20]. Seiches[24,25], another kind of MIWLOs, are basin-scale standing waves caused by wind shifting in directions or sudden cessation of wind stresses forcing[25,26]. Both meteotsunamis or seiches, amplified by nearshore transformation processes such as reflection, refraction, and shoaling[14,17], can induce strong longshore currents[24,27], which can lead to flash rips in two processes. One is the destabilized longshore shear currents in meteotsunamis or seiches to produce offshore-directed propagating vortices as flash rips[13]. Another possible process is the reflected seaward cross-shore flows of two converged meteotsunami-induced edge waves[16] to produce strong offshore shear currents as flash rips. For wind waves-induced flash rips, there are several well-documented processes. Shear instabilities of longshore currents under highly oblique incidence waves[1] generate unsteady vortices as transient out-bursting flows[28,29]. Breaking of short-crested waves under shore-normal incidence[1,30] induce instantaneous small-scale vorticities[30–32] that cascade to form large-scale surf zone eddies[33]. The interactions of incident waves with infra-gravity waves[34,35] or edge waves[5,36,37] create radiation stress gradients that drive offshore-directed flows. While mechanisms to generate flash rips can be related to both MIWLOs and wind waves, the characteristics of flash rips induced by MIWLOs have yet been reported, as far as the authors are aware.

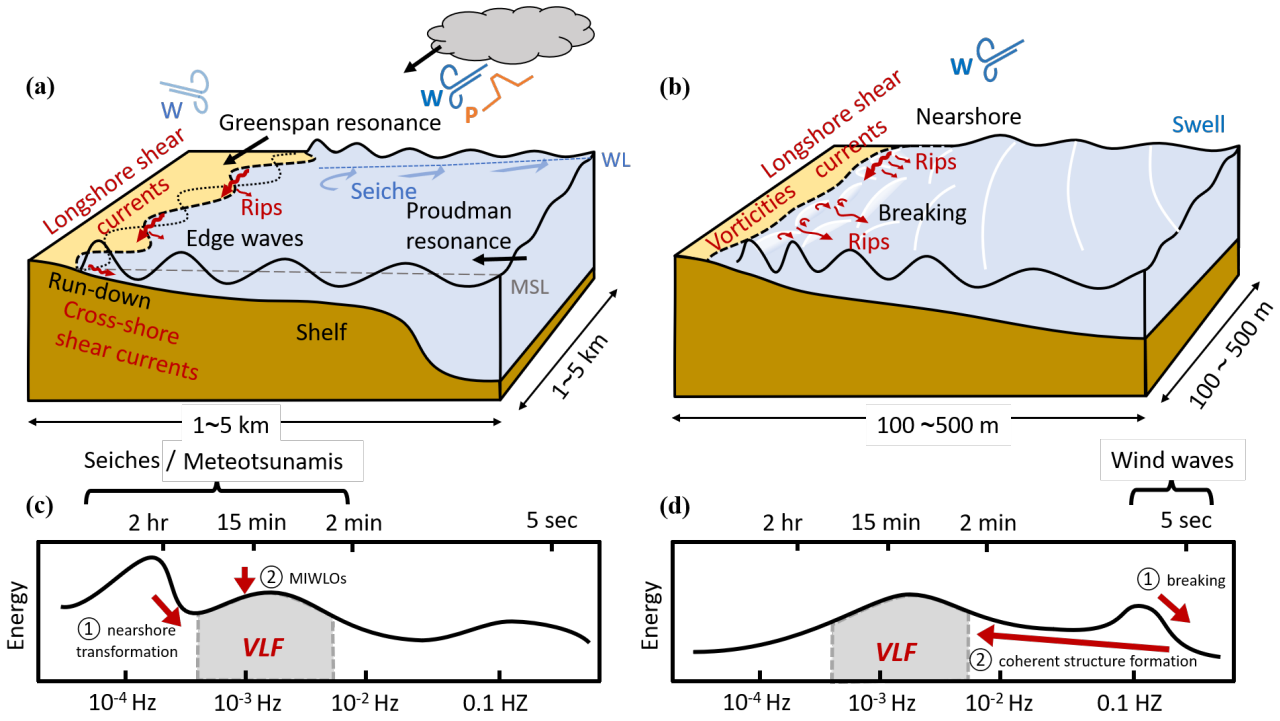

Fig 3-1. Schematics of flash rips induced by (a) meteorologically induced water level oscillations (MIWLOs) like meteotsunamis and seiches, and (b) wind waves and swells. Correspondingly, the very low frequency motions (VLFs) can be excited by energy transfer pathways through (c) ① nearshore transformation or ② direct input of MIWLOs; and (d) ① generation of wave-breaking induced vortices and ② formation of coherent eddies.

Temporal and spatial characteristics of flash rips are associated with the very low frequency motions (VLFs, ~0.4 mHz <f< 4 mHz)[38–40]. For flash rips induced by wind waves[11,40,41], temporally intermittency in flash rips exhibit pulsations in the VLF range[38] and spatially nonstationary locations in flash rips are inherit feature in VLFs, which are excited by the generation of wave-breaking induced vortices and the formation of coherent eddies[42] (see Fig 3-1d). Specifically, VLFs consists of two parts. One is the "extrinsic"[28] (or "forced"[43]) VLFs, which are associated with the stochastic wave forcing due to randomness in directionally spread incident waves or wave groups[30,43]. Another is the "intrinsic" VLFs, independent from the variations in wave forcing[42], are associated with the nonlinear instability of shear currents[29], or by modulation

of atmospheric wind or ocean tides[44]. For flash rips generated by MIWLOs mechanisms, the VLFs are likely induced by two pathways (see Fig 3-1c). First, VLFs can be excited through nearshore transformation processes by MIWLO induced longshore currents to generate nonlinear shear instabilities, similar to the "intrinsic" VLFs[29,42]. Second, VLFs can be induced from the MIWLOs with periods around 2 min - 2 hours in meteotsunamis[14] and a few hours in seiches[25], which are coinciding partially with the very low frequency range. To date, temporally intermittent and spatially nonstationary characteristics in flash rips associated with VLFs caused by MIWLOs have not reported.

The objective of this paper is to elucidate temporal and spatial characteristics of flash rips generated by meteorologically induced water level oscillations for revealing unrecognized beach hazards for beachgoers. Here, we compile webcam images, Next Generation weather radar (NEXRAD) reflectivity images, water level, waves, surface winds, atmospheric pressure observations, as well as nearshore velocity and vorticity fields reconstructed using state-of-art integrated atmospheric-hydrodynamic modeling. Transient, intermittent flash rip with VLFs pulsations with spatially nonstationary but ubiquitous locations are associated with MIWLOs processes including meteotsunamis, seiches, and combined effects with wind waves. The hidden hazard of flash rips due to the temporally and spatially repeatable occurrences are elucidated at a Lake Michigan beach as an example. Further examination of the drowning incident statistics suggests that MIWLOs can be an overlooked cause for inducing rip currents in Great Lakes and oceanic coasts of the United States.

3.2 Results

Repeated flash rips at the North Beach of Port Washington, WI. under three events, July 12, 2017 (*Event I*), May 25, 2019 (*Event II*), and May 22, 2019 (*Event III*) are discussed here. Visual signatures of rip-induced sediment plumes throughout the events appeared intermittently: in *Event I* a total of 51 flash rip occurrences between 10:09-17:54, in *Event II* a total of 52 occurrences between 05:15 -16:15, and in *Event III* a total of 76 occurrences between 05:10-17:26. Fig 3-2 (a-c) show the snapshots of sediment plumes that occurred at non-fixed locations. At 10:15 of *Event I*, five pulses of flash rips appeared, mostly with uniform lengths close to 20 m but exhibiting rip spacings of 30 - 500 m apart (see Fig 3-2a). At 12:07 of *Event II*, seven pulses of flash rips appeared with varying lengths between 20 - 50 m and spacings of 40 - 160 m apart (see Fig 3-2b). At 06:20 of *Event III*, four pulses of flash rips appeared between the white crests of intensely breaking waves, with rip lengths extending beyond 50 m from the shoreline and rip spacings of 20 -450 m apart (see Fig 3-2c). Interestingly, distinct weather and wave conditions are exhibited in the three observed events: *Event I* was featured with cloudy weather and low waves, *Event II* was featured with sunny weather and low waves, while *Event II* was featured with cloudy weather and high waves.

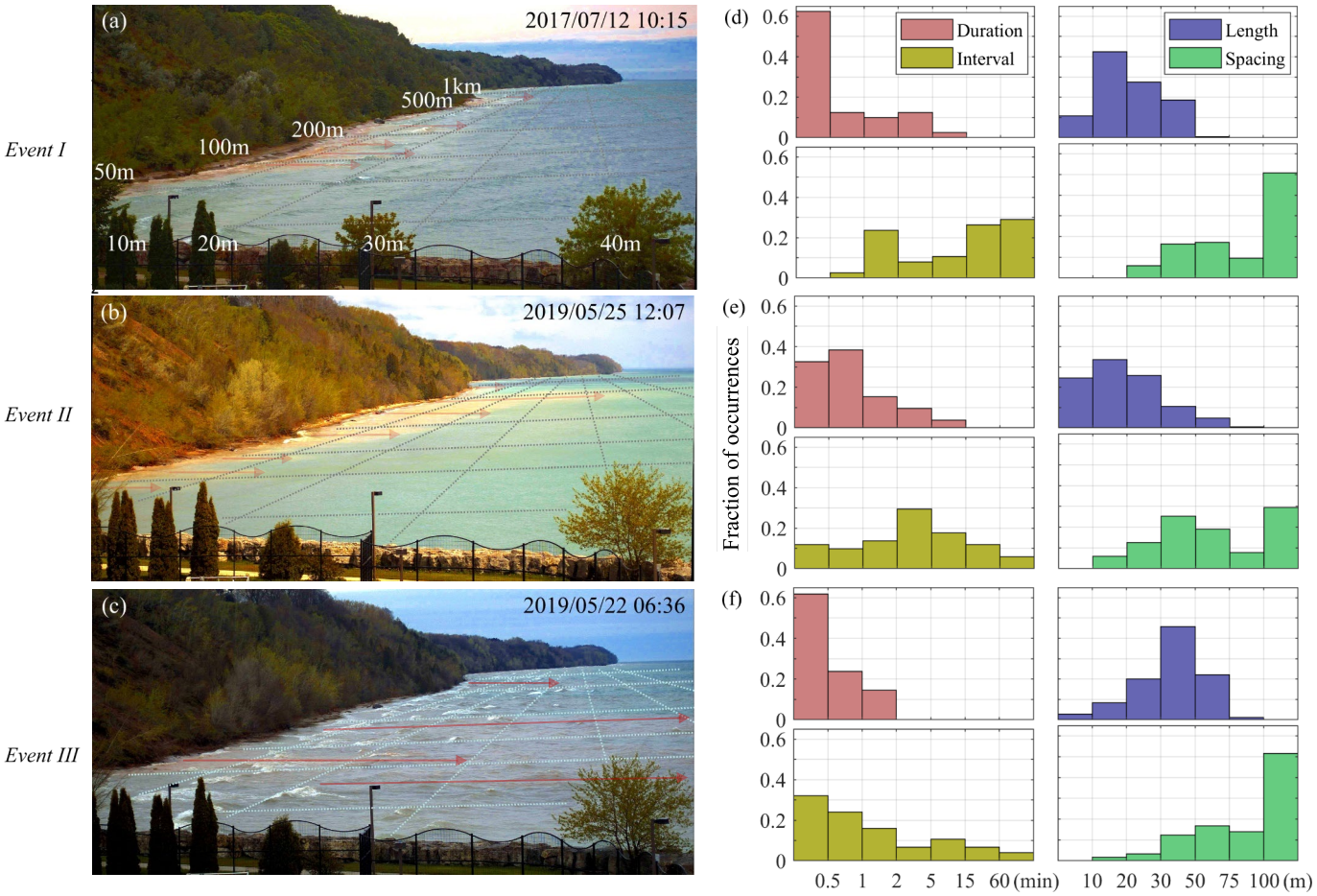

Fig 3-2. Three flash rip events observed at the North Beach of Port Washington, WI on cloudy (Event I), sunny (Event II) and wave (Event III) days. **(a-c)** Images show rip-induced sediment plumes (highlighted in red arrows) as visual evidence of flash rips. The overlaid gray dotted lines represent the georeferenced scales for visual distortion correction. **(d-f)** Histograms for characteristics of all flash rips observed throughout the days of the three events. Four parameters are used: durations (pink) of each individual rip plume pulse, intervals (gold) as the time between consecutive rip pulses, lengths (blue) measured as the offshore extents from shoreline, and spacing (green) measured as distance between centroids of neighboring plumes.

Characteristics of temporally and spatially repeating flash rips are compared among the three events. Fig 3-2 (d-f) shows histograms of four characterized parameters: duration, interval, length, and spacing. Temporally, transiency in flash rips, depicted by rip durations, is mostly (~85-100%) between a few seconds (<30 sec) and less than 2 minutes in all three events and are

consistent with previous studies[11,12]. Pulsation of flash rips, measured by the interval between two consecutive occurrences, exhibits significantly lower frequencies in the cloudy day *Event I* (July 12, 2017, mean ~21 min) than in the sunny day *Event II* (May 25, 2019, mean ~3 min), and in the high-wave day *Event III* (May 22, 2019, mean ~54 sec). Very low frequency motions (VLFs, >2 min) are also seen pronounced in *Event I* and *II* (see Fig 3-2d, e) with occurrence fractions of 73% and 65%, compared with those of 28% for the high-wave day *Event III* (Fig 3-2e). Spatially, the extent of flash rips, described by rip lengths measured away from the shore, shows more than 50 m in all three events. Specifically, flash rips in *Event III* of high waves tend to develop offshore distances (median ~ 41m) approximately twice those observed in *Event I* (median ~19 m) and *II* (median ~18 m) under the relatively low waves. The spacing of flash rips, defined as the distances between the centroid locations of neighboring rip-induced plumes, reveals smaller spacings but more rip pulses in *Event II* (see Fig 3-2b, e), in comparison with the larger spacings but fewer rip pulses on *Event I* (see Fig 3-2a, e) and *III* (see Fig 3-2c, f). Furthermore, high variability in rip locations (σ~200 m) during the *Event I* and *II* is about twice of that during the high-wave event *III* (σ ~100m), suggesting that ubiquitous but uniformly distributed flash rips can be more likely in conditions without large waves. Overall, in all three events, transient flash rips exhibit intermittent pulsations of VLFs (> 2 min) are observed. Interestingly, flash rips occurring on the low wave days (*Event I, II*) tend to appear more ubiquitously with larger spatial variations than those on the high wave day (*Event III*), thus imposing higher risks of the hidden and unexpected dangers to beach swimmers.

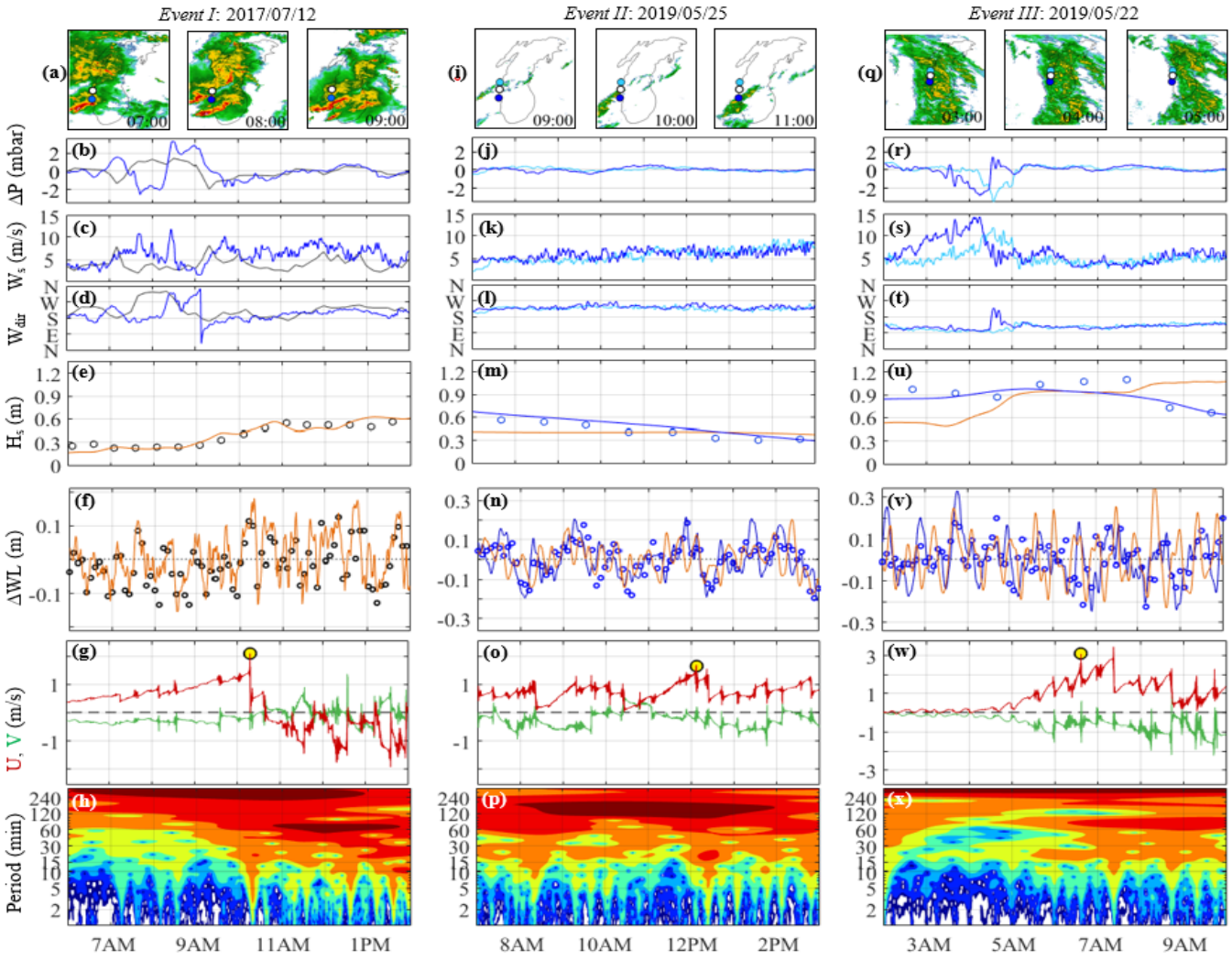

Fig 3-3 (**a,i,q**) Atmospheric conditions of radar reflectivity images showing propagation of associated convective storms, with dots overlaid to represent observation stations (white-PW, blue -KMKE, cyan - KSBM). Time series of (**b,j,r**) air pressure disturbances (ΔP), (**c,k,s**) wind speed (W_s), and (**d,l,t**) wind directions (W_{dir}). (**e,m,u**) Time series of wave heights (H_s) measured at PW (black dots) and measured at the South Lake Michigan (SLM) buoy (45007, blue dots), with model outputs for the same locations of PW (orange lines) and SLM (blue lines). (**f,n,v**) Time series of water level fluctuations at PW (black dots) and nearby gage MKE (blue dots), with model outputs for the same locations of PW (orange lines) and MKE (blue lines). (**g,o,w**) Time series of model outputs of velocities (U, cross-shore in red lines, and V, alongshore in green lines, also see Fig 3-4 for coordinate definition) at locations indicated by the yellow dots in Fig 3-4. (**h,p,x**) Time series of wavelet power spectrum for velocities at the same location as shown in velocity timer series plots (g,o,w).

Meteorological conditions leading to the observed flash rips of the three events are investigated here. Fig 3-3 (a-d, i-l, q-t) shows atmospheric observations including convective storms, atmospheric pressure perturbations (ΔP), surface winds speed (W_s), and directions (W_{dir}). The *Event I* on July 12, 2017, the cloudy day event, is associated with convective bows which propagated across Lake Michigan easterly (~100° clockwise relative to the True North) at a speed of 13.3 m/s and arrived on the west coasts between 07:00 and 09:00 (see Fig 3-3a). The atmospheric pressure perturbations were up to 3.4 hPa at Port Washington, WI (PW, see the grey line in Fig 3-3b) and reached up to 5.9 hPa at the nearby ASOS station in Milwaukee, WI (KMKE, see blue line) with a maximum gradient of 3.5 hPa/10 min to initiate meteotsunamis. Surface wind disturbances exhibited sporadic peaks above 5 m/s with a maximum speed of 8.1 m/s at PW and 11.8 m/s at KMKE (see Fig 3-3c). The south winds also shifted into north winds during the passage of the storms (see Fig 3-3d). The atmospheric disturbances could potentially induce meteotsunamis of initial height near 9.2 cm, with 65% contributed from the pressure perturbations dominantly. The *Event II* of May 25, 2019, the sunny day event, occurred after a convective cluster had propagated southward (~ 178°) along the west shore at a speed of 11.1 m/s and passed PW around 10:00 (see Fig 3-3i). Though at PW observation was temporally unavailable, the atmospheric pressures and surface winds can be inferred from data of two nearby stations at Sheboygan, WI (KSBM, see cyan lines), and KMKE (see blue lines). As shown in Fig 3-3 (j), barely any pressure perturbation was induced by the convective cluster. Surface winds (see Fig 3-3k), with speeds, gradually increasing from ~5 m/s to ~10 m/s and the directions (see Fig 3-3l) maintained at the southwest, were the dominant driver. Lastly, the *Event III* of May 22, 2019, the high-wave event, occurred after a convective complex had propagated northwards (~14°) across Lake Michigan at a speed of 13.8 m/s as shown in Fig 3-3(q). The storm-induced perturbations were observed

consequently at KMKE (blue lines) and KSBM (cyan lines) with a 30-min time delay. Atmospheric pressures exhibited drops close to 4 hPa at both stations (see Fig 3-3r). Surface winds had reached the maximum speeds of 14.4 m/s at KMKE and 11.8 m/s at KSBM (see Fig 3-3s) consequently and sustained above 5 m/s hours afterward. The east wind directions were observed throughout the day while a transient shift (lasting ~20 min) into the southwest direction was observed at KMKE around 09:30 when the complex left. The atmospheric disturbances ended up with not only large wind waves as observed in images (see Fig 3-2c), but also meteotsunamis of an initial height estimated to be 22.6 cm, of which 78% were contributed from the wind stresses dominantly. In short, pressure perturbations observed in *Event I* and wind stresses in *Event II, III*, exhibiting similar atmospheric features as previously reported events in Lake Michigan[13], are closely related to the observed flash rips.

Hydrodynamic conditions of wind waves (H_s) and high-frequency water level fluctuations (ΔWL) associated with the observed flash rips are examined in Fig 3-3. In *Event I*, nearshore waves at PW exhibited increasing heights but remained H_s < ~0.6 m (see black dots in Fig 3-3e), in consistency with visual signatures shown in Fig 3-2(a). High-frequency water level oscillations at PW also exhibited an increase in fluctuations (ΔWL) from ~0.15 m before the storm to ~0.25 m afterward (see black dots in Fig 3-3f). Nearing the time of the flash rips snapshot (10:15 as shown in Fig 3-2a), the largest oscillations of ΔWL = 0.33 m at a period T_{WL} = 42 min were identified as meteotsunamis, likely the cause for flash rips occurred on July 12, 2017. In *Event II*, decreasing wave heights were observed in south Lake Michigan at the NDBC buoy (45007, see blue dots in Fig 3-3m). At PW nearshore, low waves were found with H_s ~ 0.3 m (see orange line). Pronounced high-frequency water level oscillations were observed at the nearby Milwaukee gage (see blue dots in Fig 3-3n), also affecting PW (see orange line). When flash rips were observed, sustained

ΔWL ~0.4 m with periods near T_{WL} ~ 2.2 hours, which coincides with the standing wave mode in Lake Michigan[25], i.e. the seiches, thus considered as the possible cause for flash rips observed on May 25, 2019. In *Event III*, observed hydrodynamic conditions show that wind waves in south Lake Michigan had reached H_s >0.9 m (see blue dots in Fig 3-3u). Nearshore waves at PW (see orange line in Fig 3-3u) is also found to increase with the storm arrival and sustained above H_s> 0.9 m for hours, resulting in intensely wave breaking as depicted in Fig 3-2 (c). Meteotsunamis of a maximum height ΔWL = 0.4 m and a period of T_{WL} = 74 minutes were also identified at the nearby Milwaukee gage near the same time of storm disturbances (see blue dots in Fig 3-3v). At PW (see orange line), associated high-frequency water level fluctuations also reached ΔWL = 0.5 m, becoming particularly pronounced after 08:00. Wind waves and meteotsunamis are both possible to cause the flash rips observed on May 22, 2019. Overall, results suggest that hydrodynamic conditions of meteotsunamis (*Event I*, *III*), seiches (*Event II*), and wind waves (*Event III*) are causes for the observed flash rips.

Very low frequency motions (VLFs) in flash rips related to the MIWLOs are examined using the integrated atmospheric-hydrodynamic modeling. Specifically, temporal characteristics of VLFs are illustrated by the repeating velocity spikes of flash rips in the three events. Fig 3-3 (g, o, w) shows the time series of nearshore currents (cross-shore velocity U in red lines, the alongshore velocity V in green lines), revealing that flash rips with durations ~ 1 min pulsate in intervals from a few minutes to about an hour, which is consistent with the temporal pattern observed in Fig 3-2 (d, e, f). For each event, linkages between flash rip VLFs and MIWLOs are depicted by the energetic oscillations in the velocity wavelet power spectrum (WPS, normalized by variance, see Fig 3-3h, p, x). For *Event I* in Fig 3-3 (h), the VLFs are particularly pronounced at 10:15, 12:30, 13:30 with the energetic oscillations are seen at periods around 10-25 min and

around 45 min. The VLF signatures are exhibited to connect between the flash rip velocity spikes (~1 min) and lower frequency oscillations (~75 min, around 11:00-13:30) of the meteotsunamis (see Fig 3-3f). For *Event II* in Fig 3-3 (p), VLF signatures that connect to the flash rip velocity spikes, are pronounced at 8:20, 12:30, and 13:40, and 14:40 with periods same as in *Event I* (see Fig 3-3h) around 10-25 min. Meanwhile, the lower frequency oscillations from 08:00 to 14:00 are related to the seiches with the period around 2.2 hours (see Fig 3-3n). Lastly, for *Event III* in Fig 3-3x, similarly, the VLFs of period 10-40 min are exhibited connecting the flash rips such as at 6:00, 7:20 and 8:40, while the energetic lower frequency oscillations (60~90 min) are also related to the meteotsunamis that occurred simultaneously (see Fig 3-3v). Furthermore, the energic velocity oscillations with similar periods as those of associated meteotsunamis (*Event I, III*) or seiches (*Event II*) suggest that the observed VLFs likely are directly induced by the MIWLOs (see path ② in Fig 3-1c). Overall, signatures of VLF depicted by the time series and the WPS of velocities further elucidate that the temporal characteristics of flash rips induced by MIWLOs, i.e. transiency and intermittency, pose repeatable dangers to beach users.

Processes of generating the observed flash rips are elucidated in the spatial patterns of velocities and vorticities shown in Fig 3-4 (a, b, c) for the three events, respectively. For *Event I*, the meteotsunami induces five flash rips (see yellow arrows in Fig 3-4a, labeled from ① to ⑤) are revealed in the eddies induced by shear instability of meandering longshore currents. At the instant (10:15), the speed of the flash rip ③ has reached the velocity spike of >2 m/s (see the yellow circle in Fig 3-3g). Meanwhile, rapidly increasing water levels of the meteotsunamis (see Fig 3-3f) induces the longshore currents of speeds ~1 m/s as shown in Fig 3-4 (a), which suggest that the observed VLFs are also related to the nearshore transformation processes (see path ① in Fig 3-1c). The strong longshore currents drive flash rip vortex pairs, but also act the barrier of the eddies

to shed farther offshore-wards, resulting in that flash rips are mostly constrained within ~20 m distance from the shoreline. The spatial pattern of flash rips in rip spacings of ~50 m is in consistency with the observed plumes shown in Fig 3-2 (a, d). The repeatable dangers due to VLFs of flash rips in *Event I* can be further elevated, due to spatial characteristic of ubiquitous locations of the flash rips induced by meteotsunamis.

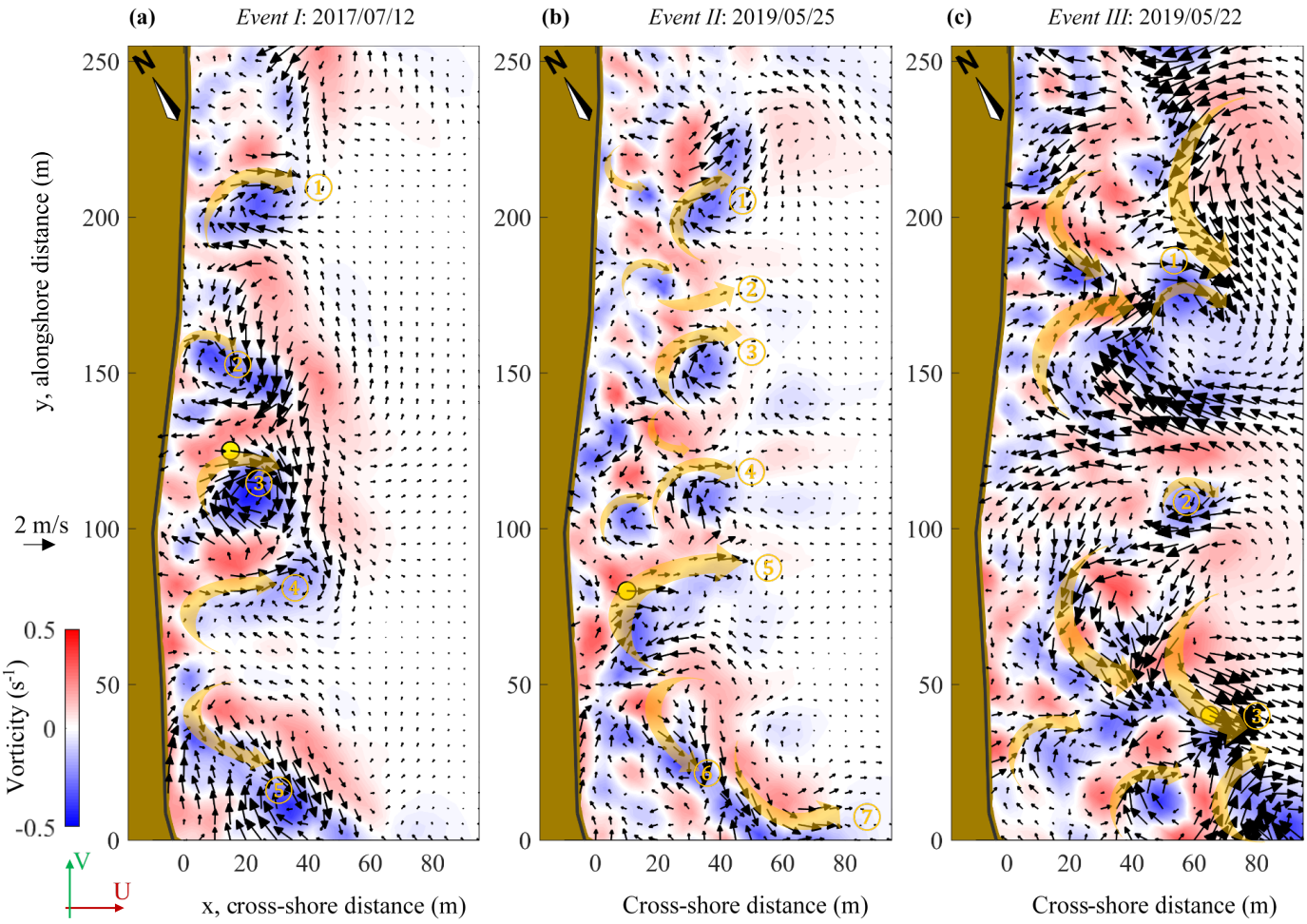

Fig 3-4. Flash rips revealed in nearshore current velocity vectors (black arrows) plotted on top of vorticity color contours at the instances indicated by yellow dots on Fig 3-3 (g,o,w). Pronounced flash rip plumes are highlighted in shaded yellow arrows and labeled in numbers.

For *Event II*, seiches induce seven flash rips (see yellow arrows) resolved in Fig 3-4(b) at the time of 12:06. When the velocities of flash rip ⑤ reach the spike of 1.5 m/s (see the yellow circle in Fig 3-3(o), the water level is decreasing rapidly (Fig 3-3n) but the wind wave height remains as low as 0.4 m (Fig 3-3m). The seiche receding water levels create offshore-directed currents and the cross-shore shear instability induces eddies (see Fig 3-4b). Flash rips, generated from the vortex pairs of size ~20 m, are mostly located at distances of 30-40 m from the shoreline and in non-uniform spacings between 10 - 60 m, in consistency with the spatial characteristics observed in images (see Fig 3-2b, e). Different from those induced by meteotsunamis in Fig 3-4 (a), flash rips induced by seiches can potentially propagate farther offshore into the deep water without strong longshore currents as a barrier, such as the flash rip ⑦ in Fig 3-4 (b). In addition to the ubiquity, flash rips in *Event II* also exhibit spatially variability in offshore extents, elucidating the characteristics of spatial unpredictability in flash rips induced by seiches.

For *Event III*, combined effects of meteotsunamis and wind waves induce three flash rips, mostly are converged from offshore-directed flows of multiples eddies as shown in Fig 3-4 (c). At the instant (6:36), velocity spike of flash rip ③ reaches speed >3 m/s (see the yellow circle in Fig 3-3w), when the wave heights have increased to H_s ~ 0.9 m (see Fig 3-3u) and the water level is about to start receding after a peak (see Fig 3-3v). The flash rips are mostly located at 40-60 meters from the shoreline, where surf zone eddies of size ~50 m are generated by wave breaking. In comparison with the previous two events (Fig 3-4a, b), the spatial offshore extents of flash rips reach beyond farther >90 m into deep water, also in consistency with the trend of observed rip lengths (see Fig 3-2c, f). Meanwhile, nearer to the shoreline at x ~20 m, additional vortex pairs in opposite directions are also seen due to the modulations of the meteotsunami on water depths that change breaking locations. The combined effects of meteotsunamis and wind waves further add

spatial variability to the nonstationary locations of flash rips. In brief, processes of flash rip generation include the meteotsunami-induced shear instability of longshore currents (*Event I*), which is similar to previously reported event[13], and the cross-shore shear instability of seiches-induced receding flows (*Event II*) and meteotsunami-modulated wave breaking vorticities (*Event III*), which are reported for the first time.

3.3 Discussion

Flash rips characteristics induced by meteorologically induced water level oscillations (MIWLOs) can result in repeating hazards that were previously not recognized. Specifically, the temporal characteristics of very low frequency motions (VLFs) lead to transient and intermittent occurrences, adding upon by the spatial characteristics of ubiquitous and unpredictable locations to further elevate flash rip risks to the unawareness of beach users. Both meteotsunamis and seiches, two kinds of MIWLOs, are revealed to generate flash rips in offshore-shedding eddies of meteotsunami-induced longshore meandering currents and two newly uncovered processes. One is the seiches-induced cross-shore shear instability currents and the other is the meteotsunami-modulated wave breaking vortices. Occurrences of flash rips are observed in cloudy and sunny weathers, low and high waves. The mix conditions of MIWLOs-induced flash rips suggest that the hidden, unexpected hazards can occur more ubiquitous and frequently than expected nor recognized.

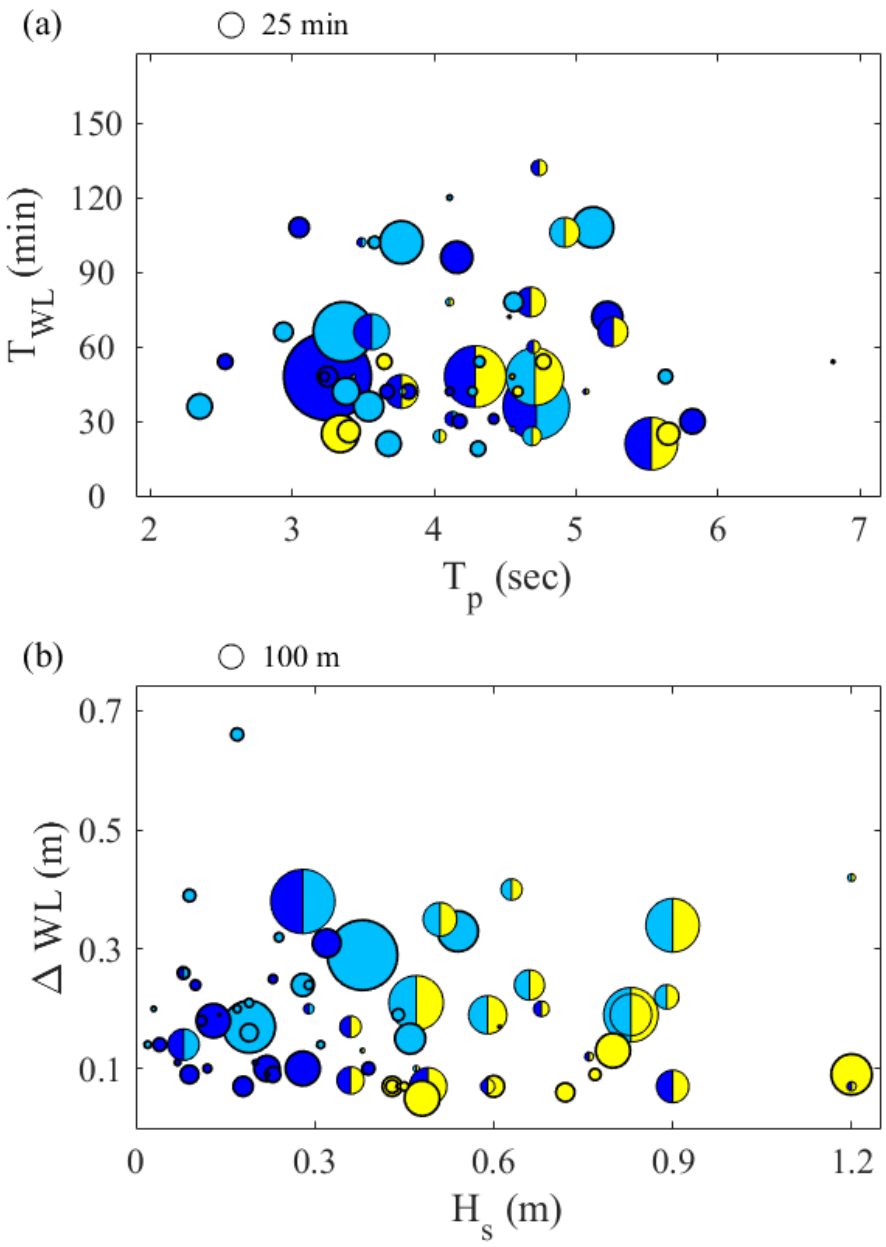

Fig 3-5. Distributions of associated processes in a total of 69 events of flash rip-induced sediment plumes observed at North Beach of Port Washington in 2016-2019. Each flash rip event is represented in a circle, color coded according to associated processes that can lead to the observed flash rips: meteotsunamis (such as *Event I* on 2017/07/12) in light blue, seiches (such as *Event II* on 2019/05/25) in dark blue, wind waves in yellow, or the combinations (such as *M&W Event III* on 2019/05/22). The distributions are plotted in (**a**) wind wave period (T_p) versus water level fluctuation period (T_{WL}), with event circles scaled based on the rip pulsations, and (**b**) significant wave heights (H_s) versus water level fluctuations (ΔWL), with event circles scaled based on the rip extents of observed rip plumes.

How many flash rips are induced by MIWLOs, in comparison with wind waves, during the study period? Compiling observations for a total of 69 events during 2016-2019 at the North Beach of Port Washington, the causative processes including meteotsunamis (denoted as *M*), seiches (denoted as *S*), wind waves (denoted as *W*) and the combinations are listed in Table 3- 1. Fraction-wise, a majority of 55% events are associated with only meteorologically induced water level fluctuations (i.e. *M*, *S*, or *M*&*S*), and 38% with combinations of both (i.e. *M*&*W*, *S*&*W*), in comparison with the 17% with wind waves only. Furthermore, types of atmospheric disturbances show that events associated with meteotsunamis (*M*, *M*&*W*) are mostly featured with pronounced pressure perturbations ΔP ~3 hPa, while events associated with wind waves and/or seiches (*S*, *W*, *S*&*W*) are usually during large wind speeds W_s >10 m/s and long durations Δt_w ~ 7-8 hours (see Table 3- 1). This result suggests that MIWLOs can be induced by either pathway of atmospheric disturbances, in comparison with wind generated waves. Overall, event statistics show that MIWLOs can result in flash rip occurrences more frequently than wind waves.

Table 3-1. Summary of flash rip events at North Beach, Port Washington

Processes	Fractions	Rip pulsations (min)	Rip extents (m)	ΔP (hPa)	W_s (m/s)	Δt_w (min)
M	26%	25	79	2.9	10.4	1.5
S	23%	22	67	0.9	10.2	8.5
W	13%	23	95	0.7	8.1	7.6
M & *S*	6%	32	122	1.4	8.4	3.2
M & *W*	17%	18	129	2.7	10.3	4.8
S & *W*	15%	25	74	1.0	10.3	8.1

How are flash rip characteristics affected by the hydrodynamic conditions under MIWLOs or wind waves? For all events during the study period, observed flash rips show average rip pulsations ~ 25 min and rip extents ~100 m despite different causative processes (see Table 3- 1), exhibiting that the VLFs characteristics and spatial scales, consistent with those in the three example events, are ubiquitous in flash rips. For each event individually, the temporal rip pulsations are related to the wind wave periods (T_p) and the water level fluctuation period (T_{WL}) as shown in Fig 3-5 (a), and in Fig 3-5 (b) the spatial rip extents are related to the significant heights of wind waves (H_s) and the water level fluctuations (ΔWL). Fig 3-5 (a) shows that flash rips are mostly (71%) occur under wind wave periods T_p ~3-5 sec and mostly (68%) under high-frequency water level fluctuations of periods T_{WL}< 1 hr. Interestingly, events with rip pulsations >60 min (large circles) or those <10 min (small circles) are mostly associated with combination processes (*M&S, M&W, S&W*), while events with pulsations close to the average of 25 min are mostly associated with *M*, *S*, or *W* alone. This finding suggests that the interactions between MIWLOs and wind waves could change the VLFs in either direction, thus adding the unpredictability in recurring flash rips and the repeatable dangers to beach swimmers. In Fig 3-5 (b), events associated with meteotsunamis (*M,* light blue) tend to cluster at large water level fluctuations ΔWL >0.1 m, those associated with seiches (*S,* dark blue) tend to cluster at low wave heights, and those associated with wind waves (*W*, yellow) tend to cluster at large wave heights. Flash rips with large extents (large circles) are mostly associated with the combined process (*M&W, M&S*), shown in Fig 3-5 (b) and Table 3- 1, suggesting that interactions between meteotsunamis and wind waves/seiches can amplify flash rips than the those generated by meteotsunamis alone. We particularly pay attention to flash rips events under both low wave heights and low water level fluctuations below 0.3 m due to the hidden danger. The 39% events are also mostly associated

with seiches (dark blue circles), such as the observed *Event II* during a sunny weather day on 2019/05/25 (see Fig 3-2b), suggesting that MIWLOs, in comparison with wind waves, can pose higher risks due to unrecognized or unexpected hazards. When the water appears misleadingly calm and the weather seems attractively sunny, unaware beachgoers may decide to get into the water and be exposed to a dangerous condition due to the hidden flash rip hazards.

How ubiquitous are flash rips induced by MIWLOs? We compile statistics of rip current related incidents on the Great Lakes coasts from the Great Lakes Current Incident Database (data since 2002) and those of the ocean coasts of the continental Unites States from the National Weather Service Storm Data database[2] (data since 1996). A total of 2083 rip current events including 293 on the Great Lakes are plotted on the United State continental map as shown in Fig 3-6 (a). Note that we use one "event" to consolidate for multiple records of incidents (fatalities or rescues) on the same day/location, due to the characteristics of repeated occurrences in rip current events. Spatially, rip incident events are seen clustered mostly on the East Coasts (30%) and the Gulf Coasts (46%), while some hotspots (>2 incidents/year) also occur on the Great Lakes coasts (14%). Furthermore, possible causative processes for incident events are categorized into MILWOs (blue circle), wind waves or swells (yellow), and unknowns (green). An event is categorized as MIWLOs if high-frequency water level oscillations (meteotsunamis or seiches) are detected[14,24] based on nearby water level gage data for the Great Lakes coasts, or as wind waves/wells if high wave conditions[2] are documented in incident reports, and the rest as unknowns. Note that a hotspot region for MILWOs associated rip currents is the Lake Michigan, where at least 7 events per year are estimated, including meteotsunamis related events[13]. Percentage-wise (see Fig 3-6b), on the Great Lake coasts, the MIWLOs (blue color) are found the possibly causative processes for about 70% of the rip current incidents. For each lake, the percentages of MIWLOs

are 75% in Lake Michigan, 67% in Lake Eire, 61% in Lake Superior, 82% in Lake Huron, and 54% in Lake Ontario. On the ocean coasts, though wind waves or swells (yellow color) are the dominant processes to cause the rip current incidents, there are still 24% of the incidents on the East coast, 27% on the Gulf coast, and 30% on the West coast, occurred in days without large waves or swells reported. Among those unknown (green) incidents, we further discovered that storm conditions were mentioned in 47% of the incidents reported. This finding suggests that storm-related MIWLOs, such as meteotsunamis which have been observed to occur on US oceanic coasts[45,46], are possible causes for the unknown incidents. Detailed data investigation for these rip current events can be further conducted in the future. Overall, in view of the high percentage of MIWLOs associated rip currents on the Great Lakes coasts, the co-occurrences of storms and incidents on oceanic coasts suggest that rip currents generated by MIWLOs can occur ubiquitously, posing unrecognized hazards to all coastal communities.

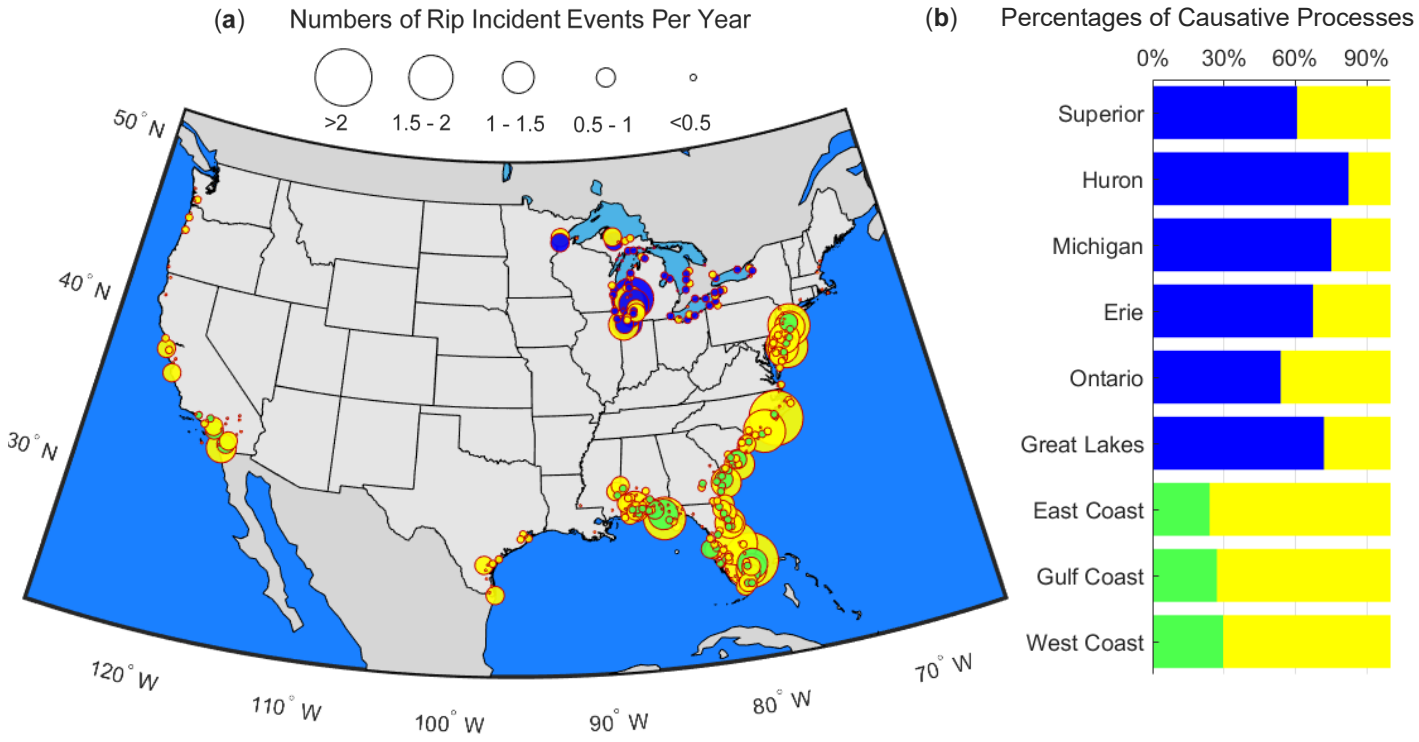

Fig 3- 6. (**a**) Rip current incident events on major coasts of the United States, including the Great Lakes. Number of incidents per year shown by the circle size. The circle color indicates the likely causative processes of rip current generation (see Fig 3-1): blue – MIWLOs (meteotsunamis or seiches), yellow - wind waves or swells, green – unknown/others. (**b**) Percentages of causative processes in reported rip current incidents on the five Great Lakes coasts, and on the East, Gulf and West coasts.

3.4 Methods

Flash rips occurrences are characterized using images captured by the Lifeguarding Operational Camera Kiosk System (LOCKS)[12] at the North Beach of Port Washington, WI. Images are recorded continuously throughout the day in full resolution (3072 by 2048 pixels) and a sampling interval of 5 sec. Flash rips are identified based on signatures of sediment plumes using image processing procedures described in LOCKS, including segmenting morphological features,

ortho-rectifying coordinates, and detecting plumes[12]. Temporal and spatial features of flash rips are parameterized in duration, interval, length and spacings. Duration is counted from the first detected presence of sediment plumes until no offshore-directed propagations for the same plume are detected. Interval is the time between the last appearance of sediment plumes and the first detected appearance of new plumes perceived with different shapes or locations. Length is measured as the distance from the shoreline to the maximum offshore extent in each plume. Spacing is the distance shore-parallel direction between the centroid of two neighboring plumes.

Environmental conditions of atmospheric and hydrodynamic observations are compiled from multiple sources. First, reflectivity radar NEXRAD composite images from the Iowa Environmental Mesonet with 1-km spatial resolution and 5-min interval are used to identify atmospheric storm structures. Second, meteorology data of surface winds and atmospheric pressure data are obtained from nearby stations, including (i) PWAW3 (see white dots in Fig 3-3a, i, q), of the NOAA National Data Buoy Center (NDBC) network at the Port Washington Marina providing data at 10-min interval; (ii) the LOCKS weather unit, which is a Young ResponseONE Weather Transmitter of the providing 1-min data; (iii) KMEK (see blue dots in Fig 3-3a, i, q) and KSBM (see cyan dots in Fig 3-3i, q), the two nearby Automated Surface Observing System (ASOS) at Milwaukee and Sheboygan providing 1-min data. A high-pass digital filter with a 2-hour cut-off frequency is used to obtain to storm-related high-frequency atmospheric pressure perturbations. The pressure perturbations and wind shear stresses associated with storm structures are used to calculate relative contributions of atmospheric pressure (%P) and wind (%W) disturbances[24]. Third, an ultrasonic Echologger sensor with a 5 Hz sampling frequency was at Port Washington to obtain nearshore wind wave climates. The nearshore significant wave heights and peak wave periods are calculated using a 5-min window. The offshore NDBC buoy 45007

providing 1-hour wave climates in the southern Lake Michigan basin is used. Lastly, water level data include water altitude measurements by the Echologger with applying a 1-min moving average filter and the 6-min interval data from the NOAA National Ocean Service gage at Milwaukee. A high-pass digital filter with a 6-hour cut-off frequency is applied on water level time series to obtain oscillations in the frequency band of meteotsunamis and seiches[17]. The zero-crossing method is employed to calculate individual wave height from the filtered time series[47]. Meteotsunamis are identified if water level oscillations are identified as if the wave height exceeds gage-specific thresholds, the period falls in the 2-min to 6-hour range, and atmospheric disturbances are associated with storm structures[24]. Seiches are identified if water level oscillations meet the meteotsunami criteria but there was no storm associated atmospheric disturbance[24].

Nearshore hydrodynamics of flash rips are revealed using integrated atmospheric-hydrodynamic modeling, a Semi-implicit Cross-scale Hydroscience Integrated System Model (SCHISM[48]) coupled with the 3rd generation spectral Wind Wave Model (WWM III[49]). Atmospheric forcings are created from the hourly spatial fields of NOAA High-Resolution Rapid Refresh (HRRR) atmospheric model outputs and refined in time and space to match with the discrete point observations at ASOS stations across Lake Michigan, since atmospheric storm disturbances with frequency of O (1min) are critical in initiating meteotsunamis. Currents velocity and waves fields are solved in SCHISM-WWM based on the time- and depth-averaged Reynolds-averaged Navier–Stokes (RANS) equations, and wave fields are repetitively updated based on the evolving currents[50,51]. Wave averaging approach has been successfully deployed in modeling flash rip caused by meterotsunmmis[24], longshore shear currents[29] and wave group-generated vortices[41]. Furthermore, we specify coupling to take place at every time step of the two models to resolve wave-induced vortices in generating flash rips[13,1]. Spatial grid resolutions are refined to O (1m) at

the shoreline of Port Washington and gradually increased to O (100 m) towards offshore to seamlessly merge into the large lake scale mesh. High-spatial resolution coastal bathymetry from the 2012 USACE NCMP Topography Survey is used. Details of the model configurations have been documented in previous studies[13], which have successfully simulated the generation of flash rips related to convective storms and meteotsunamis at several other beaches along the Lake Michigan coasts. Model simulations for events of July 12, 2017, May 22, and May 25, 2019, are presented in this study. The model outputs are compared with observed wind waves and water level fluctuations (see Fig 3-3). Wave climates at nearshore PW (Fig 3-3e) and in southern Lake Michigan basin (Fig 3-3m, u) show reasonable matching of the wave heights. The water level fluctuations at PW (Fig 3-3f) and MKE (Fig 3-3n, v) also show that the dominant fluctuations were resolved in the model. Also, note that embedded higher frequency components are present in the model result but not in observation data, likely due to the coarser sampling schemes of the NOS water level gages that were used in this study. Flash rips are successfully simulated. Time series of the nearshore velocities and spatial fields of vorticities and velocity vectors are plotted in Fig 3-3. Wavelet analysis[52,53] is also used to reveal the time and frequency features of flash rip pulsations. The wavelet power spectrum of current speeds is calculated using a Morlet mother wavelet function and normalized by the variance[52]. Overall, the integrated atmospheric-hydrodynamic modeling is successfully employed to provide additional information on the characteristics and generation processes of flash rips.

3.5 Acknowledgements

This study was supported by the Wisconsin Coastal Management Program (WCMP), National Oceanic and Atmospheric Administration (NOAA) Coastal Storms Program, University of Wisconsin Sea Grant Institute (UW-Sea Grant), and local friends of Port Washington group. We would like to thank Mr. Todd Breiby, Ms. Angel Kathleen, and Mr. Michael Friis, from WCMP for their support in coordination, education, and outreach for rip current safety. In addition, Ms. Moira Harrington at UW-Sea Grant for their dedication to communicating rip current hazards to the Great Lakes community is acknowledged. Mr. Dan Buehler, Mr. Dennis Cherny, Mr. Jon Crain, and Ms. Kiley Schulte, and many staff at the City of Port Washington, WI for the assistance in field measurements and maintenance of the real-time camera observation system are acknowledged. The authors especially thank Mr. Tom Mlada and Marty Becker, former and current Mayor of the City of Port Washington, respectively, for their support to emphasize the importance of providing rip current warning for beach safety. We specifically thank Dr. Alvaro Linares for guiding the multiple-scale integrated atmospheric-hydrodynamic modeling.

3.6 References

1. Castelle, B., Scott, T., Brander, R. W. W. & McCarroll, R. J. J. *Rip current types, circulation and hazard*. *Earth-Science Reviews* vol. 163 1–21 (Elsevier, 2016).
2. Gensini, V. A. & Ashley, W. S. An examination of rip current fatalities in the United States. *Nat. Hazards* **54**, 159–175 (2010).
3. MacMahan, J. H., Thornton, E. B. & Reniers, A. J. H. M. Rip current review. *Coast. Eng.* **53**, 191–208 (2006).
4. Winter, G., van Dongeren, A. R. R., de Schipper, M. A. A. & van Thiel de Vries, J. S. M. S. M. Rip currents under obliquely incident wind waves and tidal longshore currents. *Coast. Eng.* **89**, 106–119 (2014).
5. Reniers, A. J. H. M., MacMahan, J. H., Thornton, E. B. & Stanton, T. P. Modelling infragravity motions on a rip-channel beach. *Coast. Eng.* **53**, 209–222 (2006).
6. Castelle, B. & Coco, G. Surf zone flushing on embayed beaches. *Geophys. Res. Lett.* **40**, 2206–2210 (2013).
7. Scott, T., Austin, M., Masselink, G. & Russell, P. Dynamics of rip currents associated with groynes — field measurements, modelling and implications for beach safety. *Coast. Eng.* **107**, 53–69 (2016).
8. Pattiaratchi, C., Olsson, D., Hetzel, Y. & Lowe, R. Wave-driven circulation patterns in the lee of groynes. *Cont. Shelf Res.* **29**, 1961–1974 (2009).
9. Dalrymple, R. A., MacMahan, J. H., Reniers, A. J. H. M. & Nelko, V. Rip Currents. *Annu. Rev. Fluid Mech.* **43**, 551–581 (2011).
10. Murray, T., Cartwright, N. & Tomlinson, R. Video-imaging of transient rip currents on the Gold Coast open beaches. *J. Coast. Res.* **165**, 1809–1814 (2013).

11. Floc'h, F. *et al.* Flash Rip Statistics from Video Images. *J. Coast. Res.* **81**, 100–106 (2018).

12. Liu, Y. & Wu, C. H. Lifeguarding Operational Camera Kiosk System (LOCKS) for flash rip warning: Development and application. *Coast. Eng.* **152**, 103537 (2019).

13. Linares, Á., Wu, C. H., Bechle, A. J., Anderson, E. J. & Kristovich, D. A. R. Unexpected rip currents induced by a meteotsunami. *Sci. Rep.* **9**, 2105 (2019).

14. Bechle, A. J. *et al.* Meteotsunamis in the Laurentian Great Lakes. *Sci. Rep.* **6**, 37832 (2016).

15. Anderson, E. J. *et al.* Reconstruction of a meteotsunami in Lake Erie on 27 May 2012: Roles of atmospheric conditions on hydrodynamic response in enclosed basins. *J. Geophys. Res. Ocean.* **120**, 8020–8038 (2015).

16. Bechle, A. J. & Wu, C. H. The Lake Michigan meteotsunamis of 1954 revisited. *Nat. Hazards* **74**, 155–177 (2014).

17. Linares, Á., Bechle, A. J. & Wu, C. H. Characterization and assessment of the meteotsunami hazard in northern Lake Michigan. *J. Geophys. Res. Ocean.* **121**, 7141–7158 (2016).

18. Monserrat, S., Vilibić, I. & Rabinovich, A. B. Meteotsunamis: atmospherically induced destructive ocean waves in the tsunami frequency band. *Nat. Hazards Earth Syst. Sci.* **6**, 1035–1051 (2006).

19. Šepić, J., Vilibić, I. & Monserrat, S. Quantifying the probability of meteotsunami occurrence from synoptic atmospheric patterns. *Geophys. Res. Lett.* **43**, 10,377-10,384 (2016).

20. Pattiaratchi, C. B. & Wijeratne, E. M. S. Are meteotsunamis an underrated hazard? *Philosophical Transactions of the Royal Society A: Mathematical, Physical and Engineering Sciences* vol. 373 (2015).

21. Proudman, J. The Effects on the Sea of Changes in Atmospheric Pressure. *Geophys. J. Int.*

2, 197–209 (1929).

22. Greenspan, H. P. The generation of edge waves by moving pressure distributions. (2020) doi:10.1017/S002211205600038X.

23. Munk, W., Snodgrass, F. & Carrier, G. *Edge Waves on the Continental Shelf*. *Source: Science, New Series* vol. 123 https://www.jstor.org/stable/pdf/1750948.pdf?refreqid=excelsior%3A76263e6ef2d6245878faec0261b31b7e (1956).

24. Linares, Á., Wu, C. H., Anderson, E. J. & Chu, P. Y. Role of Meteorologically Induced Water Level Oscillations on Bottom Shear Stress in Freshwater Estuaries in the Great Lakes. *J. Geophys. Res. Ocean.* **123**, 4970–4987 (2018).

25. As-Salek, J. A. & Schwab, D. J. High-Frequency Water Level Fluctuations in Lake Michigan. *J. Waterw. Port, Coastal, Ocean Eng.* **130**, 45–53 (2004).

26. Rabinovich, A. B. Seiches and Harbor Oscillations. in *Handbook of Coastal and Ocean Engineering* 193–236 (WORLD SCIENTIFIC, 2009). doi:10.1142/9789812819307_0009.

27. Bedford, K. W. The Physical Effects of the Great Lakes on Tributaries and Wetlands. *J. Great Lakes Res.* **18**, 571–589 (1992).

28. Feddersen, F. The Generation of Surfzone Eddies in a Strong Alongshore Current. *J. Phys. Oceanogr.* **44**, 600–617 (2014).

29. Özkan-Haller, H. T. & Kirby, J. T. Nonlinear evolution of shear instabilities of the longshore current: A comparison of observations and computations. *J. Geophys. Res. Ocean.* **104**, 25953–25984 (1999).

30. Peregrine, D. H. Surf Zone Currents. *Theor. Comput. Fluid Dyn.* **10**, 295–309 (1998).

31. Clark, D. B., Elgar, S. & Raubenheimer, B. Vorticity generation by short-crested wave

breaking. *Geophys. Res. Lett.* **39**, 2012GL054034 (2012).

32. Kirby, J. T. & Derakhti, M. Short-crested wave breaking. *Eur. J. Mech. - B/Fluids* **73**, 100–111 (2019).

33. Spydell, M. & Feddersen, F. Lagrangian Drifter Dispersion in the Surf Zone: Directionally Spread, Normally Incident Waves. *J. Phys. Oceanogr.* **39**, 809–830 (2009).

34. Dalrymple, R. A. A mechanism for rip current generation on an open coast. *J. Geophys. Res.* **80**, 3485–3487 (1975).

35. Johnson, D. & Pattiaratchi, C. Boussinesq modelling of transient rip currents. *Coast. Eng.* **53**, 419–439 (2006).

36. Sasaki, T. O. & Horikawa, K. Observation of Nearshore Current and Edge Waves. in *Coastal Engineering 1978* 791–809 (American Society of Civil Engineers, 1978). doi:10.1061/9780872621909.047.

37. Symonds, G. & Ranasinghe, R. On the Formation of Rip Currents on a Plane Beach. in *Coastal Engineering 2000* vol. 276 468–481 (American Society of Civil Engineers, 2001).

38. Bruneau, N., Castelle, B., Bonneton, P. & Pedreros, R. *Very Low Frequency motions of a rip current system: observations and modeling*. *Source: Journal of Coastal Research* vol. II (2009).

39. Elgar, S., Raubenheimer, B., Clark, D. B. & Moulton, M. Extremely Low Frequency (0.1 to 1.0 mHz) Surf Zone Currents. *Geophys. Res. Lett.* (2018) doi:10.1029/2018GL081106.

40. MacMahan, J. H., Reniers, A. J. H. M. & Thornton, E. B. Vortical surf zone velocity fluctuations with 0(10) min period. *J. Geophys. Res.* **115**, C06007 (2010).

41. Long, J. W. & Özkan-Haller, H. T. Low-frequency characteristics of wave group–forced vortices. *J. Geophys. Res.* **114**, C08004 (2009).

42. Geiman, J. D. & Kirby, J. T. Unforced oscillation of rip-current vortex cells. *J. Phys. Oceanogr.* **43**, 477–497 (2013).

43. Uchiyama, Y., McWilliams, J. C. & Akan, C. Three-dimensional transient rip currents: Bathymetric excitation of low-frequency intrinsic variability. *J. Geophys. Res. Ocean.* **122**, 5826–5849 (2017).

44. Marchesiello, P. *et al.* On tridimensional rip current modeling. *Ocean Model.* **96**, 36–48 (2015).

45. Shi, L., Olabarrieta, M., Nolan, D. S. & Warner, J. C. Tropical cyclone rainbands can trigger meteotsunamis. *Nat. Commun.* **11**, 1–14 (2020).

46. Šepić, J. & Rabinovich, A. B. Meteotsunami in the Great Lakes and on the Atlantic coast of the United States generated by the "derecho" of June 29–30, 2012. *Nat. Hazards* **74**, 75–107 (2014).

47. Bechle, A. J., Kristovich, D. A. R. & Wu, C. H. Meteotsunami occurrences and causes in Lake Michigan. *J. Geophys. Res. Ocean.* **120**, 8422–8438 (2015).

48. Zhang, Y. J., Ye, F., Stanev, E. V. & Grashorn, S. Seamless cross-scale modeling with SCHISM. *Ocean Model.* **102**, 64–81 (2016).

49. Roland, A. *et al.* A fully coupled 3D wave-current interaction model on unstructured grids. *J. Geophys. Res. Ocean.* **117**, (2012).

50. Yu, J. & Slinn, D. N. Effects of wave-current interaction on rip currents. *J. Geophys. Res. C Ocean.* **108**, 33–1 (2003).

51. Haas, K. A., Svendsen, I. A., Haller, M. C. & Zhao, Q. Quasi-three-dimensional modeling of rip current systems. **108**, 10–1 (2003).

52. Torrence, C., Compo, G. P., Torrence, C. & Compo, G. P. A Practical Guide to Wavelet

Analysis. *BAMS* **79**, 61–78 (1998).

53. Daubechies, I. & Sweldens, W. Factoring Wavelet Transforms into Lifting Steps. *J. Fourier Anal. Appl.* **4**, (1998).

4. Hidden flash rips related to convective storms in Lake Michigan

The following has been submitted to *Nature Communications*.

4.1 Introduction

Several drowning incidents spanning over the coast of Lake Michigan were reported during a series of convective storms in a 4-day period from July 18 to 21, 2019 (Fig. 4-1). The first storm starting at 1130 UTC of July 18 crossed the southwest shoreline. A few hours later, a drowning incident was reported around 0000 UTC of July 19 on the east coast near Ludington. At 0755 UTC, the second storm hit the northwest shore. Two incident rescues occurred around 1630-1700 UTC on the southeast shore near South Haven and one fatal incident was reported at 2300 UTC on the southwest shore near Kenosha. The third storm reported as a strong "derecho," landed on the northwest shore at 0225 UTC of July 20 and was followed by the fourth storm, which hit the northwest shore again at 1655 UTC. During these two storms, damages were reported around 0630-1045 UTC on the northeast shore near Little Traverse Bay and the north shore near Manistique due to rapidly increasing water levels, similar to the previously reported meteotsunami events in Lake Michigan[1]. Afterward, another drowning occurred on the south shore near Michigan City around 0130 UTC of July 21. The last two storms crossed the southeast shoreline at 0455 UTC and 1625 UTC, respectively. Shortly after, two incidents including one rescue on the east coast at Ludington around 1600-1900 UTC and one fatality on the southeast coast at Chicago around 2030 UTC occurred. The simultaneous occurrence of incidents and convective storms has been reported before. Linares et al.[2] found that 16% of incidents occurred on the same day of convective storms on the Lake Michigan, based on a fifteen-year (2002-2017) rip current database. Interestingly, a recent study on the west coast of Lake Michigan[3] over a two-year period (2016-

2017) showed that 90% of convective storms coincided with occurrences of flash rips[4,5], which are transient and intermittent rip currents[4]. In view of these observations, the cause of drownings is hypothesized to be convective storm induced flash rips, a hidden hazard to beach swimmers.

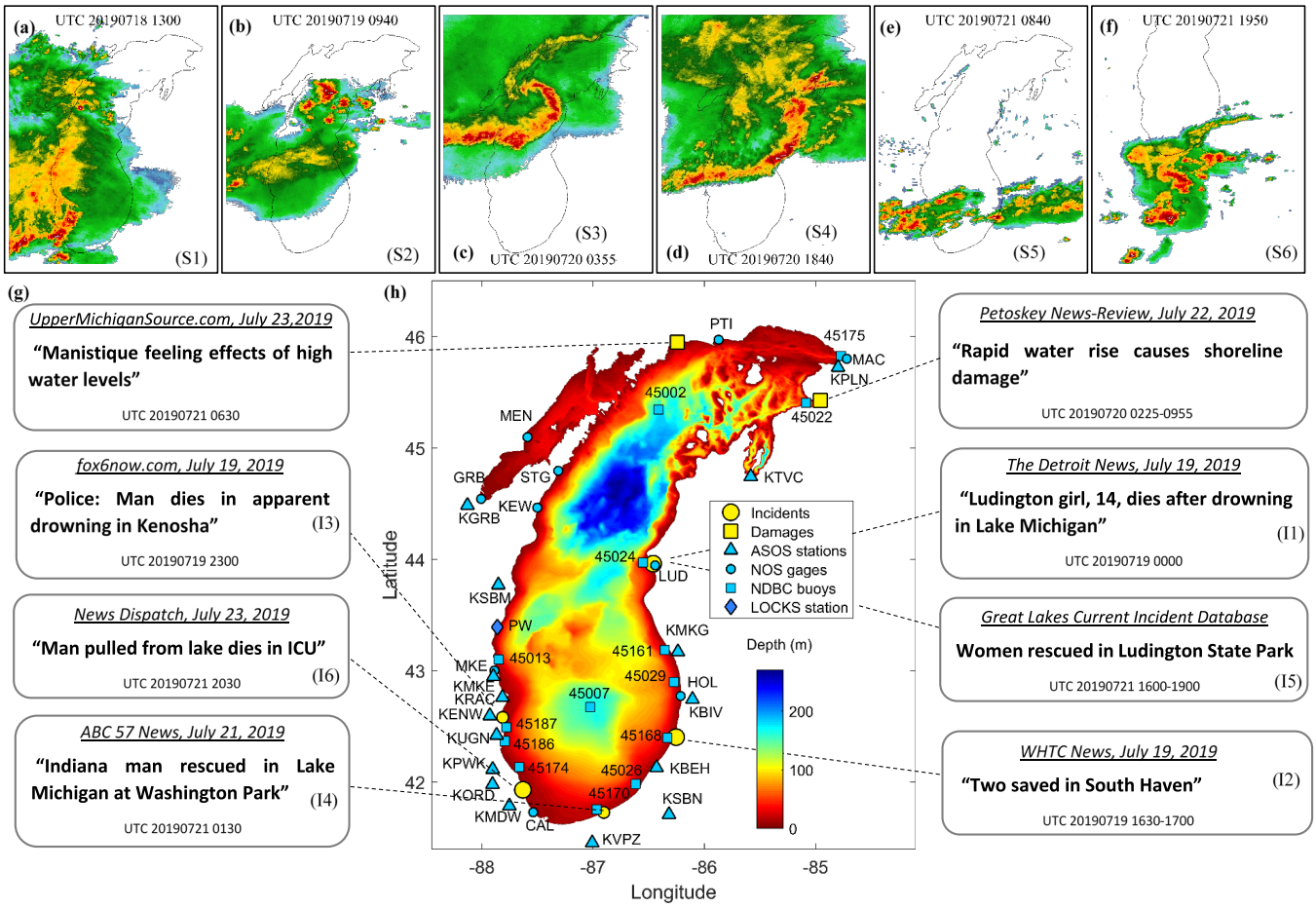

Fig. 4-1: Convective storms and drowning incidents in Lake Michigan. (a-f) A series of six convective storms crossed Lake Michigan on July 18-21, 2019 with reflectivity imagery from the Iowa Environmental Mesonet NEXRAD Composite database, (g) newspaper reports on drowning incidents (yellow dots) and water level-related damages (yellow squares) during the 4-day storm event. (h) Bathymetry of Lake Michigan. Available observations include 16 Automated Surface Observation System (ASOS) meteorology stations, 10 water level gauges operated by the National Ocean Service (NOS), 15 wave buoys operated by the National Data Buoy Center (NDBC), and 1 webcam (LOCKS) at Port Washington (PW).

Mechanisms of generating flash rips, which occur at featureless beaches or planar sections[4], involve various types of nearshore hydrodynamic processes. First, shear instabilities of longshore currents, under highly oblique incidence waves[6], can generate unsteady vortices as transient and non-fixed flows to offshore[7]. Second, short-crested wave breaking creates along-crest variations in wave dissipation[8,9]. Differential forcing between the breaking and the non-breaking regions results in changes in vorticity[4,10]. A fraction of the short-scale vorticity that is not dissipated by bottom friction can cascade into larger-scale surf zone eddies as out-busting water jets[6,11]. Third, wave groups and infra-gravity waves[12,13] can generate alongshore variations of radiation stress gradients that are imbalanced by spatial pressure gradients. The induced wave set-ups of high temporal variability[14] result in pulsating flows as transient rip currents[15,16]. Different from energic incident waves, meteorologically induced water level fluctuations like meteotsunamis (high-frequency water level oscillations with periods from a few minutes to two hours[17]) or seiches (basin-scale standing waves in an enclosed or semi-enclosed water body[18,19]) can induce nearshore currents during rapid runups and drawdowns of water levels, yielding unsteady vortices that shed offshore, as a new mechanism to generate flash rips[2,20]. Overall, mechanisms that generate flash rips involve nearshore hydrodynamic processes forced by energetic incident waves or fluctuations of meteorologically induced water levels.

Convective storms, featured with atmospheric disturbances of strong winds and rapid air pressure perturbations[21–23], are generally classified into four categories: cluster, complex, linear, and bow, based upon criteria for storm structures in the Great Lakes area[1,24–26]. A cluster is an area of unorganized convection, consisting of multiple (>3) small (<40 km^2) cells that are separated in distances of less than twice the cell sizes[24,27]. Wind shifts with large gust fronts and pressure jumps can be created when the isolated cells produce combined effects[27]. In contrast, a complex is defined

as an organized, long-lived (>3 hours), large (>500 km^2) structure[25]. A linear storm, similar to a complex storm in terms of duration and size, has a curvilinear shape with large length-width ratio (>3:1)[25]. In both complex and linear storms, sustained wind stresses and pressure perturbations can occur. These two categories are relatively stable and weakened less by environmental temperature changes when crossing a large body of cooler water[24]. Lastly, a bow storm has a quasi-linear structure similar to linear but with a curved region[1]. An example is "derechos," which are commonly known as convectively induced windstorms[28]. Bow storms are responsible for most severe winds[29] and several well-defined pressure anomaly events[21,22]. All four convective storms mentioned can lead to flash rips, based on the high (90%) coincidence rate previously observed[3]. Nevertheless, it is unknown, as far as the authors are aware, how convective storms initiate, transform, and generate flash rips and how they pose unawareness of the hidden danger.

The objective of this paper is to depict causes of the 2019 drowning incidents in Lake Michigan and reveal nearshore processes that generate flash rips. Specifically, observations are used to characterize atmospheric storm disturbances and hydrodynamic forcings that lead to the possible occurrences of flash rips across Lake Michigan. At reported incident locations, nearshore processes generating hidden flash rips are uncovered using state-of-the-art integrated atmospheric-hydrodynamic modeling. This study, for the first time, finds that transient and intermittent flash rips due to convective storms are a widespread phenomenon in the Laurentian Great Lakes. Hidden flash rip hazards are frequent under both low meteorologically induced water level oscillations and low wind waves, which have not been recognized before. These low water level oscillations and wind wave conditions, together with timing delay of flash rip occurrences relative to events of convective storms can pose unawareness of hidden danger to further elevate the highest risk to beach swimmers, a crucial message that need to be delivered among coastal communities.

4.2 Results

4.2.1 Flash rip occurrences and hydrodynamic conditions

Characteristics of flash rip occurrences and nearshore hydrodynamic conditions during the 4-day convective storms are described here. A total of 11 flash rip occurrences, denoted chronologically as R1 to R11 (Fig. 4-2a, b), are identified based on image evidence of rip-induced sediment plumes[3,30] captured by the real-time nearshore camera of the Lifeguarding Operational Camera Kiosk System (LOCKS)[3] at Port Washington, WI (see PW in Fig. 4-1h). Intermittency of flash rips is depicted as the numbers of flash rips in each occurrence were irregular and discontinuous, represented by the color of rectangles in Fig. 4-2a, b. Transiency of flash rips is shown with durations between 25 to 245 sec and intervals of less than an hour, consistent with previously reported observations[3,30,31]. Timing of flash rip occurrences relative to the six convective storms, denoted chronologically as S1 to S6, is registered as shaded blue color in Fig. 4-2a, b. For example, Both R1 and R4 flash rips in Fig. 4-2c and Fig. 4-2d appeared after the storm (S1) and (S2) with delays of 1 hour and 5 hours, respectively. Flash rip R7 (Fig. 4-2e) occurred during the beginning of the storm (S4), while R10 flash rip (Fig. 4-2f) was found during the later hours of the storm (S5). No occurrence of flash rips was identified during or after the storm (S6). Fig. 4-2a, b also show nearshore hydrodynamic conditions including wind wave heights (H_s) at the nearby NDBC buoy (45013, see Fig. 4-1h) and water level fluctuations ($\Delta\eta$, displacement relative to mean water level) at the nearby NOS water level gauge (MKE, see Fig. 4-1h). Both R1 and R7 flash rips in Fig. 4-2c and Fig. 4-2e occurred under moderate H_s and large $\Delta\eta$; R4 flash rip (Fig. 4-2d) appeared under low H_s and small $\Delta\eta$; and flash rip R10 (Fig. 4-2f) was under low H_s but large $\Delta\eta$. For all observed occurrences, approximately 87% of flash rips occurred when H_s were below 0.9 m, i.e. moderate or low wind waves (Fig. 4-2a). Approximately 74% of flash rips

exhibited fluctuating water level changes (*ΔWL*, height from crest to trough) from 0.1 m to 0.32 m (Fig. 4-2b). Overall, observations show that intermittent and transient flash rips at Port Washington, WI occurred during and after storms. Overall, storm induced nearshore hydrodynamic conditions with low to moderate wind waves or large water level fluctuations can initiate unawareness of the hazardous flash rips.

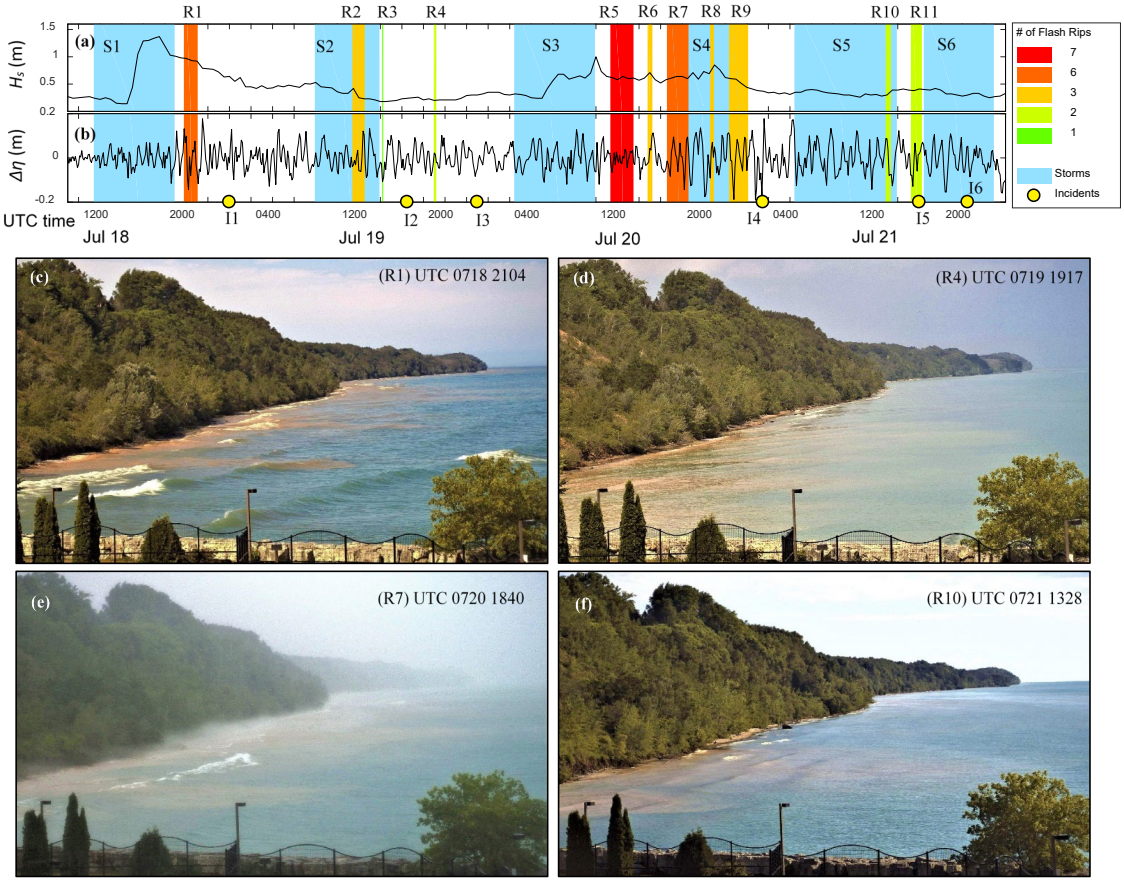

Fig. 4-2: Flash rip occurrences and hydrodynamic conditions during the 4-day convective storms. A total of eleven flash rip occurrences at Port Washington, WI and the six convective storms in colored rectangles plotted on the time series of: **(a)** significant waves heights (H_s) at the NDBC buoy 45013, and **(b)** water level oscillations ($\Delta\eta$) at the MKE gage. The number (#) of flash rips in each occurrence is represented by colors in the legend box. The six reported incidents are shown in yellow solid dots. Images of flash rips were captured at **(c)** UTC2104 of July 18, **(d)** UTC1917 of July 19, **(e)** UTC 1840 of July 20, and **(f)** UTC 1328 of July 21 by the real-time nearshore camera of the Lifeguarding Operational Camera Kiosk System (LOCKS)[3]

4.2.2 Characterization of atmospheric convective storms

Features of atmospheric storm structures with pressure and wind disturbances of the six convective storms from July 18 to 21 across Lake Michigan are chronologically characterized here. The first storm (S1, Fig. 4-1a), a convective complex, propagated southeasterly at 14.6 m/s. The KMKG gauge (abbreviated as KMKG) on the east side of Lake Michigan (see Fig. 4-1h) measured a pressure drop with a rate of 1.4 hPa/10min and wind increase to the maximum speed of 15.4 m/s with a direction change along the storm propagation (see Fig. 4-3a). At the farther southeastern KBIV gauge (abbreviated as KBIV, see Fig. 4-1h), Fig. 4-3a shows that a steep pressure dip with a rate of 2.3 hPa/10min but the increase of wind occurred approximately 20 minutes later. The second storm was a convective cluster (see S2, Fig. 4-1b) that propagated eastwards at 22.8 m/s. Fig. 4-3b shows the cluster storm with a pressure gradient of 1.9 hPa/10min and a wind speed of 12.3 m/s when it initially appeared on the west coast at the KMKE gauge (abbreviated as KMKE, see Fig. 4-1h). After arriving on the east coast at KMKG, the storm became weaker with a pressure gradient of 1.0 hPa/10min and wind speeds under 10 m/s. This feature is consistent with the previous finding that atmospheric perturbations of clusters usually become weaker after crossing the lake[24]. The third and fourth storms, reported as derechos of July 2019[32], were a convective bow (S3, Fig. 4-1c) propagating southwards at 16.5 m/s and a linear convection (S4, Fig. 4-1d) moving at 20.7 m/s toward the southeast, respectively. The KGRB gauge (abbreviated as KGRB) on the northwestern coast (see Fig. 4-1h) recorded a train of pressure perturbations with a pressure jump of 3.7 hPa/10 min during S3 and two pressure jumps of 6.2 hPa/10min and 6.9 hPa /10min during S4 (Fig. 4-3c). These pressure disturbances were comparable to or even greater than the magnitude of 2-5 hPa/10 min in largest meteotsunami events wordwide[21]. Corresponding maximum speeds were 15.9 m/s and 18.0 m/s in S3 and S4, respectively. The fifth and sixth storms were a convective

cluster (S5, Fig. 4-1e) and a convective complex (S6, Fig. 4-1f) that propagated eastward at 9.8 m/s and 7.0 m/s, respectively. These two storms had relatively small pressure gradients (less than 1 hPa/10min) and wind speeds (less than 8 m/s), as shown in Fig. 4-3d. Table 4-1 summarizes characterization of the six convective storm structures and percentage contributions due to atmospheric pressure (P) or wind (W) disturbances to initiate water level fluctuations. Among the six storms, two (S2 and S6) were wind-dominated (W>60%), one (S5) was pressure-dominated (P>60%), and the other three (S1, S3 and S4) had equal contributions of wind and pressure (40%≤W≤60% and 40%≤P≤60%). Interestingly, storms with equal contributions of wind and pressure disturbances, which can initiate wind waves and meteorologically induced water level fluctuations (e.g. meteotsunamis or seiches), tend to result in more hazardous flash rips (see the red-marked regions after S1, S3 and S4 storm in Fig. 4-2a).

Table 4-1. Summary of convective storms with atmospheric disturbances, meteotsunamis and wave conditions, and related drowning incidents.

Convective storms					**Atmospheric Disturbances**				**Meteotsunamis**				**Waves**			**Incidents**		
#S	UTC	Type*	Speed (m/s)	Dir	max ΔP/10min (hPa)	W_{max} (m/s)	%P	%W	UTC	Gage	max ΔWL (m)	T (min)	H_s (m)	T_p (sec)	MWD	UTC	Location	#I
S1	0718 1125 -1855	C	14.6	127	2.3	15.4	58	42	0718 1857-2357	CAL	0.36	48	1.28	5.5	247	0719 0000	Ludington	I1
S2	0719 0755-1355	CL	22.8	119	1.9	12.3	28	72	0719 1457-1703	CAL	0.31	118	0.6	4.2	280	0719 1630-1700	South Haven	I2
													0.13	1.6	92	0719 2300	Kenosha	I3
S3	0720 0225-0955	B	16.5	179	3.7	15.9	40	60	-	-	-	-	0.75	4.8	4	0721 0130	Michigan City	I4
S4	0720 1655 -2325	L	20.7	162	6.9	18.0	41	59	0720 1809 -0721 0957	LUD	0.32	72						
									0720 1903 -0721 0145	MKE	0.35	39						
									0720 2336 -0721 0151	CAL	0.77	99						
S5	0721 0455-1325	CL	9.8	108	0.9	7.2	64	36	0721 1003-1157	CAL	0.55	114	0.44	2.8	307	0721 1600-1900	Ludington	I5
S6	0721 1625 -2255	C	7.0	82	0.3	10.3	23	77	-	-	-	-	0.93	3.7	33	0721 2030	Chicago	I6

* C: Complex, CL: Cluster, B: Bow, L: Linear

4.2.3 Possible causes of flash rips

Meteorologically induced water level fluctuations, one kind of hydrodynamic forcings, can generate transient rip currents, i.e. flash rips[2,20], through three possible causes. One possibility is meteotsunami-induced edge waves that generate longshore currents, which have been documented in several studies of meteotsunamis in the Great Lakes[33–35]. In Fig. 4-3e, meteotsunamis (green box) occurred at the CAL gauge (abbreviated as CAL) located on the southwest corner of the lake (see Fig. 4-1h). Meanwhile, near the incident I1 at Ludington (see Fig. 4-1h), water level fluctuations with a period of 55 min were observed at the gauge LUD (abbreviated as LUD), which can be propagating edge waves along the coast. Similarly, Fig. 4-3f shows that after the meteotsunami event at CAL, water level fluctuations with a period of 35 min were observed on the southwest shore at the MKE gauge (abbreviated as MKE) near where incident I3 happened (Fig. 4-1h). The calculated time for propagating edge waves with speeds of $c = gT\tan[\beta(2n+1)]/2\pi$, where g is the gravitationally acceleration, T is the edge wave period, β is the bottom slope, and the mode n is set to 0 here, along the southwest coast between Port Washington and Kenosha is 218 min, close to 223 min inferred from the time between observed R4 occurrence of flash rips and the incident I3 in Fig. 4-2a,b. The matching between the calculated time and observation time suggests that meteotsunami-induced edge waves may induce strong longshore currents that result in flash rips at multiple locations. The second possibility is meteotsunami-induced water level drawdowns, which have been shown to generate unexpected rip currents and caused several drownings in Lake Michigan[2]. In Fig. 4-3g, the incident I4 (Fig. 4-1h) at Michigan City occurred during fast-receding water levels after a large meteotsunami event at CAL. Wave transformation via superposition of the two meteotsunami-induced edge waves from the east coast (LUD) and the west coast (MKE) could converge at the south shore, similar to the condition in a

severe 1954 meteotsunami event[33], to generate strong return currents or flash rips near the incident location. The third possibility is meteotsunami-induced seiches. Before the incident I5 (see Fig. 3h), the meteotsunamis occurred during UTC0330-1130 at LUD and during UTC0330-UTC1500 at CAL. Water levels at LUD continued to fluctuate from UTC1600 to UTC1830 with a period of 50 min like the situation at MKE. The time lag between LUD and MKE is 25-min, half of the oscillation period, which suggests that the observed meteorologically induced water level fluctuations can be standing waves like seiches[36]. Unforeseen meteotsunami-induced seiches could lead to hidden rip current risks[20]. Overall, meteotsunami-induced longshore currents, drawdowns, and seiches are possible causes of generating transient rip currents.

Wind waves, another hydrodynamic driving forcing, can generate flash rips[4] through two likely causes. One possibility is shear instability of longshore currents generated under oblique incident waves[7]. Fig. 4-3i shows that at UTC2355 oblique incident waves from southwest were approaching toward the east coast near Ludington where the incident (I1) happed. The statement is based on the wave climate, obtained from the NDBC wave buoy 45024 (see Fig. 4-1h), with significant wave height (H_s) of 1.28 m, a peak wave period (T_p) of 5.5 sec, and a mean wave direction (*MWD*, relative to the True North) of 247° (Table 4- 1). Similarly, near Michigan City during the incident I4 (Fig. 4-3k) and near Chicago during I6 (Fig. 4-3l), oblique incident waves with moderate to high wave heights (H_s = 0.75 m ~ 0.93 m, Table 4- 1) were also observed. The oblique incident waves could possibly generate shear instabilities of longshore currents to cause flash rips. The second possibility is breaking-induced vorticities[9,12,13] under shore-normal incidence waves. In Fig. 4-3j, at the time of the incident I2, moderate wind waves with H_s= 0.6 m were approaching from west with *MWD* of 280° towards South Haven on the east coast. The shore-normal incidence waves may create breaking-induced vortices to cause episodic offshore-directed

flash rips[15,16]. Overall, energetic wind waves under oblique or shore-normal incidence are two possible causes of flash rips.

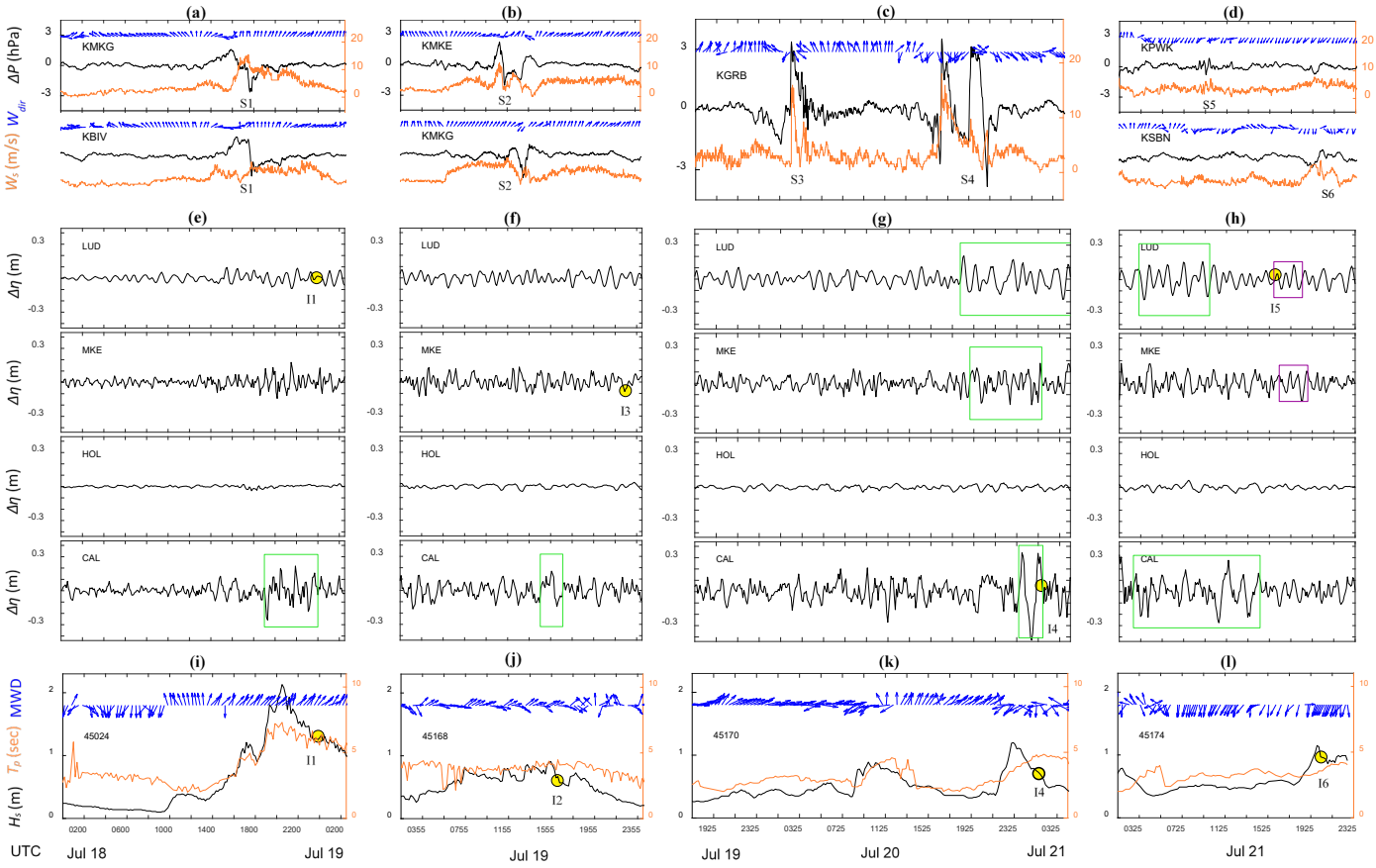

Fig. 4-3: Atmospheric and hydrodynamic observations near locations of incidents. Time series of the convective storm event of July 18-21, 2019 for: (a-d) atmospheric pressure fluctuations (ΔP), surface wind speeds (W_s) and directions (W_{dir}) observed at ASOS stations; **(e-h)** water level fluctuations ($\Delta\eta$) observed at NOS water level gauges, with meteotsunamis identified in green boxes and seiches in purple boxes; **(i-l)** significant wave height (H_s), peak wave period (T_p) and mean wave direction (MWD) observed at NDBC wave buoys. Timing of the reported incidents are labeled as yellow solid dots at the nearest NOS or NDBC stations in **(e-l)**.

4.2.4 Nearshore processes generating flash rips

The integrated atmospheric-hydrodynamic modeling with the feature of resolving multiple scales, i.e., from the whole lake domain to detailed nearshore regions, is employed to reveal nearshore processes that generate hazardous flash rips at incident locations in the following four cases. In Case 1, water level fluctuations $\Delta\eta$ of amplitudes less than 0.05 m (Fig. 4-4a) have negligible effects on generating currents near Ludington of the incident I1 (Fig. 4-4b). Instead, energetic wind waves with a significant wave height of $H_s \sim 1.3$ m due to the southeastern winds (Fig. 4-3a, i) obliquely approach toward Ludington (Fig. 4-4c). Driven by wave-induced strong meandering shear currents, pairs of negative (blue) and positive (red) vortices with the magnitude of 0.1 s^{-1} are induced on the nearshore region (see the zoom-in view in Fig. 4-4d). The vorticities are 15 ~ 30 meters apart, consistent to the length scale of previously observed flash rips[4]. Four identified flash rip jets are numbered. Spacings of the generated rips are between 50 ~ 100 m with offshore distances up to 100 m in rip ②, similar to those commonly observed in Great Lakes and oceans[3,6,31,37]. Series of flash rip jets with the speed higher than 1.0 m/s due to energic wave-induced shear instabilities flow offshore, which possibly swept swimmers away from the beach. resulting in the drowning tragedy near Ludington. Similar results for incident I6 near Chicago, not shown here for brevity, are also found.

In Case 2, water level fluctuations with $\Delta\eta \sim 0.10$ m (Fig. 4-4e) are meteotsunami-generated propagating edge waves, which induce northward longshore currents near South Haven in incident I2 (Fig. 4-4f). Low to moderate waves with $H_s \sim 0.6$ m caused by the southeastern winds (see Fig. 4-3b, j) are developed (Fig. 4-4g). In the zoom-in nearshore region, several sporadic small flash rips (see ②-④ in Fig. 4-4h) with vorticity values of ~0.05 s^{-1} are generated through the circulation cell due to interactions of edge wave induced longshore currents and

southeastern wind waves. A pronounced rip jet ① with a speed of 0.5 m/s is created from a vortex pair shedding offshore, similar to the process that the meteotsunami-generated flash rips reported in a previous study[2]. The jet spatially extends to 100 m from the shoreline, comparable to those in Case I (Fig. 4-4d). The sporadic rip jets caused by unnoticeable water level fluctuations and low to moderate wind waves might impose hidden risks to the unaware swimmers in incident I2. Similar results for the drowning tragedy of incident I3 at Kenosha, not shown here for brevity, are also found.

In Case 3, receding water levels or drawdowns with $\Delta\eta > 0.15$ m on the south shore in Fig. 4-4i are created by the reflection of the two converged meteotsunami-induced edge waves from the east and west coasts, similar to the condition in the 1954 event[33]. As a result, seaward cross-shore currents, i.e., reflected outward currents, are generated near Michigan City where incident I4 occurred (Fig. 4-4i, j). The outflow destabilizes persisting inward longshore currents, creating a meandering behavior (Fig. 4-4j). Moderate waves with $H_s \sim 0.7$ m caused by the rapidly changing winds (Fig. 4-3c, k) are developed (Fig. 4-4k). In the zoom-in nearshore region (Fig. 4-4l), three flash rip jets are driven by vorticity pairs of magnitudes larger than 0.1 s^{-1} and lengths of 30-50 meters. Offshore velocities in rip ① are larger than 1.0 m/s, same as those in Fig. 4-4d. Rip spacings are up to 150 m between rip ②-③ and the offshore distances extend beyond 100 meters from the shoreline, larger than those in Fig. 4-4d. The combined effects of meteotsunami drawdown-induced offshore currents and wave-induced nearshore currents tend to amplify the spatial scales of transient flash rips, which may explain why the swimmer was trapped in the high-speed outward flows near Michigan City in incident I4.

In Case 4, seiches induced by meteotsunamis are exhibited by the spatial distribution of water level fluctuations (Fig. 4-4m). Near Ludington where the incident I5 occurred, southward

longshore currents are generated near the nodal points, i.e., $\Delta\eta \sim 0$ (Fig. 4-4n). Low wind waves with H_s ~0.45 m caused by the northern winds (Fig. 4-3d, l) are developed (Fig. 4-4o). In the zoom-in nearshore region (Fig. 4-4p), six flash rip jets are identified in the 300-m nearshore span, more than those in Fig 4. d (1-3). Flash rips ①, ② and ③ are seiche-induced meandering shear currents, which are destabilized under the incident waves and turn into the offshore-directed rip flows. Closer to the shoreline, flash rip ④, ⑤ and ⑥ are generated through vorticity pairs with the magnitude of 0.05 s^{-1}. Under the relatively low $\Delta\eta$ and H_s, the offshore extent of rip ① and ② are less than 100 m. Nevertheless, the maximum velocities of rip jets reach to 0.5 m/s, comparable to the rip velocities under relatively high $\Delta\eta$ in the edge wave-generated rip (Fig. 4-4h). For the first time, unforeseen flash rips caused by instability of longshore shear currents in meteotsunami-induced seiches are elucidated, which supports the conjecture of seiche-induced rip currents[20] and may explain drowning incident I5 in Ludington State Park (Fig. 4-1g).

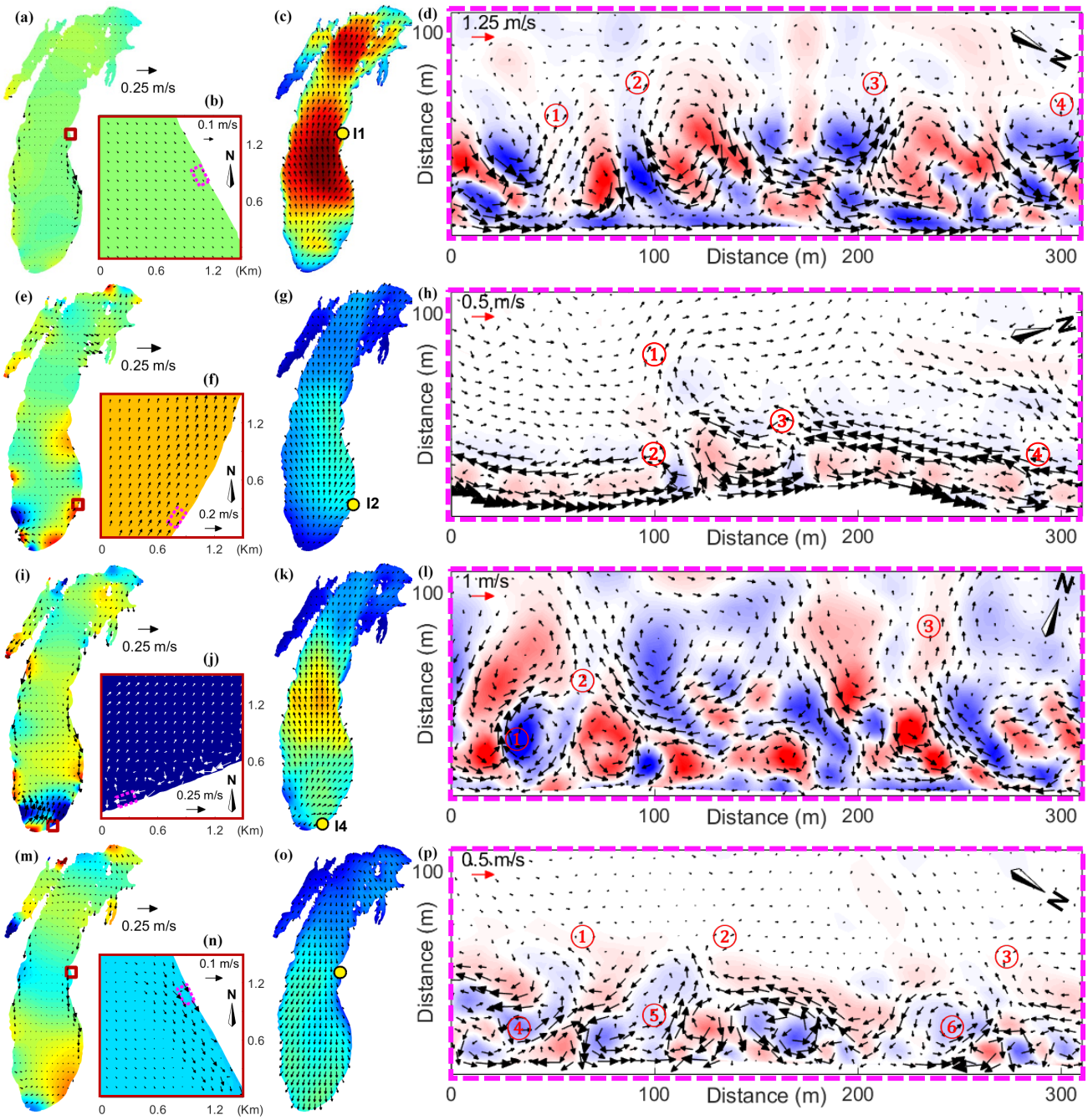

Fig 4-4: Hydrodynamic processes of generating flash rips at locations of incidents. Modeling results of incidents I1 in **(a-d)**, I2 in **(e-h)**, I4 in **(i-l)**, and I5 in **(m-p)**. **(a,e,i,m)** Currents plotted in arrows on water level fluctuations ($\Delta\eta$) colormaps for whole Lake Michigan with zoom-in views (red box) in **(b,f,j,n)**; **(c,g,k,o)** wind wave directions plotted in arrows on significant wave height (H_s) colormaps for whole Lake Michigan, with incident locations shown in yellow circles; and **(d,h,l,p)** zoom-in nearshore views (pink dashed box) of current velocities plotted on vorticity (ω) colormaps, with identified flash rips numbered in circles.

4.3 Discussion

Several drowning incidents spanning over the coast of Lake Michigan were reported during a series of convective storms in a 4-day period. Features of observed atmospheric storm disturbances and hydrodynamic forcing conditions are characterized to depict possible causes of the drowning incidents. Results show that four convective storm structures with atmospheric pressure, wind, and pressure-wind disturbances generated energetic wind waves, meteotsunami-induced longshore currents, water level drawdowns, and seiches, which can cause the possible occurrences of flash rips near incident locations across Lake Michigan. The integrated atmospheric-hydrodynamic model resolves meteorologically induced water level fluctuations and wind waves from the whole lake to detailed nearshore area throughout the convective storms. Results reveal that hazardous flash rips can be generated by four distinct processes: longshore shear instabilities due to breaking of wind waves[7]; nearshore circulation cells resulting from interactions of meteotsunami-induced edge waves and wind waves[2]; seaward cross-shore currents through the reflection of two converged meteotsunami-induced edge waves[33]; and longshore shear instability of meteotsunami-induced seiche currents. Overall, the findings of this study, for the first time, support the hypothesis that drowning incidents are caused by convective storms induced hidden flash rips. Particularly, meteotsunami-induced water level oscillations unlike energetic wind waves, misleadingly perceived as calm and safe environmental conditions, can generate unexpected hazardous flash rips[2], that are hidden to the perception of swimmers.

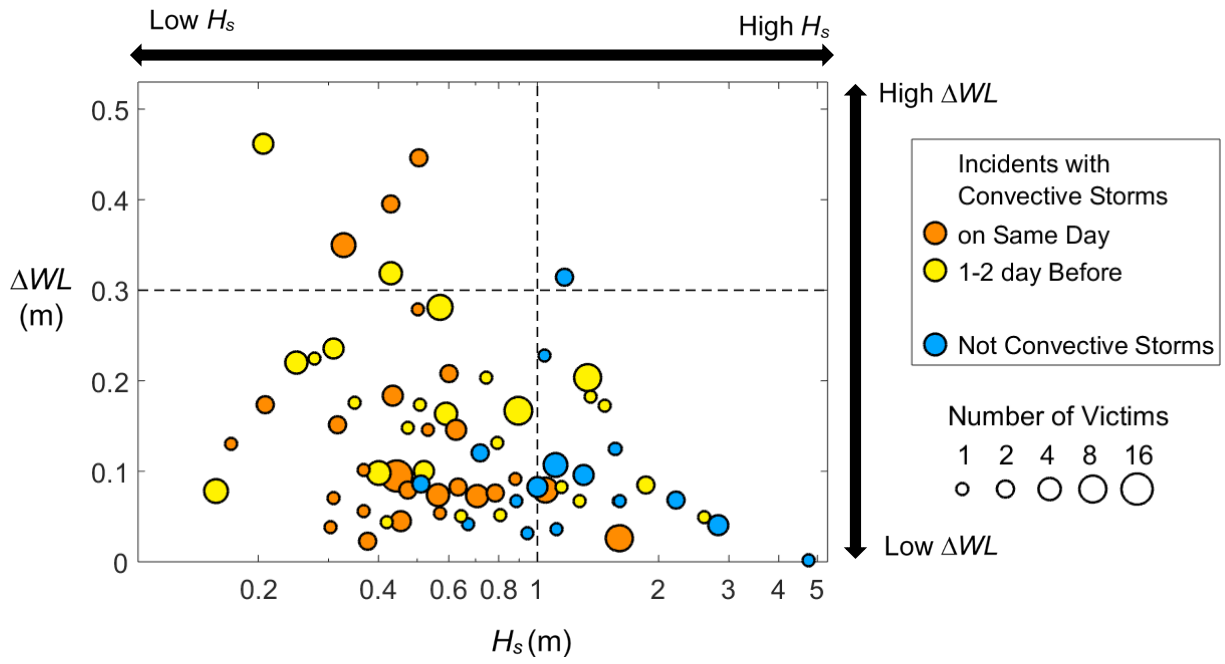

Fig 4-5: Distribution of flash rip related incidents in Lake Michigan. Incident events (based on GLCID data) plotted in terms of the meteorologically induced water level changes ΔWL versus the significant wave height of wind waves H_s (in log scale). The size of dots is proportional to the number of victims in each incident. Orange dots represent incidents associated with convective storms on the same day; yellow dots represent those associated with convective storms crossing over the lake 1-2 days before; and blue dots represent those associated with not convective types of storms.

How frequently are flash rips a hidden danger in Lake Michigan? Fig. 4-5 discusses 79 possible flash rip incidents in Lake Michigan based on the Great Lake Current Incident Database (GLCID)[38] since 2002. The flash rip incidents are extracted out from a total of 186 records by excluding those that occurred in channels (bathymetry-controlled rip currents[4]), near structures (boundary-controlled rip currents[4]), or at river outlets[39]. Incidents are associated with the two hydrodynamic forcings: water level changes (ΔWL) and significant wave heights (H_s), compiled from historical data of the NOS gages and NDBC buoys (see Fig 4-1h). Among the extracted possible flash rip incidents that had resulted in a total of 185 individual victims, 65% of the incidents (117 victims) occurred under the conditions with $\Delta WL < 0.3$ m and $H_s < 1$ m, i.e. the

"Low-Low" quadrant of Fig. 4-5 and the remaining 35% of incidents were in other quadrants: 25% in the "High (H_s)-Low (ΔWL)" quadrant; 9% in the "Low (H_s)-High (ΔWL)" quadrant; and 1% in the "High-High" quadrant. Among the 10 incidents that yielded more than four victims in one single incident, 6 were in the "Low-Low" quadrant. Both the high occurrence and the *severe* vulnerability of incidents under the "Low" meteorologically induced water level oscillations and "Low" wind waves indicate that the hidden flash rip hazards are frequent and the risks to beach swimmers are high, which have not been recognized in the past.

How are the hidden flash rips related to a wide range of atmospheric storm types in Lake Michigan? This question is addressed in the following three aspects. First, observations of radar reflectivity from the NEXRAD composite image database show that annually about 50% of convective storm events, like the event depicted in Fig. 4-1, tend to occur consecutively for 3 days or even more. Particularly, complex and linear convection, are most common during late-spring to mid-summer[40]. The seasonality of convective storms, which overlaps with the peak season of beachgoers, would prompt many coastal populations to be vulnerable to storm-induced flash rip hazards. Second, convective storms, in comparison with non-convective storms[1,40,41] like frontal, cyclonic systems, and atmospheric gravity waves, are found to be associated with the majority of the flash rip related incidents (see yellow and orange dots in Fig. 4-5).The dots associated with convective-storm incidents tend to cluster in the left quadrants, suggesting that the role of wind waves is less significant but the effect of water level changes like meteotsunamis is more crucial to induce flash rips (see Cases 2, 3, and 4). This statement is consistent with the recent finding that meteotsunami-induced rips are not sporadic but more frequently related to each other[2]. In comparison, the other 25% of incidents associated with non-convective storms (see blue dots in Fig. 4-5) tend to occur with noticeably large wave height H_s generated by energic incident waves.

Third, the timing of storms is found to occur up to 1-2 days before the flash rip incidents, which counts for almost 50% of all convective-associated incidents (see yellow dots in Fig. 4-5). After storm disturbances have already past the lake, the initiated water level fluctuations e.g., meteotsunamis, would continuously propagate like edge waves or rebound as seiches. These meteorologically induced water level oscillations would be transformed through distinct nearshore processes to generate flash rips at locations under a clear sky and nice weather, i.e. far from the event of initial storms. Two good examples are storms S3 and S5 that led to incidents I3 and I5 in this study (Table 4-1). This timing delay of flash rip occurrences relative to convective storm events can pose a hidden danger, further elevating the risk to the unawareness of beach swimmers**.** Adding the previous findings that drowning incidents are caused by convective storms induced flash rips during the swimming season and most flash-rip related drowning incidents occurred under clam conditions, i.e., low meteorologically induced water level oscillations and low wind waves, beachgoers who are not aware of this hidden hazard entering the water are unknowingly exposed to the highest danger of hidden flash rips. An urgent need is called for communication, education, and nowcast/forecast of storm-induced flash rips for coastal communities.

4.4 Methods

4.4.1 Images and atmospheric observations

Images of flash rips are captured by the Lifeguarding Operational Camera Kiosk System (LOCKS)[3] at the North Beach of Port Washington, WI. Image processing procedures with segmentation, ortho-rectification, and detection[3] are employed to characterize occurrences of flash rip with sediment plume morphological features. Durations of flash rips are counted from the first emergence of sediment plumes until no offshore-directed propagations for the same plume are

detected. Multiple flash rips that appear intermittently with time intervals of less than 1 hour are consolidated to be a single occurrence.

Reflectivity radar NEXRAD composite images (see Fig. 4-1a-f) from the Iowa Environmental Mesonet with 1-km spatial resolution and 5-min intervals are used to characterize atmospheric storm structures. The timing for convective storms crossing Lake Michigan (see in Table 4- 1) is determined as starting when reflectivity areas with values >25dBZ initially crossed the shoreline and ending when the reflectivity areas completely left the entire lake perimeter. A widely used storm classification criteria[1] is used to define storm structures as convective types, such as complex, cluster, linear and bow; and not convective types, such as frontal or cyclonic systems. Atmospheric storm disturbances are characterized based on 1-min data of air pressures, surface wind speeds and directions from the 16 Automated Surface Observing System (ASOS) around Lake Michigan (see Fig. 4-1h). A high-pass digital filter with 2-hour cut-off frequency is used to obtain storm-related high-frequency atmospheric pressure fluctuations (ΔP in Fig 3a). The isochronal analysis method[42] is used to determine propagation speeds and directions. The temporal gradients of pressure perturbations and wind shear stresses at maximum speeds[21,40,43] are used to calculate relative contributions of atmospheric pressure (P) and wind (W) disturbances.

4.4.2 Characterization of hydrodynamic conditions

Procedures to characterize hydrodynamic conditions are described here. First, water level data in 6-min intervals at 10 observation stations in Lake Michigan NOAA National Ocean Service (see Fig. 4-1h) are downloaded. Second, a high-pass digital filter with a 6-hour cut-off frequency[1] is used to obtain oscillations in the meteotsunami wave frequency band. The zero-crossing method[43] is employed to calculate individual waves from the filtered time series. Third, a well-

recognized meteotsunami-identification criteria[43]: the (long) wave height exceeding gauge-specific thresholds[40] and the period falling in the 2-min to 2-hour high-frequency range is applied to identify meteotsunamis (see Table 4- 1). Fourth, wind wave data from 15 available wave buoys in Lake Michigan (see Fig. 4-1h) operated by the NOAA National Data Buoy Center (NDBC) are compiled. Wave statistics including significant wave height (H_s), mean wave direction (*MWD*) and peak wave period (T_p) are represented in 30-min or 1-hour intervals.

4.4.3 Integrated atmospheric-hydrodynamic modeling

Integrated atmospheric-hydrodynamic modeling is implemented using the Semi-implicit Cross-scale Hydroscience Integrated System Model ((SCHISM)[45,46] coupled with the 3rd generation spectral Wind Wave Model (WWM III)[47], forced by atmospheric storm disturbances during July 18-21, 2019 in Lake Michigan. There are three components. First, the atmospheric forcing is reconstructed from wind and pressure fields with the hourly outputs of the NOAA High-Resolution Rapid Refresh (HRRR) atmospheric model and time series of discrete point observation data at ASOS stations. The HRRR outputs are temporally and spatially interpolated to match with the ASOS observation so that the high frequency, i.e., O (1min), of atmospheric storm disturbances is depicted to initiate meteorologically induced water level fluctuations and wind waves[43]. Second, multi-scale domain discretization is used. On the lake scale, the entire domain of Lake Michigan is discretized into a total of 1,125,678 triangular unstructured mesh elements. High-spatial resolution LiDAR data from the 2012 USACE NCMP Topography Survey is used to precisely delineate the shoreline and coastal bathymetry for modeling meteotsunami transformation including edge wave propagations[33]. Depth interpolation in coastal regions for the entire coastline of Lake Michigan with horizontal 100 m resolution is performed. On the nearshore

scale, detailed meshes with the spatial magnitude of O (1m) are created to resolve fine-scale hydrodynamic processes that involve interactions of water level fluctuations and wind waves[2]. At the five locations of reported incidents (Ludington, MI; South Haven, MI; Michigan City, IN; Chicago, IL; Kenosha, WI) and at Port Washington (where the model was validated with the observed flash rips), grid resolutions are refined to be 2 m at the shoreline and increasing gradually to 100 m toward offshore to seamlessly merge into the large lake scale mesh. Third, two-way coupling of SCHISM and WWM III is employed to simulate nearshore wave-current interactions. Specifically, coupling takes place at every model time step (dt = 5 sec) to simulate wave-induced vortices, a critical factor in flash rip generation[2,4]. Current velocity fields are solved in time- and depth-averaged Reynolds-averaged Navier–Stokes (RANS) equations, and wave fields are repetitively updated based on the evolving currents[48,49]. The wave-averaged approach has been successfully deployed in modeling flash rip caused by meterotsunmmis[2], longshore shear currents[7] and wave group-generated vortices[12].

4.5 Data availability

Radar reflectivity imagery from Iowa Mesonet (https://mesonet.agron.iastate.edu/archive/data/), meteorological data from ASOS stations (ftp://ftp.ncdc.noaa.gov/pub/data/asos-onemin/), High Resolution Rapid Refresh model outputs from the HRRR Archive at the University of Utah (http://home.chpc.utah.edu/~u0553130/Brian_Blaylock/cgi-bin/hrrr_download.cgi), water level data from NOAA Tides & Currents (https://tidesandcurrents.noaa.gov/), wave climate data from NOAA NDBC (https://www.ndbc.noaa.gov/station_page.php?station=45007), bathymetry from NOAA- NCEI (https://maps.ngdc.noaa.gov/viewers/bathymetry/) and from 2012 USACE NCMP Topobathy Lidar (https://coast.noaa.gov/htdata/lidar1_z/geoid12a/data/2644/), incidents data

from GLCID (https://www.michiganseagrant.org/dcd/dcdsearch.php), news data from Google News search are used in this study and are all publicly available. Image data at the North Beach in City of Port Washington are available upon request and will be provided by authors.

4.6 Code availability

The SCHISM[45] and WWM-III[46] modeling system is an open source code and can be downloaded from http://ccrm.vims.edu/schismweb/. The MATLAB (http://www.mathworks.com/) scripts for data analysis and figure generation are available from the authors.

4.7 Acknowledgements

This work was supported in part by NOAA Coastal Storms Program, University of Wisconsin Sea Grant Institute (UW-Sea Grant), and Wisconsin Coastal Management Program. We specifically thank Dr. Alvaro Linares for guiding the multiple-scale integrated atmospheric-hydrodynamic modeling and providing suggestions to clarify the processes of meteotsunamis-induced hazardous flash rips, and Dr. Adam Bechle for his critical comments and suggestion on intepreting the data. In addition, Ms Marie Zhuikov at UW-Sea Grant and Ms Mary Possin at Dept. of Civil and Environmental Engineering at UW-Madison are acknowledged for their helpful editorial comments. Ms. Moira Harrington at UW-Sea Grant for her dedication to communicating rip current hazards to the Great Lakes community are acknowledged.

4.8 References

1. Bechle, A. J., Kristovich, D. A. R. & Wu, C. H. Meteotsunami occurrences and causes in Lake Michigan. *J. Geophys. Res. Ocean.* **120**, 8422–8438 (2015).
2. Linares, Á., Wu, C. H., Bechle, A. J., Anderson, E. J. & Kristovich, D. A. R. Unexpected rip currents induced by a meteotsunami. *Sci. Rep.* **9**, 2105 (2019).
3. Liu, Y. & Wu, C. H. Lifeguarding Operational Camera Kiosk System (LOCKS) for flash rip warning: Development and application. *Coast. Eng.* **152**, 103537 (2019).
4. Castelle, B., Scott, T., Brander, R. W. W. & McCarroll, R. J. J. *Rip current types, circulation and hazard*. *Earth-Science Reviews* vol. 163 1–21 (Elsevier, 2016).
5. Brander, R. & Scott, T. Science of the rip current hazard. in *The Science of Beach Lifeguarding* 67–85 (CRC Press, 2019). doi:10.4324/9781315371641-5.
6. Feddersen, F. The Generation of Surfzone Eddies in a Strong Alongshore Current. *J. Phys. Oceanogr.* **44**, 600–617 (2014).
7. Özkan-Haller, H. T. & Kirby, J. T. Nonlinear evolution of shear instabilities of the longshore current: A comparison of observations and computations. *J. Geophys. Res. Ocean.* **104**, 25953–25984 (1999).
8. Peregrine, D. H. Surf Zone Currents. *Theor. Comput. Fluid Dyn.* **10**, 295–309 (1998).
9. Kirby, J. T. & Derakhti, M. Short-crested wave breaking. *Eur. J. Mech. - B/Fluids* **73**, 100–111 (2019).
10. Clark, D. B., Elgar, S. & Raubenheimer, B. Vorticity generation by short-crested wave breaking. *Geophys. Res. Lett.* **39**, 2012GL054034 (2012).
11. Spydell, M. & Feddersen, F. Lagrangian Drifter Dispersion in the Surf Zone: Directionally Spread, Normally Incident Waves. *J. Phys. Oceanogr.* **39**, 809–830 (2009).

12. Long, J. W. & Özkan-Haller, H. T. Low-frequency characteristics of wave group–forced vortices. *J. Geophys. Res.* **114**, C08004 (2009).

13. MacMahan, J. H., Reniers, A. J. H. M., Thornton, E. B. & Stanton, T. P. Infragravity rip current pulsations. *J. Geophys. Res. C Ocean.* **109**, (2004).

14. Johnson, D. & Pattiaratchi, C. Transient rip currents and nearshore circulation on a swell-dominated beach. *J. Geophys. Res.* **109**, C02026 (2004).

15. Dalrymple, R. A. A mechanism for rip current generation on an open coast. *J. Geophys. Res.* **80**, 3485–3487 (1975).

16. Uchiyama, Y., McWilliams, J. C. & Akan, C. Three-dimensional transient rip currents: Bathymetric excitation of low-frequency intrinsic variability. *J. Geophys. Res. Ocean.* **122**, 5826–5849 (2017).

17. Monserrat, S., Vilibić, I. & Rabinovich, A. B. Meteotsunamis: atmospherically induced destructive ocean waves in the tsunami frequency band. *Nat. Hazards Earth Syst. Sci.* **6**, 1035–1051 (2006).

18. As-Salek, J. A. & Schwab, D. J. High-Frequency Water Level Fluctuations in Lake Michigan. *J. Waterw. Port, Coastal, Ocean Eng.* **130**, 45–53 (2004).

19. Bedford, K. W. The Physical Effects of the Great Lakes on Tributaries and Wetlands. *J. Great Lakes Res.* **18**, 571–589 (1992).

20. Meadows, G. *et al.* Rip Currents in the Great Lakes: An Unfortunate Truth. in *Rip Currents: Beach Safety, Physical Oceanography, and Wave Modeling* (eds. Leatherman, S. & Fletemeyer, J.) 199–214 (CRC Press, 2011).

21. Šepić, J. & Rabinovich, A. B. Meteotsunami in the Great Lakes and on the Atlantic coast of the United States generated by the “derecho” of June 29–30, 2012. *Nat. Hazards* **74**, 75–

107 (2014).

22. Wertman, C. A. *et al.* Mesoscale convective system surface pressure anomalies responsible for meteotsunamis along the U.S. East Coast on June 13th, 2013. *Sci. Rep.* **4**, (2014).

23. Šepić, J., Vilibić, I. & Strelec Mahović, N. Northern Adriatic meteorological tsunamis: Observations, link to the atmosphere, and predictability. *J. Geophys. Res. Ocean.* **117**, (2012).

24. Workoff, T. E., Kristovich, D. A. R., Laird, N. F., LaPlante, R. & Leins, D. Influence of the Lake Erie Overlake Boundary Layer on Deep Convective Storm Evolution. *Weather Forecast.* **27**, 1279–1289 (2012).

25. Fowle, M. A. & Roebber, P. J. Short-Range (0–48 h) Numerical Prediction of Convective Occurrence, Mode, and Location. *Weather Forecast.* **18**, 782–794 (2003).

26. Gallus, W. A., Snook, N. A. & Johnson, E. V. Spring and Summer Severe Weather Reports over the Midwest as a Function of Convective Mode: A Preliminary Study. *Weather Forecast.* **23**, 101–113 (2008).

27. Weisman, M. L. & Klemp, J. B. Characteristics of Isolated Convective Storms. in *Mesoscale Meteorology and Forecasting* 331–358 (American Meteorological Society, 1986). doi:10.1007/978-1-935704-20-1_15.

28. Johns, R. H. & Hirt, W. D. Derechos: Widespread Convectively Induced Windstorms. *Weather Forecast.* **2**, 32–49 (1987).

29. Changnon, S. A. & Kunkel, K. E. *Severe storms in the Midwest*. *Illinois State Water Survey, Informational/Educational Material 2006-06* (2006).

30. Floc'h, F. *et al.* Flash Rip Statistics from Video Images. *J. Coast. Res.* **81**, 100–106 (2018).

31. Murray, T., Cartwright, N. & Tomlinson, R. Video-imaging of transient rip currents on the

Gold Coast open beaches. *J. Coast. Res.* **165**, 1809–1814 (2013).

32. Erdman, J. A Derecho, a Widespread Destructive Thunderstorm Wind Event, Swept Across Minnesota, Wisconsin and Michigan | The Weather Channel. (2019).

33. Bechle, A. J. & Wu, C. H. The Lake Michigan meteotsunamis of 1954 revisited. *Nat. Hazards* **74**, 155–177 (2014).

34. Anderson, E. J. *et al.* Reconstruction of a meteotsunami in Lake Erie on 27 May 2012: Roles of atmospheric conditions on hydrodynamic response in enclosed basins. *J. Geophys. Res. Ocean.* **120**, 8020–8038 (2015).

35. Ewing, M., Press, F. & Donn, W. L. An Explanation of the Lake Michigan Wave of 26 June 1954. *Science* **120**, 684–6 (1954).

36. Linares, Á., Wu, C. H., Anderson, E. J. & Chu, P. Y. Role of Meteorologically Induced Water Level Oscillations on Bottom Shear Stress in Freshwater Estuaries in the Great Lakes. *J. Geophys. Res. Ocean.* **123**, 4970–4987 (2018).

37. Suanda, S. H. & Feddersen, F. A self-similar scaling for cross-shelf exchange driven by transient rip currents. *Geophys. Res. Lett.* **42**, 5427–5434 (2015).

38. Great Lakes Current Incident Database. https://www.michiganseagrant.org/dcd/dcdsearch.php (2019).

39. Great Lakes Swim Season Summaries. https://www.weather.gov/iwx/beach_season_summaries (2020).

40. Bechle, A. J. *et al.* Meteotsunamis in the Laurentian Great Lakes. *Sci. Rep.* **6**, 37832 (2016).

41. Shi, L., Olabarrieta, M., Nolan, D. S. & Warner, J. C. Tropical cyclone rainbands can trigger meteotsunamis. *Nat. Commun.* **11**, 1–14 (2020).

42. Šepić, J., Vilibić, I. & Belušić, D. Source of the 2007 Ist meteotsunami (Adriatic Sea). *J.*

Geophys. Res. **114**, C03016 (2009).

43. Linares, Á., Bechle, A. J. & Wu, C. H. Characterization and assessment of the meteotsunami hazard in northern Lake Michigan. *J. Geophys. Res. Ocean.* **121**, 7141–7158 (2016).
44. Vincent C. L. *Water wave mechanics*. (2002).
45. Zhang, Y. & Baptista, A. M. SELFE: A semi-implicit Eulerian–Lagrangian finite-element model for cross-scale ocean circulation. *Ocean Model.* **21**, 71–96 (2008).
46. Zhang, Y. J., Ye, F., Stanev, E. V. & Grashorn, S. Seamless cross-scale modeling with SCHISM. *Ocean Model.* **102**, 64–81 (2016).
47. Roland, A. *et al.* A fully coupled 3D wave-current interaction model on unstructured grids. *J. Geophys. Res. Ocean.* **117**, (2012).
48. Yu, J. & Slinn, D. N. Effects of wave-current interaction on rip currents. *J. Geophys. Res. C Ocean.* **108**, 33–1 (2003).
49. Haas, K. A., Svendsen, I. A., Haller, M. C. & Zhao, Q. Quasi-three-dimensional modeling of rip current systems. **108**, 10–1 (2003).

5. Rip currents near coastal structures in Lake Michigan: characterization and assessment for warnings

The following is in preparation to be submitted to *Journal of Great Lakes Research*.

5.1 Introduction

Rip currents, narrow seaward water jets near coastal structures, or at beaches, can quickly sweep swimmers to deeper water (Castelle et al., 2016; Dalrymple et al., 2011; MacMahan et al., 2006). Panicked swimmers can become fatigued by trying to swim against rip currents back to shore, which leads to drowning (Brander et al., 2011). Hundreds of drowning incidents have been reported across the world (Arozarena et al., 2015; Brewster et al., 2019; Brighton et al., 2013; Gensini and Ashley, 2010; Short and Hogan, 1994; Woodward et al., 2013). According to the Great Lakes Current Incident Database (GLCID), a total of 624 drowning incidents including 195 fatalities occurred from 2002-2019. More than 50% of those reported were in the vicinities of coastal structures ("Great Lakes Current Incident Database," 2019). In Lake Michigan alone, 257 coastal structure-related incidents were at 38 distinct sites spanning across 18 counties. While a great amount of progress in documenting rip current hazards has been made over the past decades (Brander and Scott, 2019; Brander and MacMahan, 2011; Castelle et al., 2016; Short and Hogan, 1994), lack of timely warning of rip currents near structures often lead swimmers to tragic incidents. In view of the importance and concern, characterizing and assessing the potential occurrences of rip currents near structures would foster the resilience of recreational water users to beach hazards in the Great Lakes (Meadows et al., 2011).

Characteristics for rip currents near coastal structures can be classified into two types (Castelle et al., 2016). First, deflection rip currents occur at the wave-exposed side as offshore-

directed flows propagating along the structure (Castelle et al., 2016; Castelle and Coco, 2012; Horta et al., 2018; Scott et al., 2016; Van Rijn, 2011). The formation is caused by deflected longshore currents towards the structures when encountering the rigid boundary (Dalrymple et al., 2011). Speeds of deflected rip currents tend to increase at large wave heights and oblique wave incidence close to a 45° angle with respect to the shoreline direction (Scott et al., 2016). Strengths of deflection rip currents depend on structure geometries. For example, deflection rip currents are found to extend far outside of the surf zone when the structure is longer than the surf zone width or when the spacings between two structures (such as in groins or headlands) are 2 to 4 times of the length (Castelle and Coco, 2013; Scott et al., 2016; Van Rijn, 2011). Second, shadow rip currents occur on the lee-wave side as the offshore velocities in large recirculation eddies (Aelbrecht and Denot, 1999; Gourlay, 1974; Pattiaratchi et al., 2009; Scott et al., 2016; Wind and Vreugdenhil, 1986). The formation of the eddy is caused by differences in radiation stress gradients between large wave set-ups and the shadowed side of the structure (Gourlay, 1974; McCarroll et al., 2014; Shi et al., 2003). Flow patterns of shadow rip currents have been observed in narrow embayment between headlands (Castelle and Coco, 2013, 2012). As a result, recirculation shadow currents and offshore deflected currents can appear on both ends of the headland boundaries. Studies regarding the characterization of rip currents near groins (Aelbrecht and Denot, 1999; Pattiaratchi et al., 2009; Scott et al., 2016;) and headlands (Castelle and Coco, 2013, 2012; Gourlay, 1974; Horta et al., 2018) have been well documented (Castelle et al., 2016). Nevertheless, there is limited information related to rip currents near breakwaters (Liu and Mei, 1976; Gourlay, 1974; Kim et al., 2016, Castelle et al., 2016). For instance, it is unclear if the breakwater geometries with lengths on the order of several hundred meters beyond the surf zone can affect the formation and strength of the two types of rip currents. Therefore, characterizing rip

currents near harbor breakwaters, common coastal structures adjacent to recreation beaches in the Great Lakes, are critically needed.

Assessment of the occurrences of rip currents has been conducted in several ways. Direct observations can be achieved using in-situ velocity instrument like acoustic Doppler velocimeters or acoustic doppler current profilers at fixed locations near coastal structures (MacMahan et al., 2005; Pattiaratchi et al., 2009; Scott et al., 2016) but the cost and maintenance of the instrument can be expensive. Visual observation by trained lifeguards can detect rip currents which appear as bubble-laden or breaking-absent region (Dalrymple et al., 2011; Leatherman and Leatherman, 2017) but lifeguard detections are limited in views and not available in unpatrolled sites. In recent years, low-cost and continuous video cameras are used to facilitate visual observation with large fields of view (Holman and Haller, 2013; Holman and Stanley, 2007). For example, automated image systems for detecting rip-current induced sediment plumes using color contrasts to the water (Floc'h et al., 2018; Murray et al., 2013) have been successfully implemented on open beaches to detect occurrences of flash rips (Liu and Wu, 2019) and channeled rips (Pitman et al., 2016; Silva-Cavalcanti et al., 2018). Indirect methods based upon environmental proxies are commonly used to assess potential occurrences of rip currents (Dalrymple et al., 2011; Gensini and Ashley, 2010). On oceanic coasts, the Lushine Rip Currents scale (LURCS) and modified derivatives are based on causative factors like wind speed and direction, swell height and period, tidal range, and beach morphology (Alvarez-Ellacuria et al., 2009; Arun Kumar and Prasad, 2014; Engle, 2003; Lascody, 1998; Lushine, 1991; Schrader, 2004). In the Great Lakes, the Great Lakes Rip Current Checklist (GLRCC) considers factors like wave height, wave period, wind speed, wind direction, and water level (Meadows et al., 2011). Recently, high-frequency water level oscillations due to storm-induced meteotsunamis (Bechle et al., 2016; Monserrat et al., 2006) and seiches (As-Salek and

Schwab, 2004; Rabinovich, 2009), one of the key factors to cause rip currents in open beaches in the Great Lakes (Linares et al., 2019), are further added to the Flash Rip Occurrence Checklist (FROC) by Liu and Wu (2019). While a great deal of progress has been made in employing environmental proxies to assess rip currents in open beaches, no tools to assess rip currents near coastal breakwater structures have been reported, as far as the authors are aware.

The objective of this paper is to characterize rip current occurrences near breakwater structures and develop assessment tools for providing timely rip current warnings to beachgoers. Specifically, the occurrences of rip currents are identified and associated with environmental conditions using in-situ measurements and remote imaging observations at the north breakwater of the City of Port Washington, Wisconsin, as an example. Pulsating flow characteristics in observed rip currents are related to atmospheric and hydrodynamic conditions using wavelet and cross-wavelet analysis, respectively. A Structure Rip Checklist and Assessment Matrix (SRiCAM) tool for assessing potential occurrences of rip currents near structures is developed and validated at the study site. Consistent and trustworthy results based upon the SRiCAM are discussed. The SRiCAM tool is integrated into the cyberinfrastructure with a data contingency plan to provide reliable and real-time warnings to the public. Lastly, we apply the SRiCAM to other locations around Lake Michigan for assessing rip current hazards near coastal structures to foster coastal community resilience in the Great Lakes.

5.2 Methods

5.2.1 Site description

The study site is located on the western shore of Lake Michigan at the City of Port Washington, Wisconsin. The harbor, representing a typical coastal structure on the Great Lakes,

is bounded by two concrete breakwaters as shown in Fig 5-1. The two breakwaters are 850 meters apart on the land and the two tips are 400 meters apart. The north breakwater has a length of 750 meters and forms an oblique angle of 115° with the shoreline. The south breakwater has a length of 500 meters and forms a normal angle with the shoreline. The shoreline is orientated in angle about 30° clockwise from the true North. Correspondingly, the shore-normal incidence is 120°. Two recreational beaches, the North Beach and the South Beach shown in Fig 5-1, are connected to the two ends of breakwaters. At the two beaches, the surf zone widths are approximately 100 m - 150 meters. The beach slope is 0.03-0.04 in the surf zone and becomes 0.01-0.015 at offshore outside the surf zone. Nearby the study site, eight drownings and over ten rescue incidents have been reported according to the GLCID (2019) and reports from the Great Lakes Surf Rescue Project (2019).

5.2.2 Data sources and field measurements

Bathymetry data (Fig 5-1) is integrated by combining three sources: nearshore surveyed depths, coastal LiDAR topographic data (Office for Coastal Management, 2014), and NOAA offshore bathymetry of Lake Michigan (National Geophysical Data Center, 1996). The nearshore survey was conducted in 2017 using a Sontek River Surveyor with a 0.5 MHz downward-looking vertical acoustic beam (Lin et al., 2009), with a horizontal resolution of 0.5 m and a depth resolution of 1 millimeter. The survey covered a nearshore region (2000 m x 250 m) north of the Port Washington harbor. The coastal LiDAR topographic data, which was collected by the USACE NCMP Topobathy Lidar Survey in 2012 (Office for Coastal Management, 2014), covers coastal regions up to 500 meters offshore with horizontal resolutions of 1–3 meters and the vertical resolution of 1 millimeter. The NOAA offshore bathymetry for the entire Lake Michigan has a

spatial resolution of 3 geographic seconds. The integrated bathymetry employs unified coordinates based on the UTM NAD83 and NAVD88 datum and overlaid points are averaged using inverse distances weighting.

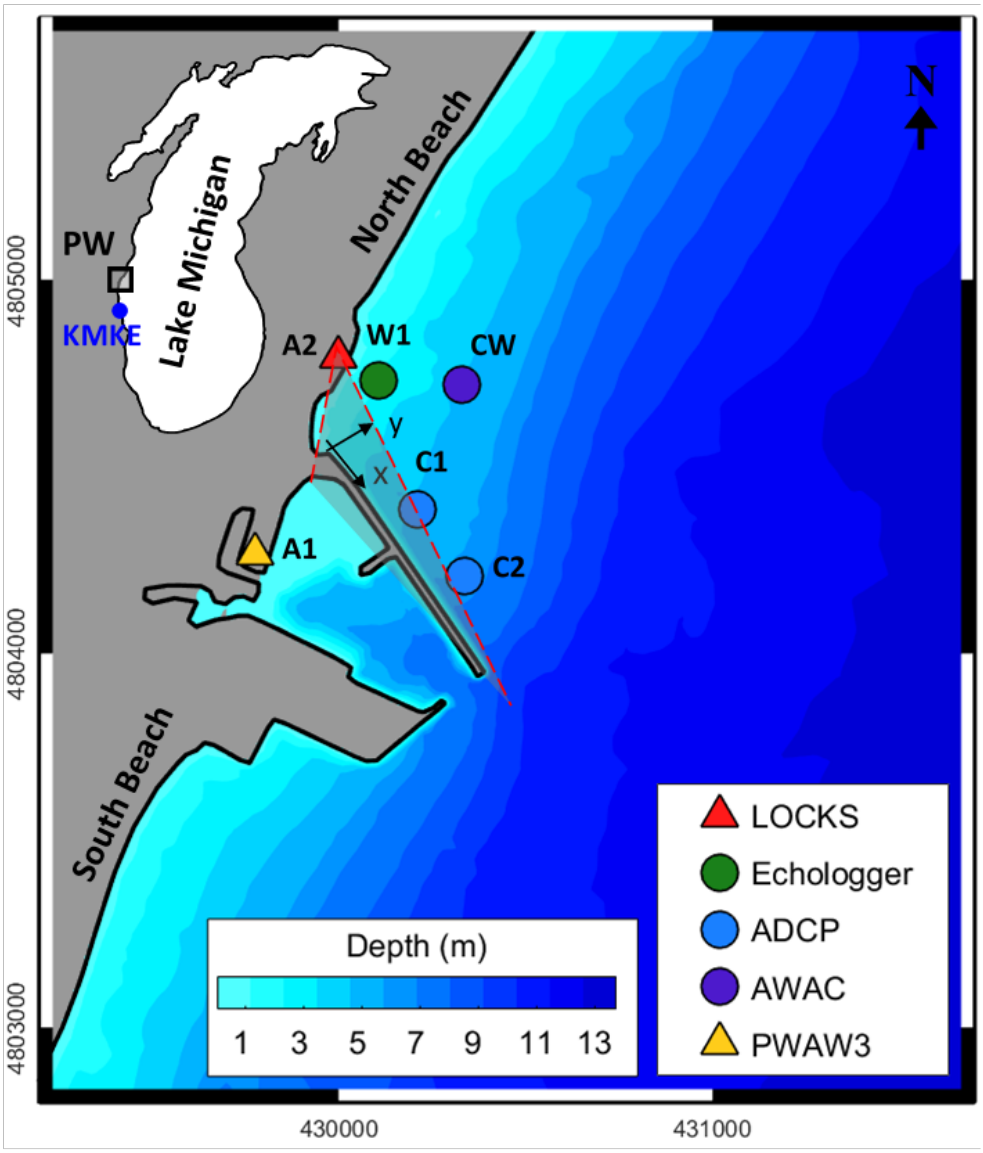

Fig 5-1. Map of the study site at Port Washington, WI (shortened as PW). Color contours show the nearshore bathymetry. Locations of observation stations and field measurement sensors are depicted in markers denoted with specific letters and numbers. A1 is NDBC meteorology station (PWAW3). A2 is the real-time camera and the weather station of the LOCKS. C1, C2 are up-looking ADCPs deployed on north side of the North Breakwater; CW is an AWAC and W1 is an Echologger that were deployed near the North Beach. KMKE is the ASOS station at Milwaukee.

Atmosphere data including surface wind speeds, directions, atmospheric pressures, and radar reflectivity images are compiled from multiple sources. First, data at 10-min interval is obtained from the NOAA weather station PWAW3 (A1 in Fig 5-1) which was established since 2006 as part of the Great Lakes Observation System (GLOS) Weather Station network. Second, 1-min time interval data was collected by a Young ResponseONE Weather Transmitter (#92000) in 2019 as part of the swim season deployment of the Lifeguarding Operational Camera Kiosk System (LOCKS) at the North Beach (Liu and Wu, 2019). Third, 1-min data is obtained from the nearby Automated Surface Observing System (ASOS) at the General Mitchell International Airport in Milwaukee, WI (KMKE, see Fig 5-1). Next Generation Radar (NEXRAD) reflectivity images are obtained from the NOAA National Climatic Data Center at 5-min interval and are used to detect passages of convective storms, which can induce high-frequency water level oscillations, i.e. meteotsunamis (Bechle et al., 2015; Linares et al., 2018).

Hydrodynamic data including nearshore currents, water levels, and wind waves were measured for a 35-day period from July 27, 2016, to August 31, 2016, and a 10-day period from Aug 9, 2017, to Aug 19, 2017. Nearshore currents on the north side of the Port Washington harbor were measured at three locations (see Fig 5-1). Near the north breakwater, two Teledyne RDI Acoustic Doppler Current Profilers (ADCPs) sensors (denoted a C1 and C2 in Fig 5-1) were deployed about 20 meters from the breakwater at a water depth of 4.6 meters and 6.7 meters, respectively. Profiles of current velocities were sampled at 3 Hz for 2.5 min in every 5-min interval. Farther away from the structure, a Nortek 1 MHz Acoustic Wave and Current Profiler (AWAC) sensor (denoted as CW in Fig 5-1) was deployed at a water depth of 5.5 meters. Velocity profiles and wind waves using the acoustic surface tracker technique (Nortek AS, 2005) were sampled in a burst mode of 2 Hz for 8.5 min in every 10-min interval. In addition, an ultrasonic

Echologger sensor (denoted as W1 in Fig 5-1) was deployed to measure the time series of water surface displacements at 5 Hz.

Visual images at the study site were recorded using a real-time Mobotix 6MP resolution dual-lens camera on the rooftop of Wastewater Treatment Plant (denoted as A2 in Fig 5-1). The camera view toward the north side of the breakwater provides a 45°×34° field of view (FOV). The camera's central control unit can automatically adjust the brightness based on the different lighting conditions during the day. High-resolution images were sampled every 5 seconds. The image data are used to detect visual signatures of rip currents, such as sediment plumes (Dalrymple et al., 2011; Leatherman and Leatherman, 2017) or bubble-laden water jets (Castelle et al., 2016).

5.2.3 Rip current identification

Rip currents are identified based upon directions and magnitudes of measured velocities during the 2016 field measurement. Rip currents with speed greater than 0.5 m/s are hazardous to swimmers (Castelle et al., 2016) and studies found that offshore-directed flows at speeds of 0.1 – 0.2 m/s could develop into strong rips with speeds larger than 1 m/s (Moulton et al., 2017; Scott et al., 2016). In this study, rip current occurrences are identified using two criteria: (i) velocity direction within +/- 15 degrees from the angle of the nearby structure toward offshore and (ii) velocity magnitude larger than 0.1 m/s, which corresponds to above the 95^{th} percentile for measured velocities of 35-day data set in 2016. The time series of measured current velocities are processed in the following three steps. First, velocity profiles in each sampling interval are averaged over time and water depth. Next, the time and depth-averaged velocities are converted from the universal ENU (East, North, Upward) coordinate system by the sensors to a location-specific CAU (Cross-shore in x, Alongshore in y, Upward in z) coordinate system, as shown in

Fig 5-1 for the x-y plane. Lastly, calculated velocity magnitudes and directions are checked using the two criteria (i) and (ii).

Rip currents are also identified based upon sediment plumes that appeared in the camera images. To facilitate the detection, we follow the method in Liu and Wu (2019) to process the recorded images in the following three steps. First, original images in RGB color space are transformed into the HSV color space, which resembles closely human perceived colors. Second, all transformed HSV pixels are partitioned into segments using a k-means clustering method. The regions representing different morphological features, such as the water, the breakwater structure, and rip currents-induced sediment plumes, are separated. Third, images in oblique views are ortho-rectified and transformed into geo-referenced coordinates using parameters obtained from on-site calibration methods (Bechle et al., 2012; Wanek and Wu, 2006). The processed images are checked against the three criteria: (i) pixels in the colors of sediment plumes (Hue<0.167) are detected; (ii) the detected sediment plume in pixel clusters have sizes larger than an area threshold (20 m^2), where the threshold is determined by minimizing any discrepancies between the detections and human eye perceived plumes; and (iii) the centroid locations of detected sediment plumes are in the vicinity of the North breakwater. (Liu and Wu, 2019)

5.2.4 Environmental proxies and association

Environmental proxies like hydrodynamic and atmospheric conditions are used to associate with identified rip current events in the following steps. First, nearshore hydrodynamic conditions include factors like significant wave height (H_s), peak wave period (T_p), and high-frequency water level fluctuations (HFWLFs, denoted as ΔWL). HFWLFs are calculated by applying a band-pass filter on the water surface displacement data with cut-off periods of 2 min and 2 hours,

corresponding to the definition of meteotsunami frequency range (Monserrat et al., 2006). Second, atmospheric conditions include factors like surface wind speeds (W_s), wind directions (Dir_w) measured from the angle clockwise relative to True North and reported in the sixteen-wind compass, wind shifts (ΔDir_w) calculated as the gradients of wind directions, pressure disturbances (ΔP) calculated obtained from differences between local maximum and minimum of filtered air pressures using a 2-hour cut-off period. In addition, convective storms are detected from radar reflectivity images based on storm structure criteria (Bechle et al., 2015). Lastly, all environmental proxies including detected storm structures are associated with the occurrences of rip currents near the structure using time series analysis (Pattiaratchi et al., 2009; Scott et al., 2016) and wavelet analysis, which will be described next.

5.2.5 Wavelet analysis

Wavelet analysis is capable of simultaneously revealing the time and frequency features of time series signals. Wavelet analysis (Daubechies and Sweldens, 1998; Torrence et al., 1998) has been employed to study nearshore processes including rip channel evolutions (Barrett and Houser, 2012), wave breaking patterns (Liu and Babanin, 2004), and high-frequency water level fluctuations (Linares et al., 2016). In this study, we employ a Morlet mother wavelet function (Torrence et al., 1998) to calculate the wavelet power spectrum (WPS) of current speeds measured by the three sensors (C1, C2, and CW) for revealing pulsating characteristics of rip currents. To establish a causative relationship of the occurrence and the pulsating behaviors of rip currents with potential environmental proxies, the cross-wavelet spectral analysis (Grinsted et al., 2004) is employed to calculate the cross-wavelet power spectrum (CWPS) between rip current speeds and the water levels, wind speeds and air pressures.

5.2.6 Structure Rip Checklist and Assessment Matrix (SRiCAM)

A new tool, based on the Great Lakes Rip Current Checklist (GLRCC, Meadows et al., 2011) and by incorporating additional environmental proxies, is developed to assess rip current occurrences near coastal structures. Table 5-1 shows that four factors (i.e., wave height, wave period, wind speed, and lake level) in the SRiCAM are adopted from GLRCC (Meadows et al., 2011). We adjust the wave period factor by accounting for wind fetches at the study site. Five new factors including wind direction, high-frequency water level fluctuation (HFWLF), wind shift, pressure disturbance, and visual image are added. Points from each factor that meets the corresponding criterion in the SRiCAM are added to yield a total point (TP), which are used to assess the potential occurrence of rip currents by four risk tiers: very high (TP>11), high (11≥ TP>7), moderate (7 ≥ TP ≥ 4), and low (4 > TP > 0). At the very high-risk tier, rip currents will occur and can impose life-threatening hazards to people who are close to the breakwater. At the high-risk tier, rip currents are expected to occur and can be dangerous near the breakwater. At the moderate-risk tier, rip currents are possible to occur near the structure. At the low-risk tier, rip currents are generally not expected.

Table 5-1. Structure Rip Checklist and Assessment Matrix (SRiCAM)

Wave Height	Point
1 ft	0.5
2 ft	1
3-4 ft	2
5-7 ft	3
8-10 ft	4
>10 ft	5

Wave Factor _____

Wave Period	Point
3-4 sec	0.5
4-5 sec	1
5-6 sec	2
> 6 sec	3

Period Factor _____

Wind Direction	Point
Downwind	1
Upwind	2

Direction Factor _____

Wind Shift	Point
>15 Deg/hr	1

Wind Shifting Factor _____

Pressure Disturbance	Point
> 0.5 hPa	1

Pressure Factor _____

Wind Speed	Point
0-5 kt	0.5
6-8 kt	1
9-11 kt	1.5
12-14 kt	2
15-17 kt	3
18-20 kt	4
>20 kt	5

Wind Factor _____

Lake Level vs Normal	Point
> 3 in	-0.5
normal	0
-6 to -10 in	1
> -11 in	2

Lake level Factor _____

High Frequency Water Level Fluctuations	Point
1.5 to 3 in	0.5
>3 in	1

HFWLO Factor _____

Visual Image	Point
Storm structure	1
Sediment plume	4

Visual Factor _____

Total Points (TP) _____

TP<4	4 ≤ TP ≤ 7	7 < TP ≤11	TP >11
Low	Moderate	High	Very High

5.3 Results

5.3.1 Rip current characteristics

Fig. 5-2 shows the time series of measured current speeds and directions at C1 and C2 near the structure. With a threshold of 0.1 m/s, fourteen events of rip currents are highlighted by shaded rectangles and numbered chronologically with a letter *A* or *D* to denote forms of accelerating or decelerating currents, respectively. Table 5-2 summarizes the maximum rip current speeds (U_{max}) and durations (ΔT), and the associated *A*- or *D*-form currents for each event. The speeds of the identified rip currents are between 0.10 – 0.23 m/s and the durations are between 1.7 – 27.1 hours. Eight rip events (#1, #3, #4, #6, #7, #8, #11 and #14) with an average speed of 0.13 m/s and an average duration of 7.1 hours are categorized as the *A*-form currents. The other seven (#2, #5, #9, #10, #12, and #13) with an average speed of 0.10 m/s and an average duration of 3.1 hours are categorized as *D*-form currents. Rip current feeding flows are measured at CW located farther away from the breakwater. The magnitudes of currents at CW are consistent with those of the rip currents at C1 and C2 but the directions of currents are mostly longshore southward (averagely ~ 190° clockwise from the True North) for *A*-form currents and southeastward (~213°) for the *D*-form currents, respectively. Note that for the *A*-form currents, the angle between the approaching longshore currents and the orientation of north breakwater (see Fig 5-1) is approximately 45°, coinciding with an optimum angle for currents to deflect out to offshore along the breakwater (Scott et al., 2016). As a result, the average speed and duration of *A*-form currents tend to be larger and longer than those of *D*-form currents, respectively. Overall, two forms of observed rip currents near the breakwater, along with the strong longshore feeding currents, are characterized.

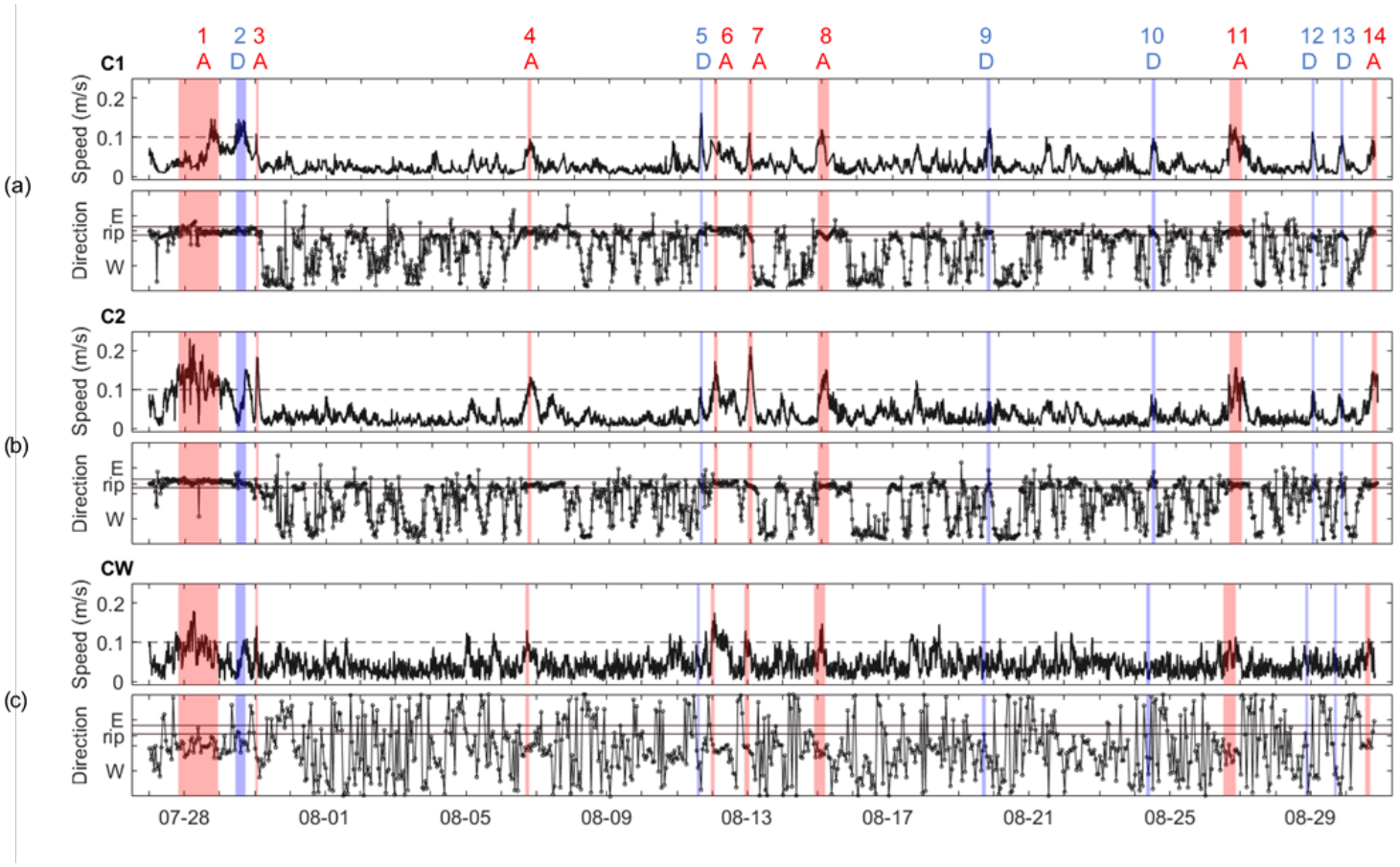

Fig 5-2. Time series of current speeds and directions measured at three locations of (a) C1, (b) C2, and (c) CW during the field measurements from 2016/07/27 to 2016/08/31. Gray lines represent the rip identification thresholds for speeds (dashed line) and for directions (solid lines). A total of fourteen rip current events are highlighted in shaded rectangles, and labeled chronologically from 1 to 14, followed by a letter *A* or *D* to denote forms of accelerating or decelerating currents.

Table 5-2. Summary of rip current events identified during 2016 field measurements and associated environmental conditions

Events in 2016		Currents			Proxy Type	Waves		Water Level Changes	Wind & Pressure Disturbances				Storms
#	Date & time	Form	U_{max} (m/s)	ΔT (hr)		H_s (m)	T_p (sec)	ΔWL (m)	W_s (m/s)	Dir_w (from)	ΔDir_w (°/hr)	ΔP (hPa)	
1	07/28 14:00 – 07/29 17:00	A	0.23	27.1	I,V,VI,VII	0.67	4.9	0.08	7.1	NE	0	0.57	cluster
2	07/30 05:00 – 07/30 13:30	D	0.15	8.5	I,V,VII	0.72	4.5	0.05	5.1	NE	3	0.39	cluster
3	07/30 18:35 – 07/30 20:20	A	0.18	1.7	II,VII	0.43	3.8	0.03	5.2	NE	22	0.46	cluster
4	08/07 10:40 – 08/07 13:15	A	0.13	2.5	I	0.55	4.0	0.03	3.2	ENE	1	0.45	none
5	08/12 07:45 – 08/12 09:30	D	0.16	1.7	IV,V,VI,VII	0.12	3.5	0.04	2.1	ENE	15	0.71	linear
6	08/12 17:05 – 08/12 19:35	A	0.17	2.5	II,V,VI,VII	0.40	2.7	0.10	5	NE	4	0.57	linear
7	08/13 16:00 – 08/13 19:25	A	0.21	3.4	II,V	0.18	3.0	0.05	5.1	NNW	17	0.38	none
8	08/15 15:30 – 08/15 23:10	A	0.15	7.6	II,V,VII	0.16	2.8	0.06	3.5	NE	6	0.41	complex
9	08/20 10:05 – 08/20 12:35	D	0.12	2.5	III,V,VI, VII	0.84	4.9	0.08	5.8	S	2	0.98	bow
10	08/25 02:00 – 08/25 04:35	D	0.10	2.5	II,V,VI, VII	0.21	3.9	0.05	2.3	NE	0	0.71	cluster
11	08/27 06:40 – 08/27 15:05	A	0.16	8.5	I,V,VI,VII	0.61	4.0	0.09	5.2	NE	2	1.12	complex
12	08/29 14:35 – 08/29 16:20	D	0.11	1.7	IV,V	0.13	3.6	0.06	1.4	E	36	0.43	none
13	08/30 10:10 – 08/30 11:50	D	0.10	1.7	IV,VI	0.12	3.3	0.03	4.4	SSE	25	0.52	none
14	08/31 07:20 – 08/31 10:45	A	0.15	3.4	I	0.76	5.4	0.02	3.9	N	22	0.39	none

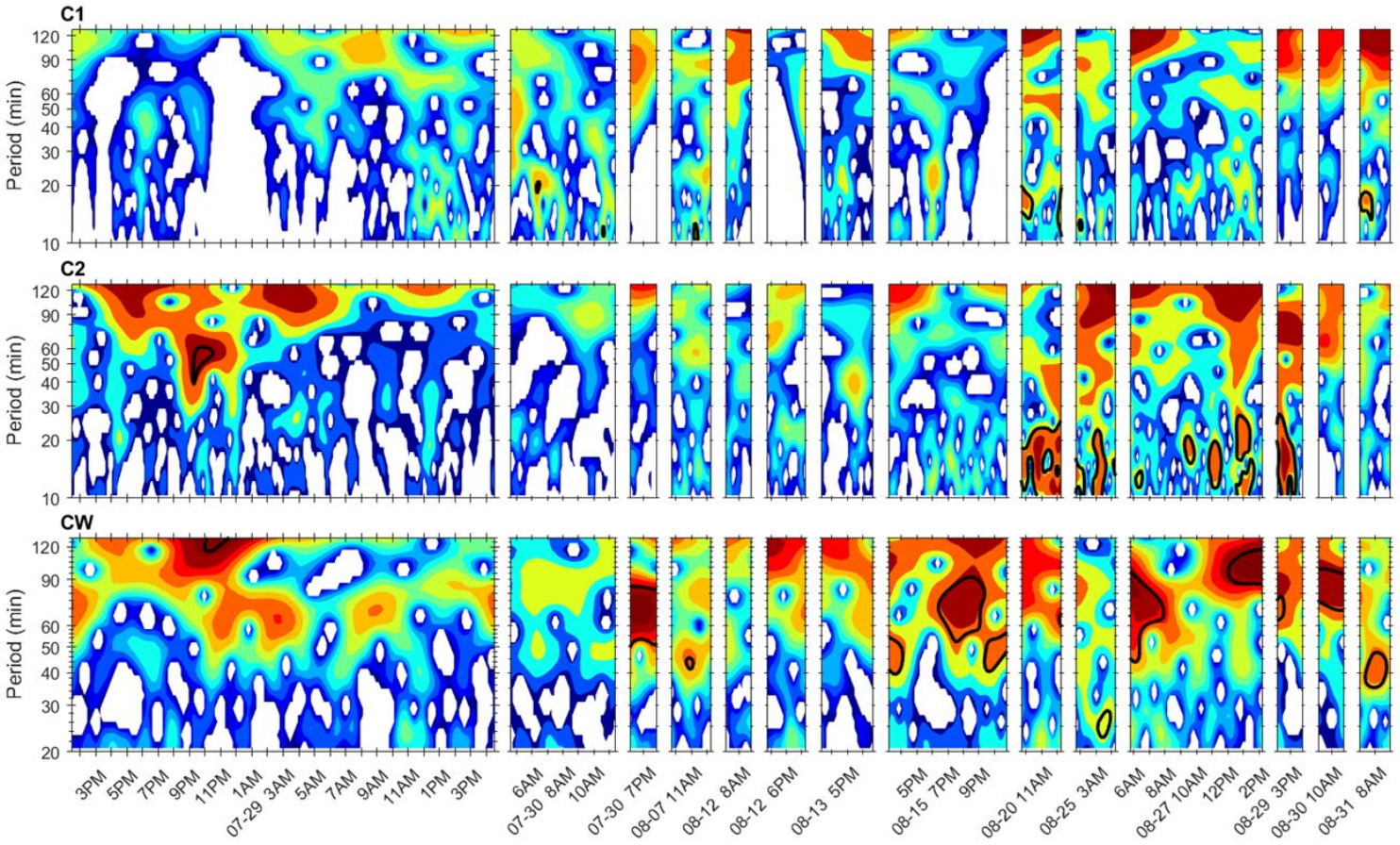

Fig 5-3. Wavelet power spectrum (in log scale) of current speeds at three locations of (a) C1, (b) C2, and (c) CW during the fourteen identified rip current events. Warm color regions represent high spectrum energy. Black solid contours represent the 95% confidence level.

Velocity pulsations measured by the three sensors at C1, C2, and CW during the fourteen identified rip current events are discussed here. Fig 5-3 shows the wavelet power spectrum (WPS) of speeds normalized against the variance in log scaled color contours. Warm colors represent high energy levels and the black lines represent WPS at the 95% significance level. Pulsations of high energies are mostly observed with the periods between 60 and 120 min, which may be caused by atmospheric disturbances. Pulsations of so-called Very Low Frequencies (VLFs, f<0.004 Hz, MacMahan et al., 2010) with periods of ~ O(10 min) are apparent at C1 (events #2, #4, #9, #10

and #14) and at C2 (events #9, #10, #11 and #12) but less obvious at CW. Interestingly, *D*-form currents (#9 and #10) show marked VLFs signatures at both C1 and C2, In comparison, *A*-form currents (events #1, #3, #6, #7 and #8) do not exhibit notable signatures of VLFs. The results indicate that the offshore-directed flows in rip currents near the breakwater are oscillatory with signatures of VLFs.

5.3.2 Environmental proxies for rip current occurrences

Four types of environmental proxies with factors of nearshore significant wave heights (H_s), wave periods (T_p), wind speeds (W_s), and wind directions (Dir_w) are associated with the identified rip current events, as shown in Fig 5-4 (a-b). The first (I) type of proxy, featured with high waves and N-E winds, is associated with events #1, #2, #4, #11, and #14 (see Table 2). The significant wave heights were all larger than 0.45 m (1.5 ft) with the peak wave periods above 4 sec. Winds with an average speed of 5.1 m/s were consistently from N to E directions. Generated wave-driven longshore currents propagated toward the structure to form rip currents in the offshore directions. The second (II) type of proxy, featured with moderate to low waves (H_s>0.15 m or 0.5 ft) and N winds (Dir_w < 45°), are associated with events #3, #6, #7, #8, and #10. Either the waves in a highly oblique incidence or the direct wind stresses parallel to the shoreline (~ 30°) induced strong longshore currents toward the breakwater to generate the deflected rip currents. The third (III) type of proxy, featured with high waves and S winds, is associated with event #9. With the significant wave height as high as H_s = 0.84 m at CW, wave-induced currents can form shadow rip currents on the north side of the breakwater, sheltered behind the breakwater. The fourth (IV) type of proxy, featured with wind direction shifts at low waves (H_s<0.15 m), is associated with events #5, #12, and #13. Winds from E to S directions with more than 15 degrees per hour of

change in directions were observed. Note that the low-wave conditions seem unfavorable to cause rip currents but the wind shifting could create temporary rip currents near the breakwater. The durations (ΔT) in rip currents was observed less than 2 hours, in comparison with the other 10 events (see Table 5-2).

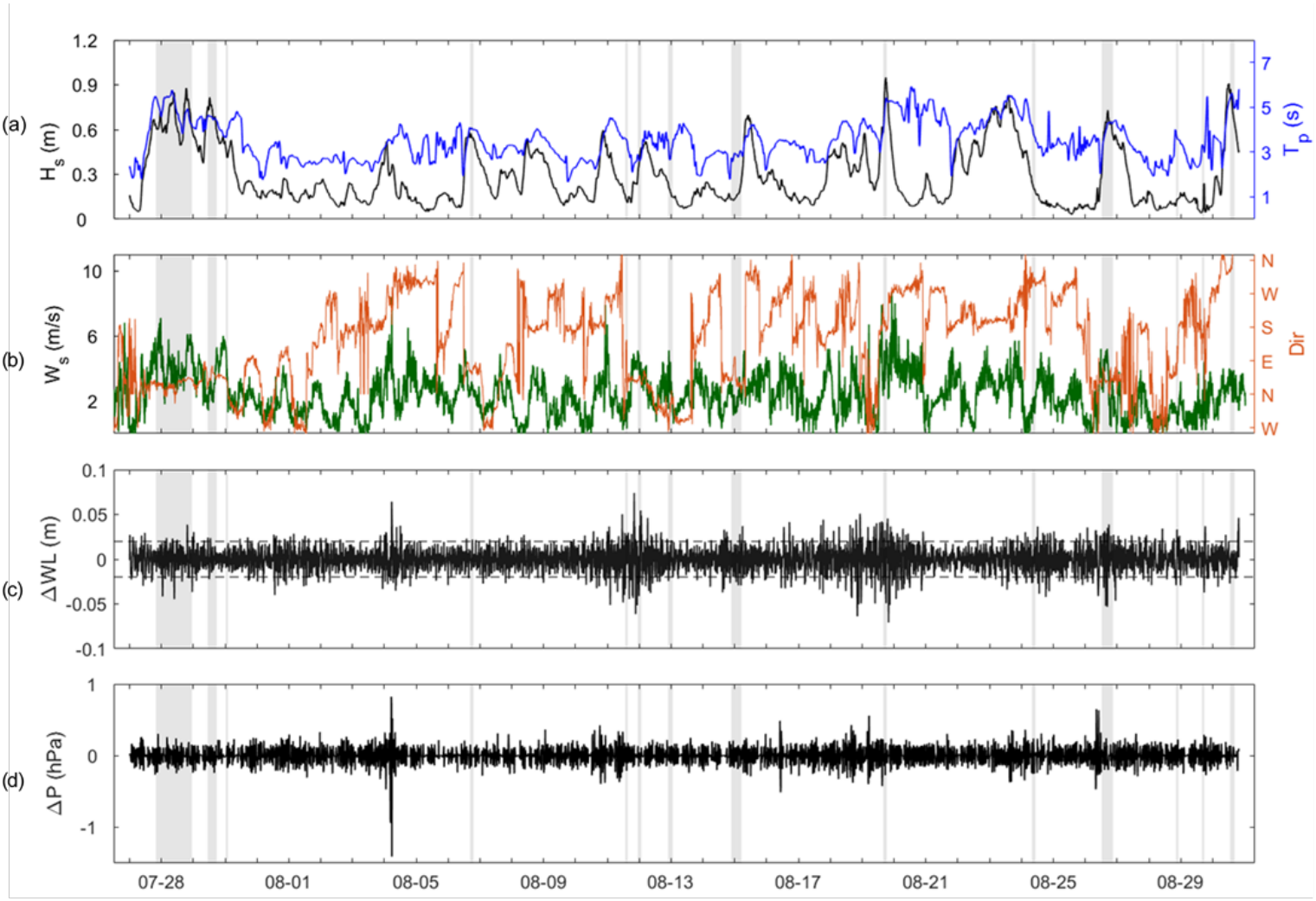

Fig 5-4. Time series of environmental conditions during the period from 2016/07/27 to 2016/08/31: (a) nearshore wave significant height (H_s), peak wave period (T_p) measured at CW location; (b) surface wind speeds (W_s) and directions (Dir_w) at A1 location; (c) high-pass filtered water level fluctuations (ΔWL) at CW location; and (d) high-pass filter atmospheric pressure disturbances (ΔP) at A1 location.

Three additional types of environmental proxies including new factors like high-frequency water level fluctuations (*ΔWL*), atmospheric pressures disturbances (*ΔP*), and storm structures related to identified rip currents are assessed in this study. The fifth (V) proxy type, featured with ΔWL with magnitudes above the standard deviation σ of 0.04 m (1.5 in), is observed in a majority (10 out of the 14) of events, as shown in Fig 5-4 (c). During the two events (#6 and #11), water level oscillations reached $\Delta WL > 2\sigma$ (3 in) and relatively large rip speeds occurred (>0.15 m/s, see Table 2). The sixth (VI) proxy type, featured with atmospheric pressure disturbances of $\Delta P >\sim 0.5$ hPa, happened during or before the rip current events (#1, #5, #6, #9, #10, #13), as shown in Fig 5-4 (d). Nevertheless, the two proxies (types V and VI) on the days of 2016/08/04, 2016/08/17, and 2016/08/19 in Fig 5-4 (c-d) met the criteria but there were no identified rip currents (Fig. 5-2). One possible reason is that the observed water level fluctuations (type V) might be infra-gravity waves (Bertin et al., 2018), which are different from meteorologically induced water fluctuations to cause rip currents near structures (Linares et al., 2019). The other possibility is that the pressure perturbations (type VI) induced water level fluctuations were propagating to the shoreline normally, which could not generate longshore currents to form deflected currents along the breakwater structure. The seventh (VII) proxy type, featured with storm structures (Bechle et al., 2015), is found to co-occur with rip currents (9 out of the 14 events in Table 5-2).

Environmental proxies correlated with velocity pulsations of identified rip current events are further revealed here. Fig. 5-5 a, b, and c are the cross-wavelet power spectrum (CWPS) of the observed current velocities at C2 with water levels, atmospheric pressures disturbances, and wind speeds, respectively. Significant CWPS between rip currents and the three environmental proxies are observed at periods <30 min, suggesting that the VLFs in rip velocities are highly associated with or even caused by these environmental proxies. Furthermore, time evolutions of different

environmental proxies within a rip current event are observed. A typical example is event #1. At around 5 PM on 07-28, the distinct CWPS in the wind speed is seen at periods between 15 – 60 min (Fig. 5-5c), suggesting that pulsating currents are associated with type I proxy. Later at 10 PM, the CWPS appears in the three factors at periods of a narrower band between 30 – 60 min (Fig. 5-5a, b, c), suggesting that pulsating currents are associated with type I, V, and VI simultaneously. At 4 AM on 07-29, the marked CWPS in atmospheric pressure disturbances appears at periods approximately at 15 - 30 min (Fig. 5-5b), suggesting that pulsating currents are associated with type VI. These results based upon CWPS analysis support the previous finding that atmospheric disturbances or/and induced water level fluctuations can lead to dangerous rip currents near structures (Linares et al., 2019).

To sum up, based on the time series (Fig. 5-4) and cross-wavelet analysis (Fig. 5-5), identified rip currents near the breakwater structure are associated with the seven environmental proxies. Type I and III proxies are associated with high waves and the preferred wind directions for deflection or shadow rip currents (Castelle et al., 2016). Type II proxy is related to the shore-parallel winds (Scott et al., 2016). Type IV proxy is associated with shifting winds. Type V, VI, and VII proxies are related to high-frequency water level oscillations, atmospheric pressure disturbances, and convective storm structures, respectively (Linares et al., 2019; Liu and Wu, 2019). Furthermore, most occurrences (12 out 14, see Table 5-2) and velocity pulsations of rip currents near the structure can be associated with more than one environmental proxy during a rip current event.

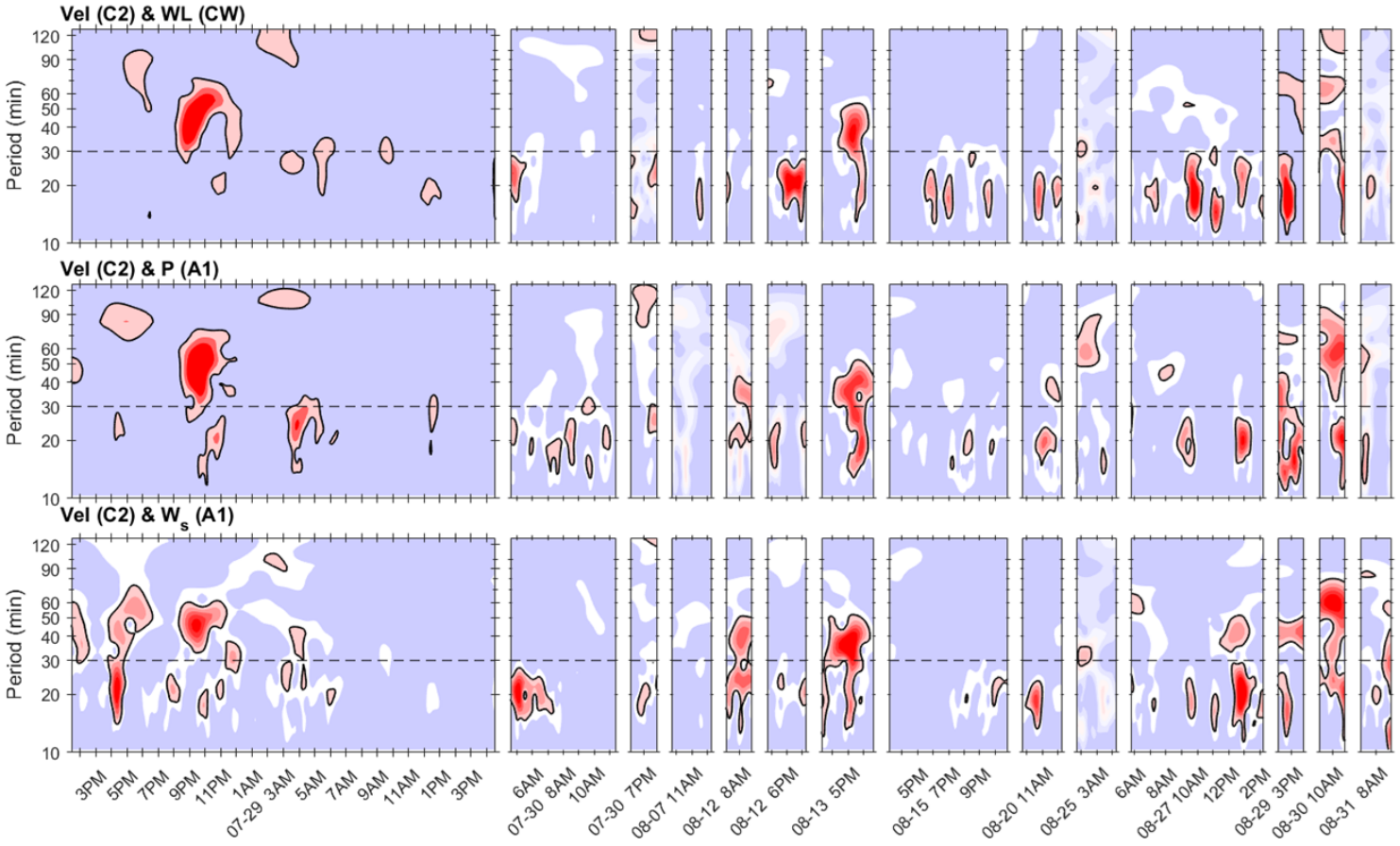

Fig 5-5. Cross-wavelet spectrum of current velocities measured at C2 (*Vel*) (a) water levels (*WL*) at CW, (b) atmospheric pressure perturbations (*P*) at A1, and (c) wind speeds (W_s) at A1. Each tick represents 1-hour interval. The spectrum is normalized by the 95% confidence level (power relative to significant level) and black solid contours represent CWPS that are statistically significant at the $\alpha = 5\%$ level.

5.3.3 Visual signatures of rip currents

Visual signatures of sediment plumes captured by the camera A2 viewing toward the north breakwater at Port Washington can be the evidence of rip currents. Fig. 5-6 shows the four example images of rip current events. Features of rip-current induced sediment plumes in the four events (#1, #3, #9, and #5) appear different. In the event #1, a plume patch was exhibited near the breakwater with no apparent feeding longshore currents. In event #3, the noticeable longshore currents were deflected to generate a narrow band of rip-current induced sediment plumes along the breakwater. In the event #9, a patch of plumes due to the longshore feeding currents was apparent but the deflected currents were not visible along the breakwater. In the event #5, the water appeared calm with no sediment plume features. Nevertheless, velocity measurements at C1 show offshore rip currents up to 0.16 m/s (see Table 5-2), indicating that rip currents near the breakwater can be a hidden hazard to those who are unaware. Events #1, #9, and #5 are associated with storm-related proxy types of V, VI, and VII, respectively, inferring that the cloudy weather, seen in Fig 5-6a, c, and d, can be used as a visual proxy of the occurrence of rip currents. Note that the event #3 is associated with a cluster storm (type VII), which crossed the southern Lake Michigan but did not pass the study site. As a result, the weather in the image (Fig. 5-6b) seemed sunny but the danger of rip currents was disguised. Overall, visual signatures of sediment plumes can directly provide vivid evidence for the occurrences of rip currents. When no apparent sediment plumes near the structure, environmental proxies like storm-related proxies could be used to assess hidden rip currents near coastal structures.

Fig 5-6. Examples of camera images viewing north breakwater at Port Washington, WI at events: (a) #1 on 2016/07/29 12:16, (b) #3 on 2016/07/30 19:01, (c) #9 on 2016/08/20 10:17, (d) #5 on 2016/08/12 09:17. For the events #1, #3, and #9 in (a-c), visual signatures of sediment plumes induced by rip currents and longshore feeding currents, highlighted in red arrows, are evident.

5.3.4 Evaluation of SRiCAM

New factors added to the SRiCAM in Table 5-1 with assigned points are rationalized here. A wind direction factor accounts for the type I and II proxies for deflection rip currents (Upwind) and the type III proxy for shadow rip currents (Downwind). As rip currents under the type I and II proxies are more frequently observed, two points are assigned to the Upwind criteria. A wind shift factor addresses the type IV proxy for a changing driver condition to initiate rip currents. A high-frequency water level fluctuation factor addresses the type V proxy for the potential occurrences

of rip currents due to meteotsunamis (Linares et al., 2019) or seiches (Meadows et al., 2011). A pressure disturbance factor addresses the type VI proxy for rip currents with dangerous pulsating velocities. Lastly, a visual image factor addresses two situations: (i) the type VII proxy for storm structures leading to rip currents through nearshore transformations (Linares et al., 2019) and (ii) direct visual signatures of sediment plumes caused by rip currents.

Outcomes of SRiCAM assessing rip current occurrences near coastal structures are evaluated. Table 5-3 shows 22 rip current events including 14 in 2016 and additional 8, which are identified based on velocity measurements conducted from Aug 9 to Aug 19, 2017 (denoted as "Velocity") or visual evidence of rip currents imaged from the A2 camera (denoted as "Image") in 2017-2019. Assessment results show that all the identified rip current events are in the *moderate*-, *high*-, or *very high*-risk tier. Contributions of the five new factors are 75% on average for all events. For events assessed in the *very high*-risk tier (#1, #16, #18, #20, #21), the contributions from new factors are on the range of 70-80% including the type I with large waves and strong winds and types V, VI, VII with convective storms. For events assessed in the *high*-risk tier (#2, #3, #9, #19, #22), the new factor contributions exhibit large variations from 56% (#19) to 95% (#22). For events assessed in the *moderate*-risk tier, similarly, the large variation in new factor contributions are exhibited. For example, a low 50% contribution from new factors in the event #14 is associated with the proxy I. A high 91% contribution from new factors in the event #5 is associated with newly identified proxies IV, V, VI, VII (see Table 5-2). In short, the new factors in the SRiCAM reflect important contributions to different degrees. In addition, 9 out of 10 events assessed in *very high*- or *high*- risk tier have visual evidence of sediment plumes, supporting the effectiveness of new visual image factor in SRiCAM to reflect associated risks. Overall, the

SRiCAM is developed and validated. The new assessment tool, SRiCAM, effectively provides warning messages of potential occurrences of rip currents near the breakwater.

Table 5-3. Validation of SRiCAM on rip current events identified near the north breakwater at PW

#	Rip Current Events (2016-2019)	Velocity	Image	Total Points	Assessment	Contribution from New Factors
1	7/29/2016 03:30	yes	yes	12.5	*very high*	72%
2	7/30/2016 08:25	yes	yes	10.5	*high*	71%
3	7/30/2016 19:25	yes	yes	10.5	*high*	81%
4	8/07/2016 12:00	yes		4.5	*moderate*	56%
5	8/12/2016 08:35	yes		5.5	*moderate*	91%
6	8/12/2016 18:25	yes		6.5	*moderate*	77%
7	8/13/2016 17:40	yes		4.5	*moderate*	78%
8	8/15/2016 19:20	yes		4	*moderate*	88%
9	8/20/2016 11:20	yes	yes	11	*high*	73%
10	8/25/2016 03:20	yes		5	*moderate*	90%
11	8/27/2016 10:50	yes		7	*moderate*	71%
12	8/29/2016 15:30	yes		4	*moderate*	88%
13	8/30/2016 11:00	yes		4.5	*moderate*	78%
14	8/31/2016 09:00	yes		7	*moderate*	50%
15	8/11/2017 01:05	yes		6.5	*moderate*	77%
16	8/15/2017 12:05	yes	yes	11.5	*very high*	78%
17	8/16/2017 22:25	yes		6	*moderate*	83%
18	8/17/2017 09:05	yes	yes	12	*very high*	75%
19	8/17/2017 14:55	yes		9	*high*	56%
20	8/17/2018 10:10		yes	11.5	*very high*	70%
21	6/28/2019 08:15		yes	12.5	*very high*	72%
22	8/15/2019 15:25		yes	10.5	*high*	95%

5.4 Discussion

5.4.1 Multi-tiered risk assessments

Four- and three-tiered risk assessments are compared and discussed here. First, the four-tiered risks in SRiCAM are compared with three-tiered risks in SRiCAM (TP ≥ 5 as moderate and TP ≥ 10 as high). Based upon the SRiCAM checklist, for a hidden rip event such as #7 the Total Point (TP) yields 4.5. The four-tiered level assesses the event as a moderate risk. In comparison, the three-tiered level would assess the TP=4.5 too low to reach a moderate risk. Similarly, 5 out of the 12 (moderate in the four-tiered level) in Table 5-1 would be assessed into a low risk in the three-tiered level. Furthermore, event #19 (high in four-tiered level) would be assessed to a moderate-risk tier in the three-tiered level. In other words, the three-tiered risk assessment tends to underestimate risk levels and can be perceived as overly cautious, resulting in low confident trust to the public (Houser et al., 2019). Second, we compare the four-tiered risks in the SRiCAM with the three-tiered risks in the GLRCC. By incorporating new proxy factors and building upon the weighting of original GLRCC factors for wind wave-driven rip currents in open beaches (Meadows et al., 2011), the SRiCAM addresses rip currents occurring near structures. Under wind waves dominating conditions (type I, III proxies), the SRiCAM adds points contributed from the original factors in the GLRCC, yielding a consistent assessment. Under mixed conditions such as strong shore-parallel winds (type II), shifting winds (type IV), meteorologically induced (type VI, VII), or water level fluctuations (type V) including meteotsunamis and seiches (Linares et al., 2019; Meadows et al., 2011), the SRiCAM considers significant contributions (>50%, see Table 3) from new factors to capture hidden rip currents, which would otherwise be assessed as low-risk by the GLRCC. Lastly, four-tiered risk assessments, instead of three-tiered risk assessments, have been recently adopted by several rip current warning systems (Arun Kumar and Prasad, 2014; “US

National Weather Service Grand Rapids Michigan"). Overall, the four-tiered risks in the SRiCAM is a trust-worthy and consistent tool to assess potential rip currents occurring near coastal breakwater structures.

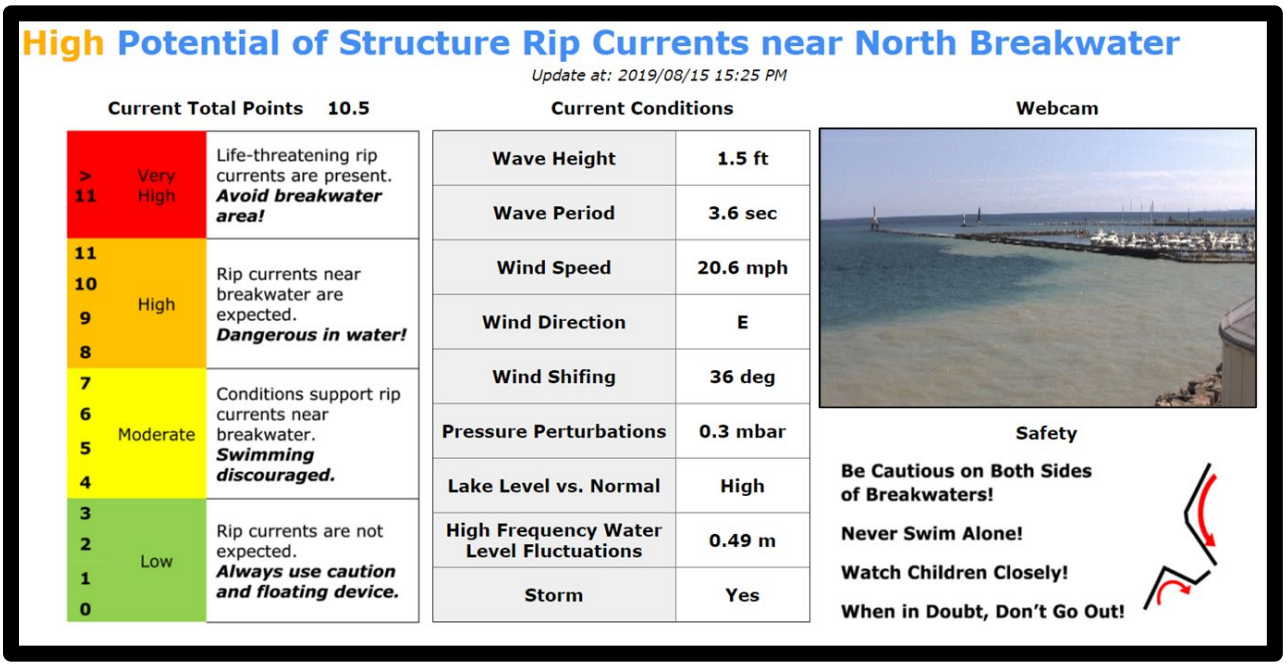

Fig 5-7. A webpage display for providing real-time assessment for the potential occurrence of rip currents near north breakwater at Port Washington, WI. A rip current event on 2019/08/15, as an example, is assessed as high-risk tier with a total point of 10.5 calculated using the SRiCAM tool. Current conditions of the nine environmental parameters, real-time webcam image, and safety messages are included on the webpage.

5.4.2 Integration of cyberinfrastructure

Cyberinfrastructure technology has been widely employed to provide real-time hazard-related warnings in recent years. For example, an Integrated Nowcast Forecast Operation System (INFOS) cyberinfrastructure has been served as an effective tool for water information and water-related hazards in the Great Lakes region (Anderson and Wu, 2018; Liu and Wu, 2019; Reimer and Wu, 2016). In this study, the SRiCAM is integrated into the INFOS (Liu and Wu, 2019) for

providing real-time warnings of rip currents near the north breakwater at City of Port Washington, WI (URL: https://infosportwashington.cee.wisc.edu/Northbreakwaterwatch1.html). Fig. 5-7 shows the webpage display during the rip current event (#22) on 2019/08/15 at 15:25 PM as an example. On the top of the page, the assessment of a *very high*-risk tier is highlighted in bolded red color. The text color is accordingly changed based upon the four risk tiers. Underneath are the main contents with three columns to describe the detailed information related to rip currents. On the left column, total points with four-tiered risk assessment of rip current risks are shown. Particularly, the explanations for "*very high*", "*high*", "*moderate*", "*low*" risks are given to describe the corresponding communication messages, emphasized in the bolded font, for each risk tier. The wordings are taken from those used in the local signage provided by the City of Port Washington (Liu and Wu, 2019) and the forecast provided by the NOAA National Weather Service (https://www.weather.gov/safety/ripcurrent-forecasts). In the middle column, current conditions of the nine factors as environmental proxies for the SRiCAM are shown. On the right column, a webcam image viewing toward the north breakwater provides visual information of weather and hydrodynamic conditions and sediment plumes induced by rip currents near the structure. For example, the rip length during the event #22 (Fig.5-7) is estimated to be 750m using the Direct Linear Transformation equation (Bechle et al., 2012; Wanek and Wu, 2006). By tracking sediment plumes over multiple images, the estimated rip speed is 0.2 m/s, consistent with the measurements during events of 2016 (see Table 5-2). Lastly, safety education is incorporated at the right bottom corner. The message, "Be Cautious on Both Sides of Breakwater!" with a schematic for visual illustration, is emphasized since deflection and shadow currents can occur near coastal structures at the same time (Scott et al., 2016). Other messages in Fig. 5-7 are also given to enhance communications and awareness of rip current hazards. Overall, integration of the SRiCAM into

the INFOS provides real-time warnings of rip current hazards near coastal structures in the Great Lakes for the first time, as far as the authors are aware.

5.4.3 Data contingency plan

Reliable real-time assessment for hazard-related risks requires a data contingency plan (Anderson and Wu, 2018). During temporary station downtime or seasonal sensor unavailability, environmental factors like wave height, wave period, wind speed, wind direction, and pressure disturbance, or water level fluctuations cannot be accounted for, yielding lower total points to a lower-tier risk. Two-step data contingency procedures are designed to ensure that all factors are counted. In step (I), alternative observations from nearby sensors are used to replace the missing data. Specifically, wave information can be obtained from two wave buoys: (i) NDBC station 45013 at Atwater Park, located 20 miles south of Port Washington Harbor, and (ii) NOAA station 45007 in central South Lake Michigan. Nearshore waves at the study site are estimated by adjusting the offshore wave observations through the linear-wave dispersion relation (Dean and Dalrymple, 1991). Additional meteorological wind and atmospheric pressure data are obtained from the three stations: the NDBC stations MLWW3 at Port of Milwaukee, SGNW3 at Sheboygan, and an Automated Weather Observing System (AWOS III) station KETB at West Bend to further augment the observations at the NDBC station PWAW3 and ASOS station KMKE. Water level oscillations at the NOAA gauge (9087057) and the other nine gauges in Lake Michigan from the nearest to the farthest order are used. The high-frequency water level fluctuations criteria are adjusted to the station-specific thresholds determined in previous meteotsunami studies (Bechle et al., 2015, 2016). In step (II), outputs from the Great Lakes Coastal Forecasting System (GLCFS),

downloaded from the GLOS Thredds Server (http://tds.glos.us/thredds/catalog/catalog.html) for gridded wind, pressure, and wave fields, are used if no alternative observations are available after step (I). The GLCFS, developed by the Great Lakes Environmental Research Laboratory (Alves et al., 2014; Liu et al., 1984; Schwab et al., 1986), is operated to provide real-time nowcasting/forecasting of hydrodynamic condition across the Great Lakes. In short, the data contingency plan for the implemented SRiCAM-INFOS cyberinfrastructure is essential to provide reliable warning messages of rip current occurrences near the breakwater structure.

5.4.4 Applicability to other locations in Lake Michigan

The applicability of the SRiCAM to other locations near harbor breakwaters around Lake Michigan is examined. Assessments are based on observation data from multiple sources including 12 NDBC offshore wave buoys for wave factors, 20 NDBC and ASOS weather stations for winds and pressure factors, and 10 NOAA water level gages for the high-frequency water level fluctuation factor in Lake Michigan. Specifically, nearshore waves are estimated using the dispersion relation (Dean and Dalrymple, 1991). Observed wind directions are examined with specific shoreline and structure orientations at each location individually to determine the "Upwind" or "Downwind." Fig. 5-8a shows an example of applying the SRiCAM to assess risks of rip currents on 2019/07/20 at the 39 locations including Port Washington, WI in Lake Michigan. The majority (27 out of the total 39) of locations are assessed as the *moderate* risk, 10 are assessed as the *high* risk, and 2 as the *low* risk. The assessed risks are consistent with visual images of rip current occurrences at three locations spanning across west, south, and east coasts of the Lake Michigan at #[1] Port Washington, WI (Fig 5-8b), #[14] Michigan City, IN (Fig 5-8c), and #[21] Grand Haven, MI (Fig 5-8d), respectively. The three visual images of rip-induced sediment

plumes, shown as red arrows in Fig 8b-d, were captured by the camera at LOCKS, the webcam by the Great Lakes Meteorological Real-Time Coastal Observation Network, and the EarthCam (earthcam.com), respectively. Note that the image (Fig 5-8e) shows water appeared choppy without apparent sediment plumes at #[17] South Haven. The assessment is a *moderate* risk, suggesting possible hidden rip currents near the breakwater. In some cases, the assessment outcome is not yet certain. The assessment at #[8] Sheridan Park and #[9] Chicago, IL, two locations close to each other, are a *moderate* risk (*TP*=5) and a *low risk* (*TP*=2), respectively. Further study is needed to adjust the environmental proxies in the SRiCAM to the risk tier due to differences in site-specific conditions and local structure configurations. Overall, the applicability of the SRiCAM for assessing potential rip current occurrences to locations near harbor breakwaters in Lake Michigan is promising. Future work should be devoted to incorporating and integrating the SRiCAM into regional cyberinfrastructures like the Great Lakes Beach Hazards (US Department of Commerce, NOAA, 2020) for providing real-time warnings for rip currents near harbor breakwaters in the Laurentian Great Lakes.

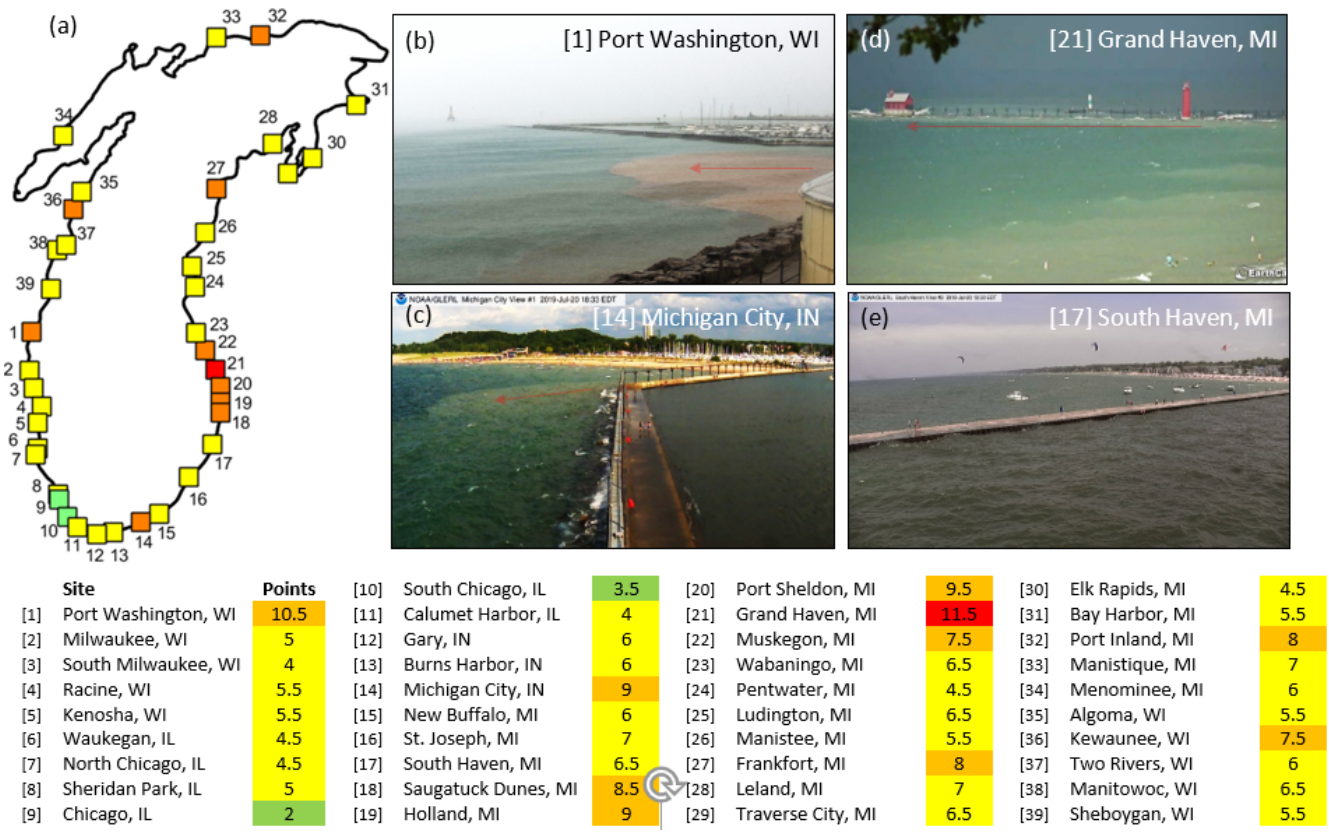

	Site	Points
[1]	Port Washington, WI	10.5
[2]	Milwaukee, WI	5
[3]	South Milwaukee, WI	4
[4]	Racine, WI	5.5
[5]	Kenosha, WI	5.5
[6]	Waukegan, IL	4.5
[7]	North Chicago, IL	4.5
[8]	Sheridan Park, IL	5
[9]	Chicago, IL	2
[10]	South Chicago, IL	3.5
[11]	Calumet Harbor, IL	4
[12]	Gary, IN	6
[13]	Burns Harbor, IN	6
[14]	Michigan City, IN	9
[15]	New Buffalo, MI	6
[16]	St. Joseph, MI	7
[17]	South Haven, MI	6.5
[18]	Saugatuck Dunes, MI	8.5
[19]	Holland, MI	9
[20]	Port Sheldon, MI	9.5
[21]	Grand Haven, MI	11.5
[22]	Muskegon, MI	7.5
[23]	Wabaningo, MI	6.5
[24]	Pentwater, MI	4.5
[25]	Ludington, MI	6.5
[26]	Manistee, MI	5.5
[27]	Frankfort, MI	8
[28]	Leland, MI	7
[29]	Traverse City, MI	6.5
[30]	Elk Rapids, MI	4.5
[31]	Bay Harbor, MI	5.5
[32]	Port Inland, MI	8
[33]	Manistique, MI	7
[34]	Menominee, MI	6
[35]	Algoma, WI	5.5
[36]	Kewaunee, WI	7.5
[37]	Two Rivers, WI	6
[38]	Manitowoc, WI	6.5
[39]	Sheboygan, WI	5.5

Fig 5-8. (a) Assessment of rip current potential occurrences on July 20, 2019 at 39 locations near harbor breakwaters in Lake Michigan. (b-d) images with sediment plume signatures (marked as red arrows) obtained from the three webcams at sites #[1] Port Washington (west coast of Lake Michigan), #[14] Michigan City, IN (south coast), and #[21] Grand Haven, MI (east coast). (e) Image with no sediment plume signatures at site #[17] South Haven, MI.

5.5 Summary and Conclusions

Rip currents at the study site near the north breakwater of the City of Port Washington, WI are characterized. Occurrences of rip currents were identified using field measurements of current velocities and image observations. Hidden dangers of rip current near coastal structures are illustrated in images, time series, and wavelet analysis. There are three findings. First, rip currents are usually accompanied by strong longshore currents that can carry unalerted swimmers far away from the structure to the offshore. Second, environmental proxies related to rip current occurrences

near coastal structures include four factors (wave height, wave period, wind speed, and lake level) and other five new factors (shifting winds, atmospheric pressure disturbances, and induced high-frequency water level oscillations) that have not been recognized before. Third, rip currents can still be present near coastal structures when the water appears seemingly safe with no apparent visual signatures. Overall, rip currents near the breakwater type structure are characterized and associated with environmental proxies in Lake Michigan for the first time.

A Structure Rip Checklist and Assessment Matrix (SRiCAM) tool is developed and validated at the study site. The SRiCAM is an environmental proxy-based tool for assessing rip current occurrences near coastal structures. Particularly, the SRiCAM uses factors to address less-recognized environmental proxies including strong shore-parallel winds, shifting winds, and atmospheric pressure disturbances, meteorologically induced water level fluctuations like meteotsunamis and seiches, and storm structures. Four-tiered risk assessments are employed to faithfully assess potential rip currents near coastal structures. Both the integration of the SRiCAM into the INFOS cyberinfrastructure and the implementation of the data contingency plan reliably provide real-time rip current warnings to the public. Applicability of the SRiCAM to 39 locations near harbor breakwaters around Lake Michigan is promising. Overall, the SRiCAM can be widely extended to the larger regions of the Great Lakes in the future to foster the resilience of coastal communities to rip current hazards.

5.6 Acknowledgments

This study was supported by the Wisconsin Coastal Management Program (WCMP), National Oceanic and Atmospheric Administration (NOAA) Coastal Storms Program, University of Wisconsin Sea Grant Institute (UW-Sea Grant), and gift funds from WE Energies and local friends of Port Washington group. We would like to thank Mr. Todd Breiby, Ms. Angel Kathleen, and Mr. Michael Friis, from WCMP for their support in coordination, education, and outreach for rip current safety. In addition, Ms. Moira Harrington at UW-Sea Grant for their dedication to communicating rip current hazards to the Great Lakes community is acknowledged. Outreach activities related to the NOAA rip current outlook by Mr. Marc Kavinsky, Lead Forecaster of Marine Program Leader at NOAA-National Weather Service – Milwaukee/Sullivan, are noted. Mr. Jon Crain and Ms. Kiley Schulte, Mr. Dennis Cherny, Mr. Dan Buehler, and many staff at the City of Port Washington, WI, and Mr. Michael Diemer and Mr. Tom Phelps at DigiCorp INC for the assistances in real-time field measurements acknowledged. Last but not least, the authors especially thank Mr. Tom Mlada and Marty Becker, former and current Mayor of the City of Port Washington, respectively, for their support to emphasize the importance of providing rip current warning for beach safety.

5.7 References

Aelbrecht, D., Denot, T., 1999. 2D & 3D Modelling of Wave-Driven Currents in Presence of a Groin System in a Tidal Sea, Transactions on the Built Environment.

Alvarez-Ellacuria, A., Orfila, A., Olabarrieta, M., Gómez-pujol, L., Medina, R., Tintoré, J., 2009. An Alert System for Beach Hazard Management in the Balearic Islands. Coast. Manag. 37, 569–584. https://doi.org/10.1080/08920750903150662

Alves, J.-H.G.M., Chawla, A., Tolman, H.L., Schwab, D., Lang, G., Mann, G., Alves, J.-H.G.M., Chawla, A., Tolman, H.L., Schwab, D., Lang, G., Mann, G., 2014. The Operational Implementation of a Great Lakes Wave Forecasting System at NOAA/NCEP*. Weather Forecast. 29, 1473–1497. https://doi.org/10.1175/WAF-D-12-00049.1

Anderson, J.D., Wu, C.H., 2018. Development and application of a real-time water environment cyberinfrastructure for kayaker safety in the Apostle Islands, Lake Superior. J. Great Lakes Res. 44, 990–1001. https://doi.org/10.1016/J.JGLR.2018.07.006

Arozarena, I., Houser, C., Echeverria, A.G., Brannstrom, C., 2015. The rip current hazard in Costa Rica. Nat. Hazards 77, 753–768. https://doi.org/10.1007/s11069-015-1626-9

Arun Kumar, S.V. V., Prasad, K.V.S.R., 2014. Rip current-related fatalities in India: a new predictive risk scale for forecasting rip currents. Nat. Hazards 70, 313–335. https://doi.org/10.1007/s11069-013-0812-x

As-Salek, J.A., Schwab, D.J., 2004. High-Frequency Water Level Fluctuations in Lake Michigan. J. Waterw. Port, Coastal, Ocean Eng. 130, 45–53. https://doi.org/10.1061/(ASCE)0733-950X(2004)130:1(45)

Barrett, G., Houser, C., 2012. Identifying hotspots of rip current activity using wavelet analysis at Pensacola Beach, Florida. Phys. Geogr. 33, 32–49. https://doi.org/10.2747/0272-

3646.33.1.32

Bechle, A.J., Kristovich, D.A.R., Wu, C.H., 2015. Meteotsunami occurrences and causes in Lake Michigan. J. Geophys. Res. Ocean. 120, 8422–8438. https://doi.org/10.1002/2015JC011317

Bechle, A.J., Wu, C.H., Kristovich, D.A.R., Anderson, E.J., Schwab, D.J., Rabinovich, A.B., 2016. Meteotsunamis in the Laurentian Great Lakes. Sci. Rep. 6, 37832. https://doi.org/10.1038/srep37832

Bechle, A.J., Wu, C.H., Liu, W.-C., Kimura, N., 2012. Development and Application of an Automated River-Estuary Discharge Imaging System. J. Hydraul. Eng. 138, 327–339. https://doi.org/10.1061/(ASCE)HY.1943-7900.0000521

Bertin, X., De Bakker, A., Van Dongeren, A., Coco, G., André, G., Ardhuin, F., Bonneton, P., Bouchette, F., Castelle, B., Crawford, W.C., Davidson, M., Deen, M., Dodet, G., Guérin, T., Inch, K., Leckler, F., Mccall, R., Muller, H., Olabarrieta, M., Roelvink, D., Ruessink, G., Sous, D., Stutzmann, É., Tissier, M., Roelvink, (D, Nl, B.G.R., Ruessink, (G, 2018. Infragravity waves: From driving mechanisms to impacts. Earth-Science Rev. 177, 774–799. https://doi.org/10.1016/j.earscirev.2018.01.002

Brander, R., Scott, T., 2019. Science of the rip current hazard, in: The Science of Beach Lifeguarding. CRC Press, pp. 67–85. https://doi.org/10.4324/9781315371641-5

Brander, R.W., Bradstreet, A., Sherker, S., MacMahan, J., 2011. Responses of Swimmers Caught in Rip Currents: Perspectives on Mitigating the Global Rip Current Hazard. Int. J. Aquat. Res. Educ. 5. https://doi.org/10.25035/ijare.05.04.11

Brander, R.W., MacMahan, J.H., 2011. Future Challenges for Rip Current Research and Outreach, in: Leatherman, S., Fletemeyer, J. (Eds.), Rip Currents: Beach Safety, Physical Oceanography, and Wave Modeling. CRC Press, pp. 1–29.

Brewster, B.C., Gould, R.E., Brander, R.W., 2019. Estimations of rip current rescues and drowning in the United States. Nat. Hazards Earth Syst. Sci. 19, 389–397. https://doi.org/10.5194/nhess-19-389-2019

Brighton, B., Sherker, S., Brander, R., Thompson, M., Bradstreet, A., 2013. Rip current related drowning deaths and rescues in Australia 2004–2011. Nat. Hazards Earth Syst. Sci. 13, 1069–1075. https://doi.org/10.5194/nhess-13-1069-2013

Castelle, B., Coco, G., 2013. Surf zone flushing on embayed beaches. Geophys. Res. Lett. 40, 2206–2210. https://doi.org/10.1002/grl.50485

Castelle, B., Coco, G., 2012. The morphodynamics of rip channels on embayed beaches. Cont. Shelf Res. 43, 10–23. https://doi.org/10.1016/j.csr.2012.04.010

Castelle, B., Scott, T., Brander, R.W.W., McCarroll, R.J.J., 2016. Rip current types, circulation and hazard, Earth-Science Reviews. Elsevier. https://doi.org/10.1016/j.earscirev.2016.09.008

Dalrymple, R.A., MacMahan, J.H., Reniers, A.J.H.M., Nelko, V., 2011. Rip Currents. Annu. Rev. Fluid Mech. 43, 551–581. https://doi.org/10.1146/annurev-fluid-122109-160733

Daubechies, I., Sweldens, W., 1998. Factoring Wavelet Transforms into Lifting Steps. J. Fourier Anal. Appl. 4. https://doi.org/10.1007/bf02476026

Dean, R.G., Dalrymple, R.A., 1991. Water Wave Mechanics for Engineers and Scientists, Advanced Series on Ocean Engineering. WORLD SCIENTIFIC. https://doi.org/10.1142/1232

Engle, J., 2003. Formulation of a rip current forecasting technique through statistical analysis of rip current-related rescues. Univ. Florida.

Floc'h, F., Mabiala, G.R., Almar, R., Castelle, B., Hall, N., Du Penhoat, Y., Scott, T., Delacourt, C., 2018. Flash Rip Statistics from Video Images. J. Coast. Res. 81, 100–106.

https://doi.org/10.2112/SI81-013.1

Gensini, V.A., Ashley, W.S., 2010. An examination of rip current fatalities in the United States. Nat. Hazards 54, 159–175. https://doi.org/10.1007/s11069-009-9458-0

Gourlay, M.R., 1974. Wave Set-Up and Wave Generated Currents in the Lee of a Breakwater or Headland. American Society of Civil Engineers, New York, NY. https://doi.org/10.1061/9780872621138.118

Great Lakes Current Incident Database [WWW Document], 2019. URL https://www.michiganseagrant.org/dcd/dcdsearch.php (accessed 12.9.19).

Grinsted, A., Moore, J.C., Jevrejeva, S., 2004. Application of the cross wavelet transform and wavelet coherence to geophysical time series. Nonlinear Process. Geophys. 11, 561–566. https://doi.org/10.5194/npg-11-561-2004

Holman, R., Haller, M.C., 2013. Remote Sensing of the Nearshore. Ann. Rev. Mar. Sci. 5, 95–113. https://doi.org/10.1146/annurev-marine-121211-172408

Holman, R.A., Stanley, J., 2007. The history and technical capabilities of Argus. Coast. Eng. 54, 477–491. https://doi.org/10.1016/J.COASTALENG.2007.01.003

Horta, J., Oliveira, S., Moura, D., Ferreira, Ó., 2018. Nearshore hydrodynamics at pocket beaches with contrasting wave exposure in southern Portugal. Estuar. Coast. Shelf Sci. 204, 40–55. https://doi.org/10.1016/j.ecss.2018.02.018

Lascody, R.L., 1998. EAST CENTRAL FLORIDA RIP CURRENT PROGRAM, National Weather Digest.

Leatherman, S.P., Leatherman, S.B., 2017. Leatherman SP (2017) Techniques for Detecting and Measuring Rip Currents. Int. J. Earth Sci. Geophys. Cit. Leatherman SB 2017, 14.

Lin, Y.T., Schuettpelz, C.C., Wu, C.H., Fratta, D., 2009. A combined acoustic and electromagnetic

wave-based techniques for bathymetry and subbottom profiling in shallow waters. J. Appl. Geophys. 68, 203–218. https://doi.org/10.1016/j.jappgeo.2008.11.010

Linares, Á., Wu, C.H., Anderson, E.J., Chu, P.Y., 2018. Role of Meteorologically Induced Water Level Oscillations on Bottom Shear Stress in Freshwater Estuaries in the Great Lakes. J. Geophys. Res. Ocean. 123, 4970–4987. https://doi.org/10.1029/2017JC013741

Linares, Á., Wu, C.H., Bechle, A.J., Anderson, E.J., Kristovich, D.A.R., 2019. Unexpected rip currents induced by a meteotsunami. Sci. Rep. 9, 2105. https://doi.org/10.1038/s41598-019-38716-2

Liu, P.C., Babanin, A. V., 2004. Using wavelet spectrum analysis to resolve breaking events in the wind wave time series, Annales Geophysicae. European Geosciences Union. https://doi.org/10.5194/angeo-22-3335-2004

Liu, P.C., Schwab, D.J., Bennett, J.R., 1984. Comparison of a Two-Dimensional Wave Prediction Model with Synoptic Measurements in Lake Michigan, Journal of Physical Oceanography. American Meteorological Society. https://doi.org/10.1175/1520-0485(1984)014<1514:COATDW>2.0.CO;2

Liu, P.L.-F., Mei, C.C., 1976. Water motion on a beach in the presence of a breakwater: 2. Mean currents. J. Geophys. Res. 81, 3085–3094. https://doi.org/10.1029/jc081i018p03085

Liu, Y., Wu, C.H., 2019. Lifeguarding Operational Camera Kiosk System (LOCKS) for flash rip warning: Development and application. Coast. Eng. 152, 103537. https://doi.org/10.1016/j.coastaleng.2019.103537

Lushine, J.B., 1991. A Study of Rip Current Drownings and Related Weather Factors. NATL. WEA. DIG 13--19.

MacMahan, J.H., Reniers, A.J.H.M., Thornton, E.B., 2010. Vortical surf zone velocity fluctuations

with 0(10) min period. J. Geophys. Res. 115, C06007. https://doi.org/10.1029/2009JC005383

MacMahan, J.H., Thornton, E.B., Reniers, A.J.H.M., 2006. Rip current review. Coast. Eng. 53, 191–208.

MacMahan, J.H., Thornton, E.B., Stanton, T.P., Reniers, A.J.H.M., 2005. RIPEX: Observations of a rip current system. Mar. Geol. 218, 113–134.

McCarroll, R.J., Brander, R.W., Turner, I.L., Power, H.E., Mortlock, T.R., 2014. Lagrangian observations of circulation on an embayed beach with headland rip currents. Mar. Geol. 355, 173–188. https://doi.org/10.1016/j.margeo.2014.05.020

Meadows, G., Purcell, H., Guenther, D., Meadows, L., Kinnunen, R.E., Clark, G., 2011. Rip Currents in the Great Lakes: An Unfortunate Truth, in: Leatherman, S., Fletemeyer, J. (Eds.), Rip Currents: Beach Safety, Physical Oceanography, and Wave Modeling. CRC Press, pp. 199–214.

Monserrat, S., Vilibić, I., Rabinovich, A.B., 2006. Meteotsunamis: atmospherically induced destructive ocean waves in the tsunami frequency band. Nat. Hazards Earth Syst. Sci. 6, 1035–1051. https://doi.org/10.5194/nhess-6-1035-2006

Moulton, M., Elgar, S., Raubenheimer, B., Warner, J.C., Kumar, N., 2017. Rip currents and alongshore flows in single channels dredged in the surf zone. J. Geophys. Res. Ocean. 122, 3799–3816. https://doi.org/10.1002/2016JC012222

Murray, T., Cartwright, N., Tomlinson, R., 2013. Video-imaging of transient rip currents on the Gold Coast open beaches. J. Coast. Res. 165, 1809–1814. https://doi.org/10.2112/SI65-306.1

Pattiaratchi, C., Olsson, D., Hetzel, Y., Lowe, R., 2009. Wave-driven circulation patterns in the lee of groynes. Cont. Shelf Res. 29, 1961–1974. https://doi.org/10.1016/j.csr.2009.04.011

Pitman, S., Gallop, S.L., Haigh, I.D., Masselink, G., Ranasinghe, R., 2016. Wave breaking patterns

control rip current flow regimes and surfzone retention. Mar. Geol. 382, 176–190.

Rabinovich, A.B., 2009. Seiches and Harbor Oscillations, in: Handbook of Coastal and Ocean Engineering. WORLD SCIENTIFIC, pp. 193–236. https://doi.org/10.1142/9789812819307_0009

Reimer, J.R., Wu, C.H., 2016. Development and Application of a Nowcast and Forecast System Tool for Planning and Managing a River Chain of Lakes. Water Resour. Manag. 30, 1375–1393. https://doi.org/10.1007/s11269-016-1228-7

Schrader, M., 2004. EVALUATION OF THE MODIFIED ECFL LURCS RIP CURRENT FORECASTING SCALE AND CONDITIONS OF SELECTED RIP CURRENT EVENTS IN FLORIDA.

Schwab, D.J., Bennett, J.R., Lynn, E.W., 1986. A two-dimensional lake wave prediction system. Environ. Softw. 1, 4–9. https://doi.org/10.1016/0266-9838(86)90030-4

Scott, T., Austin, M., Masselink, G., Russell, P., 2016. Dynamics of rip currents associated with groynes — field measurements, modelling and implications for beach safety. Coast. Eng. 107, 53–69. https://doi.org/10.1016/J.COASTALENG.2015.09.013

Shi, F., Svendsen, I.A., Kirby, J.T., Smith, J.M.K., McKee Smith, J., 2003. A curvilinear version of a quasi-3D nearshore circulation model. Coast. Eng. 49, 99–124. https://doi.org/10.1016/S0378-3839(03)00049-8

Short, A.D., Hogan, C.L., 1994. Rip Currents and Beach Hazards: Their Impact on Public Safety and Implications for Coastal Management. J. Coast. Res. 197–209.

Silva-Cavalcanti, J.S., Costa, M.F., Pereira, P.S., 2018. Rip currents signaling and users behaviour at an overcrowded urban beach. Ocean Coast. Manag. 155, 90–97. https://doi.org/10.1016/j.ocecoaman.2018.01.031

Torrence, C., Compo, G.P., Torrence, C., Compo, G.P., 1998. A Practical Guide to Wavelet Analysis. BAMS 79, 61–78. https://doi.org/10.1175/1520-0477(1998)079<0061:APGTWA>2.0.CO;2

US Department of Commerce, NOAA, N.W.S., 2020. 2020 Lake Michigan Beach Forecast Services - Will You be Safe from Dangerous Swimming Conditions this Year?

Van Rijn, L.C., 2011. Coastal erosion and control. Ocean Coast. Manag. 54, 867–887. https://doi.org/10.1016/j.ocecoaman.2011.05.004

Wanek, J.M., Wu, C.H., 2006. Automated trinocular stereo imaging system for three-dimensional surface wave measurements. Ocean Eng. 33, 723–747. https://doi.org/10.1016/J.OCEANENG.2005.05.006

Wind, H.G., Vreugdenhil, C.B., 1986. Rip-current generation near structures. J. Fluid Mech. 171, 459. https://doi.org/10.1017/S0022112086001520

Woodward, E., Beaumont, E., Russell, P., Wooler, A., Macleod∞, R., Macleod, R., 2013. Analysis of Rip Current Incidents and Victim Demographics in the UK. J. Coast. Res. 65, 850–855.

6. Transient rip currents due to bathymetry changes in Lake Superior

The following is in preparation to be submitted to *Natural Hazards*.

6.1 Introduction

Rip currents are life-threatening hazards to coastal communities in the Great Lakes including Lake Superior (Gensini & Ashley, 2010). Disregard that Lake Superior is commonly perceived as less swimmable due to the relatively low water temperatures compared to the other Great Lakes, a total of 49 incidents including 17 fatalities have been reported in Lake Superior since 2002 based on the Great Lakes Current Incident Database (GLCID). Particularly on the western shore, rip currents were reported as causes of many beach drownings incidents (*Great Lakes Current Incident Database*, 2019; *Great Lakes Surf Rescue Project Statistics*, 2019). An example was on August 17, 2003, near the Minnesota Point in Duluth, Minnesota, where rip currents caused a young man drowning of seven others rescued from the fast-moving rip flows in one afternoon (Schomberg & Grant, 2006). Unfortunately, hotspots of rip currents are also usually near the populated region (Gensini & Ashley, 2010; Meadows et al., 2011). Consequently, economic impact due to rip current drownings has been estimated to go up to $105 million per year on average in the United States (Branche & Stewart, 2001). Along the 10-mile long sandbar beach near the center of the City of Duluth, MN, restaurants, tourism, parks, recreation areas, every year can attract 3.5 million visitors (https://duluthchamber.com/visitors/). Particularly, visitors are identified as one of the most vulnerable groups of people to rip current hazards due to unawareness or limited knowledge to be able to identify the presence of dangerous offshore directed rip flows not knowing the environment where rip currents are prone to occur (Schomberg, 2009). In view of the incidents and consequences, currently little has yet been documented about the rip currents

in Lake Superior, which would be critical for promoting safe waterfront and fostering resilience to dangerous current hazards of coastal communities.

Transient rip currents, which pose one of the highest risks to the unawareness of beach swimmers, are discussed in two types of rip currents. First, hydrodynamically-controlled or flash rips are inherently transient (Johnson & Pattiaratchi, 2004; Kumar & Feddersen, 2017). Several mechanisms of transient flash rips in featureless sandy beaches are well documented. Shear instabilities of longshore currents under highly oblique incidence waves (Castelle et al. 2016). generate unsteady vortices as transient out-bursting flows (Feddersen, 2014; Özkan-Haller & Kirby, 1999). Breaking of short-crested waves under shore-normal incidence (Peregrine, 1998) induce instantaneous small-scale vorticities (Clark et al., 2012; Kirby & Derakhti, 2019; Peregrine, 1998) that cascade to form large-scale surf zone eddies (Spydell & Feddersen, 2009). The interactions of incident waves with infra-gravity waves (Dalrymple, 1975; Johnson & Pattiaratchi, 2006) or edge waves (Reniers et al., 2006; Sasaki & Horikawa, 1978; Symonds & Ranasinghe, 2001) create radiation stress gradients that drive offshore-directed flows of high temporal variability. Destabilized strong longshore shear currents in meteotsunamis or seiches to produce offshore-directed propagating vortices (Linares et al., 2019). Second, bathymetry-controlled rip are also found to exhibit transient features excited by bathymetric variability (Uchiyama et al., 2017). The transiency is associated with spontaneous very low frequency motions (VLFs) due to the alongshore variability created by the interaction between wave forcing and bathymetric non-uniformity (Geiman & Kirby, 2013; Uchiyama et al., 2017). Furthermore, nearshore bar migrations (Bruno Castelle et al., 2016) can further add on the unpredictability in the time and space of occurrences of transient rips. Nevertheless, what bathymetry features and how the evolution of the features can affect the generation of transiency rip currents remain unclear.

Two kinds of bathymetry features are commonly identified to cause rip currents in sandy beaches. First, rip currents are generated in the deeper region (i.e. rip channel) between sandbars in surf zones (Castelle et al. 2016), known as the channel rips (Bruno Castelle & Coco, 2012; Haller, 2002; Moulton et al., 2017; Reniers et al., 2009). Depth-induced wave breaking is less intense than at the shallower bars, thus creating alongshore differences of radiation stress gradients to produce offshore-directed flows (Dalrymple et al., 2011; MacMahan et al., 2006). Channel rips can be detected based on the locations of the deep rip channels (Maryan et al., 2019; Pitman, Gallop, Haigh, Mahmoodi, et al., 2016), and most are persistent and stationary (Moulton et al., 2017). Second, rip currents are generated by offshore bathymetric anomalies as the focused rips (Castelle et al. 2016), which are caused by wave refraction and alongshore differences in the radiation stress gradients. Common examples of bathymetric anomalies that can lead to focused rips include transverse ridges (Houser et al., 2011), sorted bedforms (Coco et al., 2007), submarine canyon outside of surf zones (Joseph W. Long & Özkan-Haller, 2005), and multiple bar systems (Bruno Castelle et al., 2007). Focused rips are inherently nonstationary due to the alongshore viability at different offshore approaching wave heights and directions (J. W. Long et al., 2016) and can exhibit transiency feature (Uchiyama et al., 2017). In short, the two kinds of bathymetric features can both cause rip currents but may lead to distinct flow behaviors. Nearshore sandbars and offshore anomalies can be present at the same time or the two types can transform from one to another through complex nearshore sediment transport interacting with cohesive nearshore bluff erosion and depositions. Therefore, a systematic investigation of temporal and spatial characteristics of bathymetric features that can lead to transient rip currents is needed.

The objective of this chapter is to characterize bathymetric features that are possible to induce transient rip currents on the western shore of Lake Superior. Particularly, the 12th St Beach

and the 22nd St Beach in Duluth, MN (see Fig 1), both popular public beaches but with incidents reported before, are the focus locations in this study. The bathymetric features and types are characterized, and the temporal evolutions pattern of the features are also explored.

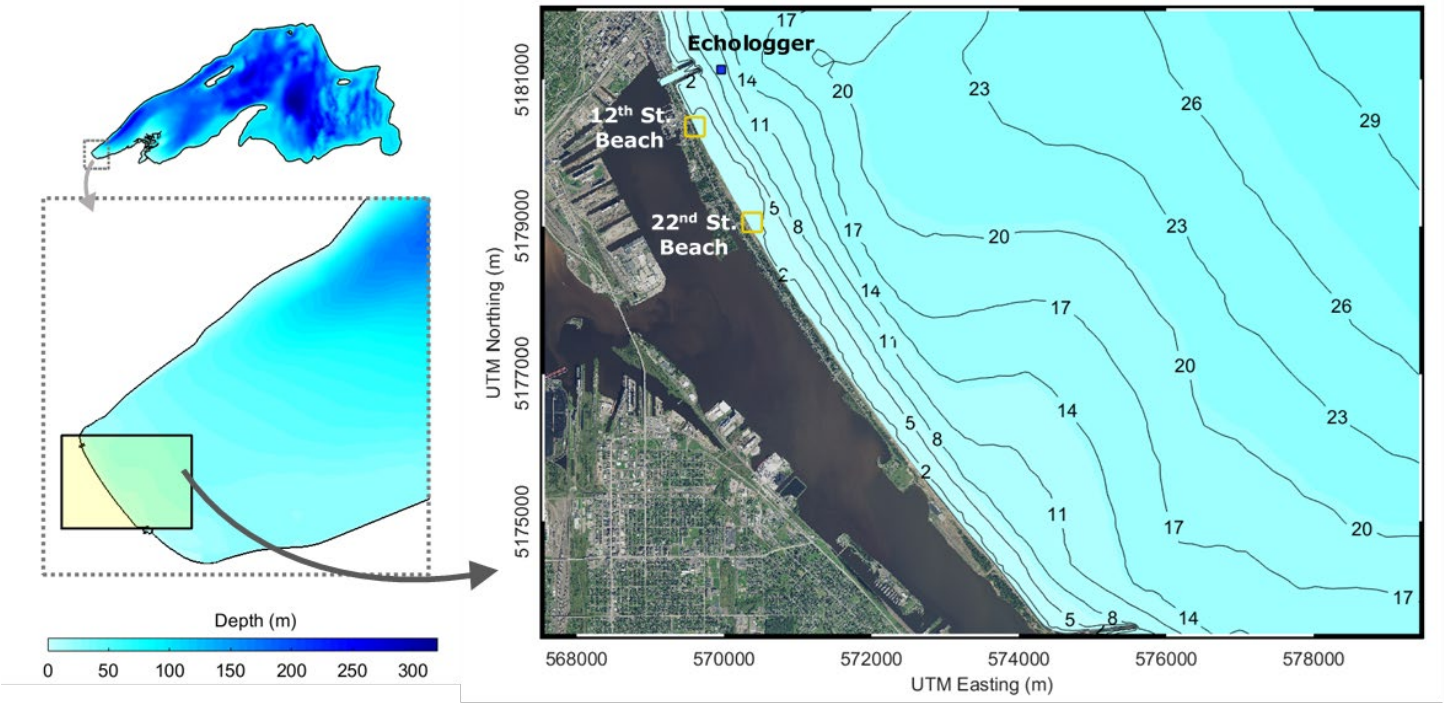

Fig 6-1. Map showing the western shore of Lake Superior and the two study sites at the 12th St. Beach and 22nd St. Beach in Duluth, MN

6.2 Methods

In-situ nearshore bathymetry survey was conducted in July 2019 at the 12th St. Beach and the 22nd St. Beach. A Sontek River Surveyor M9 was used with a 0.5 MHz downward-looking vertical acoustic beam (Lin et al., 2009), providing a depth resolution of 1 millimeter and a horizontal resolution of 0.5 m. An RTK base station was also used for kinematic position corrections at 1 HZ with a precision of 3 cm. Surveyed regions of a 450 m-by-110 m rectangle at the 12th St. Beach and a 450 m-by-150 m rectangle at the 22nd St. Beach are respectively shown in

Fig. 6-2 (a) and (b), in which the depth contours are interpolated from surveyed points. Features associated with bathymetry-controlled rip currents can be directly interpreted from the mapped contours. For example, an oblique rip channel can be visible at the 12th St, as shown in Fig. 6-2 (a), while there is no obvious rip channel but a deep (<4 m) offshore hole is instead pronounced at the 22nd St, as shown in Fig. 6-2 (b) as a comparison.

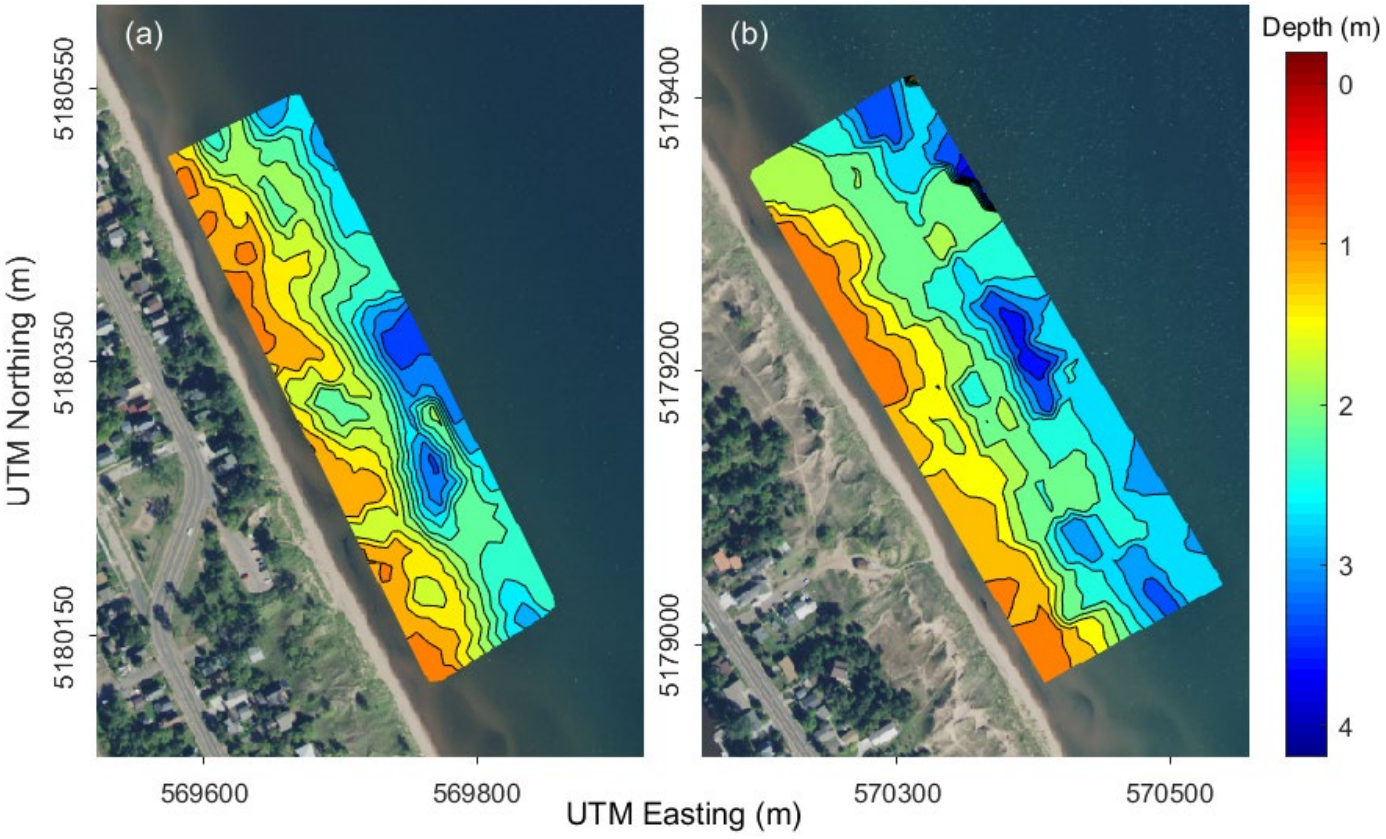

Fig 6-2. Depth contours of nearshore bathymetry surveyed in 2019 at two beaches: (a) 12th St. Beach and (b) 22nd St. Beach in Duluth, Minnesota

Remote-sensing data covering the western shore of Lake Superior are compiled from multiple sources, including aerial imagery, coastal LiDAR bathymetry, and nearshore webcam images. Data types, availability, and sources are summarized in Table 6-1. First, aerial images of National Agriculture Imagery Program (NAIP) operated by the USDA Farm Service Agency (FAS) offices are obtained from 2005 to 2017, which are available every 1 to 3 years. The NAIP

digital ortho aerial images, produced as 3.75' by 3.75' quadrangle tiles, are formatted to the UTM coordinate system using the NAD83 datum and geo-referenced using ground specifications within 6 m accuracy. Second, coastal LiDAR bathymetry includes two datasets: (i) the 2009 USACE NCMP Topobathy LiDAR by Joint Ariborne Lidar Bathymetry Technical Center of Expertise (JALBTCX), which covers the southwest shoreline of Lake Superior from the Minnesota Point in Duluth, MN to the Wisconsin Point in Superior, WI at a 0.75 m horizontal resolution, and (ii) the 2010 EPA Great Lakes Restoration Initiatives (GLRL) Bathymetric Lidar dataset, which covers the same coastal stretch from the Minnesota Point to the Wisconsin Point but at a higher 0.3 m resolution. Third, nearshore webcam images are collected at the 22nd St. Beach of Duluth since 2016. A MOBOTIX S15 dual-view camera with two CMOS sensors of a 7.9mm focal lens was installed at ~100 ft height from the still lake level. Oblique images of 45°×34° field of view with about 10° lateral overlapping are captured in full resolutions of 6 MP (3072 by 2048 pixels) at every 5 minutes. Nearshore bathymetric features like rip channels can be revealed from images using the timex (time-averaged) technique (Holman & Stanley, 2007), which uses the high-intensity pixel values to indicate locations of wave breaking continuously (i.e. sand bars), and in contrast, the deeper regions of rip channels usually appear in dark pixels (Pitman et al., 2016; Radermacher et al., 2018; Symonds & Ranasinghe, 2001).

Table 6-1. Summary of remote-sensing data along the western coastline of Lake Superior

Data type	**Availability**	**Source**
Aerial imagery	2005, 2008, 2009, 2010, 2011, 2013, 2015, 2017	NAIP
Coastal LiDAR	2009	USACE NCMP Topobathy Lidar
	2010	GLRI Bathymetric Lidar
Nearshore image	since 2016	Webcam at 22nd St. Beach

The five-step procedure of image processing to extract bathymetric features from the nearshore images of the 22nd St. Beach is described. As shown in Fig. 6-3, images captured during Sep 15, 2018, are used as an example for the illustration. In step (i), all raw snapshots (Fig. 6-3a) from the same day are timely averaged to produce a daily-timex image (Fig. 6-3b). In step (ii), the two timex images of partially overlapped views are stitched into a single near-panoramic image (see Fig. 6-3c) by matching common objects using the scale-invariant feature transform (SIFT) technique (Muja et al., 2009). In step (iii), an orthophoto (Fig. 6-3d) is generated by applying the geo-rectification (Holland et al., 1997) on the stitched image so all image pixels are converted into the actual spatial scale representing a 900 m -by -500 m rectangle region as shown. The camera parameters were obtained through in-situ field calibrations (Bechle et al., 2012; Wanek & Wu, 2006). In step (iv), bathymetry features are identified in the ortho timex images by intensity threshold and morphological transformations. The threshold values and morphological parameters used in this step are determined by minimizing the discrepancies with human perceptions. Bathymetric features are identified and categorized into four types – rip channel, sand bar, offshore holes, and offshore bars, which are color-coded as shown in Fig. 6-3e. Note that rip channel and offshore holes are differentiated based on locations relative to the shoreline. The shoreline is delineated based on the highest gradient in pixel Saturation values (in HSV color space). Lastly, in step (v), the four groups of features are quantified in parameters including the offshore distances (X, defined as the distance from the shoreline to the centroid, shown as the red cross in Fig. 6-3e), lengths (L), widths (W), and orientations (θ). For instance, the rip channel shown as the example in Fig. 6-3e is quantified with following parameters: X = 75.5 m, L = 174 m; W = 110 m, and θ = 61°. The five-step procedures are completely automated and applied to nearshore webcam images from 2016 to 2018. Furthermore, nearshore wave data measured using an Echologger ECT400

sonic altimeter with a sampling frequency of 5 HZ conducted in 2016-2018 (see Fig. 6-1) are also used in the analysis to characterize the temporal variations of bathymetric features, particularly before and after large wind wave events.

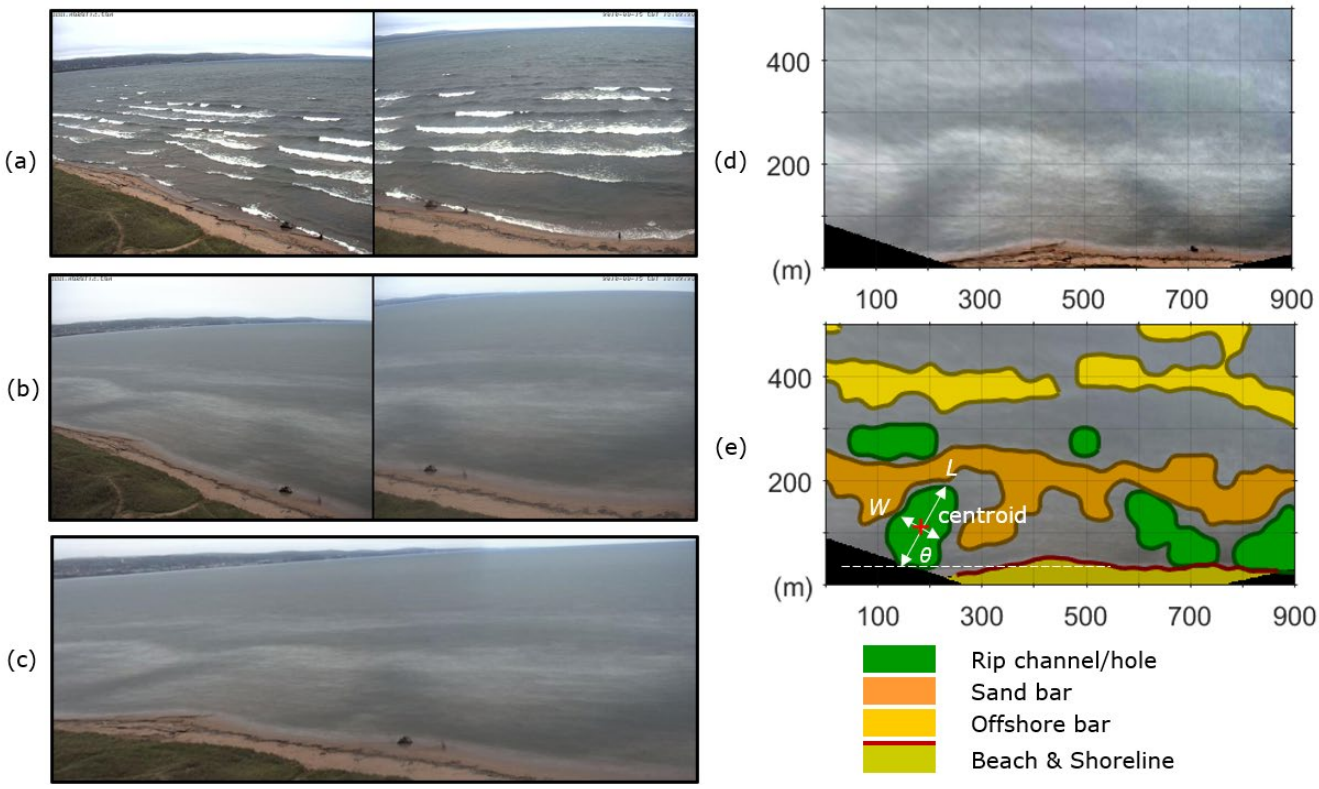

Fig 6-3. Procedures of image processing to extract bathymetric features of rip currents at 22nd Beach, Duluth, MN

6.3 Results

Qualitatively, bathymetric features of rip currents are compared at two beaches (i.e. the 12th St. Beach and the 22nd St. Beach). As shown in Fig. 6-4, a 1000 m -by- 300 m rectangle nearshore region is extracted for the two locations from aerial images of 2008-2010 and 2015, respectively. Images of the other available years have visibility too low to discern any water bottom features. Double crescent bar systems are the overall dominant features at both locations in most images, which confirms that the two beaches are potential hotspots for the channel rips and the

focused rips to occur. Nevertheless, differences exist when comparing details of the rip channel locations and offshore bar curvedness. In Fig. 6-4 (d, h), at the 12th St. Beach a pronounced rip channel extends about 50 m from the shoreline towards the north. In comparison at the 22nd St. Beach, two pronounced rip channels are seen with offshore extents close to 100 m and one is oriented towards the south. In Fig. 6-4 (a, e), at the 12th St. Beach the offshore crescent bars are located at 100-150 m offshore with the "wavelength" of about 100 m. In comparison at the 22nd St. Beach, double bars appear parallel in the 300-700 m stretch of the alongshore direction, with relatively straight outer bars extending beyond 100 m from the shore. Furthermore, temporal variations of the bathymetric features are compared in different years, which overall show consistency at the two beaches. From 2008 to 2009, the double-bar system at the two beaches is mostly preserved and locations of major curvatures in the outer bars remain unchanged. From 2009 to 2010, most bars are disappeared and a wide (~200m) nearshore hole appears in 12th St. Beach. From 2010 to 2015, the double bar systems re-appear with several pronounced rip channels, but the features are constrained within less than 100 m from the shoreline. Overall, the comparison of bathymetry features at the two beaches during the seven years shows that bathymetry-controlled rip currents are likely to occur at both locations, but the exact locations of rip currents can be dynamically varying due to temporal variations on the observed time scale of years.

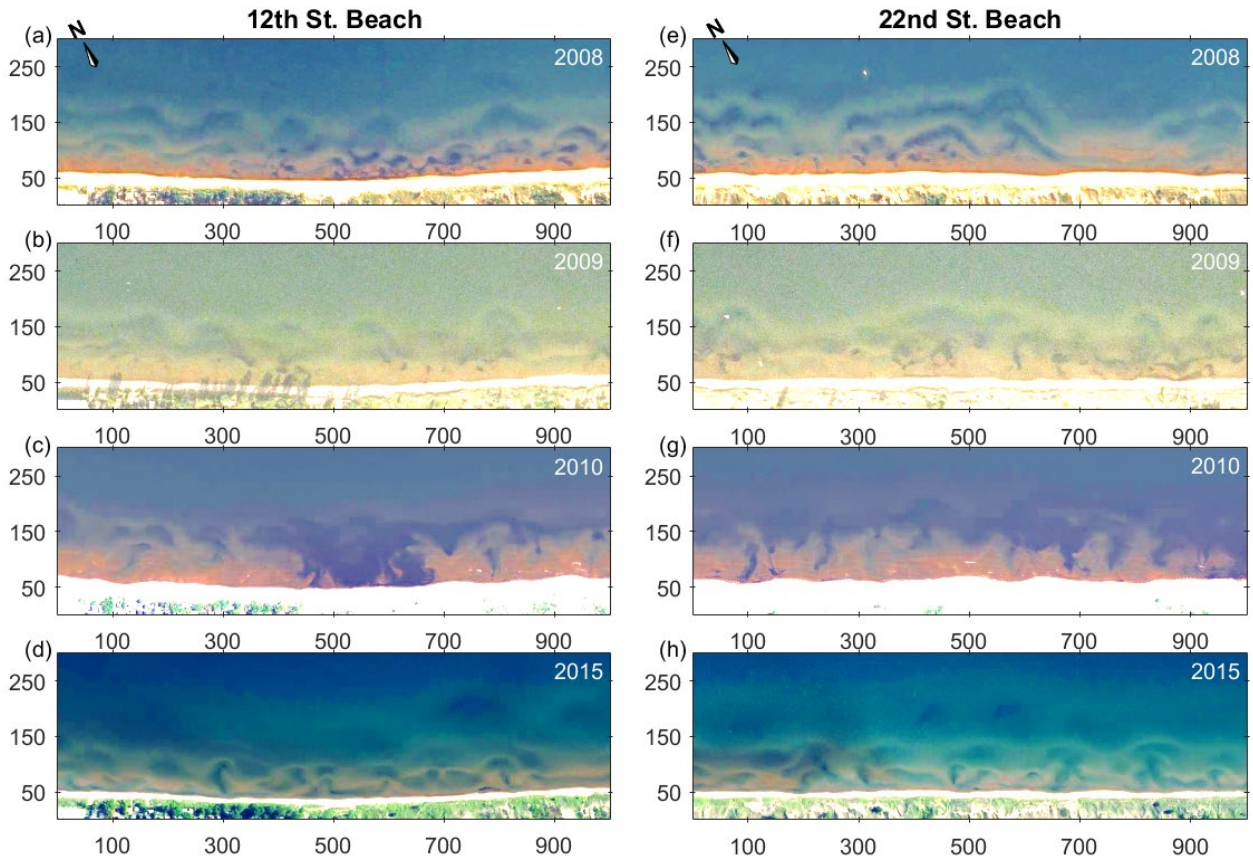

Fig 6-4. Aerial images for nearshore regions at (a-d) the 12th St. Beach and (e-h) the 22nd St. Beach

Quantitatively, characteristics parameters for bathymetry features at the 22nd St. Beach are extracted from nearshore webcam images in 2016-2018. Fig. 6-5 shows the histograms for the fraction of occurrences in rip channels (in green rectangles) and offshore bars (in yellow rectangles), as key features of the channel rip and focused rip types, respectively. For the rip channels, most centroids are within 100 m offshore extents (Fig. 6-5a). Lengths of rip channels are between 50-250 m for 95% of those detected (Fig. 6-5b). The channel widths, with a majority (~70%) are under 100 m, can also be as wide as 200 m (Fig. 6-5c). For orientations (Fig. 6-5d), 40% of rip channels are aligned near-perpendicular to the shoreline (~90°), and the others in oblique angles show a tendency towards the south (<90°) in comparison to those towards the north (>90°). For the offshore bars, the bar centroid locations show a tendency to be less than 250 m or

more than 400 m from the shoreline (Fig. 6-5e). The lengths of 80% detected bars are within 150 m (Fig. 6-5f), but those connected ones can extend up to O (100) meters, such as the example shown in Fig. 6-3 (e). The bar widths, with a 50% dominant range between 25-50 m, also exhibit considerable fractions in those as thin as less than 25 m and those as wide as greater than 100 m (Fig. 6-5g). Orientations of offshore bars are mostly (~75%) in near-parallel angles to the shoreline (>150° or < 30°, Fig. 6-5h). Overall, the parameters of the rip channels and offshore bars support the formation of bathymetry-controlled rips to occur. This is also the first time that the bathymetry features are quantitively characterized on the western shore of Lake Superior.

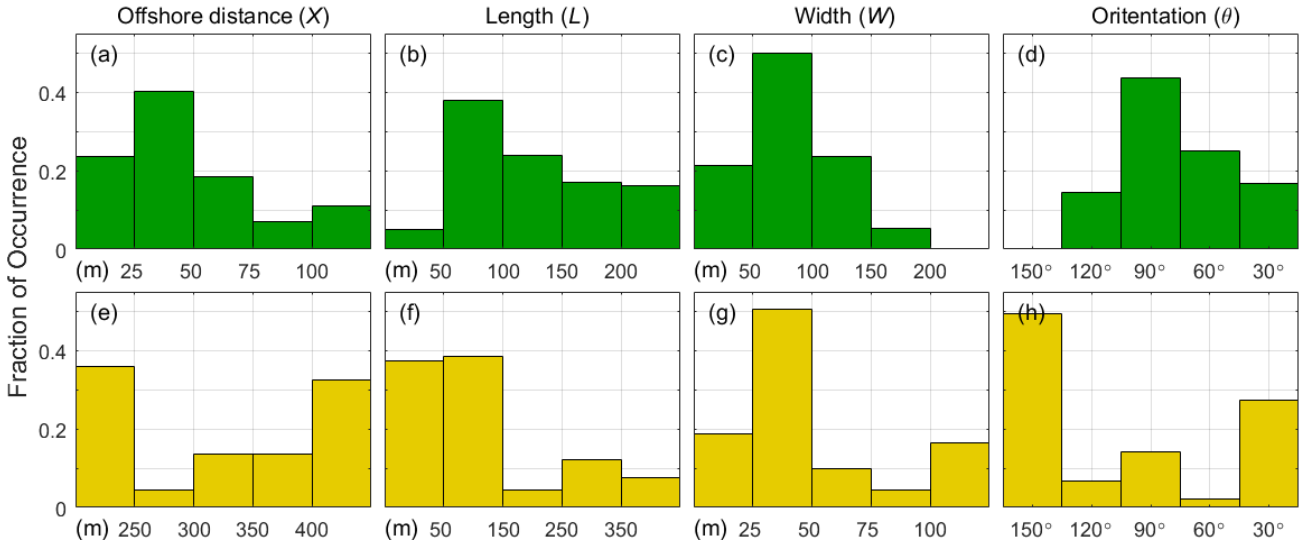

Fig 6-5. Histograms for the (a-b) rip channel and (e-h) offshore bar parameters extracted from nearshore webcam images, including offshore distance (X), length (L), width (W) and orientation (θ)

Temporal evolutions of bathymetry features at the 22nd St. Beach are further examined by comparing the numbers of the four types of detected features with daily-averaged wave heights measured by the Echologger wave sensor (see Fig. 6-1). Fig. 6-6 shows the time series for a 143-day period in 2016 as an example. In general, bathymetry features are mostly captured during large wave days. Particularly, rip channels with (nearshore) sand bars show synchronized appearance and disappearance, as compared to the trend of offshore bars with holes that can be independent

of each other. During a large wave event lasting for days, such as the one starting on 09-21 as shown in Fig. 6-6 (f), the number of bathymetry features of all four types (see Fig. 6-6a-e) exhibit changes on an hourly time scale. In addition, the number of features also changes between two events, suggesting that the bathymetry features evolve also due to other hydrodynamic processes such as large longshore currents or high-frequency water level fluctuations. This finding suggests that the bathymetry features are dynamic and prone to continuous evolutions, which can lead to uncertainties in the occurrences and locations of rip currents.

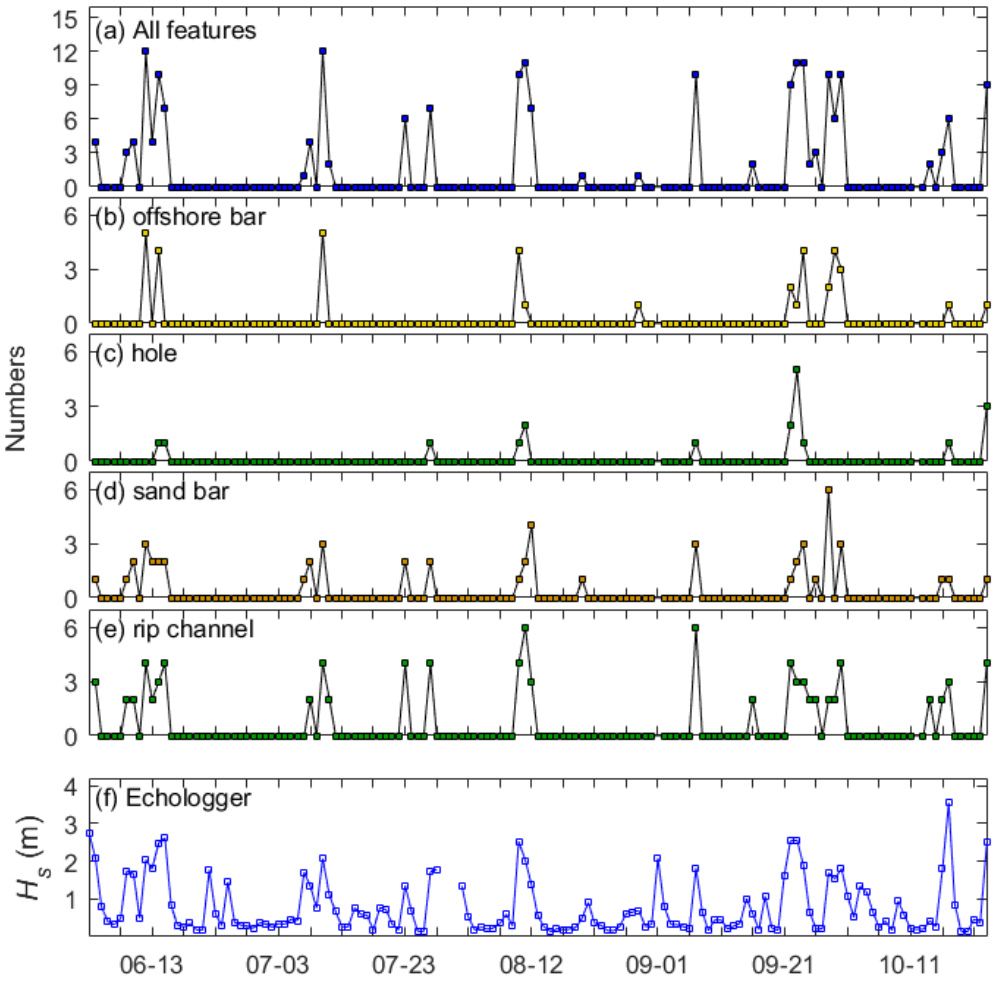

Fig 6-6. Time series of numbers of detected bathymetry features: (a) all features added, (b-e) each group of features individually, (f) measured wave heights in 2016

6.4 Summary

In this study, bathymetric features of rip current on the western shore of Lake Superior are characterized at the 12th St Beach and the 22nd St Beach in Duluth, MN. Remote-sensing data including aerial imagery, coastal LiDAR elevations, and nearshore webcam images are compiled. Image processing procedure including timexing, stitching, orthorectification, segmentation is implemented to detect bathymetry features and extract geometric parameters. Qualitatively, nearshore bathymetry features are compared at the two locations at multiple years using aerial images. It is found that the double crescent bars are the dominant features along the western shore of Lake Superior, while differences in details such as rip channel locations and offshore bar distances can vary from beach to beach, year to year. Quantitatively, the offshore extents, lengths, widths, and orientations of rip channels and offshore bars are statistically characterized based on extracted features from the nearshore images of 2016-2018 at the 22nd. St. Beach. The histogram pattern shows that the features support the formation of both channel rips and focused rips. Temporal evolutions of the bathymetry features are further explored. Dynamic and continuous evolutions of bathymetry features are observed, particularly during large wave events on the time scale of an hourly basis. Overall, bathymetry features are characterized and documented for the first time along the western shore of Lake Superior. The findings would be further extended to investigate the occurrence of transient rip currents, which may explain many drowning incidents reported in this region over the past years. A real-time system to actively monitor the rip channel evolutions and provide tier-based warnings can also be implemented for the beach safety of the Lake Superior coastal communities.

6.5 Acknowledgements

This study was supported by the University of Wisconsin Sea Grant Institute (UW-Sea Grant), National Oceanic and Atmospheric Administration (NOAA) Coastal Storms Program, and the Wisconsin Coastal Management Program (WCMP). We would like to thank Mr. Jesse D. Schomberg from Minnesota Sea Grant and Ms. Deidre Peroff for developing specific strategies and messages to reach the public on rip current education and outreach. We would like to thank Mr. Todd Breiby, Ms. Angel Kathleen, and Mr. Michael Friis, from WCMP for their support in coordination, education, and outreach for rip current safety. In addition, Ms. Moira Harrington at UW-Sea Grant for dedication to communicating rip current hazards to the Great Lakes community is acknowledged. We would like to thank Dr. Richard P. Axler and Mr. Jerald R Henneck for assistance in field measurements and support for the camera operations. The authors especially thank Mr. Gene Clark, a former coastal specialist from UW Sea Grant, for providing valuable knowledge related to nearshore processes.

6.6 References

Bechle, A. J., Wu, C. H., Liu, W.-C., & Kimura, N. (2012). Development and Application of an Automated River-Estuary Discharge Imaging System. *Journal of Hydraulic Engineering*, *138*(4), 327–339. https://doi.org/10.1061/(ASCE)HY.1943-7900.0000521

Branche, C. M., & Stewart, S. (2001). *Lifeguard Effectiveness: A Report of the Working Group*. https://stacks.cdc.gov/view/cdc/11284

Rip current types, circulation and hazard, 163 Earth-Science Reviews 1 (2016). https://doi.org/10.1016/j.earscirev.2016.09.008

Castelle, Bruno, Bonneton, P., Dupuis, H., & Sénéchal, N. (2007). *Double bar beach dynamics on the high-energy meso-macrotidal French Aquitanian Coast: A review*. https://doi.org/10.1016/j.margeo.2007.06.001

Castelle, Bruno, & Coco, G. (2012). The morphodynamics of rip channels on embayed beaches. *Continental Shelf Research*, *43*, 10–23. https://doi.org/10.1016/j.csr.2012.04.010

Castelle, Bruno, McCarroll, R. J., Brander, R. W., Scott, T., & Dubarbier, B. (2016). Modelling the alongshore variability of optimum rip current escape strategies on a multiple rip-channelled beach. *Natural Hazards*, *81*(1), 663–686. https://doi.org/10.1007/s11069-015-2101-3

Clark, D. B., Elgar, S., & Raubenheimer, B. (2012). Vorticity generation by short-crested wave breaking. *Geophysical Research Letters*, *39*(24), 2012GL054034. https://doi.org/10.1029/2012GL054034

Coco, G., Murray, A. B., Green, M. O., Thieler, E. R., & Hume, T. M. (2007). Sorted bed forms as self-organized patterns: 2. Complex forcing scenarios. *Journal of Geophysical Research*, *112*(F3), F03016. https://doi.org/10.1029/2006JF000666

Dalrymple, R. A. (1975). A mechanism for rip current generation on an open coast. *Journal of Geophysical Research*, *80*(24), 3485–3487. https://doi.org/10.1029/JC080i024p03485

Dalrymple, R. A., MacMahan, J. H., Reniers, A. J. H. M., & Nelko, V. (2011). Rip Currents. *Annual Review of Fluid Mechanics*, *43*(1), 551–581. https://doi.org/10.1146/annurev-fluid-122109-160733

Feddersen, F. (2014). The Generation of Surfzone Eddies in a Strong Alongshore Current. *Journal of Physical Oceanography*, *44*(2), 600–617. https://doi.org/10.1175/JPO-D-13-051.1

Geiman, J. D., & Kirby, J. T. (2013). Unforced oscillation of rip-current vortex cells. *Journal of Physical Oceanography*, *43*(3), 477–497. https://doi.org/10.1175/JPO-D-11-0164.1

Gensini, V. A., & Ashley, W. S. (2010). An examination of rip current fatalities in the United States. *Natural Hazards*, *54*(1), 159–175. https://doi.org/10.1007/s11069-009-9458-0

Great Lakes Current Incident Database. (2019). https://www.michiganseagrant.org/dcd/dcdsearch.php

Great Lakes Surf Rescue Project Statistics. (2019). http://www.glsrp.org/statistics/

Haller, M. C. (2002). Experimental study of nearshore dynamics on a barred beach with rip channels. *Journal of Geophysical Research*, *107*(C6). https://doi.org/10.1029/2001jc000955

Holland, K. T., Holman, R. A., Lippmann, T. C., Stanley, J., & Plant, N. (1997). Practical use of video imagery in nearshore oceanographic field studies. *IEEE Journal of Oceanic Engineering*, *22*(1), 81–92. https://doi.org/10.1109/48.557542

Holman, R. A., & Stanley, J. (2007). The history and technical capabilities of Argus. *Coastal Engineering*, *54*(6–7), 477–491. https://doi.org/10.1016/J.COASTALENG.2007.01.003

Houser, C., Barrett, G., & Labude, D. (2011). Alongshore variation in the rip current hazard at Pensacola Beach, Florida. *Natural Hazards*, *57*(2), 501–523. https://doi.org/10.1007/s11069-

010-9636-0

Johnson, D., & Pattiaratchi, C. (2004). Transient rip currents and nearshore circulation on a swell-dominated beach. *Journal of Geophysical Research*, *109*(C2), C02026. https://doi.org/10.1029/2003JC001798

Johnson, D., & Pattiaratchi, C. (2006). Boussinesq modelling of transient rip currents. *Coastal Engineering*, *53*(5–6), 419–439. https://doi.org/10.1016/J.COASTALENG.2005.11.005

Kirby, J. T., & Derakhti, M. (2019). Short-crested wave breaking. *European Journal of Mechanics - B/Fluids*, *73*, 100–111. https://doi.org/10.1016/J.EUROMECHFLU.2017.11.001

Kumar, N., & Feddersen, F. (2017). No Title. *Geophysical Research Letters*, *44*(6), 2843–2851. https://doi.org/10.1002/2017GL072611

Lin, Y. T., Schuettpelz, C. C., Wu, C. H., & Fratta, D. (2009). A combined acoustic and electromagnetic wave-based techniques for bathymetry and subbottom profiling in shallow waters. *Journal of Applied Geophysics*, *68*(2), 203–218. https://doi.org/10.1016/j.jappgeo.2008.11.010

Linares, Á., Wu, C. H., Bechle, A. J., Anderson, E. J., & Kristovich, D. A. R. (2019). Unexpected rip currents induced by a meteotsunami. *Scientific Reports*, *9*(1), 2105. https://doi.org/10.1038/s41598-019-38716-2

Long, J. W., Özkan-Haller, H. T., & Özkan-Haller, H. T. (2016). Forcing and variability of nonstationary rip currents. *Journal of Geophysical Research: Oceans*, *121*(1), 520–539. https://doi.org/10.1002/2015JC010990

Long, Joseph W., & Özkan-Haller, H. T. (2005). *Offshore controls on nearshore rip currents*. *110*. https://doi.org/10.1029/2005JC003018

MacMahan, J. H., Thornton, E. B., & Reniers, A. J. H. M. (2006). Rip current review. *Coastal*

Engineering, *53*(2–3), 191–208. https://www.sciencedirect.com/science/article/pii/S0378383905001353

Maryan, C., Hoque, M. T., Michael, C., Ioup, E., & Abdelguerfi, M. (2019). Machine learning applications in detecting rip channels from images. *Applied Soft Computing Journal*, *78*, 84–93. https://doi.org/10.1016/j.asoc.2019.02.017

Meadows, G., Purcell, H., Guenther, D., Meadows, L., Kinnunen, R. E., & Clark, G. (2011). Rip Currents in the Great Lakes: An Unfortunate Truth. In S. Leatherman & J. Fletemeyer (Eds.), *Rip Currents: Beach Safety, Physical Oceanography, and Wave Modeling* (pp. 199–214). CRC Press.

Moulton, M., Elgar, S., Raubenheimer, B., Warner, J. C., & Kumar, N. (2017). Rip currents and alongshore flows in single channels dredged in the surf zone. *Journal of Geophysical Research: Oceans*, *122*(5), 3799–3816. https://doi.org/10.1002/2016JC012222

Muja, M., Muja, M., & Lowe, D. G. (2009). Fast approximate nearest neighbors with automatic algorithm configuration. *IN VISAPP INTERNATIONAL CONFERENCE ON COMPUTER VISION THEORY AND APPLICATIONS*, 331--340. http://citeseer.ist.psu.edu/viewdoc/summary?doi=10.1.1.160.1721

Özkan-Haller, H. T., & Kirby, J. T. (1999). Nonlinear evolution of shear instabilities of the longshore current: A comparison of observations and computations. *Journal of Geophysical Research: Oceans*, *104*(C11), 25953–25984. https://doi.org/10.1029/1999JC900104

Peregrine, D. H. (1998). Surf Zone Currents. *Theoretical and Computational Fluid Dynamics*, *10*(1–4), 295–309. https://doi.org/10.1007/s001620050065

Pitman, S., Gallop, S. L., Haigh, I. D., Mahmoodi, S., Masselink, G., & Ranasinghe, R. (2016). Synthetic Imagery for the Automated Detection of Rip Currents. *Journal of Coastal*

Research, *75*(sp1), 912–916. https://doi.org/10.2112/SI75-183.1

Pitman, S., Gallop, S. L., Haigh, I. D., Masselink, G., & Ranasinghe, R. (2016). Wave breaking patterns control rip current flow regimes and surfzone retention. *Marine Geology*, *382*, 176–190. https://www.sciencedirect.com/science/article/pii/S0025322716302821?via%3Dihub

Radermacher, M., de Schipper, M. A., & Reniers, A. J. H. M. (2018). Sensitivity of rip current forecasts to errors in remotely-sensed bathymetry. *Coastal Engineering*, *135*, 66–76. https://doi.org/10.1016/J.COASTALENG.2018.01.007

Reniers, A. J. H. M., MacMahan, J. H., Thornton, E. B., & Stanton, T. P. (2006). Modelling infragravity motions on a rip-channel beach. *Coastal Engineering*, *53*(2–3), 209–222. https://doi.org/10.1016/J.COASTALENG.2005.10.010

Reniers, A. J. H. M., MacMahan, J. H., Thornton, E. B., Stanton, T. P., Henriquez, M., Brown, J. W., Brown, J. A., & Gallagher, E. (2009). Surf zone surface retention on a rip-channeled beach. *Journal of Geophysical Research*, *114*(C10), C10010. https://doi.org/10.1029/2008JC005153

Sasaki, T. O., & Horikawa, K. (1978). Observation of Nearshore Current and Edge Waves. *Coastal Engineering 1978*, 791–809. https://doi.org/10.1061/9780872621909.047

Schomberg, J. (2009). *Rip Currents: A Survey of Beach Users*. www.seagrant.umn.edu/rip

Schomberg, J., & Grant, M. S. (2006). *Rip Currents in Lake Superior*.

Spydell, M., & Feddersen, F. (2009). Lagrangian Drifter Dispersion in the Surf Zone: Directionally Spread, Normally Incident Waves. *Journal of Physical Oceanography*, *39*(4), 809–830. https://doi.org/10.1175/2008JPO3892.1

Symonds, G., & Ranasinghe, R. (2001). On the Formation of Rip Currents on a Plane Beach. *Coastal Engineering 2000*, *276*, 468–481. https://doi.org/10.1061/40549(276)37

Uchiyama, Y., McWilliams, J. C., & Akan, C. (2017). Three-dimensional transient rip currents: Bathymetric excitation of low-frequency intrinsic variability. *Journal of Geophysical Research: Oceans*, *122*(7), 5826–5849. https://doi.org/10.1002/2017JC013005

Wanek, J. M., & Wu, C. H. (2006). Automated trinocular stereo imaging system for three-dimensional surface wave measurements. *Ocean Engineering*, *33*(5–6), 723–747. https://doi.org/10.1016/J.OCEANENG.2005.05.006

7. Summary, Contribution, and Future Work

7.1 Summary

Rip current hazard has caused hundreds of drowning incidents and fatalities in the Great Lakes (Gensini and Ashley, 2010; “Great Lakes Current Incident Database,” 2019, “Great Lakes Surf Rescue Project Statistics,” 2019; Meadows et al., 2011; Schomberg, 2009), imposing a deadly and prevalent threat to coastal communities. Rip currents warnings are essential to alert beach users about dangerous water conditions (Matthews et al., 2014), nevertheless, effective warning systems remain sporadic at local beaches and overall underserved for the Great Lakes coastal communities. Furthermore, limited characterization for rip currents in the Great Lakes has been documented to date (Castelle et al., 2016; Meadows et al., 2011). The objective of this dissertation is to characterize rip currents in Lake Michigan and in Lake Superior and to develop assessment tools for effective warning of the rip current hazards to coastal communities.

In Chapter 2, a Lifeguarding Operational Camera Kiosk System (LOCKS) is developed to provide real-time flash rip warnings to beach users for the first time. LOCKS has been implemented at the North Beach of Port Washington, WI in three components. First, a real-time environmental observation system acquires timely beach view images and local environmental condition data. Second, an integrated nowcast forecast operational system, high performance and distributed computing infrastructure, digitally detects and assesses flash rip hazards in high, moderate, or low risks. Third, an automated kiosk dynamically issues real-time warnings on site by a three-color dynamic light and a digital display monitor. Results of flash rip detection show that the combined length threshold and HSV-based segmentation method can be used in both sunny and cloudy days with an overall accuracy of 83%. Nonstationary locations and intermittent occurrences of flash rips are observed and characterized. The length of the flash rip ranges between

10 and 50 m. The duration of flash rips varies from 1 to 5 min with 65% of flash rips less than 2 min. A flash rip occurrence checklist by adding two new (storm and visual observation) factors is constructed to reliably assess the likelihood of hazardous flash rips. Public communication through media mentions, news releases, and website usages show the strong interest and support of the LOCKS as a new approach to issue timely and dynamic flash rip warnings to beach users.

In Chapter 3, temporal and spatial characteristics of flash rips induced by meteorologically induced water level oscillations (MIWLOs) are elucidated for revealing the unrecognized flash rip hazards to beach users. Specifically, the occurrences of flash rips in Lake Michigan at the North Beach of Port Washington are identified by using observation of images with sediment plume signatures. The causes and processes to generate flash rips are investigated by compiling observation of wind waves, water levels, and atmospheric pressures, surface winds, radar reflectivity images. Nearshore velocities and vorticities are reconstructed using the integrated atmospheric-hydrodynamic modeling to reveal spatial patterns of flash rips. Results of the observation and hydrodynamic modeling reveal that flash rips are induced by meteorologically induced water level oscillation including meteotsunamis, seiches, or the combined effects with wind waves. Flash rips characteristics of temporal transiency and intermittency, and spatial ubiquity and unpredictability are elucidated in the very low frequency motions (VLFs), posing a repeatable hidden danger to beach swimmers. Furthermore, rip currents generated by MIWLOs are found to be associated with 70% of current related incidents on the Great Lakes coasts and possibly also the cause for many reported incidents on the ocean coasts, as unrecognized hazards to beachgoers and coastal communities.

In Chapter 4, several drowning incidents spanning over the coast of Lake during a series of convective storms in a 4-day period are investigated. Features of storm disturbances and

hydrodynamic forcing are characterized to depict possible causes of the drowning incidents. Results reveal that unexpected flash rips can be generated by multiple nearshore processes, including: (i) longshore shear instabilities due to breaking of wind waves (Özkan-Haller and Kirby, 1999); (ii) nearshore circulation cells resulting from interactions of meteotsunami-induced edge waves and wind waves (Linares et al., 2019); (iii) seaward cross-shore currents through the reflection of two converged meteotsunami-induced edge waves (Bechle and Wu, 2014); and (iv) longshore shear instability of meteotsunami-induced seiche currents. Hidden flash rips are frequent under both low meteorologically induced water level oscillations and low wind waves, a condition has not been recognized before. Flash rips occurring after convective storms passing can further elevate the risk of the hidden danger to the unaware beach swimmers. An urgent need is called for communication of the storm-induced hidden flash rips.

In Chapter 5, a Structure Rip Checklist and Assessment Matrix (SRiCAM) is developed by characterizing rip currents near breakwaters rip current near breakwater structures in Lake Michigan. Rip currents occurrences near the north breakwater of Port Washington are associated with environmental proxies, including shifting winds, storm induced pressure perturbations, and high-frequency water level fluctuations that were not recognized before. The SRiCAM utilizes a four-level tier assessment to effectively address hidden rip currents, which occur when the water appears seemingly calm near the structure. The integration of SRiCAM into a cyberinfrastructure provides real-time warnings to the public. The developed assessment tool can be potentially applied to thirty-eight other locations in Lake Michigan and to wider regions of the Great Lakes, to foster the resilience to the rip current hazards among all coastal communities.

In Chapter 6, rip currents are characterized on the western shore of Lake Superior. Remote-sensing data including aerial imagery, coastal LiDAR elevations, and nearshore webcam images

are used to detect and analyze the bathymetry features where rip currents are prone to occur. The comparison of features at two beaches, the 12th St Beach and the 22nd St Beach in Duluth, MN over multiple years has shown that the double crescent bar systems are a dominant feature of rip current to occur on the western shore of Lake Superior. Dynamic and continuous evolution in feature components such as surf zone rip channels and offshore bars are observed on the time scale of years to hours. Overall, the documented bathymetric characteristics in this chapter provide information about hotspots and can be used to facilitate the future studies of transient rip currents on the western shore of Lake Superior.

7.2 Key contributions

- **Unrecognized, hidden flash rips impose one of the most dangerous beach hazards to the Great Lake coastal communities**

Flash rips in Great Lakes are observed and characterized for the first time in this dissertation. Temporally, flash rips are found to develop in transient lifespans from few seconds to several minutes. Rip pulsation in intervals >2 min is associated with the very low frequency motions VLFs (J. H. MacMahan et al., 2010). Spatially, flash rips occur ubiquitously in featureless beaches in nonstationary, variable locations that are unpredictable. The lengths of flash rips are found to extend beyond the surf zone widths up to 50-100 meters offshore. The temporal transiency and intermittency, with the spatial ubiquity and unpredictability in flash rip characteristics (Chapter 2, 3), can pose high risks. Unalerted beach swimmers can all of sudden get caught by flash rip pluses and be swept into deeper water where panic and exhaustion often leads to drowning (Houser et al., 2017). The temporal and spatial features result in the repeating danger of flash rips which have rarely been recognized before (Chapter 3). Furthermore, flash rips also pose a hidden

danger to unawareness of beach swimmers (Chapter 4), since the occurrences of flash rips frequently are observed under conditions that can appear misleadingly safe, such as under the low water level fluctuations, low wind wave heights, or during sunny weather after convective storms (Linares et al., 2019). Overall, unrecognized, hidden dangers in flash rips can be one of most dangerous and overlooked hazards to unaware swimmers and a critical need for communication and education to coastal communities is called.

- **Meteorologically induced water level oscillations are an overlooked cause to generate rip currents in the Great Lakes**

While energetic ocean swells or wind-generated waves have widely been perceived as the primary cause of rip currents (Castelle et al., 2016), a recent study also reveals that meteorologically induced water level oscillations (MIWLOs) such as meteotsunamis in the Great Lakes (Bechle et al., 2016) can also induce rip currents (Linares et al., 2019), but has been rarely recognized. In Chapter 3 and Chapter 4, flash rips induced by two types of MIWLOs, meteotsunamis and seiches in Lake Michigan, are revealed with evidence of atmospheric, hydrodynamic observations and state-of-art integrated atmospheric-hydrodynamic modeling. Specifically, the causative processes of MIWLOs generating flash rips include: meteotsunami-induced longshore currents (Chapter 3, 4), shear instability in seaward cross-shore currents in meteorologically induced water level drawdowns (Chapter 3), and breaking vorticity modulated by meteotsunamis (Chapter 3), reflected seaward cross-shore flows of two converged meteotsunami-induced edge waves (Chapter 4), and nearshore circulation cells resulting from interactions of meteotsunami-induced edge waves and wind waves (Chapter 4). In Chapter 5, MIWLOs, particularly high-frequency fluctuations in water levels are characterized as one type of

the environmental proxies for the boundary-controlled rip current occurring near coastal breakwaters. Additional evidence of high coincident occurrences of convective storms with observed flash rip occurrences (Chapter 2), and with rip current related drowning incidents (Chapter 4) are also discussed to further support MWILOs-induced flash rips. Overall, meteorologically induced water level oscillations are demonstrated to be an important but overlooked cause of hazardous rip currents in the Great Lakes.

- **Nearshore cameras can provide visual evidence for detecting rip currents**

Nearshore camera images are processed and analyzed to detect occurrences and characterize the three types of rip currents on the coasts of Lake Michigan and Lake Superior. First, for flash rips, the Lifeguarding Operational Camera Kiosk System (LOCKS) developed in Chapter 2 demonstrates that flash rip can be effectively and reliably detected using signatures of sediment plumes. The detection based on the combined length threshold and HSV-based segmentation method can achieve an overall accuracy of 83% on both sunny and cloudy days, which is found better than the traditionally RGB-based or HSV-based segmentation methods (Floc'h et al., 2018; Murray et al., 2013). Second, for boundary-controlled rip currents occurring near coastal structures, signatures of sediment plumes are detected near coastal structures at multiple locations across Lake Michigan (Chapter 5). Third, for bathymetry-controlled rip currents that occur on sandy barred beaches such as on the western shore of Lake Superior (Chapter 6), bathymetry features like rip channels or offshore crescent bars (Castelle et al., 2007; Moulton et al., 2017) are detected and quantified using time-averaged images with processing procedures of orthorectification and intensity-threshold segmentation, which can be used for long-term monitoring the potential hotspots of rip currents. Overall, nearshore cameras are of great potential

to be widely applied on the Great Lakes coasts for real-time detections and warnings of rip currents.

- **Effective warning for rip current hazards is achieved using environmental proxy-based assessments for rip occurrences**

Two new rip current checklists are developed to address flash rips (Chapter 2) and boundary-controlled rip currents (Chapter 5) in the Great Lakes. While existing rip current assessments tools based on environmental proxies (Lushine, 1991; Meadows et al., 2011) such as the Great Lakes Rip Current Checklist (GLRCC) have been widely used by the National Weather Service offices in rip currents advisory warnings, the GLRCC was developed based on characteristics of rip current in open barred beaches, i.e. bathymetry-controlled rips only. In this dissertation, the Flash Rip Occurrence Checklist (FROC) for flash rips occurring on featureless beaches (Chapter 2), and the Structure Rip Checklist and Assessment Matrix (SRiCAM) for rip currents near coastal structures (Chapter 5) are developed. Specifically, in FROC new environmental proxies of convective storms and visual observation are employed, and assessment results show consistency with human-eye observed occurrences. In SRiCAM, a four-level tiering is used instead of the traditional three-level tiering, which is demonstrated with consistency and inclusiveness for hidden rip current occurrences. Overall, the environmental proxies are demonstrated to reliably assess hazardous flash rips and can be employed to other beaches by adjusting site-specific proxies and criteria. Furthermore, both the FROC and the SRiCAM have been integrated into the INFOS cyberinfrastructure (Liu and Wu, 2019) to provide real-time rip current warnings to the public of the Great Lakes coastal communities.

7.3 Recommendations for future work

Future studies would focus on rip current characterization on the western shore of Lake Superior. Field measurements for characterization of rip current occurrences and circulations patterns at the hotspots identified in Chapter 6 could be conducted by measuring rip current velocities using dye releases (Brander and Short, 2001; Clarke et al., 2007) or GPS-equipped drifters (Austin and Atkinson, 2004; Johnson and Pattiaratchi, 2004; J. MacMahan et al., 2010; Sabet and Barani, 2011; Schmidt et al., 2003). Observations for rip currents and bathymetric features would be continued at the 22nd St. Beach, and at the 12th St. Beach with an installation of a nearshore camera, which can provide an efficient and cost-effective way for monitoring and assessing potential occurrences of rip currents. Numerical simulations for rip currents to reveal detailed hydrodynamic forcing in rip current generation could be conducted by employing the integrated atmospheric-hydrodynamic modeling as used in Chapter 3 and 4, or using the Large-Eddy Simulation (LES) model which directly solves resolve flows under wind wave and current interactions (Shen and Yue, 2001). The characterization could shed insights on explaining the causes for several past drowning tragedies (mentioned in Chapter 6) due to rip currents on the western shore to foster the resilience of coastal communities in Lake Superior.

Studies in Lake Superior would be extended to cover the southwestern shore region, particularly investigating rip currents at the site of Chequamegon Bay. Chequamegon Bay, with the complex geometry and topographic features (headlands, breakwater, and piers), can likely be a hotspot for all three types of rip currents. Furthermore, meteorologically induced water level fluctuations oscillations can be further amplified inside the bay due to natural resonance (As-Salek and Schwab, 2004; Bechle et al., 2016; Rabinovich, 2009), which further leads to the MIWLOs induced rip currents uncovered in this dissertation. Field observations of water level fluctuations

(Linares et al., 2018), Eulerian measurements of nearshore currents using acoustic Doppler current profilers (MacMahan et al., 2005), or GPS drifters (Schmidt et al., 2003; Scott et al., 2016) could be conducted to identify rip current occurrences and association with water level fluctuations in a semi-enclosed bay environment. Numerical simulations for MIWLOs induced rip currents could be conducted using the integrated atmospheric-hydrodynamic modeling to reveal the role of bay resonance in generating rip currents. In short, investigating rip currents at Chequamegon Bay would provide new perspectives on characteristics and causative processes that can lead to the unrecognized and hidden hazards of rip currents in semi-enclosed bays.

A detailed assessment of flash rips induced by meteorologically induced water level oscillations (MIWLOs) could be conducted to extend the findings in Chapter 3 and 4. Further science questions related to the MIWLOs induced flash rips would be asked, such as: which processes of MIWLOs are mostly likely to induce flash rips? how do features of atmospheric disturbance (i.e. storm propagation speeds and directions) affect the flash rip generation? what kind of interactions between wind waves and MIWLOs are more prone to cause flash rips and affecting flash rip characteristics? The assessments could be performed by implementing the integrated atmospheric-hydrodynamic models with high-resolution (O~ 1m) nearshore bathymetries using idealized scenarios or historical flash rip events, which can be identified from image observations or incident database. The assessment would provide system evaluations on the roles of meteorologically induced water level oscillations in inducing the hazardous flash rips, as well as could shed insights on the interacted impacts due to multiple coastal hazards of rip currents and meteotsunamis on the Great Lakes coastal communities.

Lastly, real-time warnings of rip current hazards could be extended to other beaches across the Great Lakes. Timely assessments on potential occurrences of different types of rip currents

could be achieved by using (1) the existing GLRCC for rip currents occurring in barred beaches (Meadows et al., 2011), (2) the developed FROC for flash rips occurring on featureless beaches (Liu and Wu, 2019), and (3) the SRiCAM developed in this dissertation for rip currents near coastal structures. Communication, delivering and warning could be achieved by similar systems as the LOCKS kiosk or as the INFOS cyberinfrastructure described in this dissertation. Furthermore, cyberinfrastructure like INFOS could be further extended to serve advanced data acquisition, processing, storage, visualization, and communications over the internet to multiple entities (Reimer and Wu, 2016) and providing timely information on rip current warnings to wider regions in all five Great Lakes.

7.4 References

As-Salek, J.A., Schwab, D.J., 2004. High-Frequency Water Level Fluctuations in Lake Michigan. J. Waterw. Port, Coastal, Ocean Eng. 130, 45–53. https://doi.org/10.1061/(ASCE)0733-950X(2004)130:1(45)

Austin, J., Atkinson, S., 2004. The design and testing of small, low-cost GPS-tracked surface drifters. Estuaries 27, 1026–1029. https://doi.org/10.1007/BF02803428

Bechle, A.J., Wu, C.H., 2014. The Lake Michigan meteotsunamis of 1954 revisited. Nat. Hazards 74, 155–177. https://doi.org/10.1007/s11069-014-1193-5

Bechle, A.J., Wu, C.H., Kristovich, D.A.R., Anderson, E.J., Schwab, D.J., Rabinovich, A.B., 2016. Meteotsunamis in the Laurentian Great Lakes. Sci. Rep. 6, 37832. https://doi.org/10.1038/srep37832

Brander, +; W, Short, R.W., 2001. Flow Kinematics of Low-energy Rip Current Systems. J. Coast. Res. 17, 468–481.

Castelle, B., Bonneton, P., Dupuis, H., Sénéchal, N., 2007. Double bar beach dynamics on the high-energy meso-macrotidal French Aquitanian Coast: A review. https://doi.org/10.1016/j.margeo.2007.06.001

Castelle, B., Scott, T., Brander, R.W.W., McCarroll, R.J.J., 2016. Rip current types, circulation and hazard, Earth-Science Reviews. Elsevier. https://doi.org/10.1016/j.earscirev.2016.09.008

Clarke, L.B., Ackerman, D., Largier, J., 2007. Dye dispersion in the surf zone: Measurements and simple models. Cont. Shelf Res. 27, 650–669. https://doi.org/10.1016/j.csr.2006.10.010

Floc'h, F., Mabiala, G.R., Almar, R., Castelle, B., Hall, N., Du Penhoat, Y., Scott, T., Delacourt, C., 2018. Flash Rip Statistics from Video Images. J. Coast. Res. 81, 100–106. https://doi.org/10.2112/SI81-013.1

Gensini, V.A., Ashley, W.S., 2010. An examination of rip current fatalities in the United States. Nat. Hazards 54, 159–175. https://doi.org/10.1007/s11069-009-9458-0

Great Lakes Current Incident Database [WWW Document], 2019. URL https://www.michiganseagrant.org/dcd/dcdsearch.php (accessed 12.9.19).

Great Lakes Surf Rescue Project Statistics [WWW Document], 2019. URL http://www.glsrp.org/statistics/ (accessed 12.9.19).

Houser, C., Trimble, S., Brander, R., Chris Brewster, B., Dusek, G., Jones, D., Kuhn, J., 2017. Public perceptions of a rip current hazard education program: "Break the Grip of the Rip!" Nat. Hazards Earth Syst. Sci. 17, 1003–1024. https://doi.org/10.5194/nhess-17-1003-2017

Johnson, D., Pattiaratchi, C., 2004. Application, modelling and validation of surfzone drifters. Coast. Eng. 51, 455–471. https://doi.org/10.1016/j.coastaleng.2004.05.005

Linares, Á., Wu, C.H., Anderson, E.J., Chu, P.Y., 2018. Role of Meteorologically Induced Water Level Oscillations on Bottom Shear Stress in Freshwater Estuaries in the Great Lakes. J. Geophys. Res. Ocean. 123, 4970–4987. https://doi.org/10.1029/2017JC013741

Linares, Á., Wu, C.H., Bechle, A.J., Anderson, E.J., Kristovich, D.A.R., 2019. Unexpected rip currents induced by a meteotsunami. Sci. Rep. 9, 2105. https://doi.org/10.1038/s41598-019-38716-2

Liu, Y., Wu, C.H., 2019. Lifeguarding Operational Camera Kiosk System (LOCKS) for flash rip warning: Development and application. Coast. Eng. 152, 103537. https://doi.org/10.1016/j.coastaleng.2019.103537

Lushine, J.B., 1991. A Study of Rip Current Drownings and Related Weather Factors. NATL. WEA. DIG 13--19.

MacMahan, J., Brown, J.J., Brown, J.J., Thornton, E., Reniers, A., Stanton, T., Henriquez, M.,

Gallagher, E., Morrison, J., Austin, M.J., Scott, T.M., Senechal, N., 2010. Mean Lagrangian flow behavior on an open coast rip-channeled beach: A new perspective. Mar. Geol. 268, 1–15. https://doi.org/10.1016/j.margeo.2009.09.011

MacMahan, J.H., Reniers, A.J.H.M., Thornton, E.B., 2010. Vortical surf zone velocity fluctuations with 0(10) min period. J. Geophys. Res. 115, C06007. https://doi.org/10.1029/2009JC005383

MacMahan, J.H., Thornton, E.B., Stanton, T.P., Reniers, A.J.H.M., 2005. RIPEX: Observations of a rip current system. Mar. Geol. 218, 113–134.

Matthews, B., Andronaco, R., Adams, A., 2014. Warning signs at beaches: Do they work? Saf. Sci. 62, 312–318. https://doi.org/10.1016/J.SSCI.2013.09.003

Meadows, G., Purcell, H., Guenther, D., Meadows, L., Kinnunen, R.E., Clark, G., 2011. Rip Currents in the Great Lakes: An Unfortunate Truth, in: Leatherman, S., Fletemeyer, J. (Eds.), Rip Currents: Beach Safety, Physical Oceanography, and Wave Modeling. CRC Press, pp. 199–214.

Moulton, M., Elgar, S., Raubenheimer, B., Warner, J.C., Kumar, N., 2017. Rip currents and alongshore flows in single channels dredged in the surf zone. J. Geophys. Res. Ocean. 122, 3799–3816. https://doi.org/10.1002/2016JC012222

Murray, T., Cartwright, N., Tomlinson, R., 2013. Video-imaging of transient rip currents on the Gold Coast open beaches. J. Coast. Res. 165, 1809–1814. https://doi.org/10.2112/SI65-306.1

Özkan-Haller, H.T., Kirby, J.T., 1999. Nonlinear evolution of shear instabilities of the longshore current: A comparison of observations and computations. J. Geophys. Res. Ocean. 104, 25953–25984. https://doi.org/10.1029/1999JC900104

Rabinovich, A.B., 2009. Seiches and Harbor Oscillations, in: Handbook of Coastal and Ocean Engineering. WORLD SCIENTIFIC, pp. 193–236.

https://doi.org/10.1142/9789812819307_0009

Reimer, J.R., Wu, C.H., 2016. Development and Application of a Nowcast and Forecast System Tool for Planning and Managing a River Chain of Lakes. Water Resour. Manag. 30, 1375–1393. https://doi.org/10.1007/s11269-016-1228-7

Sabet, B.S., Barani, G.A., 2011. Design of small GPS drifters for current measurements in the coastal zone. Ocean Coast. Manag. 54, 158–163. https://doi.org/10.1016/j.ocecoaman.2010.10.029

Schmidt, W.E., Woodward, B.T., Millikan, K.S., Guza, R.T., Raubenheimer, B., Elgar, S., 2003. A GPS-tracked surf zone drifter. J. Atmos. Ocean. Technol. 20, 1069–1075. https://doi.org/10.1175/1460.1

Schomberg, J., 2009. Rip Currents: A Survey of Beach Users.

Scott, T., Austin, M., Masselink, G., Russell, P., 2016. Dynamics of rip currents associated with groynes — field measurements, modelling and implications for beach safety. Coast. Eng. 107, 53–69. https://doi.org/10.1016/J.COASTALENG.2015.09.013